

Unclassified

SECURITY CLASSIFICATION OF THIS PAGE (When Data Entered)

REPORT DOCUMENTATION PAGE		READ INSTRUCTIONS BEFORE COMPLETING FORM
1. REPORT NUMBER AFFDL-TR-79-3118, Volume VII	2. GOVT ACCESSION NO.	3. RECIPIENT'S CATALOG NUMBER
4. TITLE (and Subtitle) DURABILITY METHODS DEVELOPMENT VOLUME VII - PHASE II DOCUMENTATION		5. TYPE OF REPORT & PERIOD COVERED Final Report June 1979 - January 1984
		6. PERFORMING ORG. REPORT NUMBER
7. AUTHOR(s) S. D. Manning, S. M. Speaker and D. E. Gordon		8. CONTRACT OR GRANT NUMBER(s) F33615-77-C-3123
9. PERFORMING ORGANIZATION NAME AND ADDRESS General Dynamics Fort Worth Division Fort Worth, Texas		10. PROGRAM ELEMENT, PROJECT, TASK AREA & WORK UNIT NUMBERS P.E. 62201F 24010118
11. CONTROLLING OFFICE NAME AND ADDRESS Flight Dynamics Laboratory (FIBE) Air Force Wright Aeronautical Laboratories Wright-Patterson Air Force Base, OH 45433		12. REPORT DATE January 1984
		13. NUMBER OF PAGES 194
14. MONITORING AGENCY NAME & ADDRESS (if different from Controlling Office)		15. SECURITY CLASS. (of this report) UNCLASSIFIED
		15a. DECLASSIFICATION/DOWNGRADING SCHEDULE
16. DISTRIBUTION STATEMENT (of this Report) Approved for public release; distribution unlimited.		
17. DISTRIBUTION STATEMENT (of the abstract entered in Block 20, if different from Report)		
18. SUPPLEMENTARY NOTES The associate investigators for this report were J. N. Yang, George Washington University, and M. Shinozuka, Modern Analysis Inc.		
19. KEY WORDS (Continue on reverse side if necessary and identify by block number) Durability, fatigue, economic life, crack size distribution, deterministic crack growth, time-to-crack-initiation (TTCI), equivalent initial flaw size (EIFS), initial fatigue quality (IFQ), probabilistic fracture mechanics, probability of crack exceedance, extent of damage, small crack sizes, Weibull distribution.		
20. ABSTRACT (Continue on reverse side if necessary and identify by block number) A statistically-based durability analysis methodology is evaluated, refined and demonstrated in this report for advanced metallic airframes. This methodology can be used to: (1) analytically assure the U.S. Air Force's durability design requirements, (2) evaluate durability design tradeoffs, and (3) evaluate structural maintenance requirements and user options affecting life-cycle costs. The methodology accounts for initial fatigue quality, crack growth accumulation in a population of structural details, (Continued)		

Abstract (Continued)

load spectra and structural properties. Analytical procedures and guidelines are developed and described for quantifying the extent of damage due to fatigue cracking in structural details as a function of service time and design variables. An initial fatigue quality model is described and discussed. This model is based on the time-to-crack-initiation (TTCI) and the equivalent initial flaw size (EIFS) concepts and a deterministic crack growth power law. An experimental test program and the resulting fractographic data for cracks in clearance-fit fastener holes are described and discussed. The durability analysis methodology is demonstrated for a full-scale fighter structure (F-16 lower wing skin) and for a complex splice subjected to a B-1 bomber spectrum. Various durability-related studies are described and discussed: initial fatigue model calibrations, statistical crack growth, scale-up and hole interaction effects, development of crack growth transfer functions for different load spectra and parameter sensitivity analysis.

The durability analysis methodology has been demonstrated for quantifying the extent of damage due to relatively small cracks in clearance-fit fastener holes (e.g., $\leq 0.10''$). Further research is needed to extend the methodology to larger crack sizes and to verify the methodology for other details, such as fillets, cutouts and lugs. The effects of fretting, faying surface sealant, fastener clamp-up, environment, interference-fit fasteners, etc., on the initial fatigue quality needs to be investigated. A fundamentally-sound statistically-based strategy has been developed for quantifying structural durability in meaningful terms for judging economic life and optimizing life-cycle costs. Further improvements and refinements of the procedures and durability design data can be developed within the general framework established.

AFFDL-TR-79-3118
VOLUME VII

Vol. 7

LIBRARY
RESEARCH REPORTS DIVISION
NAVAL POSTGRADUATE SCHOOL
MONTEREY, CALIFORNIA 93943



DURABILITY METHODS DEVELOPMENT VOLUME VII - PHASE II DOCUMENTATION

S.D. Manning, S.M. Speaker and D.E. Gordon

ae **General Dynamics Corporation**
Ft. Worth
Fort Worth Division
P.O. Box 748
Fort Worth, Texas 76101

J.N. Yang

The George Washington University
Washington, D.C. 20052

M. Shinozuka

Modern Analysis Incorporated
Ridgewood, N.J. 07450

January 1984

FINAL REPORT JUNE 1979 - JANUARY 1984

Approved for public release; distribution unlimited


AIR FORCE FLIGHT DYNAMICS LABORATORY
AIR FORCE WRIGHT AERONAUTICAL LABORATORIES
AIR FORCE SYSTEMS COMMAND
WRIGHT-PATTERSON AIR FORCE BASE, OHIO 45433


NOTICE

When Government drawings, specifications, or other data are used for any purpose other than in connection with a definitely related Government procurement operation, the United States Government thereby incurs no responsibility nor any obligation whatsoever; and the fact that the government may have formulated, furnished, or in any way supplied the said drawings, specifications, or other data, is not to be regarded by implication or otherwise as in any manner licensing the holder or any other person or corporation, or conveying any rights or permission to manufacture use, or sell any patented invention that may in any way be related thereto.


This report has been reviewed by the Office of Public Affairs (ASD/PA) and is releasable to the National Technical Information Service (NTIS). At NTIS, it will be available to the general public, including foreign nations.

This technical report has been reviewed and is approved for publication.


James L. Rudd
Project Engineer


Davey L. Smith
Structural Integrity Branch
Structures & Dynamics Division

FOR THE COMMANDER:


Ralph L. Kuster, Jr., Colonel, USAF
Chief, Structures & Dynamics Division

"If your address has changed, if you wish to be removed from our mailing list, or if the addressee is no longer employed by your organization please notify AFWAL/FIBE, W-PAFB, OH 45433 to help us maintain a current mailing list".

Copies of this report should not be returned unless return is required by security considerations, contractual obligations, or notice on a specific document.

FOREWORD

This report was prepared by General Dynamics, Fort Worth Division, with the support of George Washington University (Dr. J. N. Yang) and Modern Analysis Inc. (Dr. M. Shinozuka). The Air Force Wright Aeronautical Laboratories (AFWAL/FIBEC) sponsored this research under the "Durability Methods Development" program (Air Force Contract F33615-77-C-3123). James L. Rudd was the Air Force Project Engineer and Dr. Jack W. Lincoln of ASD/ENFS was a technical advisor for the program. Dr. B. G. W. Yee of the General Dynamics Materials Research Laboratory was the Program Manager and Dr. Sherrell D. Manning was the Principal Investigator. Dr. J. N. Yang and Dr. M. Shinozuka were associate investigators.

All tests were performed in General Dynamics' Metallurgy Laboratory by R. O. Nay under the direction of F. C. Nordquist. W. T. Kaarlela was responsible for the fractographic data acquisition. Fractographic readings were made by D. E. Gordon, W. T. Kaarlela, A. Meder, R. O. Nay and S. M. Speaker. S. M. Speaker coordinated the testing and fractographic effort for the program. J. W. Norris developed the computer software for storing and analyzing the fractographic data acquired and supported the initial fatigue quality model calibration/evaluation studies. Dr. V. D. Smith supported the statistical analysis effort. Peggy Thomas and Ernestine Bruner typed the report and Ron Jordan prepared many of the illustrations.

This report (Vol. VII) summarizes the work performed under Phase II of the "Durability Methods Development" program. The Phase II effort is further documented in two volumes as follows:

- o Volume VIII - Test and Fractographic Data
- o Volume IX - Documentation of Durability Analysis Computer Program.

An additional volume (VI) was also prepared to document the computer programs developed under Phase I for Vol. IV - Initial Quality Representation.

Work for this report was performed from June 1979 to January 1984.

TABLE OF CONTENTS

<u>Section</u>		<u>Page</u>
I	INTRODUCTION	1
	1.1 Objective and Scope	1
	1.2 Organization	2
II	BACKGROUND	3
	2.1 Introduction	3
	2.2 Aircraft Structural Durability Problem	3
	2.3 Air Force Durability Design Requirements	5
	2.4 Economic Life	6
	2.5 Extent of Damage	6
	2.6 Durability Analysis Objectives	6
III	DURABILITY ANALYSIS METHOD	9
	3.1 Introduction	9
	3.2 General Description	9
	3.3 Assumptions	9
	3.4 Initial Fatigue Quality	12
	3.5 Initial Fatigue Quality Model	13
	3.6 General Procedure	16
IV	DURABILITY ANALYSIS DETAILS	21
	4.1 Introduction	21

TABLE OF CONTENTS (Continued)

<u>Section</u>	<u>Page</u>
4.2 Initial Fatigue Quality	21
4.2.1 Crack Growth Power Law Variations	21
4.2.2 Generic EIFS Distribution	22
4.2.3 Negative EIFS	24
4.2.4 Details Other Than Fastener Holes	31
4.3 Determination of IFQ Model Parameters	31
4.3.1 Fractographic Data Pooling	31
4.3.2 EIFS Master Curve Parameters (Q_i^* and b_i^*)	32
4.3.3 TTCI Parameters	34
4.4 Statistical Scaling of β	37
4.5 Probability Of Crack Exceedance	40
4.5.1 IFQ Based on AFXMR4 Data Set	40
4.5.2 Compatible SCGMC	42
4.5.3 Crack Exceedance Predictions	46
4.6 Formats For Presenting Durability Analysis Results	48
4.7 Demonstration of Durability Analysis Method	48
4.7.1 F-16 Lower Wing Skin	48
4.7.2 Complex Splice (B-1 Bomber Spectrum)	51

TABLE OF CONTENTS (Continued)

<u>Section</u>	<u>Page</u>
4.8 Additional Studies	54
4.8.1 IFQ Model Studies	54
4.8.2 Statistical Crack Growth Studies	57
4.8.3 Related Durability Studies	58
V DURABILITY TEST PROGRAM	59
5.1 Introduction	59
5.2 Test Matrix	59
5.3 Data Set Designations	59
5.4 Load Spectra	65
5.5 Specimen Details	65
5.6 Test Setup And Procedures	71
VI EVALUATION OF TEST AND FRACTOGRAPHIC RESULTS	75
6.1 Introduction	75
6.2 Dog-Bone Specimens	76
6.2.1 TTCI Comparisons	76
6.2.2 Fatigue Life Comparisons	76
6.2.3 Test Results For D6ac Steel	87
6.2.4 Discussion	87
6.3 Complex Splice	92

TABLE OF CONTENTS (Continued)

<u>Section</u>	<u>Page</u>
6.4 Crack Initiation Origins and Trends	94
6.4.1 No-Load Transfer Specimens	94
6.4.2 15% Load Transfer Specimens	98
6.4.3 30% and 40% Load Transfer Specimens	101
6.4.4 Complex Splice	101
6.5 F-16 Lower Wing Skin Tear-Down Inspection	101
6.6 Conclusions and Recommendations	104
VII CONCLUSIONS AND RECOMMENDATIONS	113
7.1 Conclusions	113
7.2 Recommendations	118
APPENDICES	123
A - Evaluation of IFQ Model Parameters for Straight-Bore Fastener Holes	123
A.1 Introduction	123
A.2 IFQ Model Parameters for Individual Data Sets	126
A.3 IFQ Model Parameters for Pooled Data Sets	128
A.4 Study IFQ Model Relationships	131
B - Evaluation of IFQ Model Parameters for Countersunk Fastener Holes	141
B.1 Introduction	141
B.2 IFQ Model Parameters for Individual Data Sets	143
B.3 Study IFQ Model Relationships	146

TABLE OF CONTENTS (Continued)

<u>Section</u>	<u>Page</u>
C - Related Durability Studies	153
C.1 Scale-up Effects and Hole Interaction	153
C.2 Development of Transfer Functions	156
C.3 Parametric Sensitivity Analysis	185
REFERENCES	189

LIST OF FIGURES

<u>FIGURE NO.</u>	<u>TITLE</u>	<u>PAGE NO.</u>
1	Essential Elements of the Durability Analysis Methodology	xxxiii
2	Wing Box Assembly	4
3	Initial Fatigue Quality Model	10
4	Growth of EIFS Distribution as Function of Time	11
5	Flow Diagram and Equations for Computing $y_{1i}(\tau)$ and $p(i, \tau)$	19
6	Illustration of Generic EIFS Condition	23
7	IFQ Distribution With Both Positive and Negative EIFSs	26
8	Truncated IFQ Distribution	28
9	Truncated EIFS Cumulative Distribution	29
10	Ranked EIFS Crack Growth for Truncated Distribution	30
11	Calibration Concepts for b_i^*	35
12	Conceptual Description of Procedures for Determining α and β_{1i} for Pooled TTCI Data Sets	38
13	Formats for Presenting Extent of Damage Results	49
14	Stress Zones for F-16 Lower Wing Skin	52
15	Complex-Splice Specimen	53
16	Specimen Configuration Designations	63

LIST OF FIGURES (Continued)

<u>FIGURE NO.</u>	<u>TITLE</u>	<u>PAGE NO.</u>
17	No-Load Transfer Specimen Design	66
18	15% Load Transfer Specimen Design	67
19	30% Load Transfer Specimen Design	68
20	40% Load Transfer Specimen Design	69
21	D6ac Steel Specimen Design	70
22	Load Transfer Specimen Free Body Diagram	72
23	TTCI Comparisons for Selected No-Load Transfer Data Sets (7475-T7351 Aluminum; F-16 400 Hour Spectrum; $a_0 = 0.03''$)	79
24	TTCI Comparisons for Selected 15% Load Transfer Data Sets (7475-T7351 Aluminum; F-16 400-Hour Spectrum; $a_0 = 0.03''$)	80
25	TTCI Comparisons for Selected 30% and 40% Load Transfer Data Sets (7475-T7351 Aluminum; F-16 400-Hour Spectrum; $a_0 = 0.03''$)	81
26	TTCI Comparisons for Selected No-Load Transfer Data Sets (7475-T7351 Aluminum; B-1 Bomber Spectrum; $a_0 = 0.03''$)	82
27	TTCI Comparisons for Selected 15% Load Transfer Data Sets (7475-T7351 Aluminum; B-1 Bomber Spectrum; $a_0 = 0.03''$)	83
28	TTCI Comparisons for Selected 30% and 40% Load Transfer Data Sets (7475-T7351 Aluminum; B-1 Bomber Spectrum; $a_0 = 0.03''$)	84

LIST OF FIGURES (Continued)

<u>FIGURE NO.</u>	<u>TITLE</u>	<u>PAGE NO.</u>
29	Fatigue Life as a Function of Stress Level for F-16 400-Hour Spectrum	85
30	Fatigue Life as a Function of Stress Level for B-1 Bomber Spectrum	86
31	Fatigue Life as a Function of Stress Level for D6ac Steel Specimens (F-16 400-Hour Spectrum)	89
32	Fatigue Life as a Function of Stress Level for Complex Splice Specimens (B-1 Bomber Spectrum)	95
33	Coalescence of Multiple Cracks to Form a Single Large Crack	96
34	Fatigue Crack Origin Location Designations	97
35	Typical Fatigue Crack Origins in No-Load Transfer Specimens	99
36	Typical Fracture Surface for 15% Load Transfer Specimen (ABXMR4(A); $\sigma = 38\text{ksi}$; B-1 Bomber Spectrum)	100
37	Convergence of Crack Fronts Causing Rapid Crack Growth	100
38	Identification of Fastener Holes in Outer Row of Complex Splice Specimen	102
39	F-16 Basic Wing Box Structure	103
40	Identification of Fastener Holes in the F-16 Durability Component Lower Right Hand Wing Skin with Observed Cracks (After 16000 Hrs. of Testing with F-16 500-Hour Spectrum)	105

LIST OF FIGURES (Continued)

<u>FIGURE NO.</u>	<u>TITLE</u>	<u>PAGE NO.</u>
41	Identification of Fastener Holes in the F-16 Durability Component Lower Left Hand Wing Skin with Observed Cracks (After 16000 Hrs. of Testing with F-16 500-Hour Spectrum)	106
A1	Fastener Hole Quality Specimens; (a) No-Load Transfer and (b) 15% Load Transfer	125
A2	$\ln Q_i^*$ Versus $\ln \beta_{\ell i}$ for Pooled Data Sets (Case V; Table A3)	134
A3	$\ln \beta_{\ell i}$ Versus $\ln \sigma$ for Pooled Data Sets (Case I; Table A3)	135
A4	$\ln \beta_{\ell i}$ Versus $\ln \sigma$ for Pooled Data Sets (Case V; Table A3)	136
A5	$\ln Q_i^*$ Versus $\ln \sigma$ for Pooled Data Sets (Case I; Table A3)	137
A6	$\ln Q_i^*$ Versus $\ln \sigma$ for Pooled Data Sets (Case V; Table A3)	138
B1	$\ln Q_i^*$ Versus $\ln \beta_{\ell i}$ for Pooled Data Sets (Case X; Table B2)	150
B2	$\ln Q_i^*$ Versus $\ln \sigma$ for Pooled Data Sets (Case X; Table B2)	151
B3	$\ln \beta_{\ell i}$ Versus $\ln \sigma$ for Pooled Data Sets (Case X; Table B2)	152
C1	Schematic Comparisons of Crack Growth Curves for Different Load Spectra	158
C2	Relationship Between Spectral Intensity and Flight Hours	158
C3	Crack Growth Curves for Five Load Spectra Based on CYCGRO Program	178

LIST OF FIGURES (Continued)

<u>FIGURE NO.</u>	<u>TITLE</u>	<u>PAGE NO.</u>
C4	Rms Stress Value - Flight Hour Relationship	179
C5	A Simplified Load Spectrum	182
C6	Crack Growth Under Simplified Spectra (Missions 6-15)	184

LIST OF TABLES

<u>TABLE NO.</u>	<u>TITLE</u>	<u>PAGE NO.</u>
1	Description of AFXMR4 Fractographic Data Set	41
2	IFQ Model Parameters for AFXMR4 Data Set	43
3	Analytical Crack Growth Predictions for 7475-T7351 Aluminum and the F-16 500 Hour Spectrum	43
4	Summary of SCGMC Parameters	44
5	Comparison of $a(t)$ Predictions (SCGMC) Versus Actual $a(t)$ Values	45
6	Crack Exceedance Analysis Based on Compatible SCGMC	47
7	Durability Test Matrix	60
8	Test Matrix Details	61
9	Data Set Designations	64
10	Comparison of TTCI Results for Key Fighter Data Sets (7475-T7351 Aluminum)	77
11	Comparison of TTCI Results for Key Bomber Data Sets (7475-T7351 Aluminum)	78
12	Test Results for D6ac Steel Specimens	88
13	Complex Splice Test Results	93
14	Fractographic Results for F-16 Lower Wing Skin (Right Hand; Durability Test Article) - Stress Zone I	107

LIST OF TABLES (Continued)

<u>TABLE NO.</u>	<u>TITLE</u>	<u>PAGE NO.</u>
15	Fractographic Results for F-16 Lower Wing Skin (Right Hand; Durability Test Article) - Stress Zone II	108
16	Fractographic Results for F-16 Lower Wing Skin (Right Hand; Durability Test Article) - Stress Zone III	109
17	Fractographic Results for F-16 Lower Wing Skin (Left Hand; Durability Test Article)	110
A1	FHQ Data Sets Used	124
A2	Model Parameters for Unpooled FHQ Data Sets (Straight Bore Holes; 0.005" - 0.100" Crack Size Range)	127
A3	Model Parameters for Pooled FHQ Data Sets (Straight Bore Holes; 0.005" - 0.100" Crack Size Range)	129
A4	Model Parameters for Pooled FHQ Data Sets (Straight Bore Holes; 0.005" - 0.050" Crack Size Range)	130
A5	Comparison of $Q_i^* \beta_{li}$ Values for Different Spectra and Stress Levels (15% LT, Straight Bore Holes)	132
A6	Comparison of $Q_i^* \beta_{li}$ Values for Different % LT, Stress Levels and Spectra (Straight Bore Holes)	132
A7	Summary of Model Parameters and Empirical Constants for Pooled Data Sets	133
B1	Fractographic Data Sets Used	142
B2	Model Parameters for Pooled Data Sets (Csk Rivets: 0.005" - 0.100" Crack Size Range)	144

LIST OF TABLES (Continued)

<u>TABLE NO.</u>	<u>TITLE</u>	<u>PAGE NO.</u>
B3	Comparison of $Q_i^* \beta_{\ell_i}$ Values for Different Stress Levels and Spectra (15% LT; $\frac{1}{4}$ " Dia Csk Hole)	147
B4	Comparison of $Q_i^* \beta_{\ell_i}$ Values for Different Hole Diameters (F-16 400-Hour Spectrum; Csk Hole)	148
B5	Comparison of $Q_i^* \beta_{\ell_i}$ Values for Different % LT and Stress Levels (B-1 Bomber Spectrum; Csk Hole)	149
C1	F-15 Load Spectrum (Air-Air)	161
C2	F-16 400-Hour Spectrum (FHQ Program)	167
C3	B-1 Load Spectrum (Combat)	172
C4	B-1 Load Spectrum (Crew Training)	175
C5	Simplified Amplitude Flight-by-Flight Load Spectra ($\sigma_{LIM} = 40$ ksi)	183

LIST OF SYMBOLS

a	=	Crack size
a_{DL}	=	Durability limit flaw size
a_e	=	Economic repair size limit
a_0	=	Reference crack size for given TTCI's
$a(0)$	=	Crack size at $t=0$
a_{RL}	=	Repair. limit flaw size
$a(t), a(t_1), a(t_2)$	=	Crack size at time t, t_1 and t_2 , respectively
a_U, a_L	=	Upper and lower bound fractographic crack size, respectively, used to define the IFQ model parameters
$a(\tau)$	=	Crack size at service time τ
b, Q	=	Crack growth parameters in the equation $\frac{da(t)}{dt} = Q [a(t)]^b$. Used in conjunction with the IFQ model.
b_i, Q_i	=	Crack growth constants in $\frac{da(t)}{dt} = Q_i [a(t)]^{b_i}$ for the i th stress region when this equation is used in conjunction with the service crack growth master curve (SCGMC).
b_i^*, Q_i^*	=	Crack growth constants in $\frac{da(t)}{dt} = Q_i^* [a(t)]^{b_i^*}$ for the i th fractographic data set. Notation used in conjunction with fractographic data pooling procedures and the EIFS master curve for the i th fractographic data set.

$b_{i,j}^*, Q_{i,j}^*$	=	Crack growth constants in $\frac{da(t)}{dt} = Q_{i,j}^* [a(t)]^{b_{i,j}^*}$ for the ith fractographic data set and the jth fractographic sample from the ith data set, where $b_{i,j}^* \geq 1.0$. Notation distinguishes parameters for each sample in a given fractographic data set.
c	=	b - 1; Used in conjunction with the IFQ model when the crack growth law, $\frac{da(t)}{dt} = Q[a(t)]^b$ is used and b > 1.0.
c_i	=	$b_i - 1$; Used in conjunction with the SCGMC when $\frac{da(t)}{dt} = Q_i[a(t)]^{b_i}$ is used. The subscript "i" refers to the ith stress region.
CFA	=	Conventional Fatigue Analysis (Palmgren-Miner rule)
DCGA	=	Deterministic Crack Growth Approach
$\frac{da(t)}{dt}$	=	Crack growth rate as a function of time
EIFS	=	Equivalent initial flaw size
$f_{a(0)}(x)$	=	EIFS probability density function = $\frac{dF_{a(0)}(x)}{dx}$
$f_T(t)$	=	$\frac{dF_T(t)}{dt}$
$F_{a(0)}(x)$	=	EIFS cumulative distribution function
$F_T(t)$	=	TTCI cumulative distribution function
FHQ	=	Fastener hole quality
IFQ	=	Initial fatigue quality

ℓ	=	Factor used in conjunction with the fractographic results for a single TTCI data set and the equation: $\beta = \beta_0(\ell)^{1/\alpha}$. ℓ is the number of equally-stressed fastener holes per test specimen in which <u>only</u> the largest fatigue crack in <u>any</u> "one" hole per specimen is included in the fractographic data set.
ℓ_i	=	Same as ℓ with the subscript "i" referring to the ith TTCI data set and used in the equation: $\beta_i = \beta_{\ell_i}(\ell_i)^{1/\alpha_i}$.
$L(\tau), \bar{L}(\tau)$	=	Total and average number of details, respectively, in the entire component having a crack size $>x_1$ at any service time τ
LT	=	Load transfer through the fastener
N_i	=	Total number of details in the ith stress region
N^*	=	Total number of details in the entire durability critical component
$N(i, \tau), \bar{N}(i, \tau)$	=	Total and average number of details respectively, having a crack size exceeding x_1 at any service time τ
NLT	=	No load transfer through the fastener
P	=	Probability or exceedance probability
PFMA	=	Probabilistic Fracture Mechanics Approach
$p(i, \tau)$	=	Probability that a detail in the ith stress region will have a crack size $>x_1$ at the service time τ

$$\hat{Q}_i = \frac{\text{Ave. } Q_i^* \beta_i}{\beta_i} = \frac{\frac{1}{n} \sum_{i=1}^n Q_i^* \beta_i}{\beta_i}; \text{Normalized}$$

crack growth parameter, Q_i^* , for the i th fractographic data set when the crack growth equation, $\frac{da(t)}{dt} = Q_i^* [a(t)]^{b_i^*}$

is used and $b_i^* = 1.0$. Used in conjunction with the EIFS master curve for the i th fractographic data set.

$$\hat{Q}_{\ell_i} = \frac{\text{Ave. } Q_i^* \beta_{\ell_i}}{\beta_{\ell_i}} = \frac{\frac{1}{n} \sum_{i=1}^n Q_i^* \beta_{\ell_i}}{\beta_{\ell_i}}$$

$$Q\beta = \text{Ave. } Q_i^* \beta_i = \frac{1}{n} \sum_{i=1}^n Q_i^* \beta_i = \frac{1}{n} \sum_{i=1}^n Q_i^* \beta_{\ell_i} (\ell_i)^{1/\alpha_i} =$$

constant for "generic" EIFS cumulative distribution.

$$Q\beta_{\ell} = \text{Ave } Q_i^* \beta_{\ell_i} = \frac{1}{n} \sum_{i=1}^n Q_i^* \beta_{\ell_i}$$

Used when checking IFQ model goodness-of-fit when fractography is available only for the largest fatigue crack in any one ℓ_i fastener hole per test specimen.

SCGMC = Service crack growth master curve

t, t_1, t_2 = Flight hours at t, t_1, t_2 , respectively.

T, T_{TCI} = Time-to-crack-initiation

x = Crack size

x_1 = Crack size used for $p(i, \tau)$ predictions

x_u = Upper bound limit for EIFS

$y_{1i}(\tau)$ = An EIFS in the IFQ distribution corresponding to a crack size x_1 at time τ in the i th stress region. Value determined using the SCGMC.

Z	=	No. of standard deviations from the mean
$\alpha, \beta, \epsilon,$	=	Weibull distribution parameters for shape, scale, and lower bound TTCI, respectively. Used in conjunction with the IFQ distribution or for a single TTCI data set.
$\alpha_i, \beta_i, \epsilon_i$	=	Weibull distribution parameters for the i th TTCI data set for shape, scale, and lower bound TTCI, respectively. Used in conjunction with fractographic data pooling procedures ($i = 1, \dots, n$ data sets).
β_ℓ	=	Weibull scale parameter for TTCI based on the TTCI's for a given fractographic data set in which only the fractography for the largest fatigue crack in any "one" of ℓ fastener holes per test specimen is used to define β_ℓ . Note: $\beta = \beta_\ell (\ell)^{1/\alpha}$
β_{ℓ_i}	=	Same as β_ℓ with the subscript "i" denoting the β_ℓ value for the i th TTCI data set and is used to determine β_i as follows: $\beta_i = \beta_{\ell_i} (\ell_i)^{1/\alpha_i}$.
$\Gamma()$	=	Gamma function
ξ, γ	=	Empirical constants in the equation: $Q_i = \xi \sigma^\gamma$, where σ = stress
σ	=	Stress or standard deviation
$\sigma_N^2(i, \tau), \sigma_L^2(i, \tau)$	=	Variance of $N(i, \tau)$ and $L(\tau)$, respectively
τ	=	A particular service time

TERMINOLOGY

1. Crack Size - is the length of a crack in a structural detail in the direction of crack propagation.
2. Deterministic Crack Growth - Crack growth parameters are treated as deterministic values resulting in a single value prediction for crack length.
3. Durability - is a quantitative measure of the airframe's resistance to fatigue cracking under specified service conditions. Structural durability is normally concerned with relatively small subcritical crack sizes which affect functional impairment, structural maintenance requirements and life-cycle-costs. Such cracks may not pose an immediate safety problem. However, if the structural details containing such cracks are not repaired, economical repairs cannot be made when these cracks exceed a limiting crack size. The entire population of structural details in various components is susceptible to fatigue cracking in service. Therefore, a statistical approach is essential to quantitatively assess the "durability" of a part, a component, or an airframe.
4. Durability Analysis - is concerned with quantifying the extent of structural damage due to fatigue cracking for structural details (e.g.. fastener hole, fillet, cutout, lug, etc.) as a function of service time. Results are used to ensure design compliance with Air Force's durability design requirements.
5. Economic Life - is that point in time when an aircraft structure's damage state due to fatigue, accidental damage and/or environmental deterioration reaches a point where operational readiness goals cannot be preserved by economically acceptable maintenance action.
6. Economic Life Criteria - are guidelines and formats for defining quantitative economic life requirements for aircraft structure to satisfy U.S. Air Force durability design requirements. The economic life criterion provides the basis for analytically and experimentally ensuring design compliance of aircraft structure with durability design requirements. Two recommended formats for economic life criteria are:

- o probability of crack exceedance

- o cost ratio: repair cost/replacement cost

7. Economic Repair Limit - is the maximum damage size that can be economically repaired (e.g., repair 0.03" - 0.05" radial crack in fastener holes by reaming hole to next size).
8. Equivalent Initial Flaw Size (EIFS) - is a hypothetical crack assumed to exist in the structure prior to service. It characterizes the equivalent effect of actual initial flaws in a structural detail. It is determined by back-extrapolating fractographic results. An equivalent initial flaw is assumed to have the same flaw shape and origin as the observable crack size at a given time. The EIFS concept is a convenient "mathematical tool" for quantifying the IFQ for structural details and the probability of crack exceedance or extent of damage as a function of time. An EIFS is strictly a mathematical quantity rather than an actual initial flaw size. Within this context, EIFS's can be positive or negative, depending on the fractographic results and the back extrapolation method used. EIFS values depend on several factors, including: the fractographic results used (and the test variables reflected), the fractographic crack size range used, the form of the crack growth equation used for the back-extrapolation, the goodness of the curve fit to the fractographic data, the manufacturing quality of the structural details, fastener hole type, fastener type and fit, etc. EIFS, for different fractographic data are not comparable unless the applicable IFQ model parameters are determined consistently (e.g., same fractographic crack size range used, same "b" value imposed if the $Q[a(t)]^b$ crack growth model is used, same a values imposed for comparable fractographic data sets, etc.). Fractographic data pooling is essential to quantify the IFQ for different fractographic data sets on a common baseline.
9. EIFS Master Curve - is a curve (e.g., equation, tabulation of $a(t)$ vs. t or curve without prescribed functional form) used to determine the EIFS value at $t=0$ corresponding to a given TTCI value at a specified crack size. Such a curve is needed to determine the IFQ distribution from the TTCI distribution. The EIFS master curve depends on several factors, such as the fractographic data base, the fractographic crack size range used, the functional form of the crack growth equation used in the curve fit, etc. (Ref. EIFS).

10. Extent of Damage - is a quantitative measure of structural durability at a given service time. For example, the number of structural details (e.g., fastener holes, cutouts, fillets, etc.) or percentage of details exceeding specified crack size limits. Crack length is the fundamental measure for structural damage. The predicted extent of damage is compared with the specified economic life criterion for ensuring design compliance with U.S. Air Force durability requirements.
11. Generic EIFS Distribution - An EIFS distribution is "generic" if it depends only on the material and manufacturing/fabrication processes. Theoretically, the EIFS distribution should be independent of design variables, such as load spectrum, stress level, percent load transfer, environment, etc. For "durability analysis", the EIFS distribution for fastener holes (e.g., given material, drilling procedures, fastener types/fit, etc.) should be justified for different design stress levels and load spectra.
12. Initial Fatigue Quality (IFQ) - characterizes the initial manufactured state of a structural detail or details with respect to initial flaws in a part, component, or airframe prior to service. The IFQ, represented by an equivalent initial flaw size (EIFS) distribution, must be defined using a consistent fractographic data base. The EIFS distribution depends on the fractographic crack size range used and other factors (Ref. EIFS and EIFS master curve). Whatever EIFS distribution is used, it should be defined specifically for the crack size range of interest for the structural details to be used in the durability analysis. A single EIFS distribution will not necessarily be satisfactory for a wide range of crack sizes (e.g., 0.0005" - 0.10"). Based on current understanding, the EIFS distribution should be defined for a fairly small range of crack sizes (e.g., 0.020" - 0.050" crack size for fastener holes). Further research is required to evaluate the effects and sensitivity of the crack size range on the EIFS distribution and the accuracy of the crack exceedance prediction.
13. Initial Fatigue Quality Model - is a "mathematical tool" for quantifying the IFQ distribution for applicable structural details. Using the IFQ model and fractographic results, an EIFS distribution can be determined which is compatible with the TTCI distribution.

14. Probability of Crack Exceedance ($p(i, \tau)$) - refers to the probability of exceeding a specified crack, x_i , size at a given service time, τ . It can be determined from the statistical distribution of crack sizes and can be used to quantify the extent of damage due to fatigue cracking in fastener holes, cutouts, fillets, lugs, etc.
15. Reference Crack Size (a_0) - This is the specified crack size in a detail used to reference TTCI's. The IFQ distribution is based on a selected reference crack size.
16. Service Crack Growth Master Curve (SCGMC) - This curve is used to determine the EIFS, $y_{11}(\tau)$, corresponding to an exceedance crack size x_i at time τ . The probability of crack exceedance, $p(i, \tau)$, can be determined from the EIFS cumulative distribution for a given $y_{11}(\tau)$. The SCGMC is defined for the applicable design variables (e.g., stress level, spectrum, etc.) and it can be determined using either test data or an analytical crack growth program. All SCGMC's must be consistent with the corresponding EIFS master curve and the fractographic data base. The SCGMC must be consistent with the basis for the IFQ distribution.
17. Structural Detail - is any element in a metallic structure susceptible to fatigue cracking (e.g., fastener hole, fillet, cutout, lug, etc.).
18. Time-To-Crack-Initiation (TTCI) - is the time or service hours required to initiate a specified (observable) fatigue crack size, a_0 , in a structural detail (with no initial flaws intentionally introduced).
19. TTCI Lower Bound Limit (ϵ) - ϵ is a cutoff value for TTCI's reflected in the IFQ model. It varies for a given a_0 and it depends on the EIFS upper bound limit, x_u , and the EIFS master curve. TTCI's for a given crack size, a_0 , should $\geq \epsilon$. This Weibull distribution parameter provides a basis for quantifying the EIFS distribution for different TTCI crack sizes on a common baseline.
20. Upper Bound EIFS (x_u) - defines the largest EIFS in the initial fatigue quality distribution. x_u , specified by the user, should be consistent with ϵ (TTCI lower bound limit) and the EIFS master curve.

SUMMARY

Objectives of the "Durability Methods Development" program were: (1) develop and demonstrate a durability analysis methodology capable of satisfying the U.S. Air Force's durability design requirements for metallic airframes and (2) prepare a durability design handbook.

A statistically-based durability analysis methodology was developed under Phase I of this program [1-5]. This Volume (VII) documents the Phase II effort, which was concerned with: (1) evaluating, refining and demonstrating the durability analysis method developed in Phase I for full-scale aircraft structures, (2) acquiring fractographic data for fatigue cracks in clearance-fit fastener holes, (3) developing and evaluating durability analysis procedures and guidelines and (4) performing related durability studies to further the understanding. Raw test and fractographic data are reported in Volume VIII[6] Computer programs for implementing the durability analysis method are listed in Volume IX [7]

Aircraft structure must be designed to be durable to minimize structural maintenance requirements, life-cycle-costs and functional impairment problems affecting operational readiness. Durability is normally concerned with relatively small subcritical fatigue cracks in structural details (e.g., 0.03"- 0.05" radial crack in a fastener hole). It is a measure of the structure's resistance to fatigue cracking.

The population of structural details, such as fastener holes, fillets, cutouts, lugs, etc., in aircraft structures is susceptible to fatigue cracking in service. Likewise, structural maintenance requirements and costs depend on the number of details requiring repair. To assess the durability of the structure or the extent of damage as a function of time, the entire population of structural details must be accounted for. Therefore, a statistical approach is essential to quantify the overall extent of damage as a function of time.

According to U.S. Air Force durability design requirements for metallic airframes, the economic life of the structure must exceed one design service life. Economic life is currently defined in qualitative terms: "... the occurrence of widespread damage which is uneconomical to repair and, if not repaired, could cause functional problems

affecting operational readiness" [8-10]. Acceptable limits for "widespread damage" and "uneconomical repair" must be defined for each aircraft design and such limits must be approved by the Air Force. A quantitative definition of economic life has not evolved from this program. However, guidelines and two basic formats for quantitative economic life criteria have been developed: (1) probability of crack exceedance and (2) cost ratio: repair cost/replacement cost. The analytical tools developed under this program can be used to quantify the extent of damage and show compliance with the specified economic life criterion.

The durability analysis method developed is conceptually described in Fig. 1. It accounts for initial fatigue quality, crack growth accumulation in a population of structural details, load spectra and structural properties. A "mathematical tool" has been developed for quantifying the initial fatigue quality of structural details using fractographic results. This model is based on the time-to-crack-initiation (TTCI) and equivalent initial flaw size (EIFS) concepts and a deterministic crack growth power law. Once the initial fatigue quality or EIFS distribution has been defined for a given detail type, the EIFS population for groups of details with a common stress history can be grown to a given service time (for specified design conditions) using a suitable analytical crack growth program. The extent of damage is measured by the number of details in the population expected to exceed a specified crack size at a given service time or equivalently by the probability of crack exceedance. Simple expressions, based on the binomial distribution, are used to quantify the overall extent of damage for different details, parts, components, or the entire airframe. Statistical principles can be used to estimate upper and lower bound predictions for the extent of damage. These results provide a quantitative description of the structure's resistance to cracking and a basis for judging economic life.

The durability analysis method has been evaluated and demonstrated for relatively small fatigue cracks in clearance-fit fastener holes (e.g., $\leq 0.10"$). However, the basic strategy and concepts theoretically apply to fatigue cracks in any structural detail (e.g., cutouts, fillets, lugs, etc.) as long as the dominant crack in each detail is relatively small and such cracks are statistically independent (i.e., the growth of the largest crack in one detail does not significantly affect the growth of the largest crack in neighboring details and vice versa). The durability analysis method has been successfully demonstrated for a full-scale fighter aircraft structure

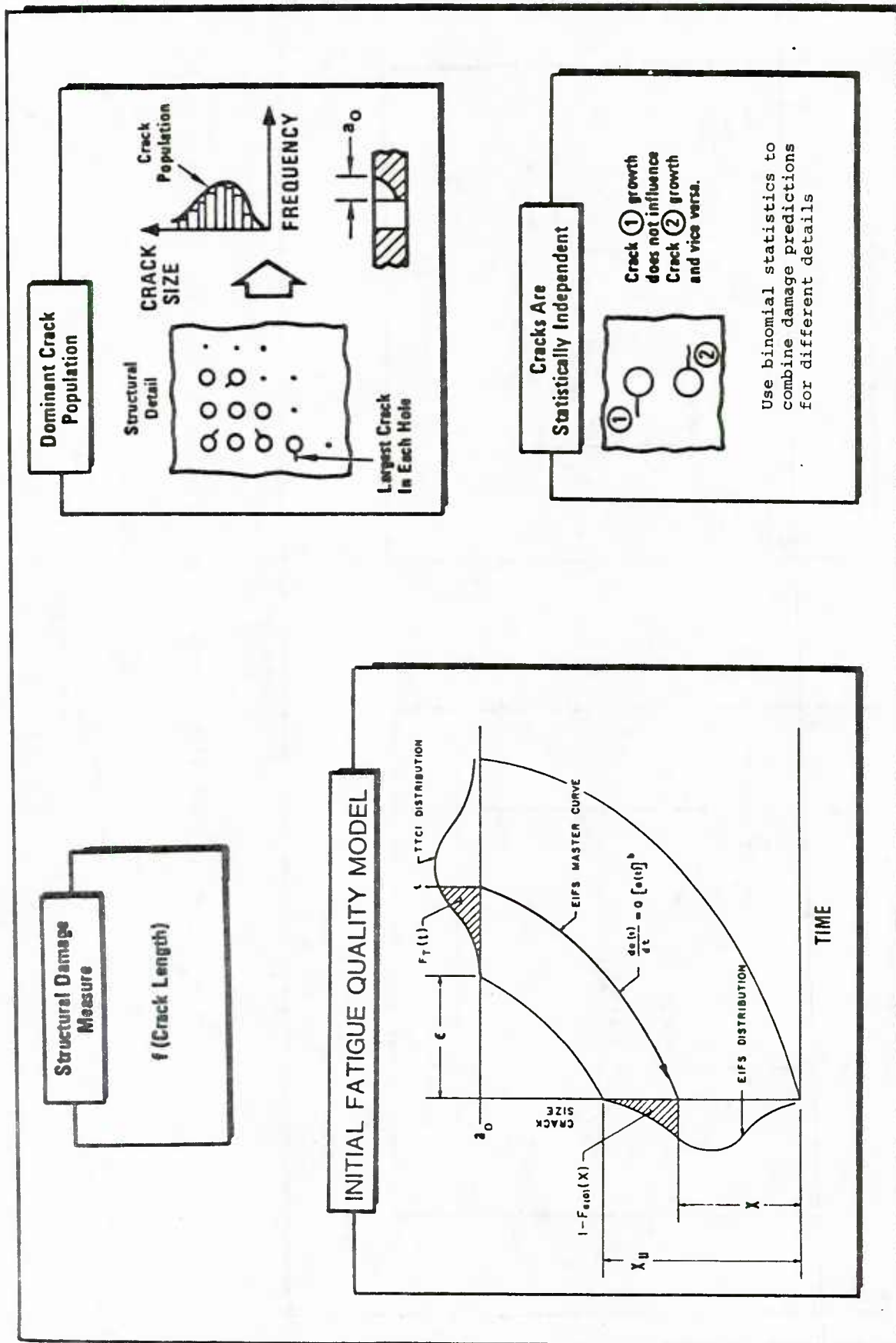


Fig. 1 Essential Elements of the Durability Analysis Methodology

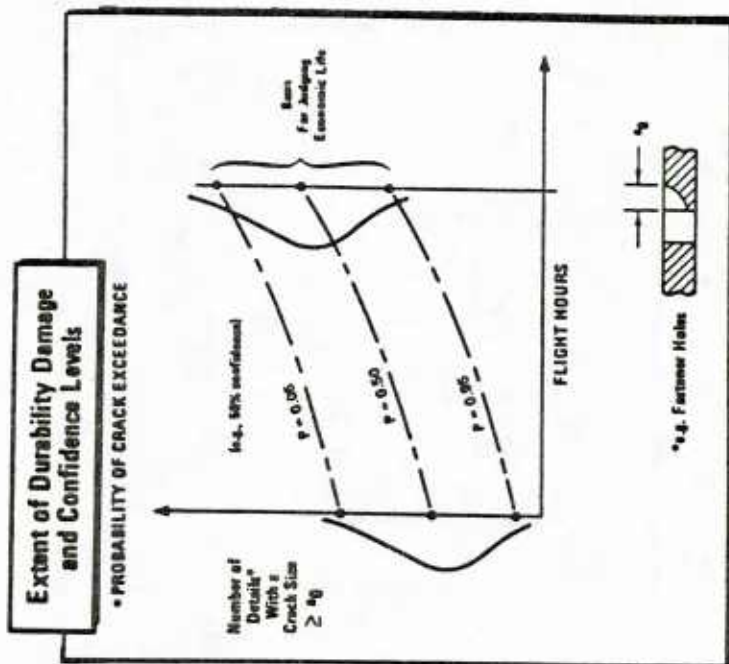
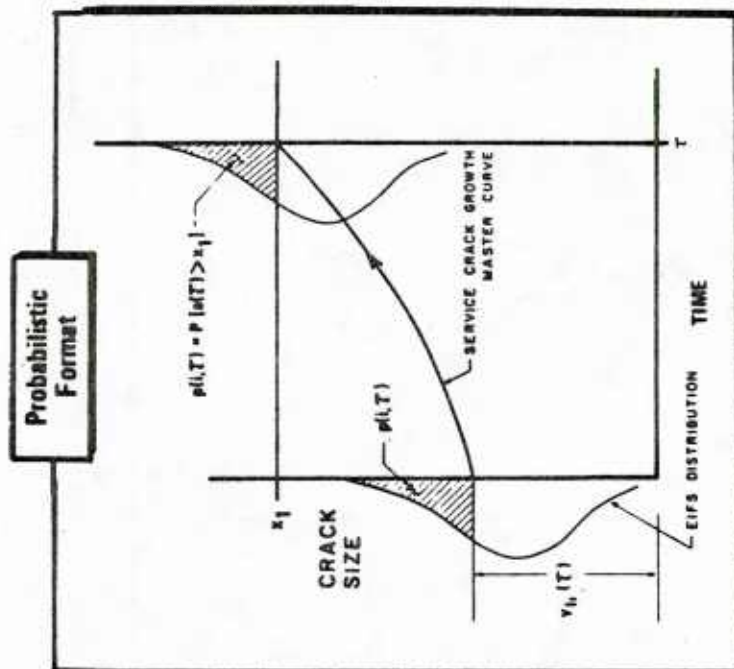


Fig. 1 Essential Elements of the Durability Analysis Methodology (Continued)

(i.e., F-16 lower wing skin) and for a complex splice subjected to a B-1 bomber spectrum.

The analytical tools and concepts developed under this program can be used to: (1) evaluate durability design trade-off options in terms of structural design variables, (2) support the full-scale durability test plan/evaluations, (3) evaluate structural maintenance requirements before or after the aircraft is committed to production or service, and (4) provide aircraft user options affecting life-cycle-costs, structural maintenance requirements and operational readiness.

A large fractographic data base was developed under this program for fatigue cracks in clearance-fit fastener holes (straight-bore and countersunk) to: (1) evaluate and demonstrate the durability analysis methodology developed (2) provide durability design data for the handbook. Fractographic results for over 800 fatigue cracks were generated. The following test parameters were considered:

- o Material (7475-T7351 Al, 2024-T851 Al, D6ac Steel)
- o Load Spectra (F-16 400-hour, F-16 500-hour, B-1 bomber)
- o % Shear Load Transfer Specimens (0%, 15%, 30%, 40%)
- o Clearance-fit Fasteners (3/16" Dia. and 1/4" Dia.)
 - Countersunk Rivet (MS 90353)
 - Countersunk Bolt (NAS 1580)
 - Protruding Head Bolt (NAS 6204)
- o Multiple Stress Levels
- o Environment (Lab Air)

A tear-down inspection of the F-16 lower wing skins from the durability test article was performed. Over 1600 fastener holes per wing skin were inspected for cracks. Results are summarized in this report and details are given in Volume VIII.

Several studies were performed to evaluate the durability analysis methodology: initial fatigue quality model calibrations, statistical crack growth, scale-up and hole interaction effects, crack growth transfer functions

for different load spectra and parameter sensitivity analyses.

Further research is required to: (1) extend the durability analysis method to larger crack sizes (e.g., $> 0.10''$), (2) demonstrate the method developed for cutouts, fillets, lugs, etc., and (3) increase confidence in the extent of damage predictions for different design conditions (e.g., materials, load spectra, stress levels, etc.). The effects and significance of factors such as fretting, faying surface sealant, environment, interference - fit fasteners, fastener clamping force, fastener diameter, coupon size, etc., on initial fatigue quality need to be investigated. A better understanding of the initial fatigue quality model parameter values, range of values and parameter sensitivities is needed for different design conditions and structural details.

SECTION I

INTRODUCTION

1.1 OBJECTIVE AND SCOPE

This report (Vol. VII) documents and summarizes the Phase II effort. The objectives and scope of this report are:

1. Evaluate, refine and demonstrate the durability analysis methodology developed under Phase I [1-5] for full-scale fighter structure (F-16 lower wing skin) and for a complex splice subjected to a B-1 bomber spectrum.

2. Summarize the essential elements of the refined durability analysis method and describe/illustrate implementation procedures,

3. Discuss important aspects of durability analysis.

4. Describe the Phase II experimental program, fractographic data, and evaluate results. Raw test/fractography data are reported in Volume VIII.

5. Document various durability-related studies that were performed to develop a better understanding of the durability analysis method/procedures. Key issues, guidelines, limitations, overall conclusions and future research needs are discussed.

The Phase II effort is documented in nine quarterly program progress reports [11-19] and two other volumes as follows:

- Volume VIII - Test and Fractography Data [6]
- Volume IX - Documentation of Durability Analysis Computer Program [7]

Volume VI, "Documentation of Computer Programs For Initial Quality Representation (Vol. IV) [20], was also prepared under Phase II to document the computer programs developed under Phase I for Volume IV.

A Durability Design Handbook [21] was prepared under Phase III. This handbook has a similar format to the USAF's Damage Tolerance Handbook [22]. It summarizes the Air Force's durability design requirements [8-10] and includes

durability analysis methodology, design data and guidelines for satisfying these requirements.

The final understandings for this program, documented in the Durability Design Handbook [21], are based on the Phase I and Phase II effort. Many studies were performed during Phase II to further the understanding of aircraft structural durability, durability analysis and related issues (e.g., initial fatigue quality, generic EIFS, IFQ model calibration procedures, etc.). Phase II was definitely a "learning process." Therefore, some of the studies and understandings from the Phase II effort are documented in this Volume for information purposes only. In any case, the Durability Design Handbook [21] is the governing document for durability analysis applications.

1.2 Organization

This report is organized into seven sections and three appendices. In general, the Phase II effort is summarized and discussed in the main text; further details are documented in applicable appendices, Volumes VIII and IX, quarterly reports and technical papers.

Durability background information is presented in Section II: the durability problem, essential Air Force durability design requirements, economic life, extent of damage, and durability analysis objectives.

Essential elements of the durability analysis method developed under Phase I and applicable refinements made under Phase II are summarized and discussed in Section III.

Durability analysis details are discussed in Section IV, including related durability studies. Procedures and guidelines are also described for implementing the durability analysis method described in Section III. Initial fatigue quality model studies and the demonstration of the durability analysis method for: (1) an F-16 lower wing skin and (2) complex splice specimens (B-1 bomber spectrum) are discussed.

The durability test program is described in Section V; test/fractographic results are evaluated and discussed in Section VI. Raw test/fractographic data are documented in Volume VIII [6].

The overall program conclusions and recommendations for further research are discussed in Section VII. This is followed by three appendix sections which support the detailed documentation of various durability aspects.

SECTION II

BACKGROUND

2.1 INTRODUCTION

The purpose of this section is to: (1) describe the aircraft durability problem and implications, (2) describe the essential elements of the Air Force durability design requirements, (3) discuss durability analysis objectives, and (4) discuss the meaning of economic life.

2.2 AIRCRAFT STRUCTURAL DURABILITY PROBLEM

Aircraft structures have thousands of structural details susceptible to fatigue cracking: fastener holes, fillets, cutouts, etc. For example, the wing box assembly shown in Fig. 2 has over 3000 fastener holes in the wing skins alone. Aircraft structural damage surveys conducted under this program showed that fatigue cracks are likely to occur in fastener holes under aircraft service conditions [3]. Similar conclusions have also been reported elsewhere [23-27].

Durability is a measure of the structure's resistance to fatigue cracking. The entire population of structural details in various components is susceptible to cracking in service. Therefore, to assess the durability of the structure or extent of damage (i.e., number or percentage of structural details in a part, a structure, a component or airframe exceeding specified crack size limits that cannot be economically repaired) as a function of time, the entire population of structural details must be accounted for. Thus, a statistical approach is essential to quantify the extent of damage as a function of time.

Structural durability is generally concerned with relatively small subcritical crack sizes which affect functional impairment, structural maintenance requirements and life-cycle-costs. Such cracks may not pose an immediate safety problem. However, if the structural details containing such cracks are not repaired, economical repairs cannot be made when these cracks exceed a limiting crack size. For example, a 0.030"-0.050" radial crack in a fastener hole can be cleaned up by reaming the hole to the next fastener size. The economical repair limit is the maximum crack size in a detail that can be cleaned-up

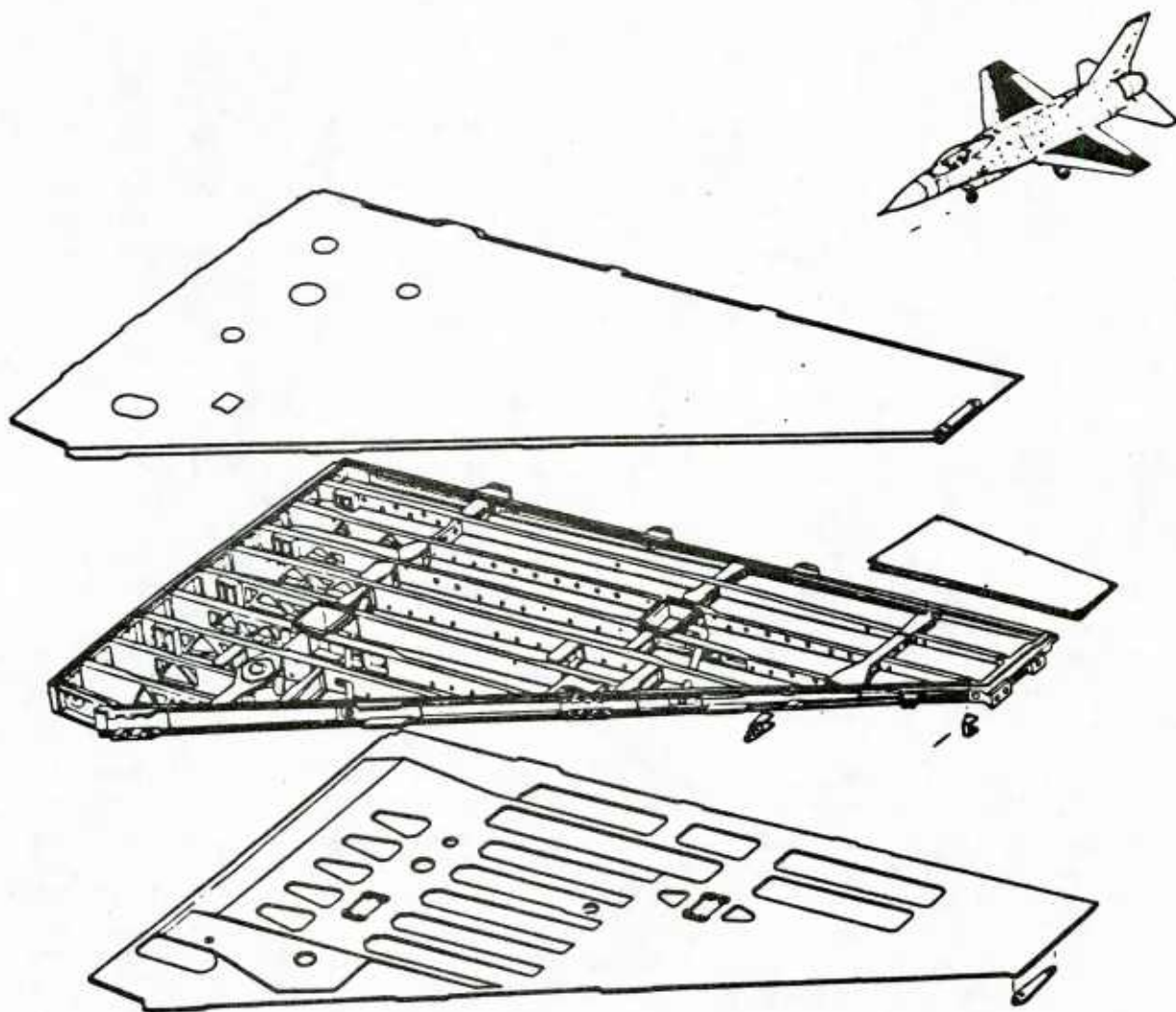


Fig. 2 Wing Box Assembly

without further repair or part replacement. If structural details are not repaired or parts replaced at an opportune time, expensive repairs or part replacement may be required. Also, unrepaired cracks may reach sizes which could affect structural safety during the design life of the aircraft.

Aircraft structural safety is ensured by satisfying damage tolerance requirements. Damage tolerance is typically concerned with the rogue flaw size in a single detail. For example, in Fig. 2 the damage tolerance analysis of the wing box is limited by a few critical structural details. On the other hand, the durability of the wing box is concerned with the entire population of structural details and the size of the largest subcritical crack in each detail.

The conventional fatigue analysis (CFA) approach (e.g., Palmgren-Miner rule, Ref. 28,29) and the deterministic crack growth approach (DCGA) [22] don't have the proper format for quantifying the "extent of damage" as a function of service time. The CFA, in its commonly used form, does not quantify crack sizes for a population of details - an essential requirement for any durability analysis method. A DCGA can be used to predict the growth of a single crack in a detail as a function of time. Using the DCGA, details can be grouped and the "worst-case" detail in the group can be used to analytically assure the largest crack size in the group of details will be = a specified size. However, the DCGA does not yield a quantitative description of the probable crack sizes or ranges of crack sizes for the population of details. CFA and the DCGA have been evaluated for potential durability analysis applications [2,30].

2.3 AIR FORCE DURABILITY DESIGN REQUIREMENTS

Air Force durability design requirements for metallic airframes are presented in three documents [8-10]. According to these requirements, the airframe must be designed to have an economic life greater than the design service life. Furthermore, the economic life must be verified by analysis and test. The analytical verification of economic life must account for the effects of initial quality variations, material property variations and the design loads/environments.

Durability analysis tools have been developed under this program for analytically quantifying the extent of damage, due to fatigue cracking, as a function of time. These tools can be used to judge the economic life of aircraft structure

for groups of details, parts, components, or an entire airframe.

2.4 ECONOMIC LIFE

The economic life of an aircraft structure is currently defined in qualitative terms: "...the occurrence of widespread damage which is uneconomical to repair and, if not repaired, could cause functional problems affecting operational readiness" [8-10]. Acceptable limits for "widespread damage" and "uneconomical repair" must be defined for each aircraft design and such limits must be approved by the Air Force.

A quantitative definition of economic life has not evolved from this program. However, guidelines have been developed for specifying economic life criterion. Various aspects of economic life and recommended formats for economic life criterion are discussed in the Durability Design Handbook [21]. In any case, the economic life of an airframe depends on the user's acceptable limits for extent of structural damage, structural maintenance requirements and costs and operational readiness.

2.5 EXTENT OF DAMAGE

The extent of damage is a quantitative measure of the number of structural details exceeding specified crack size limits as a function of service time. Structural maintenance requirements and costs depend on the number of structural details requiring repair. The "durability" of the structure depends on the extent of damage for the population of structural details in a part, component, or airframe.

The extent of damage can be predicted using the analytical tools described in this report and the handbook [21]. Extent of damage predictions provide the basis for analytically ensuring design compliance with the governing economic life criterion.

2.6 DURABILITY ANALYSIS OBJECTIVES

The basic objective of the durability analysis tools developed under this program is to analytically assure design compliance with Air Force durability design requirements [8-10] during the design stage before the

aircraft structure is committed to durability testing, production or service. Other objectives are:

1. Evaluate durability design tradeoffs for different materials, stress levels, design spectra, manufacturing variables, etc., which affect Air Force life-cycle-costs and operational readiness.

2. Support the durability verification plan and evaluation of results for full-scale aircraft structures.

3. Develop structural maintenance policy before the aircraft is committed to service.

SECTION III

DURABILITY ANALYSIS METHOD

3.1 INTRODUCTION

Essential elements and equations of the durability analysis method, including Phase II refinements, are presented in this section. Implementation procedures are described and discussed in Section IV and in the handbook [21]. Further details are given elsewhere [1,2,5, 11-19,30-36]. Recommended durability analysis procedures and guidelines are presented in the Durability Design Handbook [21]. Reference 21 is the governing document for durability analysis applications.

3.2 GENERAL DESCRIPTION

The basic objective of the durability analysis methodology is to quantify the distribution of crack sizes as a function of service time for all structural details (e.g., fastener holes, cutouts, fillets, lugs, etc.) experiencing a common load history, environment, etc. The extent of damage is measured by the number of details expected to have a crack size greater than any specified size at a given service time or equivalently by the probability of crack exceedance. Using the binomial distribution, the extent of damage for different details, parts, components, or an entire airframe can be predicted. Upper and lower bound predictions for the "extent of damage" can be estimated using statistical analysis principles. The extent of damage prediction provides a basis for analytically assuring design compliance with the selected criterion for economic life.

The durability analysis includes two essential steps: (1) quantify the initial fatigue quality (IFQ) distribution for the structural details to be included in the extent of damage assessment (Fig. 3), and (2) predict the probability of crack exceedance using the IFQ distribution and the applicable design conditions (e.g., load spectrum, stress level, percent load transfer, etc.) (Fig. 4).

3.3 ASSUMPTIONS

The durability analysis method is based on the following explicit or implied assumptions:

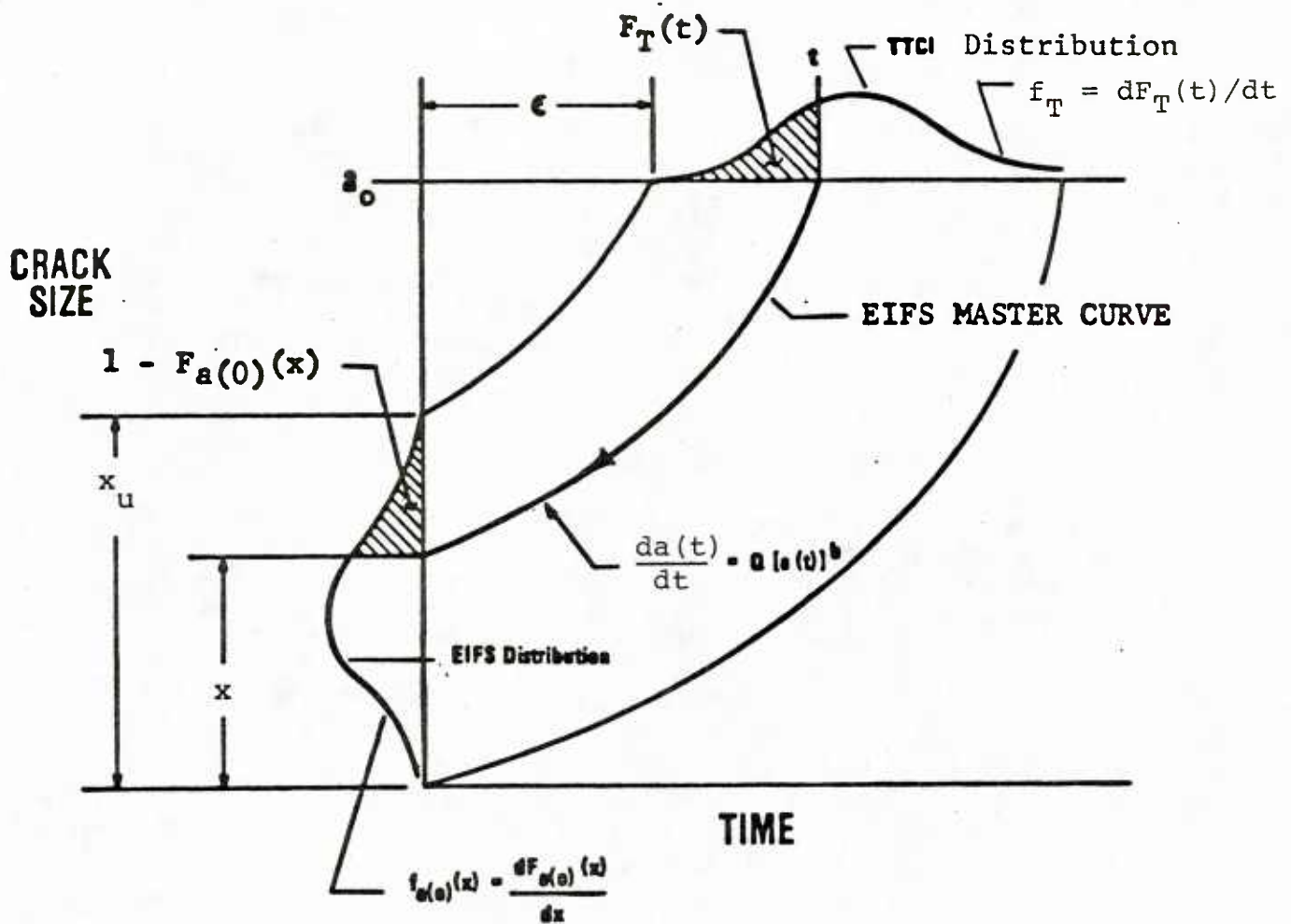


Fig. 3 Initial Fatigue Quality Model

Note: EIFSs must be grown forward the same way the fractographic results were grown backward to determine the EIFSs.

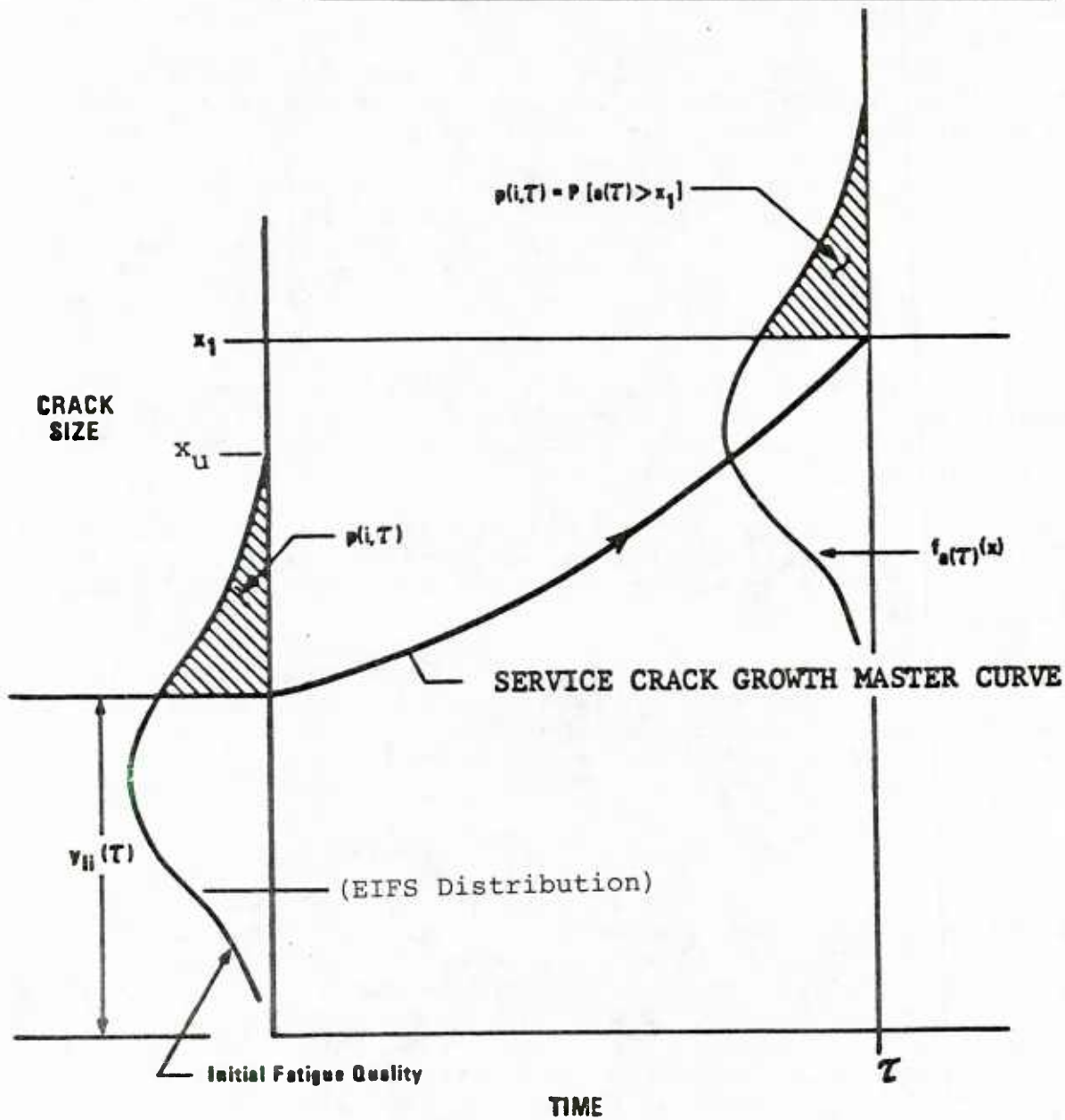


Fig. 4 Growth of EIFS Distribution as Function of Time

1. Crack length is the fundamental measure of durability damage.

2. Each detail in the population of details in an aircraft structure has a single dominant crack size; such cracks are considered to be random variables.

3. The largest crack in each detail is relatively small (e.g., ≤ 0.05 " corner crack in a fastener hole) and such cracks are statistically independent. Hence, the growth of the largest crack in one detail does not significantly affect the growth of the largest crack in neighboring details and vice versa.

4. The initial fatigue quality (IFQ) of the structural details to be included in the durability analysis can be represented by an equivalent initial flaw size (EIFS) distribution.

5. The population of dominant crack sizes for a group of structural details with a common stress history can be grown from one time to another using a single deterministic crack growth curve.

6. Once the IFQ distribution has been defined, a suitable analytical crack growth program can be used to predict the extent of damage as a function of time using applicable design variables [e.g., 37-40].

3.4 INITIAL FATIGUE QUALITY

Initial fatigue quality (IFQ) defines the initial manufactured state of a structural detail or details with respect to initial flaws in a part, component or airframe prior to service. The objective of the durability analysis is to quantify the distribution of crack sizes for structural details (e.g., fastener holes) as a function of time. An IFQ distribution provides a quantitative description of the initial flaws in the structure -- an essential starting point for all durability analyses.

The initial fatigue quality for a group of replicate details is represented by an equivalent initial flaw size (EIFS) distribution. An equivalent initial flaw is a hypothetical crack assumed to exist in a detail prior to service. An arbitrary crack size, a_0 , is selected which can be readily detected or which can be reliably observed fractographically following testing. The time required for an initial defect, of whatever type, to become a fatigue crack of size a_0 is termed the time-to-crack-initiation (TTCI). Test results of TTCI and crack growth rates using coupon specimens are employed to define the EIFS distribution. A conceptual description of the initial fatigue quality model is shown in Fig. 3. Once the EIFS

distribution (or population) has been defined for a group of details, a deterministic crack growth analysis is used to grow the entire EIFS population to any service time τ ; thus determining the time-varying crack size distribution in service (Fig. 4).

3.5 INITIAL FATIGUE QUALITY MODEL

An IFQ model was developed in Phase I for quantifying the EIFS distribution for structural details, such as fastener holes [5,32]. This model was evaluated and refined during Phase II. IFQ model refinements and EIFS distributions for two model variations will now be described and discussed. The two EIFS distributions are both based on the three-parameter Weibull distribution and variations of the same crack growth rate equation. The IFQ model, conceptually described in Fig. 3, is a "mathematical tool" for quantifying the EIFS distribution for structural details.

The time-to-crack-initiation (TTCI) distribution for coupon specimens is represented by the three-parameter Weibull distribution, $F_T(t)$.

$$F_T(t) = P[T \leq t] = 1 - \exp \left[- \left(\frac{t - \epsilon}{\beta} \right)^\alpha \right]; t \geq \epsilon \quad (1)$$

where $T = \text{TTCI}$, $\alpha = \text{shape parameter}$, $\beta = \text{scale parameter}$ and $\epsilon = \text{lower bound TTCI}$. The three Weibull parameters are determined from fractography for coupon specimens or other suitable test results.

The crack growth rate in the small crack region is assumed to be of the following form

$$\frac{da(t)}{dt} = Q[a(t)]^b \quad (2)$$

where Q and b are parameters depending on loading spectra, structural and material properties, etc.; $a(t)$ is the crack size at t . Other crack growth laws could also be used. Eq. 2 is used because of its simplicity and general ability to fit crack growth data.

The objective of the IFQ model is to define an EIFS distribution which is statistically compatible with the TTCI distribution. A crack growth law, such as Eq. 2, is used to obtain the EIFS distribution through a transformation of the TTCI distribution. Two different EIFS distributions are obtained using Eq. 2 for $b \neq 1$ (case I) and $b = 1$ (case

II). The resulting EIFS equations for case I and case II are described below.

Case I (b ≠ 1)

Integrating Eq. 2 from $t = 0$ to $t = T$, the relation between the initial crack size, $a(0)$, and the reference crack size $a_0 = a(T)$ for TTCI (flight hours) is obtained as follows:

$$\text{EIFS} = a(0) = (a_0^{-c} + cQT)^{-1/c} \quad (3)$$

where $c = b - 1$.

The distribution of $a(0)$ can be obtained from that of T given by Eq. 1 through a transformation of Eq. 3 as follows,

$$1 - F_{a(0)}(x) = F_T(t)$$

$$F_{a(0)}(x) = \exp \left\{ - \left[\frac{x^{-c} - a_0^{-c} - cQ\epsilon}{cQ\beta} \right]^\alpha \right\}; \quad 0 < x \leq x_u \quad (4)$$

$$= 1 \quad ; \quad x \geq x_u$$

where

$$\beta = \beta_\ell(\ell)^{1/\alpha} \quad (5)$$

$$x_u = (a_0^{-c} + cQ\epsilon)^{-1/c} \quad (6)$$

In Eq. 5,

β_ℓ = Weibull scale parameter for TTCI based on the TTCI's for a given fractographic data set in which only the fractography for the largest fatigue crack in any "one" of ℓ fastener holes per test specimen is used.

ℓ = Number of equally-stressed fastener holes per test specimen in which only the largest fatigue crack in any "one" hole per specimen is included in the fractographic data set.

and,

α = Weibull shape parameters for a given TTCI data set.

Details for Eq. 5 are given in Section 4.4 and Ref.14. In Eq. 4, if $x < 0$ (i.e., negative EIFS), refer to Section 3.6 (Step 4) and subsection 4.2.3.

In Eq. 6, x_u is the upper bound EIFS in the initial fatigue quality (IFQ) distribution. The lower bound TTCI, ϵ , for a given reference crack size, a_0 , is defined from Eq. 6 as follows:

$$\epsilon = \frac{1}{cQ} \left(x_u^{-c} - a_0^{-c} \right) ; \quad a_0 \geq x_u \quad (7)$$

Eq. 4 for $F_{a(0)}(x)$ can be simplified by substituting the expression for $CQ\epsilon$ from Eq. 6 into Eq. 4 as follows:

$$F_{a(0)}(x) = \exp \left\{ - \left[\frac{x^{-c} - x_u^{-c}}{cQ\beta} \right]^\alpha \right\} ; \quad 0 < x \leq x_u \quad (8)$$

$$= 1.0 \quad ; \quad x > x_u$$

In Eq. 8, β and x_u are defined by Eqs. 5 and 6, respectively.

Case II ($b = 1$)

Integrating Eq. 2 from $t = 0$ to $t = T$ and considering $b = 1$, the following relation between the initial crack size, $a(0)$, and the reference crack size $a_0 = a(T)$ for TTCI (flight hours) is obtained:

$$\text{EIFS} = a(0) = a_0 \exp(-Q\tau) \quad (9)$$

The EIFS cumulative distribution, $F_{a(0)}(x)$, is obtained by use of Eqs. 1 and 9 as follows:

$$1 - F_{a(0)}(x) = F_T(t)$$

$$F_{a(0)}(x) = \exp \left\{ - \left[\frac{\ln(a_0/x) - Q\epsilon}{Q\beta} \right]^\alpha \right\} ; \quad 0 < x \leq x_u \quad (10)$$

$$= 1 \quad ; \quad x > x_u$$

where β is defined by Eq. 5 and x_u is the selected upper bound EIFS:

$$x_u = a_0 \exp(-Q\epsilon) \quad (11)$$

The lower bound TTCI value, ϵ , for a given reference crack size, a_0 , is defined from Eq. 11 as follows:

$$\epsilon = \frac{1}{Q} \ln (a_0/x_u) \quad ; \quad a_0 \geq x_u \quad (12)$$

Eq. 10 for $F_{a(0)}(x)$ can be simplified by combining Eqs. 10 and 12 as follows:

$$F_{a(0)}(x) = \exp \left\{ - \left[\frac{\ln (x_u/x)}{Q\beta} \right]^\alpha \right\}; \quad 0 < x \leq x_u \quad (13)$$

β and x_u in Eq. 13 are defined by Eq. 5 and 6, respectively.

3.6 GENERAL PROCEDURE

The general procedure for implementing the durability analysis methods is described and discussed below and elsewhere [1,5,21,34-36]. For final details and recommendations, refer to the Durability Design Handbook [21].

1. Divide the durability component into m stress regions where the maximum stress in each region may be reasonably assumed to be equal for every location or detail (e.g., fastener hole).

2. Use the IFQ model shown in Fig. 3 and suitable fractographic results to define the EIFS cumulative distribution, $F_{a(0)}(x)$. If Case I (i.e., $b \neq 1$) is used, use Eqs. 3-8. For Case II (i.e., $b = 1$), use Eqs. 9-13.

3. Use the applicable service crack growth master curve (SCGMC) to determine, for each stress region, the corresponding EIFS value, $y_{1i}(\tau)$, which grows to crack size x_1 at service time τ as illustrated in Fig. 4. If applicable fractographic data are available for different stress levels and fractographic data pooling procedures are used, the SCGMC can be determined from Eq. 14 as follows.

Two different SCGMC's can be obtained from Eq. 14 considering $b_i \neq 1$ and $b_i = 1$.

$$\frac{da(t)}{dt} = Q_i [a(t)]^{b_i} \quad (14)$$

For example, Eq. 14, for $b_i \neq 1$, can be integrated from $a(0) = y_{1i}(\tau)$ to $a(\tau) = x_1$ to obtain $y_{1i}(\tau)$ in Eq. 15.

$$y_{1i}(\tau) = [x_1^{-c_i} + c_i Q_i \tau]^{-1/c_i} \quad (15)$$

In Eq. 15, $c_i = b_i - 1$ and Q_i is given by Eq. 16.

$$Q_i = \xi \sigma^\gamma \quad (16)$$

Q_i in Eq. 16 is assumed to be a power function of the maximum applied stress σ , and ξ and γ are constants to be determined from available fractographic data.

Equation 14, for $b_i = 1$, can be integrated from $a(0) = y_{1i}(\tau)$ to $a(\tau) = x_1$ to obtain $y_{1i}(\tau)$ in Eq. 17.

$$y_{1i}(\tau) = x_1 \exp(-Q_i \tau) \quad (17)$$

Q_i in Eq. 17 is given by Eq. 16.

If applicable fractographic results are not available for the desired design conditions (e.g., load spectra, % bolt load transfer, stress level, etc.), an analytical crack growth program [e.g., 37] can be used to generate the SCGMC needed to determine $y_{1i}(\tau)$ for a given x_1 and τ [37]. When an analytical crack growth program is used, $y_{1i}(\tau)$ must be determined in a manner which is consistent with that used to determine the EIFS distribution from the fractographic data.

4. Compute the probability of crack exceedance for each stress region, i.e., $p(i, \tau) = P[a(\tau) > x_1] = 1 - F_{a(0)}[y_{1i}(\tau)]$. Use Eq. 18 and 19 for $b \neq 1$ and for $b = 1$, respectively.

For $b \neq 1$

$$p(i, \tau) = 1 - \exp \left\{ - \left[\frac{(y_{1i}(\tau))^{-c} - x_u^{-c}}{c Q_i \beta} \right]^\alpha \right\}; 0 < y_{1i}(\tau) \leq x_u \quad (18)$$

$$= 0 \quad ; y_{1i}(\tau) \geq x_u$$

For $b = 1$

$$\left. \begin{aligned} p(i, \tau) &= 1 - \exp \left\{ - \left[\frac{\ln (x_u / y_{1i}(\tau))}{Q\beta} \right]^\alpha \right\}; \quad 0 < y_{1i}(\tau) \leq x_u \\ p(i, \tau) &= 0 \quad ; \quad y_{1i}(\tau) > x_u \end{aligned} \right\} \quad (19)$$

In Eq. 18 and 19, β is given by Eq. 5 and x_u is given by Eqs. 6 and 11. $y_{1i}(\tau)$ in Eqs. 18 and 19 is given by Eqs. 15 and 17, respectively, or by a suitable analytical SCGMC.

A flow diagram for determining $y_{1i}(\tau)$ and $p(i, \tau)$ is shown in Fig. 5 for $y_{1i}(\tau) > 0$ and for $y_{1i}(\tau) < 0$. Equations 20 and 21 are an extension of Eqs. 15 and 18, respectively. The negative EIFS issue is discussed in subsection 4.2.3.

5. The average number of details $\bar{N}(i, \tau)$ and the standard deviation $\sigma(i, \tau)$ in the i th stress region with a crack size greater than x_1 at service time τ are determined using the binomial distribution and are expressed as follows:

$$\bar{N}(i, \tau) = N_i p(i, \tau) \quad (22)$$

$$\sigma_N(i, \tau) = \left\{ N_i p(i, \tau) [1 - p(i, \tau)] \right\}^{\frac{1}{2}} \quad (23)$$

in which N_i denotes the total number of details in the i th stress region. The average number of details with a crack size exceeding x_1 at the service time τ for m stress regions, $\bar{L}(\tau)$, and its standard deviation, $\sigma_L(\tau)$, can be computed using Eqs. 24 and 25.

$$\bar{L}(\tau) = \sum_{i=1}^m \bar{N}(i, \tau) \quad (24)$$

$$\sigma_L(\tau) = \left[\sum_{i=1}^m \sigma_N^2(i, \tau) \right]^{\frac{1}{2}} \quad (25)$$

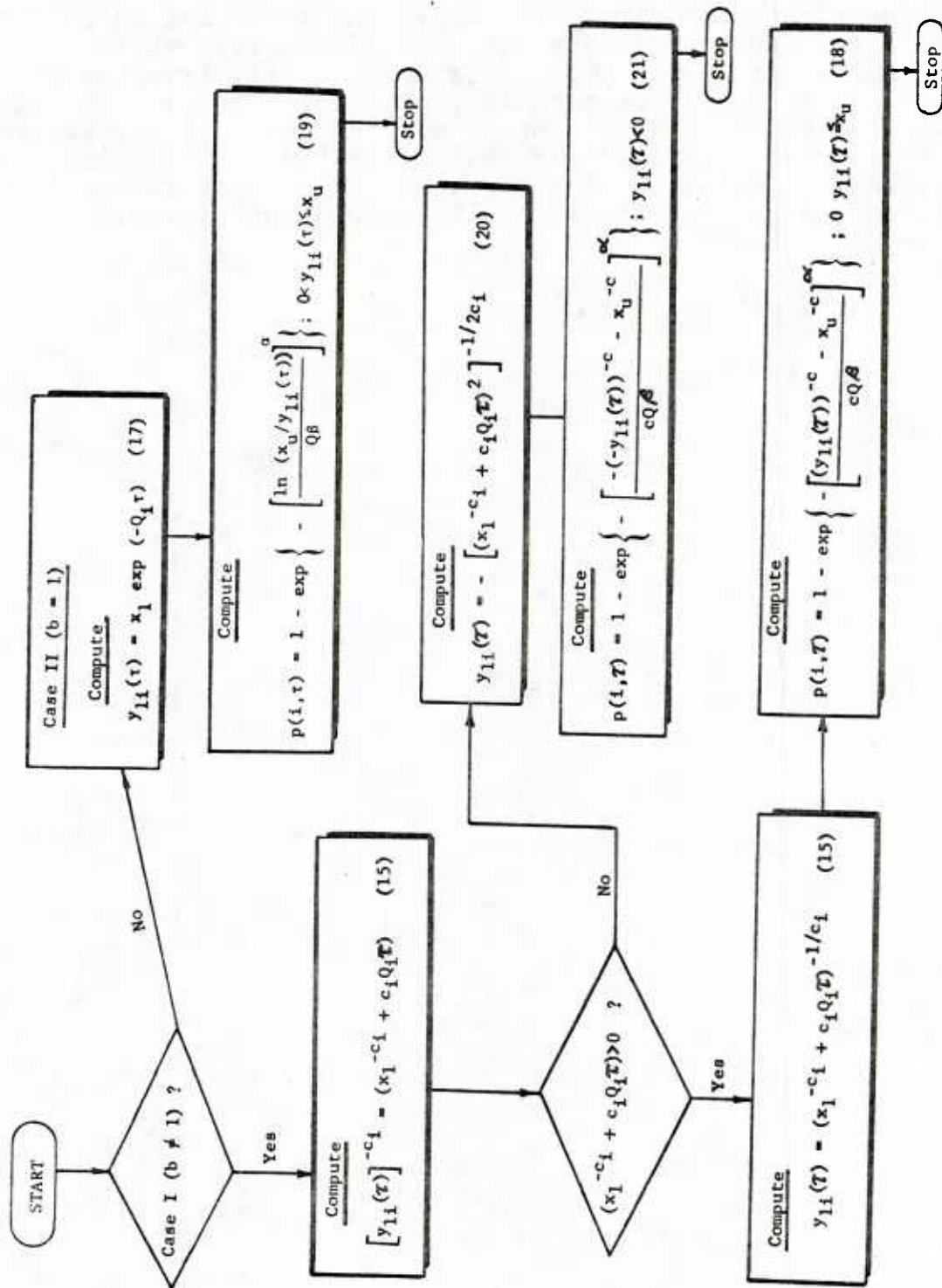


Fig. 5 Flow Diagram and Equations for Computing $y_{1i}(\tau)$ and $p(i, \tau)$

Equations 24 and 25 can be used to quantify the extent of damage for a single detail, a group of details, a part, a component, or an airframe. Upper and lower bounds for the prediction can be estimated using $L(\tau) \pm Z\sigma_L(\tau)$, where Z is the number of standard deviations, $\sigma_L(\tau)$, from the mean, $L(\tau)$. Equations 22 through 25 are valid if cracks in each detail are relatively small and the growth of the largest crack in each detail is not affected by cracks in neighboring details. Hence, the crack growth accumulation for each detail is statistically independent (Refs. 1, 5, 21, 34-36).

SECTION IV

DURABILITY ANALYSIS DETAILS

4.1 INTRODUCTION

Durability analysis concepts, procedures, and final understandings evolved from the Phase II effort. This was a "learning process." The purpose of this section is to document the evolving understandings from the Phase II effort and to support the Durability Design Handbook [21]. In any case, Ref. 21 is the governing document for durability analysis.

4.2 INITIAL FATIGUE QUALITY

Initial fatigue quality (IFQ), or EIFS distribution, is one of the most important elements of the durability analysis method developed. Four aspects of IFQ are discussed in this section: (1) crack growth power law variations, (2) generic EIFS, (3) negative EIFS and (4) details other than fastener holes. IFQ is also discussed in Section 3.4 herein and elsewhere [1,2,5,21,31,32,34-36].

4.2.1 Crack Growth Power Law Variations

Two variations of the crack growth power law, Eq. 2, were used to develop equations for the EIFS cumulative distribution, $F_{a(0)}(x)$. For example, $F_{a(0)}(x)$ based on $b \neq 1$ and $b = 1$ are discussed in this section.

Either Eq. 8 or 13 can be used to define the IFQ or EIFS cumulative distribution. However, if Eq. 8 is used and $b < 1$, negative EIFS values are theoretically possible (Ref. Fig. 5). The negative EIFS issue is discussed in subsection 4.2.3. In Eq. 8, if $b > 1$ all EIF values will be greater than zero. In Eq. 13, for $b = 1$ (Case II) all EIFS values will be positive.

Intuitively, the two-parameter form of Eq. 2 (i.e., $Q, b \neq 1$; Case I) should provide a better overall fit to the fractographic data than the one-parameter form (i.e., $Q, b = 1$; Case II). However, the one-parameter form is simpler and it worked very well for the final demonstration of the durability analysis methodology [35,36].

As long as consistent procedures are used to determine the crack growth parameters in Eq. 2 for a given fractographic data set(s), either Eq. 8 or Eq. 13 can be used to define the IFQ. If the service crack growth master curve (SCGMC) is made compatible with the applicable EIFS master curve(s), the resulting $p(i, \tau)$ predictions will be virtually the same for either variation of Eq. 2 (Ref. Subsection 4.5.3 and Table 6).

4.2.2 Generic EIFS Distribution

An EIFS distribution is "generic" if it depends only on the material and manufacturing/fabrication processes. Theoretically, the EIFS distribution should be independent of design variables, such as load spectrum, stress level, percent bolt load transfer, environment, etc.

The IFQ model parameters in Eq. 8 and 13 can be determined for fastener holes using applicable fractographic results for one or more data sets. A fractographic data set refers to the fractographic results (i.e., $a(t)$ versus t values) for replicate fatigue tests (e.g., same: material, specimen geometry, drilling procedure, load spectrum, stress level, % bolt load transfer, fastener type/fit, etc.). Since the fractography reflects specific fatigue test variables, the derived EIFS cumulative distribution, $F_{a(0)}(x)$, will not be strictly "generic". This situation is further complicated by the effects of scatter in the fatigue test results on the IFQ model parameters.

The IFQ model, described in Fig. 3, was derived for a single TTCI data set. However, the model can be applied to one or more fractographic data sets using the data pooling procedures described in the Durability Design Handbook [21]. This is a practical approach for determining a suitable EIFS distribution for durability analysis.

Suppose two sets of replicate specimens are fatigue tested using the same loading spectrum but different stress levels. Using the fractographic results for each data set, the respective TTCI's for a given a can be determined for each data set (Ref. Fig. 6). For the EIFS cumulative distribution, $F_{a(0)}(x)$, to be "generic", the TTCI distribution, $F_T(t)$, for data set 1 and 2 should transform into the same EIFS distribution as shown in Fig. 6.

Theoretically, a "generic" EIFS distribution can be obtained by forcing the IFQ model parameters, x_1 , α , b and $Q\beta$, to be constants for one or more fractographic data sets.

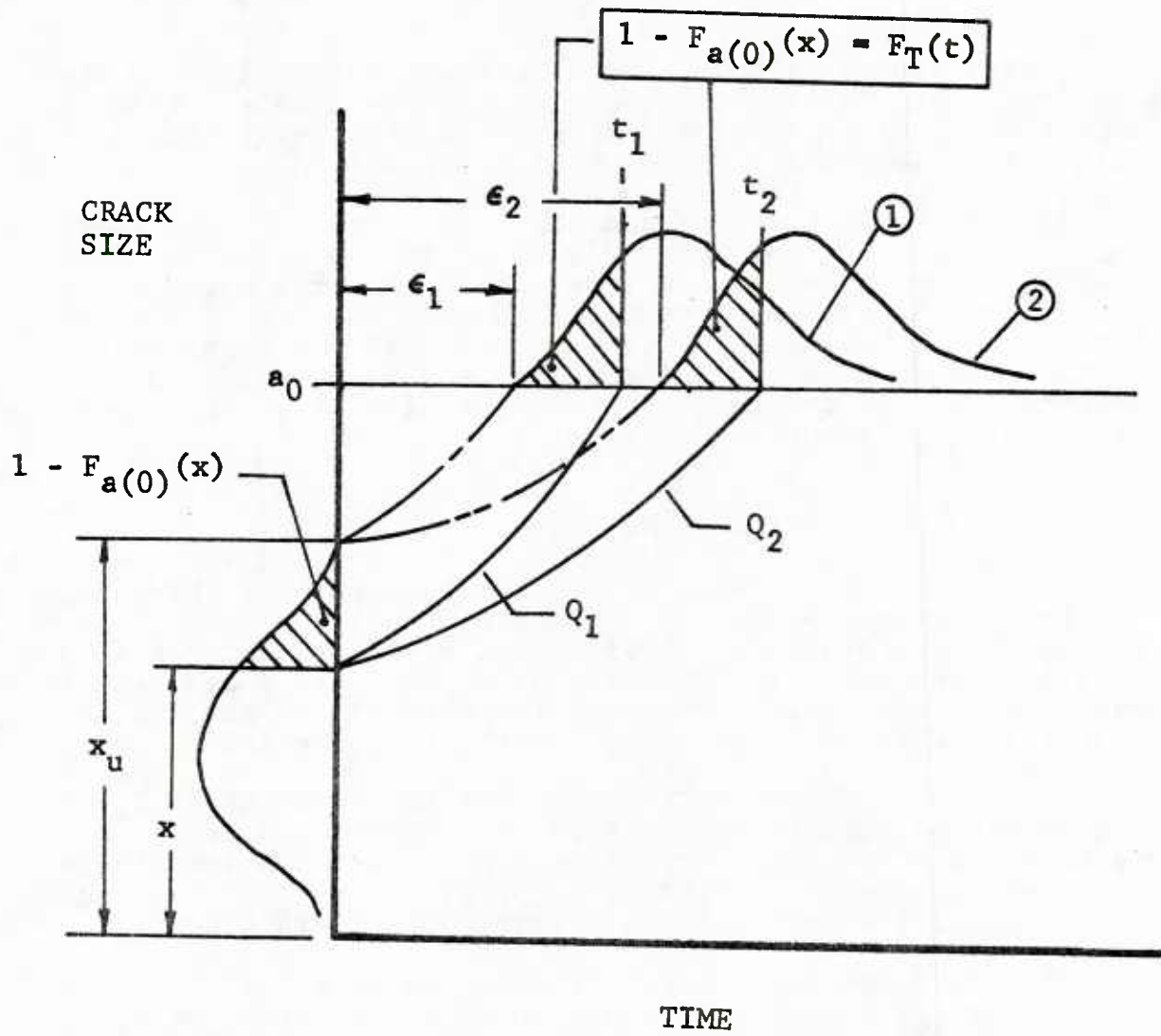


Fig. 6 Illustration of Generic EIFS Condition

Using this approach, compatible IFQ model parameters can be obtained for different fractographic data sets. This is important in order to obtain compatible EIFS values for each data set or sets and a viable EIFS distribution.

It appears that α and $Q\beta$ are material constants depending on the fastener hole drilling procedures (and quality) and type of fastener hole. Further research is needed to evaluate and compare $Q\beta$ values for different fractographic data sets [e.g., 6]. IFQ model parameter studies are documented in Appendix A and B in this volume. Recommended procedures for determining the IFQ model parameters are illustrated in Ref.21.

4.2.3 Negative EIFS

Negative EIFSs are not physically possible. However, in some cases, when fractographic results are back-extrapolated, negative EIFSs can result. The purpose of this section is to: (1) explain the conditions under which negative EIFSs can occur and (2) discuss the meaning and significance of negative EIFSs in terms of the IFQ model.

The IFQ model is a "mathematical tool" for quantifying the initial manufactured state of a structural detail in terms of an EIFS. This "tool" provides a mathematical basis for making crack exceedance predictions for design conditions different than the fractographic data base.

The EIFS master curve is obtained by curve fitting a suitable crack growth law (e.g., Eq. 2) to fractographic results. Using the same fractographic results, different EIFS master curves can be obtained for each crack growth law and curve fit criterion used. The EIFS master curve can also be numerically defined using a series of crack size-time points rather than a deterministic equation [5].

The EIFS cumulative distribution $F_a(0)(x)$ is based on a transformation of the TTCI distribution, Eq. 1, using the applicable EIFS master curve. A different $F_a(0)(x)$ equation is obtained for each EIFS master curve used. Significantly, each $F_a(0)(x)$ equation will be statistically compatible with the TTCI distribution: i.e., $F_a(0)(x) = 1 - F_T(t)$. Whatever $F_a(0)(x)$ equation is used, the resulting "service crack growth master curve" used should be compatible with the EIFS master curve for making $p(i, \tau)$ predictions (Ref. Sections 4.5.2 and 4.5.3).

Negative EIFSs will now be explained two ways using: (1) an untruncated EIFS distribution and (2) a truncated EIFS distribution. The following discussion provides additional insight into the features and flexibility of the IFQ model for durability analyses.

4.2.3.1 Untruncated EIFS Distribution

Suppose an EIFS distribution with both positive and negative EIFSs is obtained as illustrated in Fig. 7. Assume the resulting $F_{a(0)}(x)$ distribution was determined following the transformation procedure described for the IFQ model.

Since negative flaws are not physically possible, how can the IFQ model be justified for both positive and negative EIFSs? The main purpose of the IFQ model is to quantify an EIFS distribution that will track the observable distribution of crack sizes when grown outward. The fact that a portion of the EIFS population is negative may create an emotional problem (i.e., negative flaws are not physically possible). However, either positive or negative EIFSs can be handled mathematically by the IFQ model.

In Fig. 7, a positive, zero, and negative EIFS are shown. Using the applicable EIFS master curve, there is a corresponding TTCI for each EIFS value. Note that "negative EIFSs" will eventually grow to a crack size a_0 . Keep in mind that the IFQ model is simply a "mathematical tool" for making crack exceedance predictions.

The positive EIFSs support the fracture mechanics theory that initial flaws exist in a structural detail and such flaws grow according to fracture mechanics theories. On the other hand, the negative EIFSs suggest that a portion of the EIFS population may behave like an "initiation process" where no initial flaws are considered present. In any case, the IFQ model developed can be used to predict crack exceedance, $p(i, \tau)$, as a function of service time whether-or-not the EIFS distribution includes negative EIFSs (Ref. Subsection 4.5.3).

The upper tail portion of the EIFS distribution is of most interest for $p(i, \tau)$ predictions because the extent of damage is governed by the larger initial flaw sizes. Since the negative EIFSs will be in the lower tail portion of the $F_{a(0)}(x)$ distribution, in most cases negative EIFSs would not have to be considered anyway.

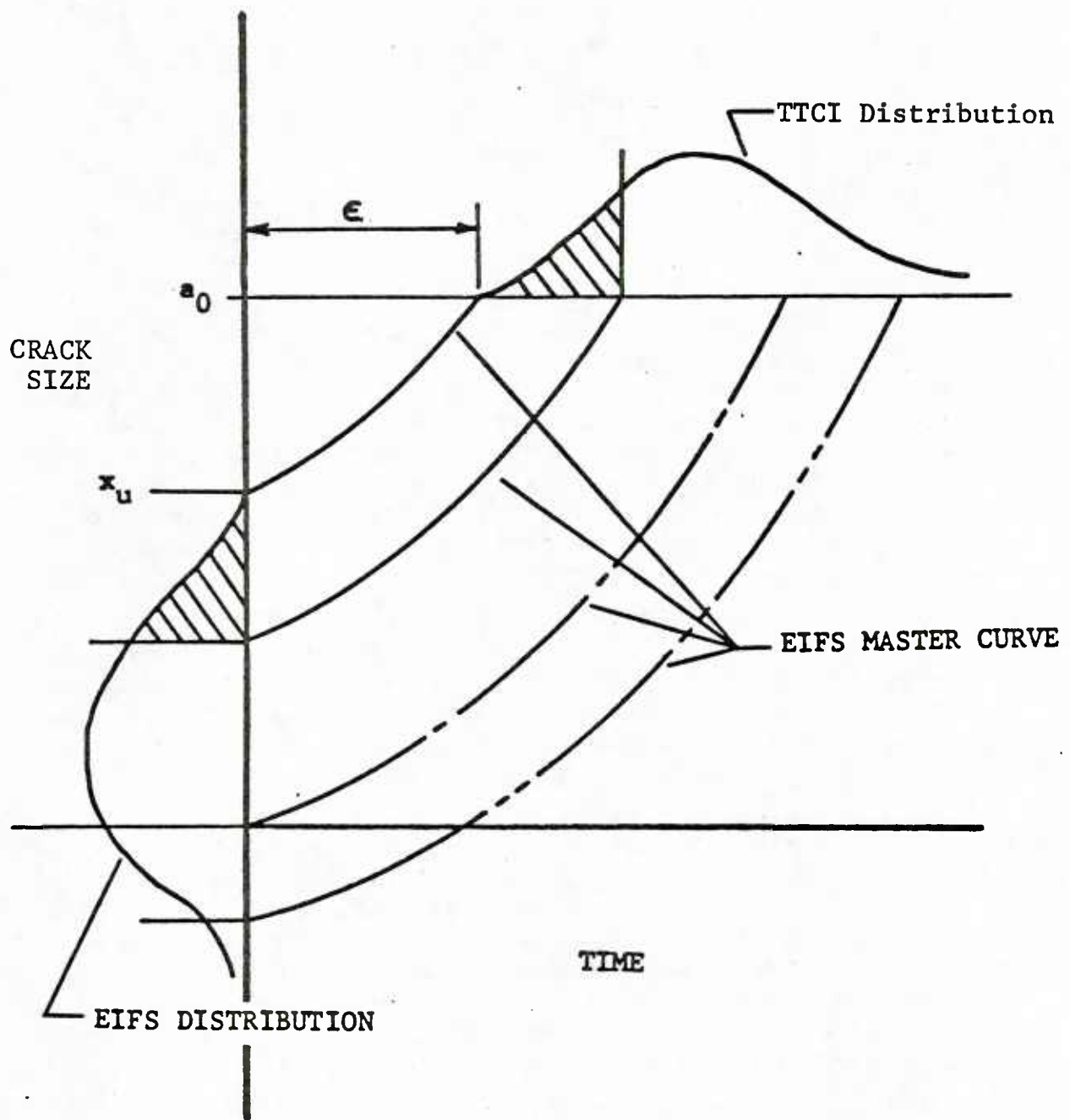


Fig. 7 IFQ Distribution With Both Positive and Negative EIFSs

4.2.3.2 Truncated EIFS Distribution

The concept of a truncated EIFS distribution is used to explain cases where a portion of the EIFS population may be negative. For example, in Fig. 8 the EIFS population includes both positive and negative values. The cross-hatched area, A_1 , under the TTCI distribution (Fig. 8) denotes the portion of the TTCI population with $TTCIs \geq \tau_1$, or the probability that $T > \tau_1$. Note that $TTCIs > \tau_1$ result in $EIFSs < 0$. The EIFS distribution is statistically compatible with the TTCI distribution. Therefore, the area A_1 under the EIFS probability density function, $f_{a(0)}(x) = dF_{a(0)}(x)/dx$, is also equal to the corresponding area A_1 under the TTCI distribution (Fig. 8).

Assume that $EIFSs < 0$ are inadmissible in Fig. 8. The area A_1 under the EIFS probability density function can be replaced by a bar of finite width with area A_1 . The "bar", located at $EIFS = 0$, can be acknowledged mathematically using the dirac δ function.

The EIFS distribution shown in Fig. 8 is called a "truncated EIFS distribution" because the $EIFS's < 0$ are treated as inadmissible quantities. The truncated EIFS distribution can also be used to represent the IFQ of replicate structural details.

In Fig. 8, notice that the distribution of crack sizes is truncated until τ_1 is reached. Also note that the bar representing the population of $EIFSs < 0$ decreases in area. For example, the bar area is A_1 at $t = 0$, A_2 at $t = \tau_1$, and zero at $t = \tau_2$. The percentile corresponding to τ_1 can be arbitrarily selected by making A_1 a selected finite quantity (e.g., 0.001).

The EIFS cumulative distribution, $F_{a(0)}(x)$, for a truncated EIFS distribution is shown in Fig. 9. Note that $F_{a(0)}(x)$ starts at " A_1 " instead of 0 when a truncated EIFS distribution is used.

EIFS and TTCI rankings are noted in Fig. 10 for a truncated EIFS distribution. Note that the truncated EIFS distribution is interpreted in the same manner as an untruncated EIFS distribution. Therefore, the derived equations for the IFQ model apply to the truncated EIFS distribution.

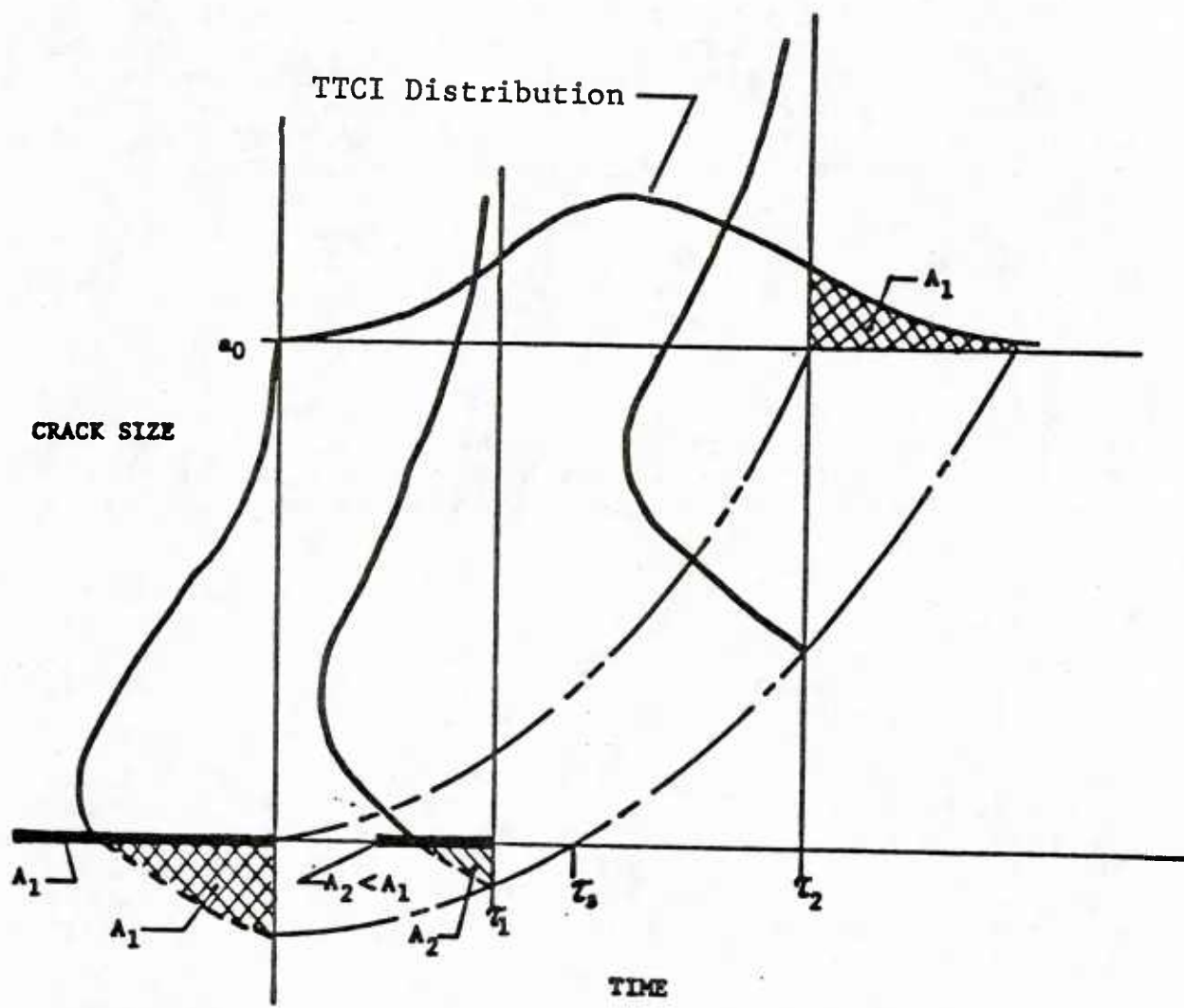


Fig. 8 Truncated IFQ Distribution

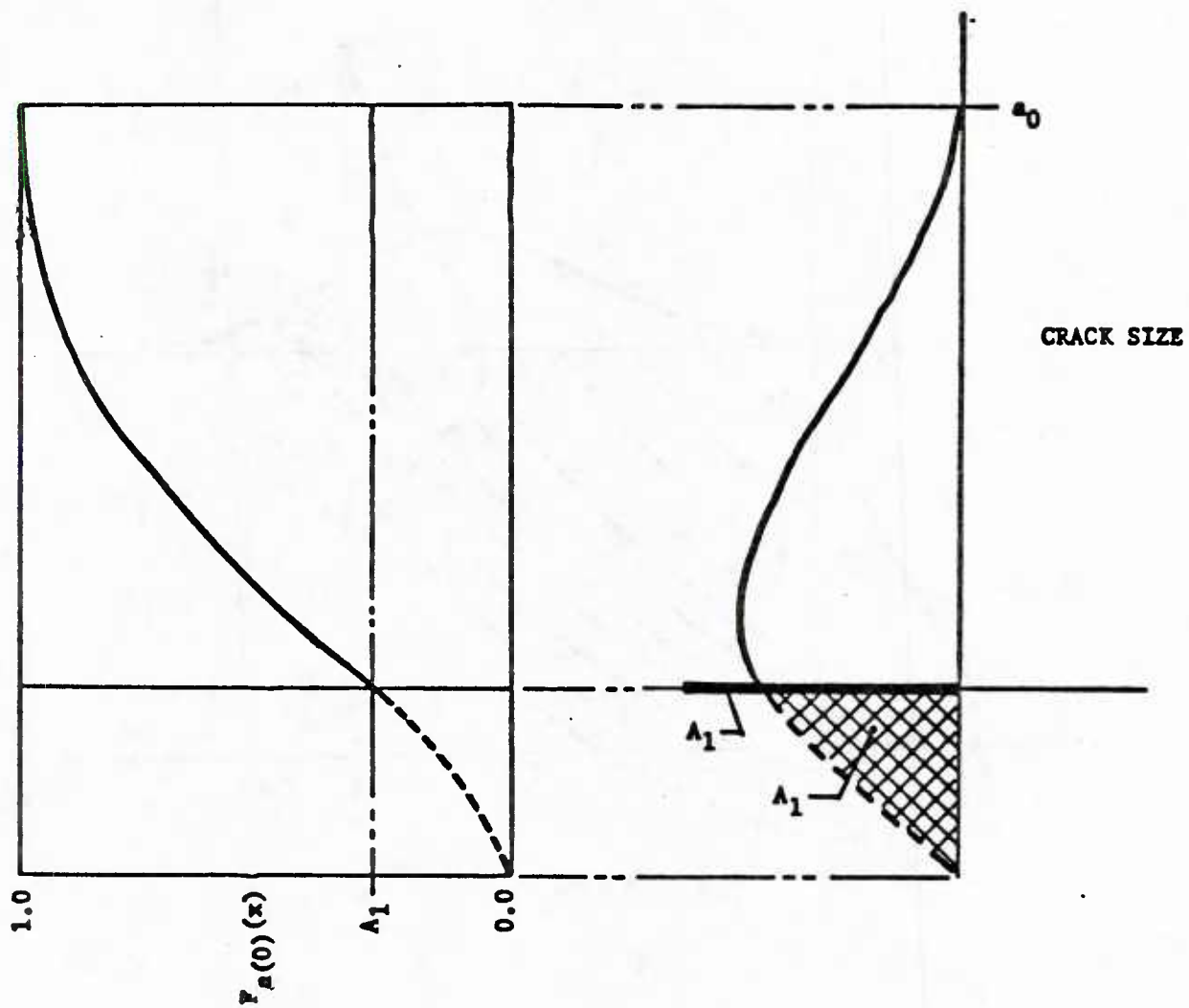


Fig. 9 Truncated EIFS Cumulative Distribution

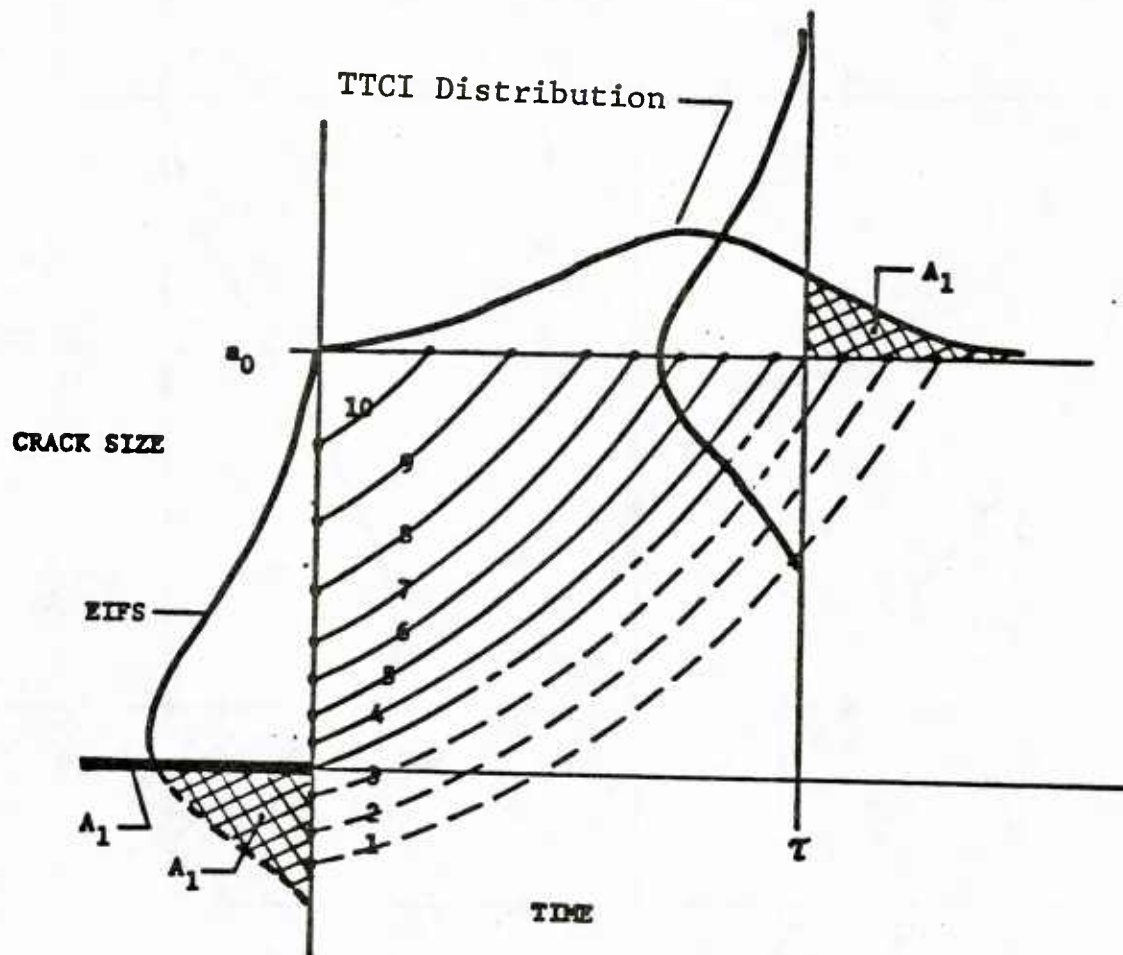


Fig. 10 Ranked EIFS Crack Growth for Truncated Distribution

4.2.4 Details Other Than Fastener Holes

The durability analysis method described in Section III theoretically applies to different types of structural details susceptible to fatigue cracking (e.g., fastener holes, lugs, cutouts, fillets, etc.). Although the method has been demonstrated for clearance-fit fastener holes, further research is required to verify the method for other detail types and for different combinations of details.

Theoretically, the IFQ for a given detail type can be quantified using applicable fractographic results for the desired detail. Suitable specimens need to be designed for acquiring fatigue cracking data for lugs, fillets, cutouts, etc. Crack initiation data should be generated for different detail types for different: materials, stress levels, load spectra, manufacturing techniques, etc. These data should be used to verify and refine, if required, the durability analysis method for those details which may have a significant effect on the structural maintenance requirements and economic life.

4.3 DETERMINATION OF IFQ MODEL PARAMETERS

An IFQ model was developed to determine the key input for the durability analysis method developed - the EIFS cumulative distribution, $F_a(0)(x)$. Because of the importance of $F_a(0)(x)$, the IFQ model was evaluated extensively, using available fractographic results for fastener holes, over the course of the program. There are many ways that the IFQ model parameters can be determined and several numerical procedures and variations thereof were investigated [e.g., 1,5,6,11-19 and 31-26].

The recommended procedures and guidelines for calibrating the IFQ model parameters, documented in the Durability Design Handbook [21], evolved from the total effort of this program. The Phase II evaluation of the IFQ model was definitely a "learning process". The purpose of this section is to document, for reference purposes, the IFQ model calibration procedures used for two Phase II studies (Ref. Appendices A & B), to discuss fractographic data pooling concepts and to support Ref. 21. In any case, Ref. 21 is the governing document for durability analysis.

4.3.1 Fractographic Data Pooling

The IFQ for fastener holes can be quantified using the IFQ model of Section III and suitable fractographic results.

IFQ model parameters must be consistently quantified to make the parameters directly comparable for different fractographic data sets. This is very important.

A "fractographic data set" refers to the set of fractographic data obtained for replicate test specimens (e.g., same material, same geometry, etc.), and fatigue test conditions (e.g., same stress level, same spectrum, etc.). Fractographic data pooling techniques have been developed and evaluated for quantifying the IFQ model parameters on a common baseline (Ref. Section 4.8.1 and Appendices A and B).

Pooling the fractographic results for different data sets is a practical approach for calibrating the IFQ model parameters. Pooling the fractographic results effectively increases the sample size. This not only increases confidence in the IFQ model parameter values but it also ensures that the resulting values will be "representative" of the overall fractographic data base used. Furthermore, since the IFQ model parameters are on the same baseline, parameter values for different fractographic data sets can be directly compared and the effects of different variables on the parameter values can be more readily evaluated. Finally, fractographic data pooling is essential to justify using the resulting IFQ distribution for different stress levels, load spectra, etc., than reflected in the fractographic data base.

4.3.2 EIFS Master Curve Parameters (Q_i^* and b_i^*)

EIFS master curves, based on two variations of Eq. 2, are given by Eqs. 3 and 9 for a single TTCI data set. To distinguish the crack growth parameters Q and b in Eq. 2 for each fractographic data set, Eq. 26 is used.

$$\frac{da(t)}{dt} = Q_i^* [a(t)]^{b_i^*} \quad (26)$$

In Eq. 26, Q_i^* and b_i^* are crack growth constants for the i th fractographic data set. To make the Q_i^* and b_i^* parameters "compatible" for different fractographic data sets, $b_i^* = b_j^* = \dots = b_n^* = \text{constant}$ must be imposed. If Eq. 26 is used for a single fatigue crack, use $Q_{i,j}^*$ and $b_{i,j}^*$ to distinguish values for the i th fractographic data set and j th fatigue crack from the i th data set.

Using the notations of Eq. 26, the EIFS master curve for $b_i^* > 1$ and $b_i^* = 1$ is given by Eqs. 27 and 28, respectively.

$$\text{EIFS} = a(0) = (a_0^{-c_i^*} + c_i^* Q_i^{*T})^{-1/c_i^*} \quad (27)$$

$$\text{EIFS} = a(0) = a_0 \exp(-Q_i^{*T}) \quad (28)$$

In Eq. 27, $c_i^* = b_i^* - 1$.

The procedures described in this section are illustrated in Appendices A and B for different fractographic data sets.

4.3.2.1 Case I (Q_i^* , $b_i^* \neq 1$)

Q_i^* and b_i^* are cross-correlated parameters. This means for a given b_i^* there is a corresponding Q_i^* and vice versa [33]. Therefore, b_i^* must be a constant to obtain compatible EIFS cumulative distributions for different fractographic data sets.

Q_i^* and b_i^* can be determined as follows:

1. Transform Eq. 26 into a linear form for least square fit as follows:

$$\ln \frac{da(t)}{dt} = \ln Q_i^* + b_i^* \ln a(t) \quad (29)$$

2. Compute b_i^* for a single crack or for pooled fractographic results using Eq. 30 (based on least square fit criterion):

$$b_i^* = \frac{N \sum xy - (\sum x)(\sum y)}{N \sum x^2 - (\sum x)^2} \quad (30)$$

where: $x = \ln a(t)$

$y = \ln [da(t)/dt]$

N = total number of x, y , pairs pooled

If fractographic results for multiple data sets are used in Eq. 30, $b = b_i^*$. The subscript "i" is used to distinguish values for individual data sets.

3. Once b_i^* has been determined, Eq. 31 can be used to quantify Q_i^* for a single specimen or for a group of specimens.

$$Q_i^* = \exp \left(\frac{\sum y - b_i^* \sum x}{N} \right) \quad (31)$$

The terms shown in Eq. 31 are defined as noted in Eq. 30.

A conceptual description of the calibration procedure is shown in Fig. 11. A computer program has been developed for determining b_1^* and Q_1^* values for individual fractographic data sets [7]. This program has been tailored for pooling fractographic data for multiple data sets.

4.3.2.2 Case II (Q_1^* , $b_1^* = 1$)

Q_1^* for Case II can be determined using Eq. 31 and $b_1^* = 1$. Q_1^* can be defined using fractographic results for one or more fatigue cracks in a fractographic data set.

4.3.3 TTCI Parameters

The purpose of this section is to document the way the Weibull parameters (α and β) in Eq. 1 were determined for two Phase II modeling studies (Appendices A and B). For these studies, $\epsilon = 0$ and $x_u = a_0$ were considered. Procedures are described for determining α and β for a single data set and for pooled fractographic data sets.

The notations for α , β and ϵ in Eq. 1 are modified to distinguish values for different fractographic data sets when the data pooling procedure is used. For example, the following notations have been adopted for the Durability Design Handbook [21].

α = Weibull shape parameter used in $F_a(x)$ based on one or more TTCI data sets and the TTCI data pooling procedure

α_i = Weibull shape parameter for the i th TTCI data set.

β_i = Weibull scale parameter for the i th TTCI data set, including "statistical scaling of β " if applicable (Ref. Section 4.4).

β_{ℓ_i} = Weibull scale parameter for the i th TTCI data set with no "statistical scaling of β ". Note: $\beta_i = \beta_{\ell_i} (\ell_i)^{1/\alpha_i}$, where ℓ_i = number of fastener holes per specimen where only the largest fatigue crack in 1 of ℓ_i holes per specimen is used to define the TTCI data set.

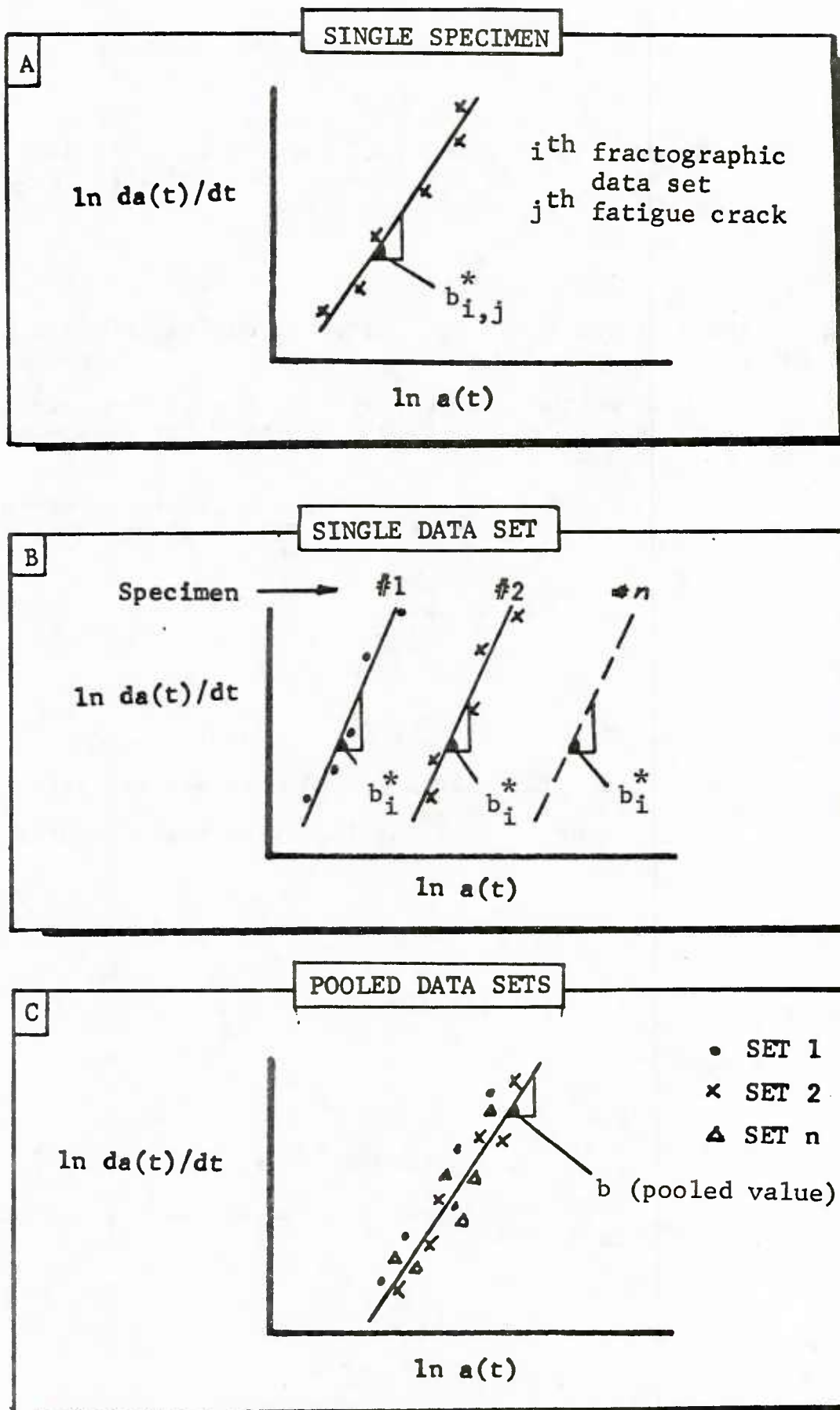


Fig. 11 Calibration Concepts for b_i^*

ϵ_i = Weibull lower bound TTCI for the i th TTCI data set
 (Note: $\epsilon_i = 0$ considered for modeling studies documented in Appendices A and B).

4.3.3.1 For One TTCI Data Set

α_i and β_i for a given TTCI data set can be determined as follows:

1. Determine the TTCI values for a selected reference crack size (e.g., $a_0 = 0.03"$) using the applicable fractographic data.

2. Rank the TTCI values in ascending order and estimate the cumulative distribution of TTCI, $F_T(t)$, using Eq. 32.

$$F_T(t) = \frac{r}{n+1} \quad (32)$$

Where r = rank of TTCI value, t (1, 2, ..., n)

n = number of TTCI values in the data set for given a_0 .

3. Transform Eq. 1 into the following least squares fit form:

$$Z = \alpha_i Y + U \quad (33)$$

where $Z = \ln \{-\ln[1-F_T(t)]\}$

$$Y = \ln t$$

$$U = -\alpha_i \ln \beta_i$$

$$\beta_i = \beta_{\ell_i} (\ell_i)^{1/\alpha_i} \text{ (Ref. Subsection 4.4)}$$

α_i and β_i can be determined using Eqs. 34 and 35, respectively. In Eq. 34,

$$\alpha_i = \frac{N \sum YZ - (\sum Y)(\sum Z)}{N \sum Y^2 - (\sum Y)^2} \quad (34)$$

N = total number of Y, Z pairs;
 Y and Z are defined in Eq. 33.

$$\beta_i = \exp \left(\frac{\alpha_i \sum Y - \sum Z}{\alpha_i N} \right) \quad (35)$$

4.3.3.2 For Pooled TTCI Data Sets

A conceptual description of the pooling procedures used to determine α and β_i in the studies of Appendices A and B is shown in Figure 12. Essential steps are as follows:

1. Determine TTCI values for a selected reference crack size (e.g., $a_0 = 0.03"$) for each fractographic data set.

2. Compute the average TTCI value for each TTCI data set (\bar{X}_i). Then, normalize the TTCI value in each data set by dividing each TTCI by the corresponding average TTCI for the data set.

3. Normalize TTCI values for each data set to be pooled and rank the pooled values in ascending order. Then, estimate $F_T(t)$ using Eq. 32.

4. The α value for the pooled data sets (Fig. 12, Frame B) can be determined using Eq. 34 and the applicable Y and Z values from Eq. 33.

5. Given α (based on pooled TTCI results), the corresponding β_i for each data set can be determined using Eq. 35 (where $\alpha = \alpha_i$) and the TTCI results for each data set separately. This procedure is conceptually illustrated in Frame C of Fig. 12 for two TTCI data sets.

4.4 STATISTICAL SCALING OF β

Laboratory tests are both expensive and time consuming. In order to save the cost and duration of experimental tests, several fastener holes, say ℓ holes, can be used in one coupon specimen. The coupon test can be stopped when a visible crack appears in any hole. Consequently, such a crack is the largest crack in ℓ holes. The time to crack

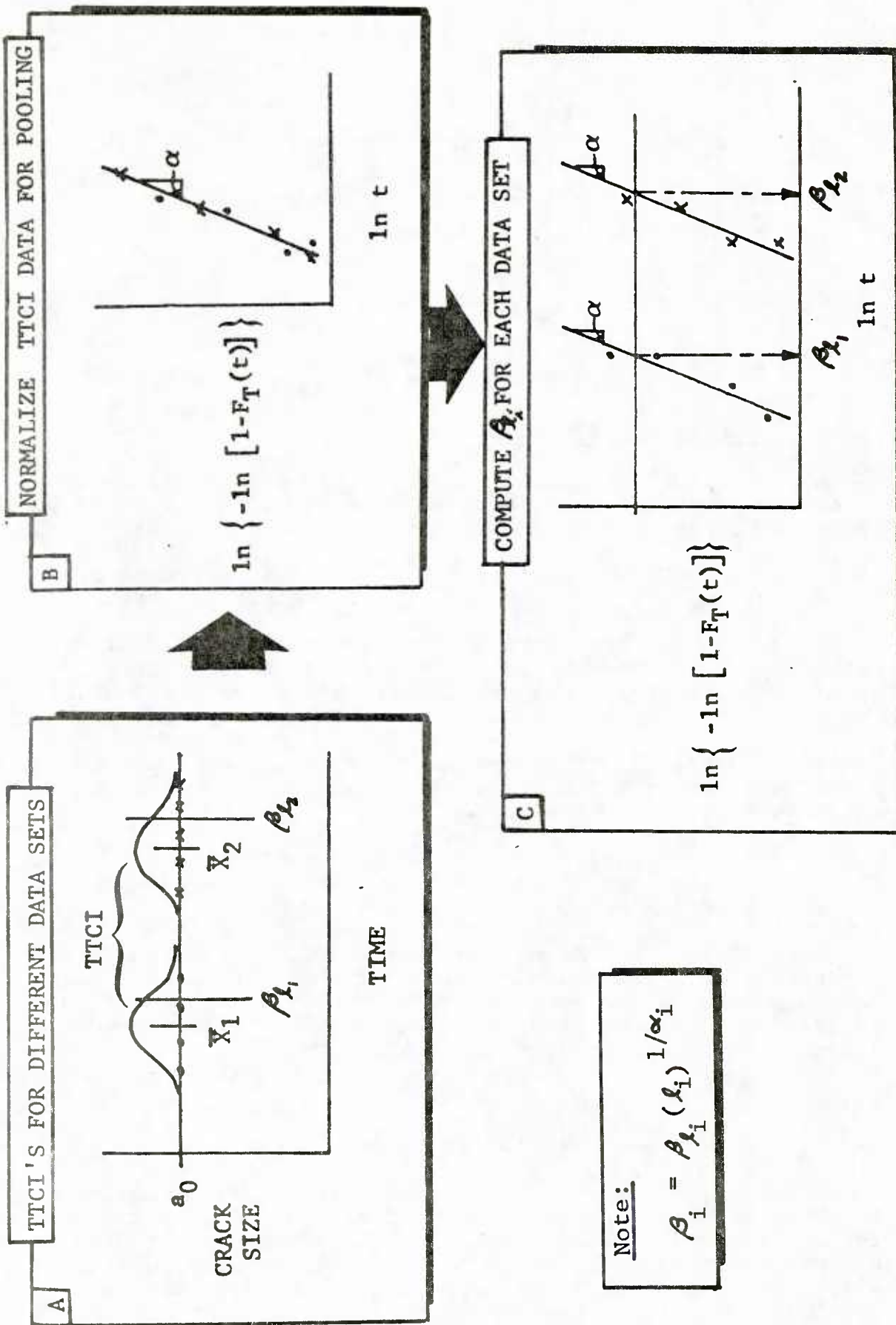


Fig. 12 Conceptual Description of Procedures for Determining α and β_i for Pooled TTIC Data Sets

initiation (TTCI) estimated from the largest crack represents the smallest TTCI in ℓ holes, i.e., the shortest TTCI of a sample of size ℓ .

As a result, one has to determine the parameter values α, β and ϵ appearing in the three parameter Weibull distribution of TTCI, Eq. 1, from a set of coupon data which represents the smallest value of TTCI of a sample of size ℓ . In this connection, the theory of minimum value of a sample of size ℓ can be used.

Let T_ℓ be the minimum TTCI of a sample of size ℓ . Then, the cumulative distribution function of T_ℓ can be derived from the three-parameter Weibull distribution of TTCI given by Eq. 1 as follows:

$$\begin{aligned} F_{T_\ell}(t) &= P[T_\ell \leq t] = 1 - P[T_\ell > t] \\ &= 1 - \{P[T > t]\}^\ell = 1 - \{1 - P[T \leq t]\}^\ell \\ &= 1 - [1 - F_T(t)]^\ell \end{aligned} \quad \left. \vphantom{\begin{aligned} F_{T_\ell}(t) &= P[T_\ell \leq t] = 1 - P[T_\ell > t] \\ &= 1 - \{P[T > t]\}^\ell = 1 - \{1 - P[T \leq t]\}^\ell \\ &= 1 - [1 - F_T(t)]^\ell \end{aligned}} \right\} \quad (36)$$

Substituting Eq. 1 into Eq. 36, one obtains the cumulative distribution for T_ℓ as

$$F_{T_\ell}(t) = 1 - \exp\left\{-\ell\left(\frac{t-\epsilon}{\beta}\right)^\alpha\right\}; \quad t \geq \epsilon \quad (37)$$

or

$$F_{T_\ell}(t) = 1 - \exp\left\{-\left(\frac{t-\epsilon}{\beta_\ell}\right)^\alpha\right\}; \quad t \geq \epsilon \quad (38)$$

in which β_ℓ is the scale parameter of the distribution of the smallest TTCI of a sample of size ℓ given by

$$\beta_\ell = \frac{\beta}{\ell^{1/\alpha}} \quad \text{or} \quad \beta = \beta_\ell \ell^{1/\alpha} \quad (39)$$

It is important to observe from Eq. 38 that the distribution of the smallest TTCI of a sample of size ℓ is also three-parameter Weibull. Furthermore, the shape parameter α and the lower bound ϵ are identical to those of the TTCI while the scale parameter β_ℓ is related to β through Eq. 39.

Thus, the test data of the smallest TTCI can be best fitted by the three-parameter Weibull distribution [see the procedures described in subsection 4.3.3] to estimate the parameter values α and β_ℓ . Then, the scale parameter, β , of TTCI is estimated from β_ℓ^ℓ using Eq. 39.

Equation 39 can be used to estimate β_i from β_ℓ (Note: $\beta_i = \beta_\ell (\ell)^{1/\alpha_i}$). This important concept is further discussed and illustrated in the Durability Design Handbook [21].

4.5 PROBABILITY OF CRACK EXCEEDANCE

The objectives of this section are: (1) show that comparable $p(i, \tau)$ predictions can be obtained using either variation of the crack growth law of Eq. 2 (i.e., $b = 1$ or $b \neq 1$), (2) illustrate how to determine a SCGMC that is compatible with the EIFS master curve, and (3) show that valid $p(i, \tau)$ predictions can be made using either $\pm y_{1i}(\tau)$ (EIFS) values.

4.5.1 IFQ Based on AFXMR4 Data Set

For illustration purposes, the IFQ model parameters were determined for the AFXMR4 data set. A description of the AFXMR4 data set is given in Table 1. Fractographic results from Vol. VIII [6] were used and included a crack size range of 0.030" - 0.050". IFQ model parameters were determined for two different variations of Eq. 26 and the results are referred to as Case I ($b_1^* \neq 1$) and Case II ($b_1^* = 1$).

Using an upper bound EIFS = $x_u = 0.0275$ ", the corresponding lower bound TTCI's (ϵ) for five different a_0 's (i.e., 0.030", 0.035", 0.040", 0.045", & 0.050") were determined. The TTCI's for five different crack sizes were normalized using the average TTCI for each a_0 . Normalized results were then pooled and α was determined using the procedures described in Subsection 4.3.3. Using α , the corresponding β_i and the corresponding $Q_i^* \beta_i$ values were determined for the five different crack sizes. IFQ model parameter results for Cases

Table 1 Description of AFXMR4 Fractographic
Data Set

Material:	7475-T7351 Al
Type Specimen:	15% Load Transfer (Reverse double dog-bone)
Fasteners:	MS 90353 ($\frac{1}{2}$ " dia.) Csk Rivets
Hole Drill:	Modified Winslow Spacematic
Gross Stress:	$\sigma_G = 34$ ksi
Load Spectrum:	F-16 400-hour (1 service life = 8000 hours)
Number of Specimens;	9
Fractography Basis:	Largest crack for 1 of 4 holes per specimen ($n = 4$)

I and II are summarized in Table 2. These results will be used in Sections 4.5.2 and 4.5.3.

4.5.2 Compatible SCGMC

Procedures are described in Section 3.6 for making the SCGMC compatible with the EIFS master curve. These procedures are discussed and illustrated in this section.

Analytical predictions for crack growth in a straight-bore fastener hole with 15% bolt load transfer in 7475-T7351 aluminum subjected to the F-16 500-hour spectrum are shown in Table 3. These results [12] were developed using an analytical crack growth program [37]. The crack growth from an initial flaw size of 0.03" (corner flaw) to 0.05" was determined as follows. The Wheeler retardation model parameter was estimated using applicable spectrum crack growth data. A multiplying factor was used to adjust the stress intensity for the 15% bolt load transfer. This factor combines the effects of tension only (no bolt load transfer or zero bearing stress) and the ratio of the bolt bearing stress to tension stress. Then, applicable da/dN versus ΔK data were used with a cycle-by-cycle crack growth program and cycle counting scheme to make the crack growth predictions.

To make the SCGMC compatible with the EIFS master curve, the same " b_i^* " value reflected in the EIFS master curve is imposed. For example, $b_i = b_i^* = 0.7372$ (Case I) and $b_i = b_i^* = 1.0$ (Case II) are used, along with the $a(t)$ versus t data from Table 3, to determine the Q_i^* values for the corresponding SCGMC. The resulting b_i 's and Q_i 's for the two different service crack growth master curves are shown in Table 4.

Predicted $a(t)$ values versus the analytical values are summarized in Table 5 for $\sigma = 22.9$ ksi and $\sigma = 28.3$ ksi. The SCGMC parameters for the two variations of the crack growth equation (Eq. 26) are indicated. The predicted $a(t)$ values were determined using $a(t_2) = 0.050$ " and Eqs. 40 and 41. Equations 40 and 41 are generalized crack size-time relationships based on Eq. 26 for $b_i \neq 1$ and $b_i = 1$, respectively (see Ref. 21 for details). In Eqs. 40 and 41,

$$a(t_1) = \left[a(t_2)^{-c_i} + c_i Q_i (t_2 - t_1) \right]^{-1/c_i} \quad (40)$$

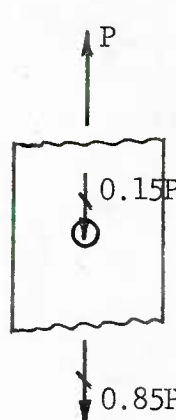
$$a(t_1) = a(t_2) \exp[-Q_i (t_2 - t_1)] \quad (41)$$

Table 2 IFQ Model Parameters for AFXMR4 Data Set

Case	b_i^*	$Q_i^* \times 10^4$	Ave. $Q_i^* \beta_{\ell_i}$	α	x_u	ℓ_i
I	0.7372	0.788	0.617	1.389	0.0275	4
II	1.0	1.854	1.451	1.389	0.0275	4

Note: $c_i^* = b_i^* - 1$

Table 3 Analytical Crack Growth Predictions for 7475-T7351 Aluminum and the F-16 500 Hour-Spectrum



σ (KSI)	$a(t)$	t (Flt.Hrs.)
22.9 ↓	0.0300	0
	0.0325	321
	0.0364	821
	0.0404	1321
	0.0444	1821
	0.0484	2321
	0.0500	2518
28.3 ↓	0.0300	0
	0.0365	313
	0.0469	813
	0.0500	959

Ref. 12

Table 4 Summary of SCGMC Parameters

σ (KSI)	Case I		Case II	
	b_i	$Q_i \times 10^4$	b_i	$Q_i \times 10^4$
22.9	0.7372	0.8586	1.0	2.0052
28.3	0.7372	2.2464	1.0	5.2333

Note: $c_i = b_i - 1$

Table 5 Comparison of $a(t)$ Predictions (SCGMC)
Versus Actual $a(t)$ Values

σ (KSI)	t (Flt. Hrs.)	a(t)		
		Analytical	Predicted	
		Table 3	Eq. 41	Eq. 40
22.9 ↓	0	0.0300	0.0302	0.0301
	321	0.0325	0.0322	0.0322
	821	0.0364	0.0356	0.0358
	1321	0.0404	0.0393	0.0396
	1821	0.0444	0.0435	0.0437
	2321	0.0484	0.0481	0.0482
	2518	0.0500	0.0500*	0.0500*
			1.0	0.7372 $\leftarrow b_i$
			2.0052	0.8586 $\leftarrow Q_i \times 10^4$
28.3 ↓	0	0.0300	0.0303	0.0302
	313	0.0365	0.0357	0.0358
	813	0.0469	0.0463	0.0465
	959	0.0500	0.0500*	0.0500*
			1.0	0.7372 $\leftarrow b_i$
			5.2333	2.2464 $\leftarrow Q_i \times 10^4$

Note

* $a(t_2) = 0.0500$ " (starting point for predictions)

$a(t_1)$ and $a(t_2)$ denote the crack size at time t_1 and t_2 , respectively; $c_i = b_i - 1$ and Q_i is a crack growth parameter.

In this case, there is excellent agreement between the analytical and predicted $a(t)$ values. Since the "b" value for the EIFS master curve is imposed on the SCGMC, the goodness-of-fit of Eq. 26 depends on the results of the analytical crack growth program (e.g., Table 3). Further work is required to evaluate "compatible SCGMC's", based on the procedure described, for different durability design conditions.

4.5.3 Crack Exceedance Predictions

It will be shown in this section that if the SCGMC is compatible with the applicable EIFS master curve: (1) it doesn't make a lot of difference which variation of Eq. 14 is used for $p(i, \tau)$ predictions (i.e., Eq. 18 or 19), and (2) comparable $p(i, \tau)$ predictions can be obtained for both positive and negative EIFS or $y_{1i}(\tau)$ values.

Crack exceedance analysis results are presented in Table 6 for two different stress levels. Results are presented for two different IFQ distributions for the AFXMR4 data set and for the corresponding service crack growth master curves. The crack exceedance predictions were based on the IFQ model parameters of Table 2 and the SCGMC parameters of Table 4. The equations used to compute $y_{1i}(\tau)$ and $p(i, \tau)$ have been appropriately modified for $y_{1i}(\tau) < 0$ (see Fig. 5). For illustration purposes, different x_1 and τ values were assumed to make $p(i, \tau)$ predictions.

In Table 6, the EIFS's for a given x_1 and τ are shown for two different cases. Although the $y_{1i}(\tau)$ values are different for Cases I and II, virtually the same $p(i, \tau)$ is obtained for a given x_1, τ . $y_{1i}(\tau)$ values < 0 resulted for Case I in two instances for $\sigma = 22.9$ ksi and 28.3 ksi. For example, for $x_1 = 0.030$ ", $\tau = 20000$ flight hours and $\sigma = 22.9$ ksi, $y_{1i}(\tau) = -0.0000144$ " and 0.000544 " were obtained for Cases I and II, respectively. As shown in Table 6, comparable $p(i, \tau)$ values were obtained (e.g., 0.635 versus 0.630) for two different EIFS's although the EIFS was negative for Case I and positive for Case II. If $p(i, \tau)$ predictions are made using an IFQ distribution and a compatible SCGMC, both \pm EIFS can be mathematically handled.

Further work is required to evaluate the accuracy of $p(i, \tau)$ predictions for different durability design

Table 6 Crack Exceedance Analysis Based on Compatible SCGMC

σ (KSI)	Case ①, ②	x_1 (Inch)	τ (Flt. Hrs.)	EIFS = $y_{11}(\tau)$ (Inch) ③	$p(1, \tau)$ ③
22.9 ↓	I	0.030	20000	-0.0000144	0.635
	II	↓	↓	0.000544	0.630
	I	0.040	4000	0.016288	0.048
	II	↓	↓	0.017936	0.045
	I	0.050	6000	0.013045	0.074
	II	↓	↓	0.015013	0.072
28.3 ↓	I	0.030	15000	-0.065027	0.926
	II	↓	↓	0.0000117	0.923
	I	0.040	4000	0.0019125	0.278
	II	↓	↓	0.0049311	0.271
	I	0.050	6000	0.0001619	0.427
	II	↓	↓	0.0021642	0.420

Notes:

- ① Ref. Table 2 for IFQ Model Parameters
- ② Ref. Table 4 for SCGMC Parameters
- ③ Ref. Fig. 5 for Appropriate Equations Used

conditions and for different crack size ranges. Also, the one and two parameter forms of Eq. 14 should be investigated further to justify using the $b_i = 1$ form for different durability analysis applications.

4.6 FORMATS FOR PRESENTING DURABILITY ANALYSIS RESULTS

The basic objective of the durability analysis is to analytically assure design compliance with the U.S. Air Force's durability requirements [8-10]. Durability analysis results can be presented in four basic formats as follows: (1) probability of crack exceedance, (2) extent of structural damage, (3) structural damage rate and (4) cost ratio: repair cost/replacement cost. The probability of crack exceedance is the fundamental output of the durability analysis.

Durability analysis results can be plotted in various forms as shown in Fig. 13. Extent of damage illustrations are presented in the Durability Design Handbook [21] and elsewhere [1,5,34-36].

4.7 DEMONSTRATION OF DURABILITY ANALYSIS METHOD

The durability analysis method developed has been demonstrated for a full-scale fighter structure (F-16 lower wing skin) and for a complex splice subjected to a B-1 bomber spectrum. Results are summarized in the Durability Design Handbook [21] and details are given elsewhere [34-36]. The durability analysis demonstrations for both fighter and bomber load spectra are discussed in this section.

4.7.1 F-16 Lower Wing Skin

A preliminary and final demonstration of the durability analysis methodology is documented in Ref. 34 and 36, respectively. Both analyses were based on coupon fractographic results for fatigue cracking in fastener holes. No scale-up of coupon data to full size structure was considered.

The preliminary analysis reflected the following:

- o IFQ of the countersunk fastener holes was based on fractographic results for straight bore fastener holes [41].

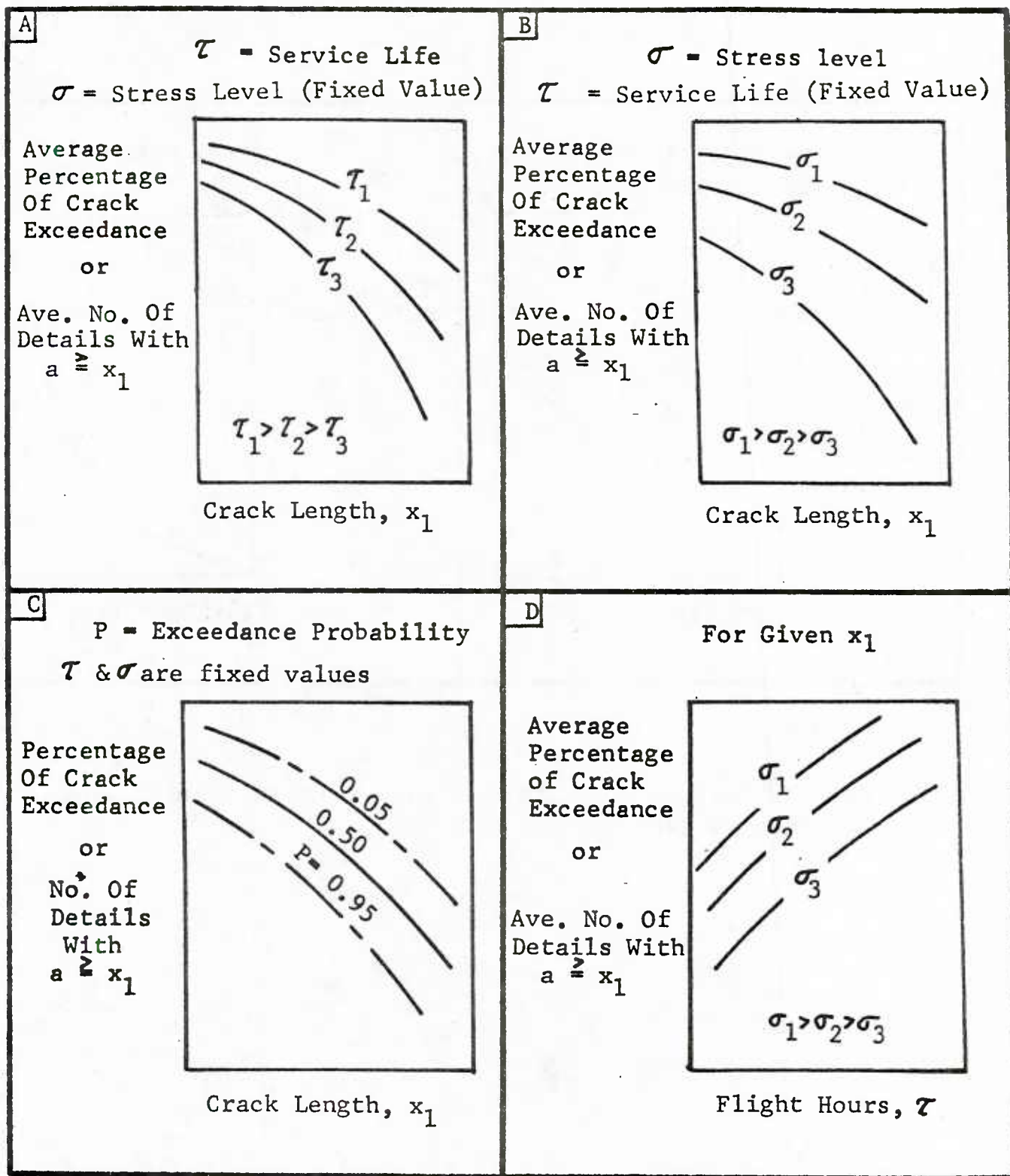


Fig. 13 Formats for Presenting Extent of Damage Results

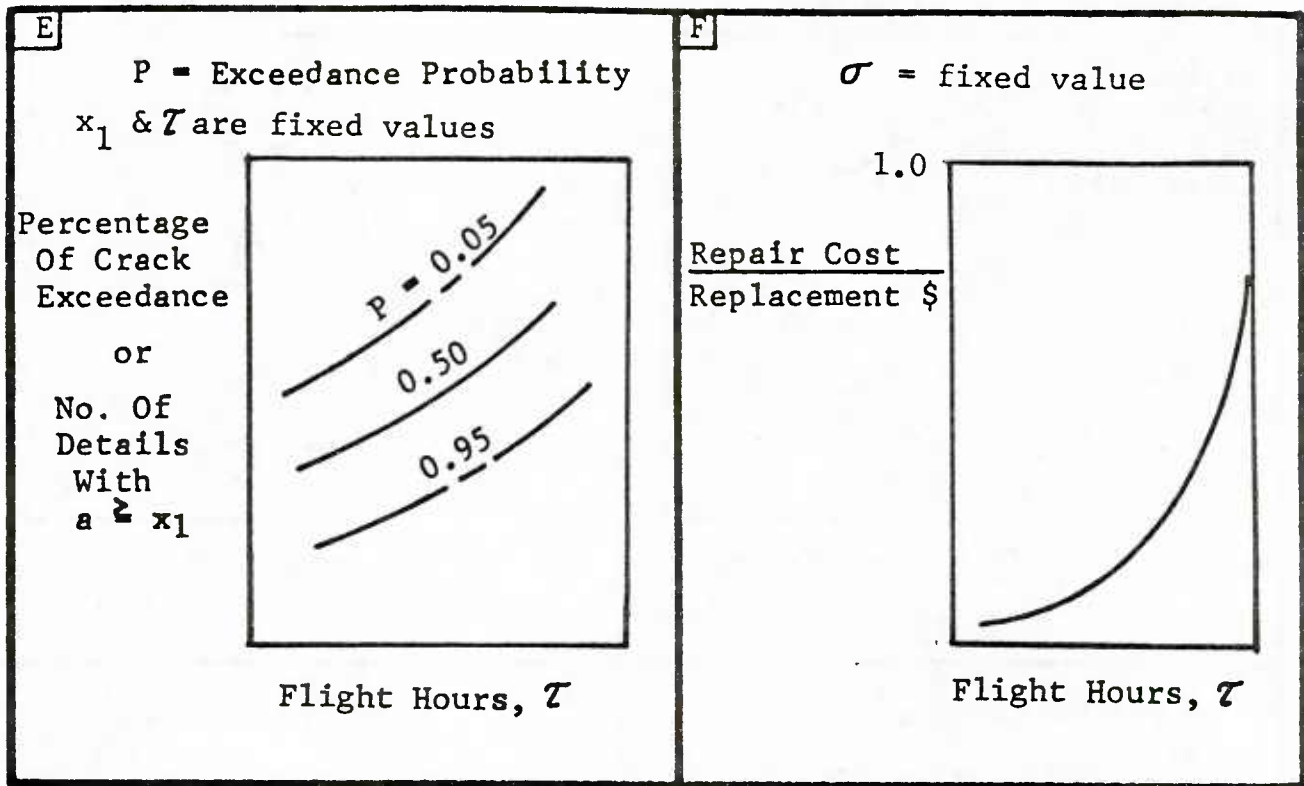


Fig. 13 Formats for Presenting Extent of Damage Results
(Continued)

- o IFQ model parameters were based on a single fractographic data set (XWPF) from Ref. 41 and $\epsilon = 0$ was used.
- o A crack growth power law, Eq. 2, for the EIFS master curve was used where $b \neq 1$.
- o "Service crack growth master curves" were used based on Ref. 37.
- o The F-16 lower wing skin was divided into three stress regions.

The final demonstration of the durability analysis method reflected the following:

- o Fractographic results for countersunk fastener holes and data pooling procedures were used to define the IFQ model parameters for the countersunk fastener holes in the F-16 lower wing skin. $\epsilon \neq 0$ was considered.
- o The F-16 lower wing skin was divided into ten stress regions (see Fig. 14).
- o A crack growth power law, Eq. 2 (with $b = 1$), was used for the EIFS master curve.
- o Average α and Q_1^{β} values were used for crack exceedance predictions.
- o The service crack growth master curve was based on pooled fractographic results and the applicable stress level for each stress region.

Tear-down inspection results from the F-16 wing durability test article (after $\tau = 16000$ hours of testing using the F-16 500-hour spectrum) were compared with extent of damage predictions. Excellent correlations and trends were obtained.

4.7.2 Complex Splice (B-1 Bomber Spectrum)

A durability analysis of the complex splice shown in Fig. 15 was performed to demonstrate the methodology for a bomber load spectrum. Details of this analysis are documented in Ref. 35. The durability analysis and basic conclusions are briefly discussed in this section.

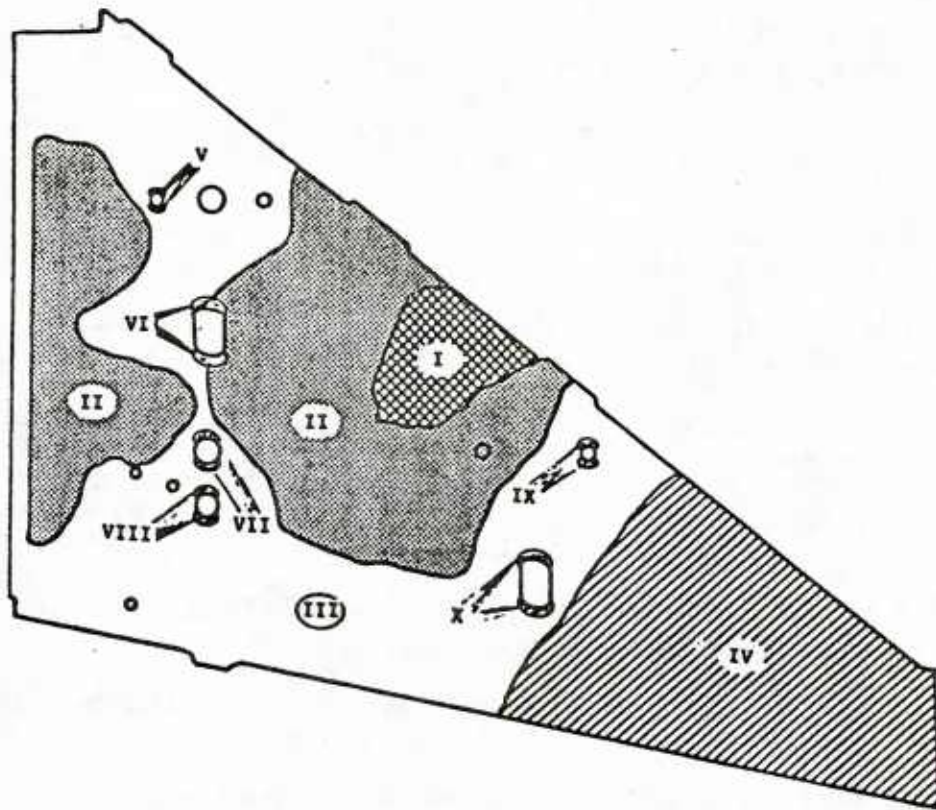


Fig. 14 Stress Zones for F-16 Lower Wing Skin

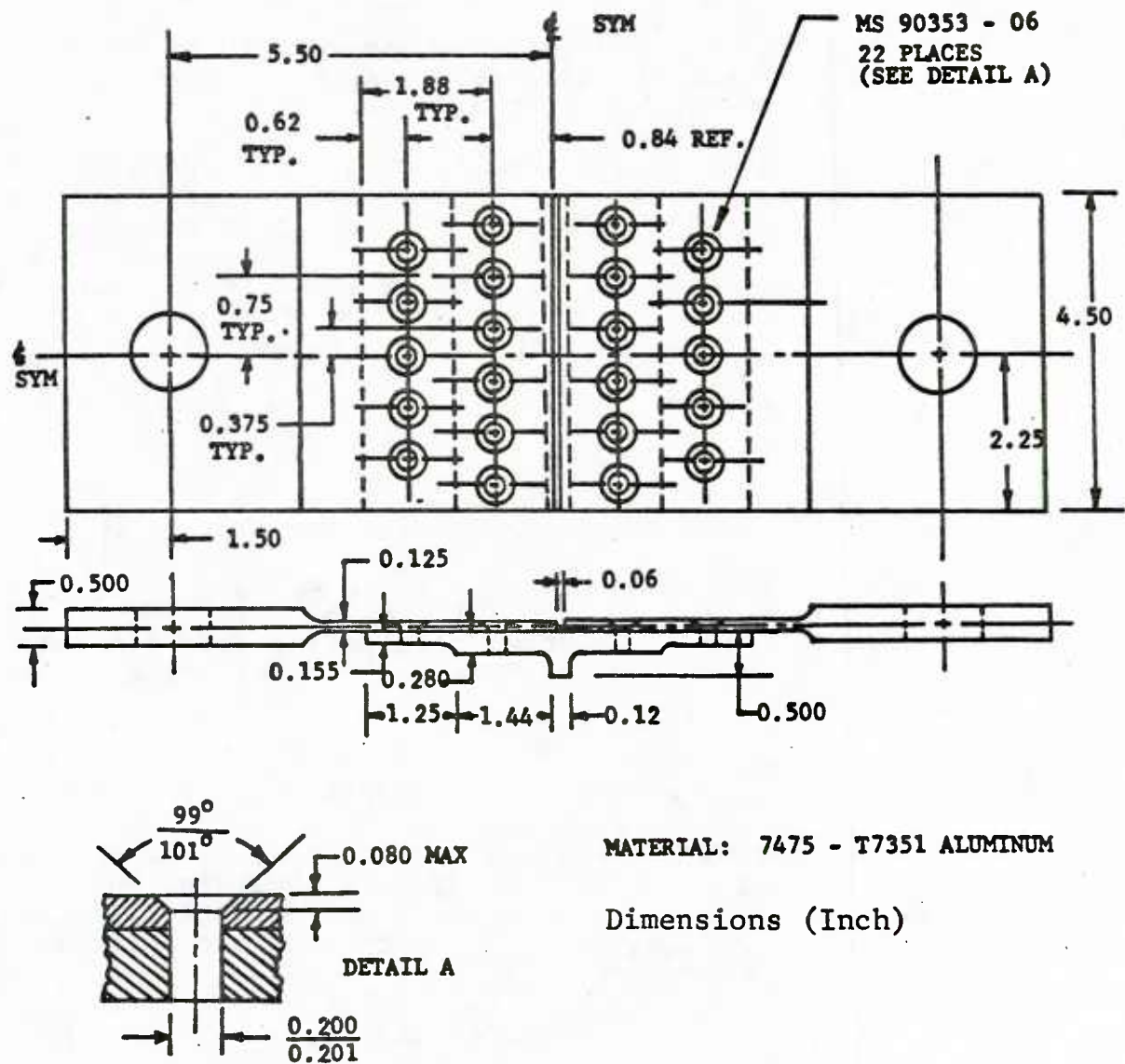


Fig. 15 Complex-Splice Specimen

Several complex splice specimens were fatigue tested using a B-1 bomber load spectrum. A tear-down inspection and fractographic evaluation were made to determine the number of fastener holes in the outer row of the splice with a crack size ≥ 0.050 " at $r = 13500$ flight hours. The extent of damage was predicted for the outer row of fastener holes and the results were compared with test results.

The durability analysis reflected the following:

- o A simplified stress analysis was used to estimate the gross stress on the cross section at the outer row of fastener holes at the interfaces.
- o The IFQ was based on fractographic results for countersunk fastener holes in reverse dog-bone specimens (15%, 30% and 40% load transfer).
- o Nine fractographic data sets were pooled to calibrate the IFQ model parameters. The fractographic crack size range used was 0.005 " - 0.10 ".
- o $a_0 = x_u = 0.050$ "
- o $\epsilon = 0$; $l = 4$
- o The EIFS master curve was based on Eq. 9 ($b = 1$)
- o The SCGMC was based on Eqs. 14, 16 and 17 with $b = 1$

In general, the predicted results and trends compared reasonably well with test results. Further details are given elsewhere [21,35].

4.8 ADDITIONAL STUDIES

Many studies were performed during Phase II to evaluate the durability analysis methodology developed in Phase I. The most important studies are discussed in this section. Miscellaneous durability-related topics are also discussed.

4.8.1 IFQ Model Studies

Initial fatigue quality (IFQ) is one of the most important elements of the durability analysis methodology developed. For this reason, several studies were made in Phase II to evaluate the IFQ model using the wealth of

fractographic data available for both straight-bore [41] and countersunk fastener holes [6].

The main objectives of these studies were to:

1. Develop, evaluate, and refine the procedures for quantifying the IFQ model parameters (i.e., α , β_i , ϵ , Q_i^* , b_i^* , x_u) on a comparable baseline for different fractographic data sets.
2. Evaluate the IFQ model and goodness-of-fit using fractographic results for different design and test variables.
3. Determine the IFQ model parameter values, including the range and variance of values, for selected fractographic data sets.
4. Evaluate the sensitivity of the IFQ model parameter values for different design and test variables.
5. Compare the IFQ model parameter values for different fractographic data sets for consistency and trends.
6. Justify using the same IFQ distribution for a given material, fastener hole type, drilling procedure and fastener type/fit for different stress levels, load spectra and percentage of fastener load transfer.
7. Develop confidence in the use of the IFQ model for different variables and applications.

The final conclusions and recommendations for IFQ, given in the Durability Design Handbook [21], were based on the "lessons learned" over the course of the program. Therefore, the IFQ model procedures and results for some studies are not in complete accord with the final understandings reached.

Two IFQ model studies are documented in Appendices A and B for straight bore and countersunk fastener holes, respectively. These studies were based on fractographic results from Ref. 41 and 6 .

The studies documented in Appendices A and B reflected the following:

1. Equation 1 was used for the TTCI distribution with $\epsilon = 0$.

2. The crack growth law of Eq. 2 was used with $b \neq 1$ (Case I).

3. $\epsilon = 0$ and $a_0 = x_u$ were used.

Based on the final understanding for the program, the following was recommended: (1) use the three-parameter Weibull distribution for TTCI with $\epsilon \geq 0$, (2) define the upper bound EIFS value, x_u , in conjunction with ϵ , (3) use the two-parameter form of Eq. 2 (i.e., Q and b) for $b > 1$; otherwise, use the one-parameter form (i.e., Q and $b = 1$). Further work is required to evaluate the one-parameter form for different design variables.

The following conclusions, based on the studies documented in Appendices A and B, are consistent with the final understandings of the program [21]:

1. IFQ model parameters should be determined using the fractographic data pooling procedure in order to make the resulting parameters compatible for different fractographic data sets.

2. α and b_i^* appear to be material constants independent of load spectra, stress level and percentage of shear load transfer.

3. α and b_i^* depend on the type of fastener hole. For example, typical α values were approximately 4.4 and 2.5 for straight bore holes and countersunk fastener holes, respectively. b_i^* values were approximately 0.88 and 0.61 for straight bore and countersunk fastener holes, respectively. Note: The one-parameter form of Eq. 2 ($b = 1$) is recommended for quantifying the IFQ if $b_i^* < 1$.

4. EIFS values < 0 are theoretically possible using the IFQ model when $b < 1.0$. This will not create a durability analysis problem as long as the IFQ model is considered as a "mathematical tool" and the SCGMC is compatible with the EIFS master curve (Ref. Section 4.2.3).

5. $Q_i^* \beta_i$ appears to depend on the material and fastener hole type. However, $Q_i^* \beta_i$ seems to be insensitive to stress level, load spectra and % shear load transfer.

6. The following empirical relationships look very promising for durability analysis applications:

$$\left. \begin{aligned} Q &= K\beta^A \\ \beta &= k\sigma^J \\ Q &= \xi\sigma^\gamma \end{aligned} \right\} \quad (42)$$

7. $Q_1^* \beta_i$ and α provide the common denominator for linking different fractographic data sets on a comparable basis and the keys for generic EIFS.

8. Q_1^* and b_1^* are cross correlated constants. For example, for a given b_1^* value there is a corresponding Q_1^* value and vice versa. Careful attention must be given to the Q_1^* and b_1^* values used to define IFQ.

9. In general, fractographic results for straight bore fastener holes exhibited less scatter than those for countersunk fastener holes [6,41].

4.8.2 Statistical Crack Growth Studies

Statistical crack growth studies, performed in Phase II of the program, are documented in Ref. 33. These studies were performed to: (1) better understand IFQ model parameters and statistical variability, (2) investigate possible relationships between parameters Q and b , and (3) study crack exceedance predictions based on probabilistic and deterministic considerations.

Two fractographic data sets from the FHQ program [41] were used: WPF and XWPF. Both data sets were for 7475-T7351 aluminum and straight bore fastener holes. The WPF specimens were designed for no load transfer and these specimens were subjected to the F-16 400-hour spectrum. The XWPF specimens were designed for 15% shear load transfer through the fasteners and these specimens were subjected to the F-16 400-hour spectrum. These studies were based on Eq. 2 with $b \neq 1$.

Essential conclusions from these studies are:

1. Crack growth rate parameters Q and b can be characterized by a log normal distribution reasonably well.

2. Since the economic repair crack size limit is usually small, the influence of the crack growth variability on the extent of damage predictions and economical life may not be very significant.

3. Since the EIFS values are determined using the TTCI data, such values indirectly account for the crack growth variability. Hence, the initial flaws can be grown deterministically to determine the probability of crack exceedance.

4. Similar studies should be made using Eq. 2 and $b = 1$.

4.8.3 Related Durability Studies

The following studies were also performed during Phase II:

1. Investigate effect of scale-up and hole interaction on crack growth.
2. Evaluate method for "scaling" the crack growth for different load spectra (development of transfer functions).
3. Parameter sensitivity analysis.

These studies were exploratory and limited in scope. Details are documented in Appendix C.

SECTION V

DURABILITY TEST PROGRAM

5.1 INTRODUCTION

An overview of the durability test program is given in this section. Essential elements of the test program are described and discussed, including the test matrix, specimen details, experimental methods and data acquisition. Details of the test program, raw fractographic data and other specifics are documented in Volume VIII [6].

A total of 701 specimens were manufactured and tested. Variables included in the test program were material, spectrum, stress level, fastener diameter/type, load transfer and specimen geometry (width and thickness). Fractographic data were obtained for over 800 fatigue cracks and a tear-down inspection of the F-16 lower wing skin from the durability test article was performed.

The basic objective of the test program and the fractographic data acquired was to: (1) provide the data base needed to evaluate, refine and demonstrate the durability analysis methodology developed and (2) provide fractographic data for quantifying the initial fatigue quality of fastener holes.

5.2 TEST MATRIX

The durability program test matrix is presented in Table 7 and is further detailed in Table 8. Different specimen configurations were used as noted in Figure 16. Data set designations and specimen details are described in Sections 5.3 and 5.4, respectively. Refer to Volume VIII for further details.

5.3 DATA SET DESIGNATIONS

Test specimens for a given test series were identified using the coding scheme shown in Table 9. Data sets were coded to identify the key parameters for a given test series. Each data set is identified by six characters, where each character represents a different test parameter, as shown in Table 9. The first symbol identifies the material used, the second identifies the spectrum, etc.

Table 7 Durability Test Matrix

MATERIAL	SPECTRUM	FASTENER	DIA.	% LOAD TRANSFER AND NUMBER					TOTAL
				0	15%	30%	40%	SPLICE	
7475-T7351	F-16 500 HR	MS 90353	1/4	20	49				69
			3/16		6				6
	F-16 400 HR	MS 90353	3/16	7	31				38
			1/4	50	31	29	31		141
		NAS 1580	1/4	10	10	6	2		28
	NAS 6204	1/4		19				19	
B-1 BOMBER	MS 90353	3/16		10	10		24	44	
		1/4	70	43	30	30		173	
	NAS 1580	1/4		32	30	30		92	
		3/16			10			10	
2024-T851	F-16 400 HR	NAS 1580	1/4		1				1
			1/4	13	10				23
	B-1 BOMBER	NAS 1580	1/4	20	20				40
D6ac STEEL	F-16 400 HR	NAS 6204	1/4	17					17
TOTAL				207	262	115	93	24	701

Table 8 Test Matrix Details

MATERIAL	SPECTRUM	LOAD TRANSFER	σ_c (KSI)	FASTENER TYPE	DIA. (IN.)	SPECIMEN TYPE	#	DATA SET DESIGNATION
7475- T7351	F-16 400 HR BLOCK	0%	32.0	MS-90353	1/4	1A	10	AFLR4
					3/16	1A	7	AFLR3
			34.0	MS-90353	1/4	1A	10	AFMR4(A)
						1B	11	AFMR4(B)
			38.0	NAS-1580	1/4	1A	10	AFMC4
				MS-90353	1/4	1A	10	AFHR4(A)
					1B	9	AFHR4(B)	
		15%	32.0	MS-90353	1/4	2A	11	AFXLR4
					3/16	2A	12	AFXLR3
			34.0	MS-90353	1/4	2A	10	AFXMR4
					3/16	2A	9	AFXMR3
				NAS-1580	1/4	2A	10	AFXMC4
				NAS-6204	1/4	2A	10	AFXMP4
			38.0	MS-90353	1/4	2A	10	AFXHR4
					3/16	2A	10	AFXHR3
			40.8	NAS-6204	1/4	2A	9	AFXHP4
		30%	30.1	MS-90353	1/4	3	9	AFYLR4
			34.0	MS-90353	1/4	3	10	AFYMR4
				NAS-1580	1/4	3	6	AFYMC4
			38.0	MS-90353	1/4	3	10	AFYHR4
		40%	27.9	MS-90353	1/4	4	6	AFZLR4
			31.2	MS-90353	1/4	4	6	AFZLR4
			33.0	MS-90353	1/4	4	4	AFZmR4
			34.0	MS-90353	1/4	4	6	AFZmR4
				NAS-1580	1/4	4	2	AFZMC4
			38.0	MS-90353	1/4	4	9	AFZHR4
			34.0	MS-90353	1/4	1A	6	AB1R4
	B-1 BOMBER	0%	36.0	MS-90353	1/4	1A	10	ABLR4(A)
						1B	11	ABLR4(B)
			38.0	MS-90353	1/4	1A	11	ABMR4(A)
						1B	11	ABMR4(B)
			40.8	MS-90353	1/4	1A	10	ABHR4(A)
						1B	11	ABHR4(B)
		15%	36.0	MS-90353	1/4	2A	11	ABXLR4
				NAS-1580	1/4	2A	12	ABXLC4
			38.0	MS-90353	1/4	2A	11	ABXMR4(A)
					2B	10	ABXMR4(B)	
						10	ABXMR3	
					3/16	2A	10	ABXMR3
				NAS-1580	1/4	2A	10	ABXMC4
				SUBTOTAL				

Table 8 Test Matrix Details (Continued)

MATERIAL	SPECTRUM	LOAD TRANSFER	σ_c (KSI)	FASTENER TYPE	DIA. (IN.)	SPECIMEN TYPE	#	DATA SET DESIGNATION
7475- T7351	B-1 BOMBER	15%	40.8	MS-90353	1/4	2A	11	ABXHR4
				NAS-1580	1/4	2A	10	ABXHC4
		30%	34.0	MS-90353	1/4	3	10	ABYLR4
				NAS-1580	1/4	3	10	ABYLC4
			36.0	MS-90353	1/4	3	10	ABYMR4
					3/16	3	10	ABYMR3
				NAS-1580	1/4	3	10	ABYMC4
					3/16	3	10	ABYMC3
			38.0	MS-90353	1/4	3	10	ABYHR4
				NAS-1580	1/4	3	10	ABYHC4
		40%	34.0	MS-90353	1/4	4	10	ABZLR4
				NAS-1580	1/4	4	10	ABZLC4
			36.0	MS-90353	1/4	4	10	ABZMR4
				NAS-1580	1/4	4	10	ABZMC4
			38.0	MS-90353	1/4	4	10	ABZHR4
				NAS-1580	1/4	4	10	ABZHC4
	F-16 500 HR RANDOM	0%	34.0	MS-90353	1/4	1A	10	ADMR4
			38.0	MS-90353	1/4	1A	10	ADHR4
		15%	29.6	MS-90353	1/4	2A	10	ADXLR4
			32.0	MS-90353	1/4	2A	10	ADXL R4
			34.0	MS-90353	1/4	2A	19	ADXMR4
					3/16	2A	6	ADXMR3
			38.0	MS-90353	1/4	2A	10	ADXHR4
2024- T851			F-16 400 HR BLOCK	0%	31.0	NAS-1580	1/4	1A
	34.0	NAS-1580			1/4	1A	8	TFMC4
	15%	31.0		NAS-1580	1/4	2A	10	TFXLC4
	B-1 BOMBER	0%	31.0	NAS-1580	1/4	1A	10	TBLC4
			34.0	NAS-1580	1/4	1A	10	TBMC4
		15%	34.0	NAS-1580	1/4	2A	10	TBXMC4
40.8	NAS-1580		1/4	2A	10	TBXHC4		
D6ac Steel	F-16 400 HR BLOCK	0%	85.0	NAS-6204	1/4	5	1	SF1P4
			100.0	NAS-6204	1/4	5	6	SFLP4
			110.0	NAS-6204	1/4	5	5	SFMP4
			125.0	NAS-6204	1/4	5	5	SFHP4
SUBTOTAL							676	

COMPLEX SPLICE								
MATERIAL	SPECTRUM	LOAD TRANSFER	σ_G (KSI)	FASTENER TYPE	DIA. (IN.)	SPECIMEN TYPE	#	DATA SET DESIGNATION
7475-T7351	B-1 BOMBER		22	MS-90353	3/16	6	1	CBS1
			25	MS-90353	3/16	6	11	CBSL
			30	MS-90353	3/16	6	12	CBSH
SUBTOTAL							24	

PHOTOELASTIC STUDY								
MATERIAL	SPECTRUM	LOAD TRANSFER	σ_c (KSI)	FASTENER TYPE	DIA. (IN.)	SPECIMEN TYPE	#	DATA SET DESIGNATION
7475-T7351		15%		MS-90353	1/4	2A	1	
SUBTOTAL							1	

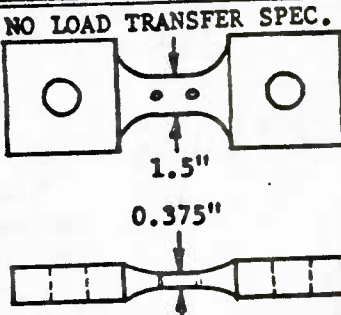
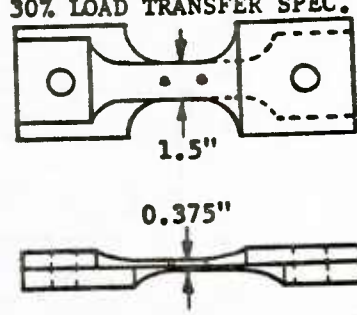
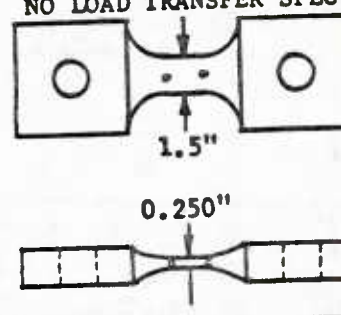
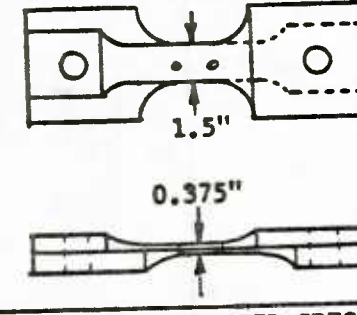
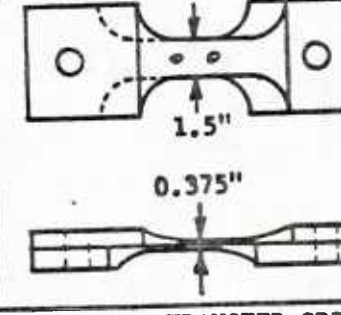
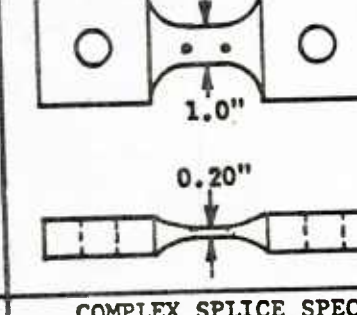
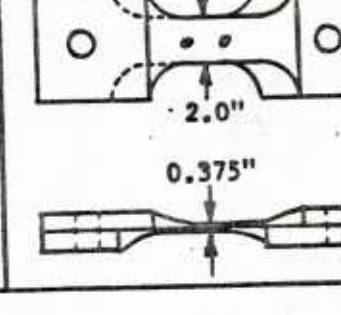
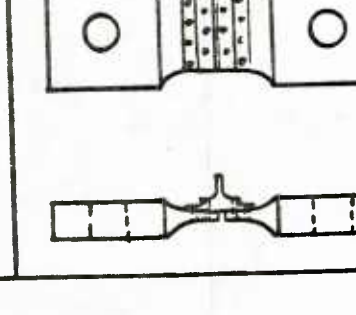
NO.	CONFIGURATION	NO.	CONFIGURATION
1A	<p>NO LOAD TRANSFER SPEC.</p> 	3	<p>30% LOAD TRANSFER SPEC.</p> 
1B	<p>NO LOAD TRANSFER SPEC.</p> 	4	<p>40% LOAD TRANSFER SPEC.</p> 
2A	<p>15% LOAD TRANSFER SPEC.</p> 	5	<p>NO LOAD TRANSFER SPEC.</p> 
2B	<p>15% LOAD TRANSFER SPEC.</p> 	6	<p>COMPLEX SPLICE SPEC.</p> 

Fig. 16 Specimen Configuration Designations

Table 9 Data Set Designations

ORDER OF SYMBOL	TEST PARAMETER	POSSIBLE SYMBOLS
1	MATERIAL	A: 7475-T7351 Al. T: 2024-T851 Al. S: D6ac STEEL
2	SPECTRUM	F: F-16 400 HR BLOCK B: B-1 BOMBER D: F-16 500 HR RANDOM
3	LOAD TRANSFER	: NO LOAD TRANSFER X: 15% LOAD TRANSFER Y: 30% LOAD TRANSFER Z: 40% LOAD TRANSFER
4	STRESS LEVEL	L: LOW M: MEDIUM H: HIGH
5	FASTENER TYPE	R: MS-90353 RIVET C: NAS 1580 C'SUNK BOLT P: NAS 6204 P.H. BOLT
6	FASTENER DIAMETER	3: 3/16 4: 4/16" or 1/4"

NOTES:

1. Lower case letters for stress level symbols represent a stress level that is lower, but in the same range as the upper case symbol.
2. CBSL: Complex Splice/Low Stress Level
CBSH: Complex Splice/High Stress Level

EXAMPLE: ABXHR3
Material: A: 7475-T7351 Al.
Spectrum: B: B-1 BOMBER
Load Transfer: X: 15%
Stress Level: H: HIGH (40.8 KSI)
Fastener Type: R: MS-90353 RIVET
Fastener Dia.: 3: 3/16"

Lower case letters for the stress level indicate a stress level that is lower than an upper case letter, but is in the same general range. Letters in parentheses at the end of a designation indicate one of the specimen configurations shown in Figure 16. Other peculiarities of the naming system are indicated in Table 9.

5.4 Load Spectra

Three load spectra were used; the F-16 400-hour wing root bending moment spectrum, the F-16 500-hour wing root bending moment durability spectrum and the B-1 bomber lower carry-through box bending moment spectrum. The F-16 400-hour block spectrum used was the same spectrum used for the "Fastener Hole Quality" program [41]. Several specimens were tested using the F-16 500-hour block spectrum, which is the same spectrum used to test the F-16 wing component for the full-scale durability demonstration.

5.5 SPECIMEN DETAILS

Five specimen designs were used for testing the 7475-T7351 aluminum material, consisting of four different amounts of load transfer and a complex splice. The details for the 0%, 15%, 30% and 40% load transfer and complex splice specimens are shown in Figs. 17-20 and 15, respectively.

Most of the 0% load transfer specimens tested were 0.375" thick as shown in Figure 17. Specimens with a 0.250" thickness were also tested. These specimens were identified with a (B) after the data set designation (Ref. Table 8).

Two different widths were used for the 15% load transfer specimen. Most of the 15% load transfer specimens tested had a width of 1.500" as shown in Figure 18. However, ten specimens with a 2.000" width were also tested. These specimens were designated as the "ABXMR4(B)" data set.

The "complex-splice" specimen, shown in Fig. 15, simulates a fuselage splice. This specimen was made from 7475-T7351 aluminum plate (1/2" thickness) and included blind, pull-through rivets (MS90353-06 (3/16" dia.)). No faying surface sealant was used.

The 0% load transfer specimen design shown in Figure 21 was used for testing the D6ac steel material.

Technical drawing of a mechanical part, showing front and top views with dimensions.

Front View (Top):

- Overall width: 2.00"
- Overall length: 13.00"
- Overall height: 4.00"
- Two circular features (possibly holes or bosses) are located on the left and right ends, each with a center cross.
- A central horizontal slot is shown, with a width of 0.375" and a depth of 1.500".
- A dimension 'S' indicates the distance from the center of the slot to the center of the right circular feature.

Top View (Bottom):

- Overall width: 0.50"
- The view shows the profile of the part, including the central slot and the circular features.

66

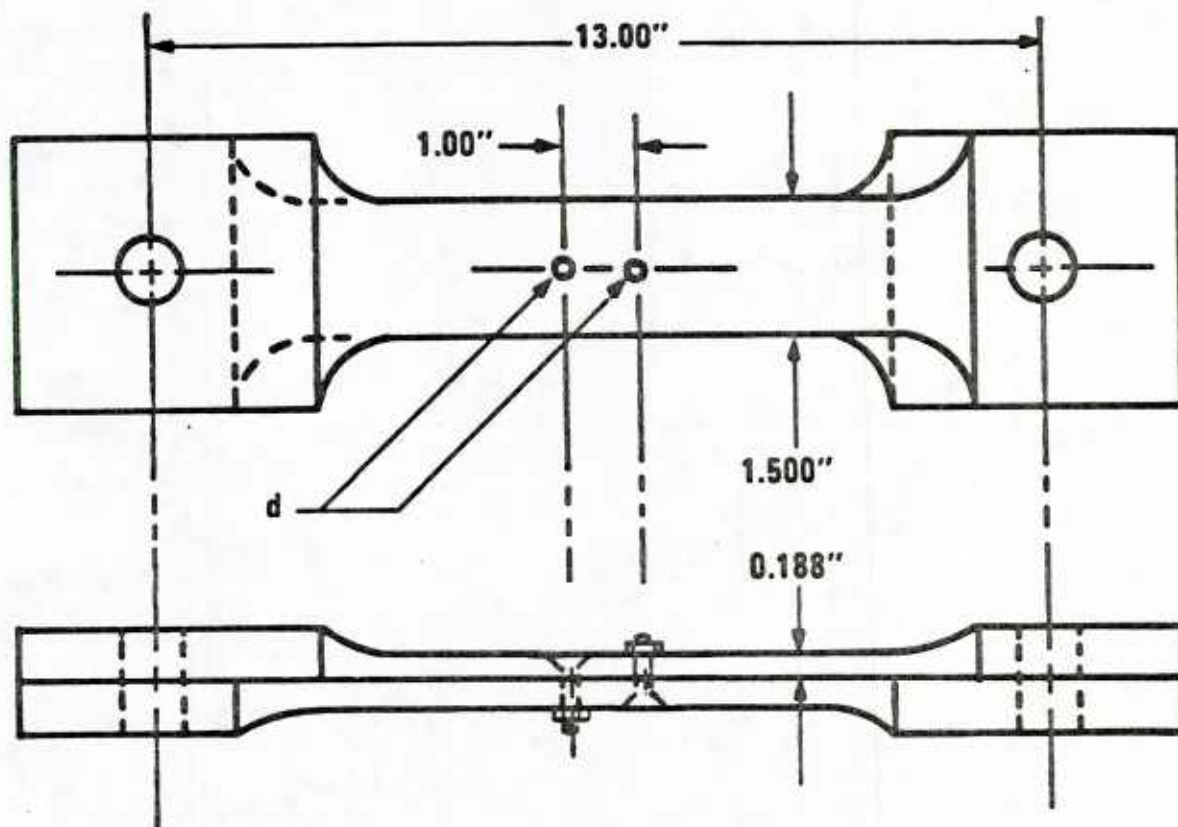
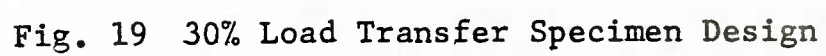


Fig. 18 15% Load Transfer Specimen Design



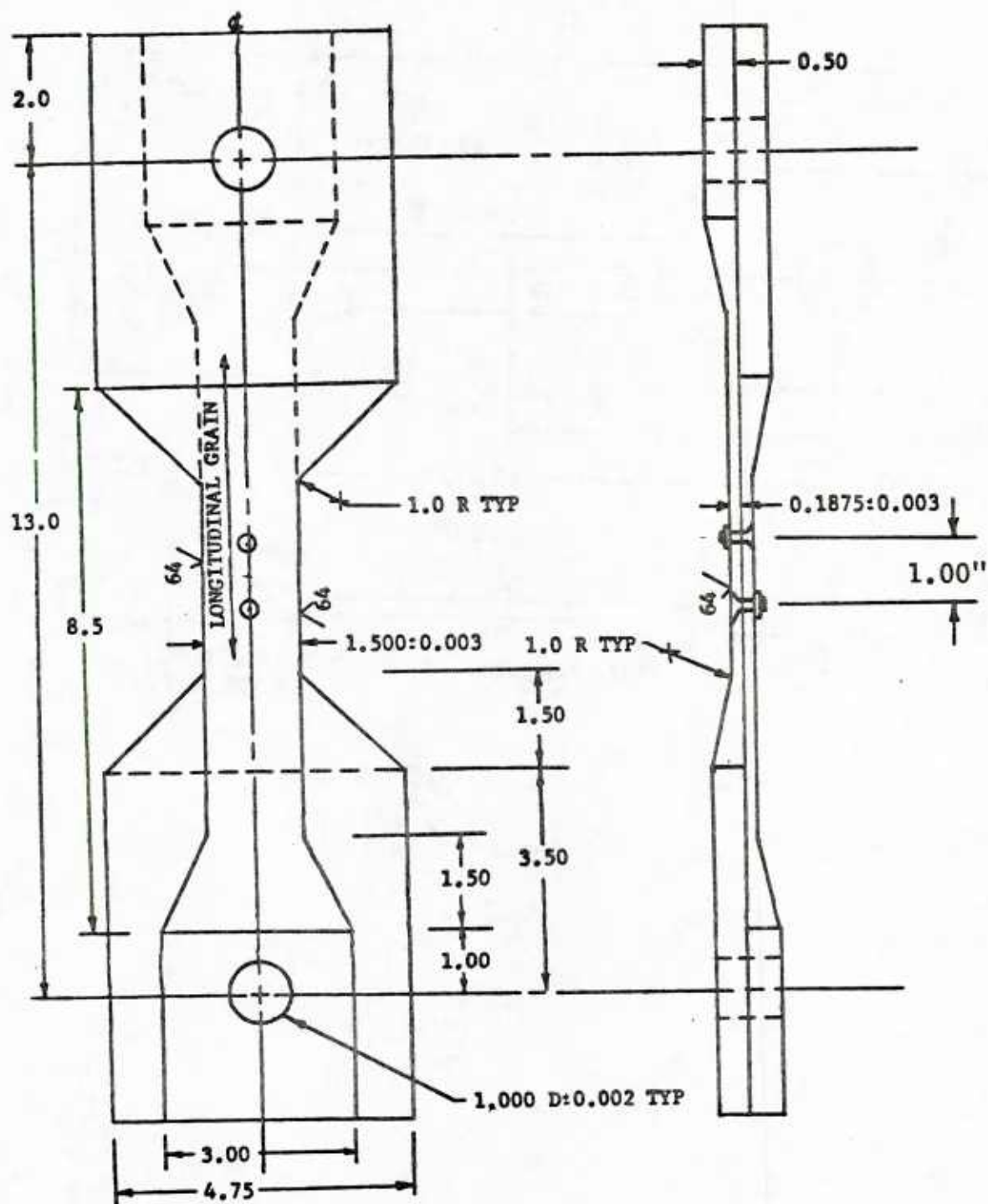


Fig. 20 40% Load Transfer Specimen Design

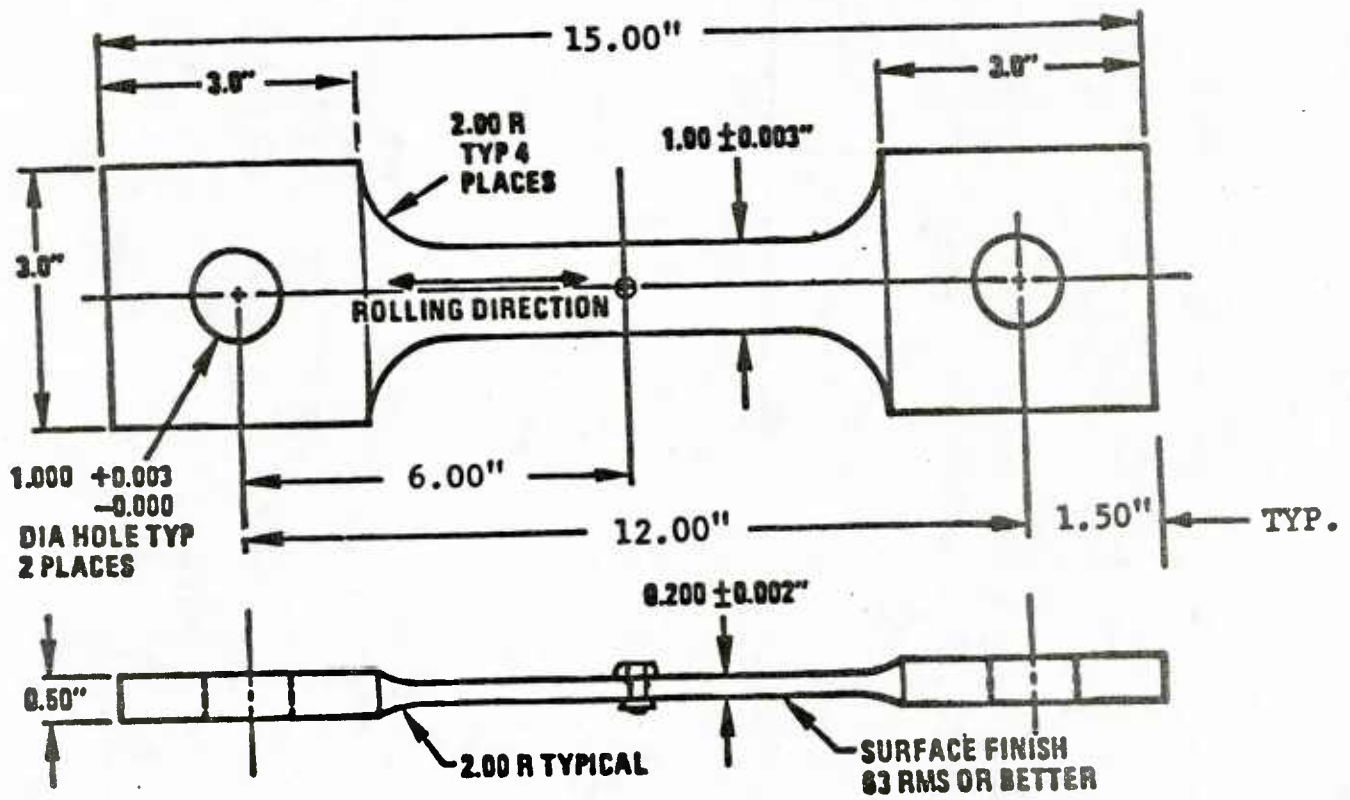


Fig. 21 D6ac Steel Specimen Design

All fastener holes for the test specimens were drilled using the modified Winslow Spacematic drill. Fasteners were installed using typical aircraft production procedures. All load transfer specimens were match-drilled in pairs.

The load transfer specimens (i.e., 15%, 30%, and 40%) were designed assuming equal longitudinal deformation for the upper and lower dog bones between lug pin and fastener. Pins and fasteners were assumed to be rigid and to "perfectly fit" their mating holes. Due to normal hole size variations and clearance fits, the actual percentage load transfer for each specimen varies depending on the load level required to take up the slop between the hole and the fastener. A free body diagram is shown in Fig. 22.

5.6 TEST SETUP AND PROCEDURES

Spectrum fatigue tests were performed at the GD/FWD on servo-controlled, hydraulically-actuated load frames. A special hardware interface was used to monitor each load frame and to assure proper load control. This system provided a permanent record of test events.

Specimen dimensions were recorded. Then, the required load for the desired stress level was determined. The hole diameters and countersink depths were also measured and recorded. Results are reported in Volume VIII [6].

Each load transfer specimen contained four fastener holes in the test section. The load transfer through the fastener affects the stress on the cross-section of each dogbone. Therefore, careful records were kept on hole positions in the specimens and the size of the largest crack in each hole. Results are documented in Volume VIII [6].

Specimens were then loaded in the test frames and left to run. When the specimens had fatigued for the desired length of time, the unbroken dogbones were pulled apart and the failure load was recorded. If the specimen failed in the load frame, no failure load was recorded. The broken dogbones were then cut up and the fatigue cracks in each hole were exposed and numbered. The D6ac steel specimens were sprayed with a clear lacquer to protect the fracture surface from rust. The final sizes of all fatigue cracks were measured and the largest crack for each specimen was read fractographically. Many specimens had more than the largest crack read and these data are also presented in Volume VIII.

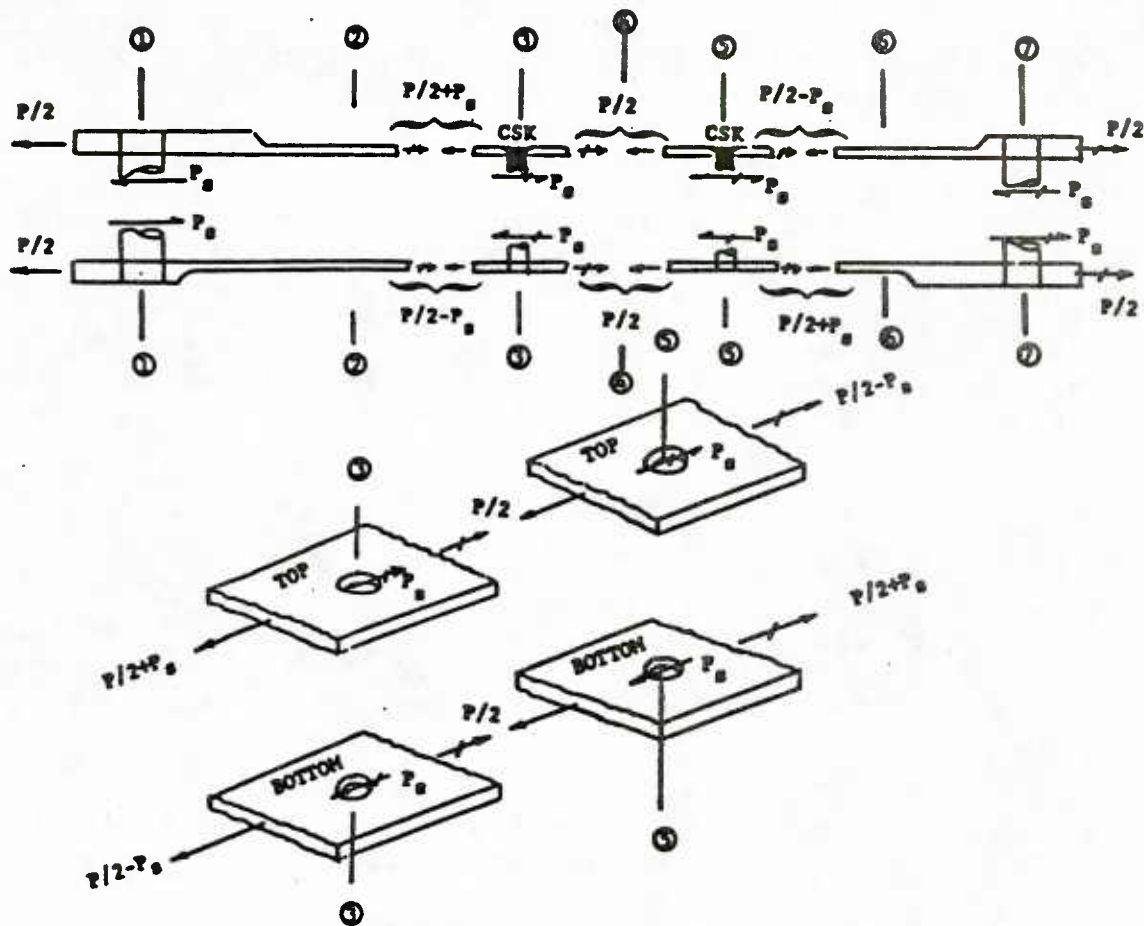


Fig. 22 Load Transfer Specimen Free Body Diagram

Details of the fractography set-up and procedures are detailed in Section VI and in Volume VIII.

The complex splice specimen, shown in Figure 15, was tested without lateral support using the same test frames used for the other tests. This same specimen design, for a different aluminum alloy (2124-T851), had been previously tested with and without lateral support [42]. Results of the strain survey indicated negligible effect of the lateral support on the resulting strains [42].

SECTION VI

EVALUATION OF TEST AND FRACTOGRAPHIC RESULTS

6.1 INTRODUCTION

The basic objective of this section is to present, compare and evaluate selected test and fractographic results from Volume VIII [6]. A comprehensive evaluation of "all the data" in Volume VIII was beyond the scope of this program. The evaluation of the test and fractographic results herein is limited to selected data sets. Further evaluation of the data in Volume VIII, including a statistical analysis, is recommended to better understand the effects of the test and specimen variables on the time-to-crack-initiation (TTCI) and the time-to-failure (TTF).

The main objectives of the Phase II test program were to:

1. provide fractographic data for evaluating the IFQ model for different conditions (e.g., material, stress level, spectrum, % load transfer, fastener type/fit, etc.),
2. develop test results and data needed to demonstrate the durability analysis methodology developed, and
3. provide a "fractographic data base" that could be used in the future to determine the IFQ for clearance-fit fastener holes.

Volume VIII documents the raw test results and the fractographic data and provides useful information (e.g., specimen dimensions, hole diameters, photographs, etc.) for future studies.

Since the "durability" of fastener holes is primarily concerned with relatively small cracks (e.g., ≤ 0.10 "), the evaluation in this section emphasizes the TTCI aspects more than the TTF. TTCI and TTF results for selected fractographic data sets (7475-T7351 aluminum) are compared for dog-bone specimens. A comprehensive evaluation of crack initiation origins and trends was made during Phase II; observations are discussed in this section. Test results for the complex splice specimen for the F-16 tear-down inspection are also presented. Overall conclusions and recommendations for the Phase II test program are presented in Section 6.6.

Several variables included in the test program were material, load spectrum, stress level, fastener diameter/type, percent bolt load transfer, and specimen geometry (width and thickness). Many of the factors which can influence fatigue life have been studied [e.g., 43-46].

6.2 DOG-BONE SPECIMENS

6.2.1 TTCI Comparisons

TTCI comparisons are presented in Tables 10 and 11 for selected fighter and bomber fractographic data sets, respectively. The fractographic data sets listed in Tables 10 and 11 were the key data sets used in Phase II to evaluate the IFQ model for countersunk, clearance-fit fastener holes. The minimum, average and maximum TTCI values are given for each data set, along with the sample size used. In some cases, the number of TTCI samples for a data set may be less than the total number of specimens tested.

The TTCI values for the selected data sets were determined by interpolation from the fractographic data given in Ref. 6. With a few exceptions, only those specimens with fractographic data encompassing $a_0=0.03$ " were used to determine the minimum, average and maximum TTCI values. Some results were used when the last fractographic crack size was near 0.03". Also, only the fractographic results for the largest fatigue crack per specimen were used.

For comparison, the minimum, average and maximum TTCI results from Table 10 are plotted in Figs. 23-25 for the "fighter" data sets (F-16 400-hour spectrum). In a similar manner, the TTCI results from Table 11 are plotted in Figs. 26-28 for the "bomber" data sets (B-1 spectrum). In Figs. 23-28, the average TTCI values are indicated by the open circles and the sample size used is shown in parentheses.

6.2.2 Fatigue Life Comparisons

Average fatigue life is plotted as a function of the maximum baseline stress for selected data sets in Fig. 29 and 30 for the F-16 400 hour spectrum and B-1 bomber spectrum, respectively. These plots are based on results from Ref. 6.

In general the results plotted in Fig. 29 and 30 appear to be fairly consistent. For example, the average fatigue life decreases as the stress level increases. Also the results tend to show that for a given stress level the fatigue life decreases as the percentage of load transfer increases. In Fig. 29, for example, the average fatigue lives for the 40%, 30%, 15%, and 0% load transfer data sets are in the order expected. Exceptions

TABLE 10 Comparison of TTCI Results for Key Fighter Data Sets (7475-T7351 Aluminum)

DATA SET	LOAD TRANSFER	SPECIMEN		FASTENER		SPECTRUM	σ (ksi)	TTCI (FLT HRS); $a_0=0.03"$			
		TYPE	NO. TESTED	TYPE	DIA (IN.)			MIN	AVE.	MAX.	SAMPLE SIZE
AFRLR4	0% ↓	1A	10	MS90353	1/4	F-16 400 Hr.	32	13755	15821	18959	7
AFRLR3		1A	7	↓	3/16		32	9926	14231	18875	5
AFMR4(A)		1A	10	↓	1/4		34	6148	13554	17624	8
AFMR4		1A	10	NAS1580	1/4		38	6181	10062	14471	10
AFHR4(A)		1A	10	MS90353	1/4		38	2595	9400	15520	10
AFHR4(B)		1B	9	↓	1/4		38	7818	13353	16200	6
AFXLR4	15% ↓	2A	11	↓	1/4		32	4246	11609	22766	10
AFXLR3		↓	12	↓	3/16		32	5893	10713	17001	12
AFXMR4		↓	10	↓	1/4		34	2947	7651	13148	8
AFXMR3		↓	9	↓	3/16		34	4965	7283	12000	9
AFXMC4		↓	10	NAS1580	1/4		34	4515	10328	15171	10
AFXHR4		↓	10	MS90353	1/4		38	2112	4747	9200	9
AFXHR3		↓	10	↓	3/16		38	1955	3825	5831	9
AFYLR4	30% ↓	3	9	↓	1/4		30.1	11783	17954	22822	5
AFYMR4		3	10	↓	↓		34	6927	9659	11846	6
AFYHR4		3	10	↓	↓		38	3723	7154	10364	7
AFZMR4	40% ↓	4	6	↓	↓		34	4648	8919	11433	6
AFZHR4		4	9	↓	↓		38	686	2216	4332	9

Notes

1. MS90353 = Countersunk, blind, pull-through rivet
2. NAS1580 = Countersunk bolt
3. σ = Gross stress
4. TTCIs from Ref. 6
5. Ref. Fig. 16 for specimen types

TABLE 11 Comparison of TTCl Results for Key Bomber Data Sets (7475-T7351 Aluminum)

DATA SET	LOAD TRANSFER	SPECIMEN		FASTENER		SPECTRUM	σ (ksi)	TTCI(NO. OF FLTS) $a_0=0.03"$				SAMPLE SIZE
		TYPE	NO. TESTED	TYPE	DIA(IN.)			MIN.	AVE.	MAX.		
ABLR4	0% ↓	1A	6	MS90353	1/4	B-1	34	3428	4317	5297	5	
ABLR4 (A)		1A	10				36	1059	1575	2327	8	
ABLR4 (B)		1B	11				36	1583	2869	3729	9	
ABMR4 (A)		1A	11				38	1544	1942	2485	10	
ABMR4 (B)		1B	11				38	708	1431	2378	9	
ABHR4 (A)		1A	10				40.8	999	1328	1740	10	
ABHR4 (B)		1B	11			40.8	477	907	1677	10		
ABXLR4	15% ↓	2A	11				36	688	1390	2000	10	
ABXLC4		2A	12	NAS1580			36	626	1177	1556	8	
ABXHR4		2A	11	MS90353			40.8	103	732	1892	9	
ABXHC4		2A	10	NAS1580			40.8	301	562	1229	9	
ABYLR4	30% ↓	3	10	MS90353			34	1130	2306	3581	7	
ABYMR4		3	10		3/16		36	878	1295	2189	8	
ABYMR3		3	10				36	503	1365	2131	10	
ABZLR4	40% ↓	4	10		1/4	↓	34	854	1965	2691	7	
ABZHR4		4	10		1/4			38	399	886	2151	8

Notes

1. MS90353 = Countersunk, blind, pull-through rivet
2. NAS1580 = Countersunk bolt
3. σ = Gross stress
4. TTCl's from Ref. 6
5. Ref. Fig. 16 for specimen types
6. 1280 flights = 13500 flight hours.

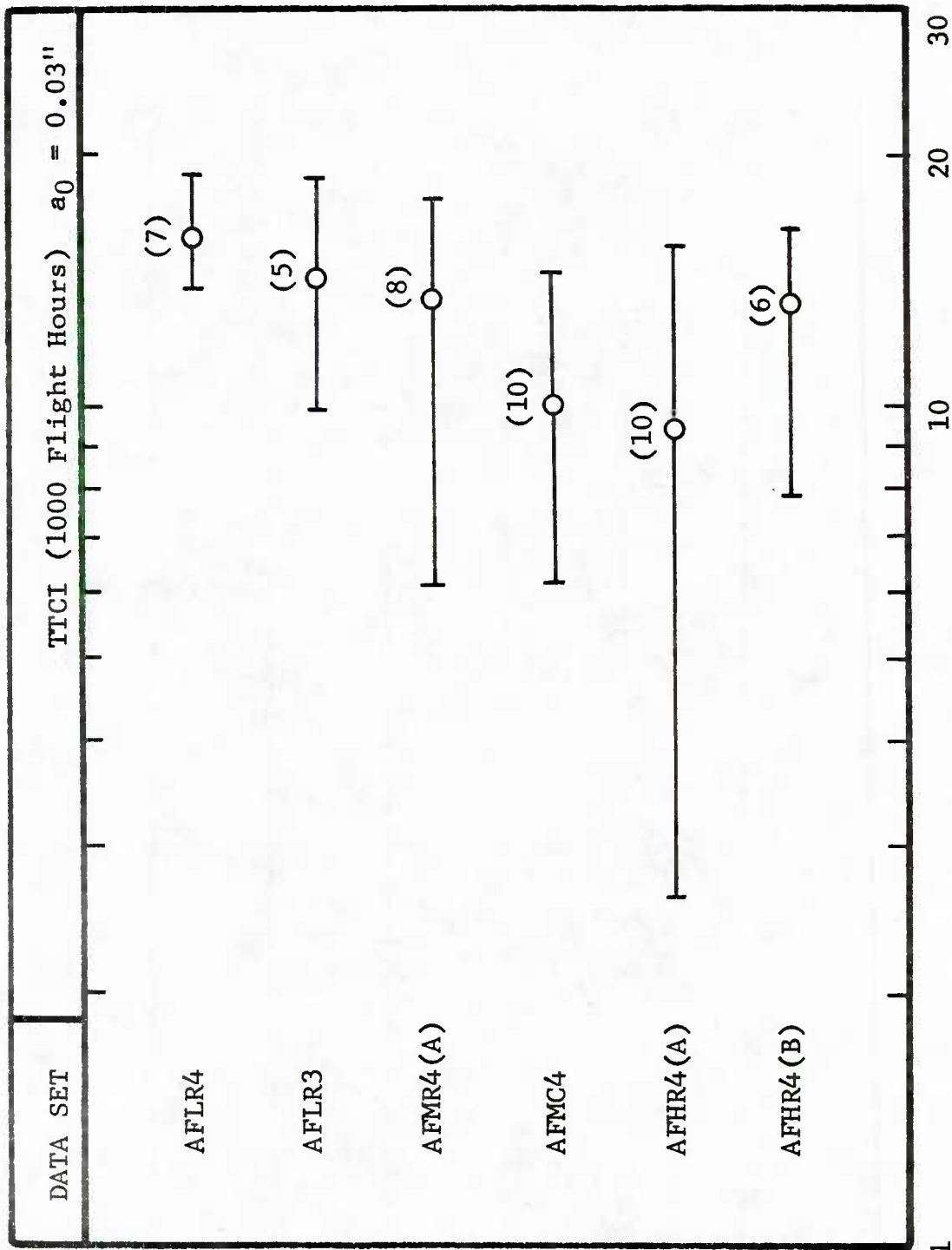


Fig. 23 TTCI Comparisons for Selected No-Load Transfer Data Sets
(7475-T7351 Aluminum; F-16 400-Hour Spectrum; $a_0 = 0.03$)

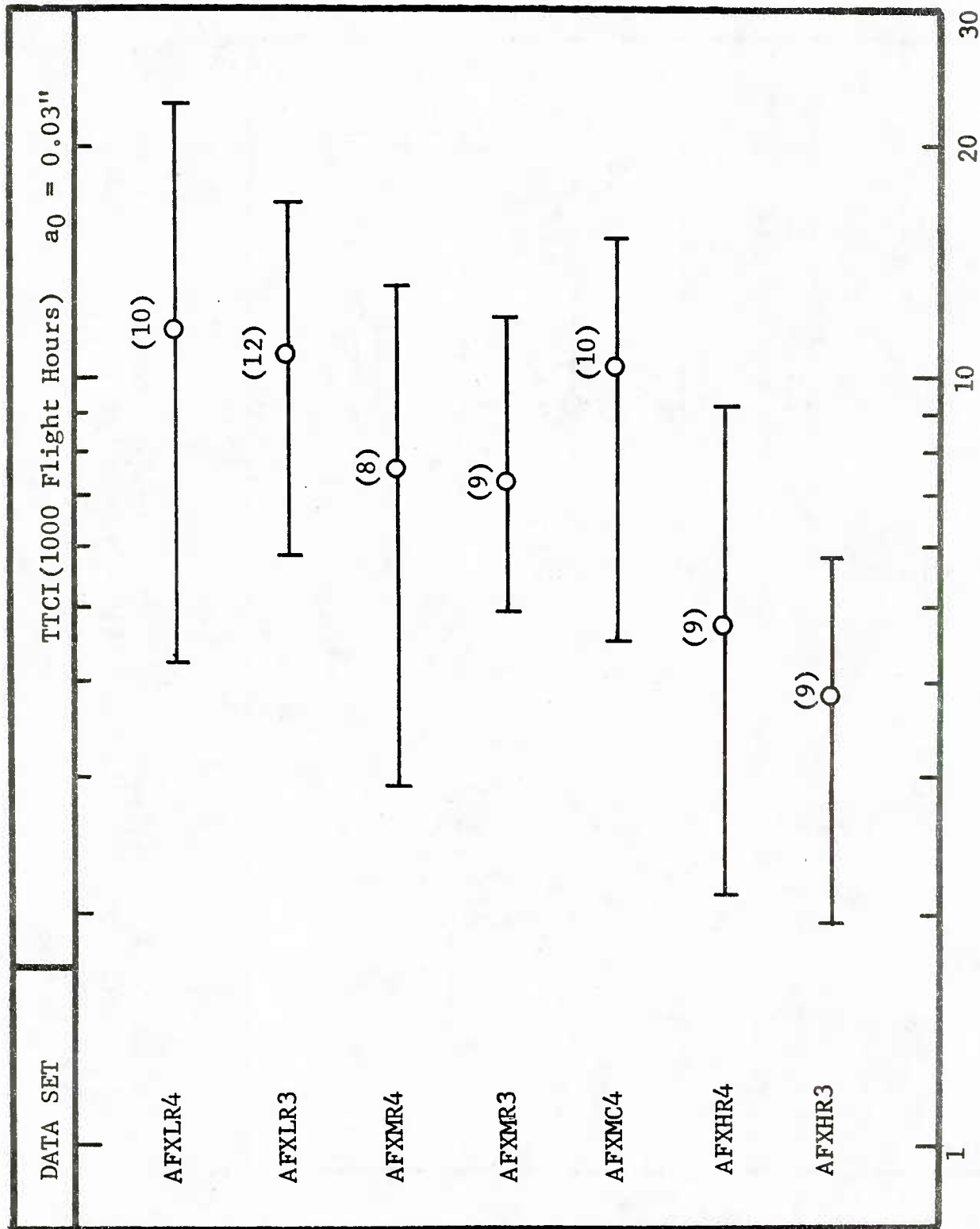


Fig. 24 TTCI Comparisons for Selected 15% Load Transfer Data Sets (7475-T7351 Aluminum; F-16 400-Hour Spectrum; $a_0 = 0.03''$)

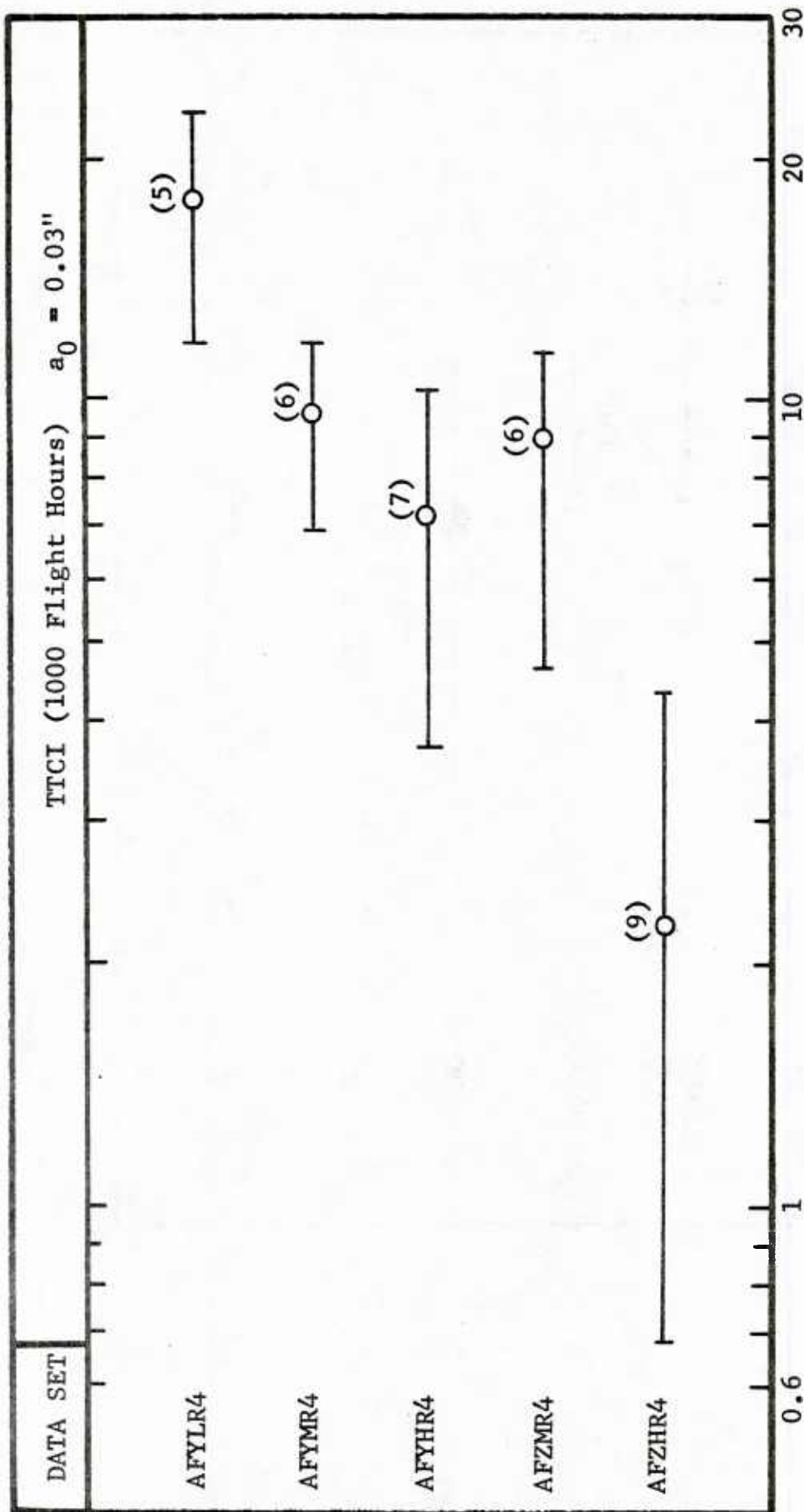


Fig. 25 TCI Comparisons for Selected 30% and 40% Load Transfer Data Sets
(7475-T7351 Aluminum; F-16 400-Hour Spectrum; $a_0 = 0.03''$)

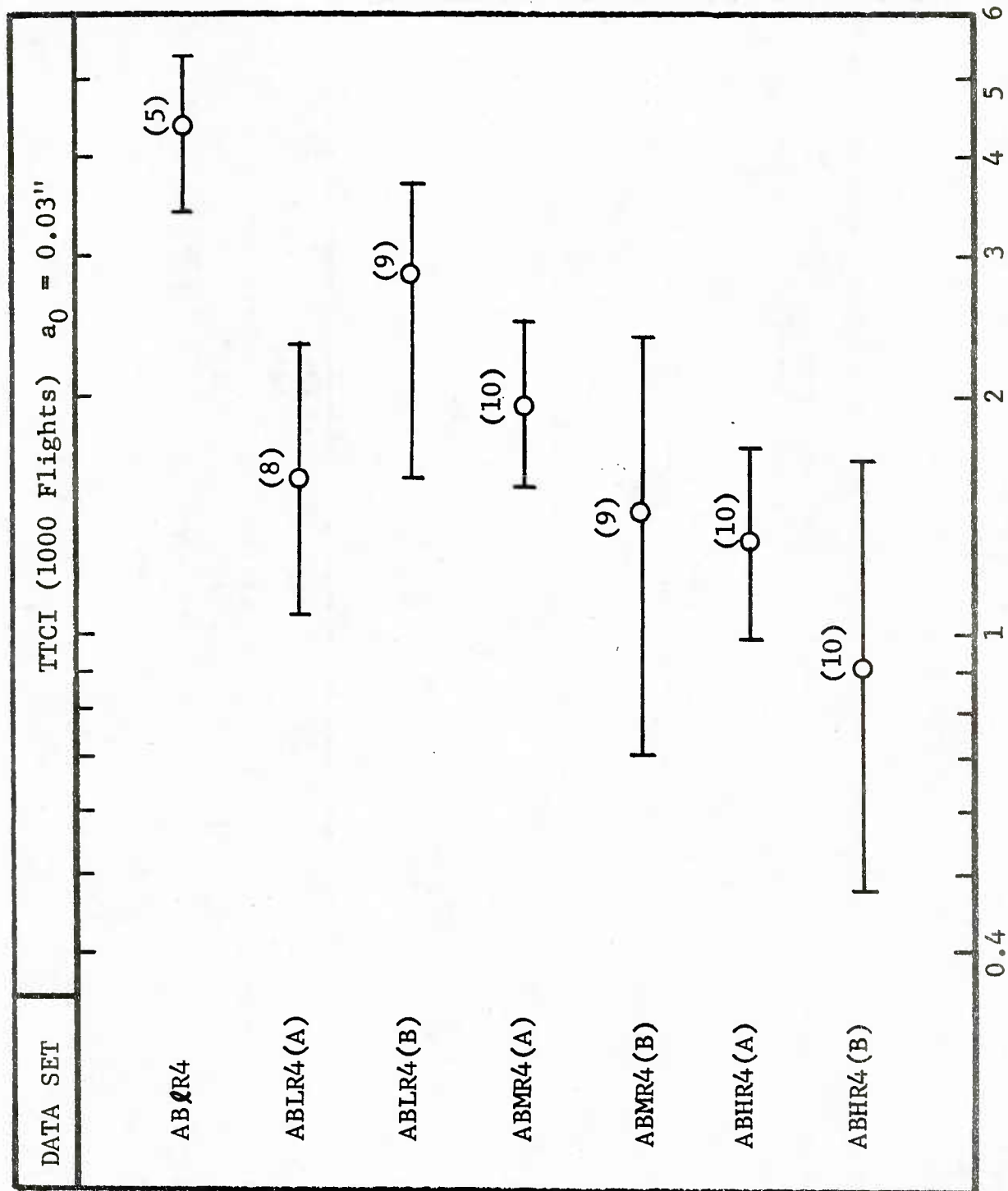


Fig. 26 TTCI Comparisons for Selected No-Load Transfer Data Sets
(7475-T7351 Aluminum; B-1 Bomber Spectrum; $a_0 = 0.03$)

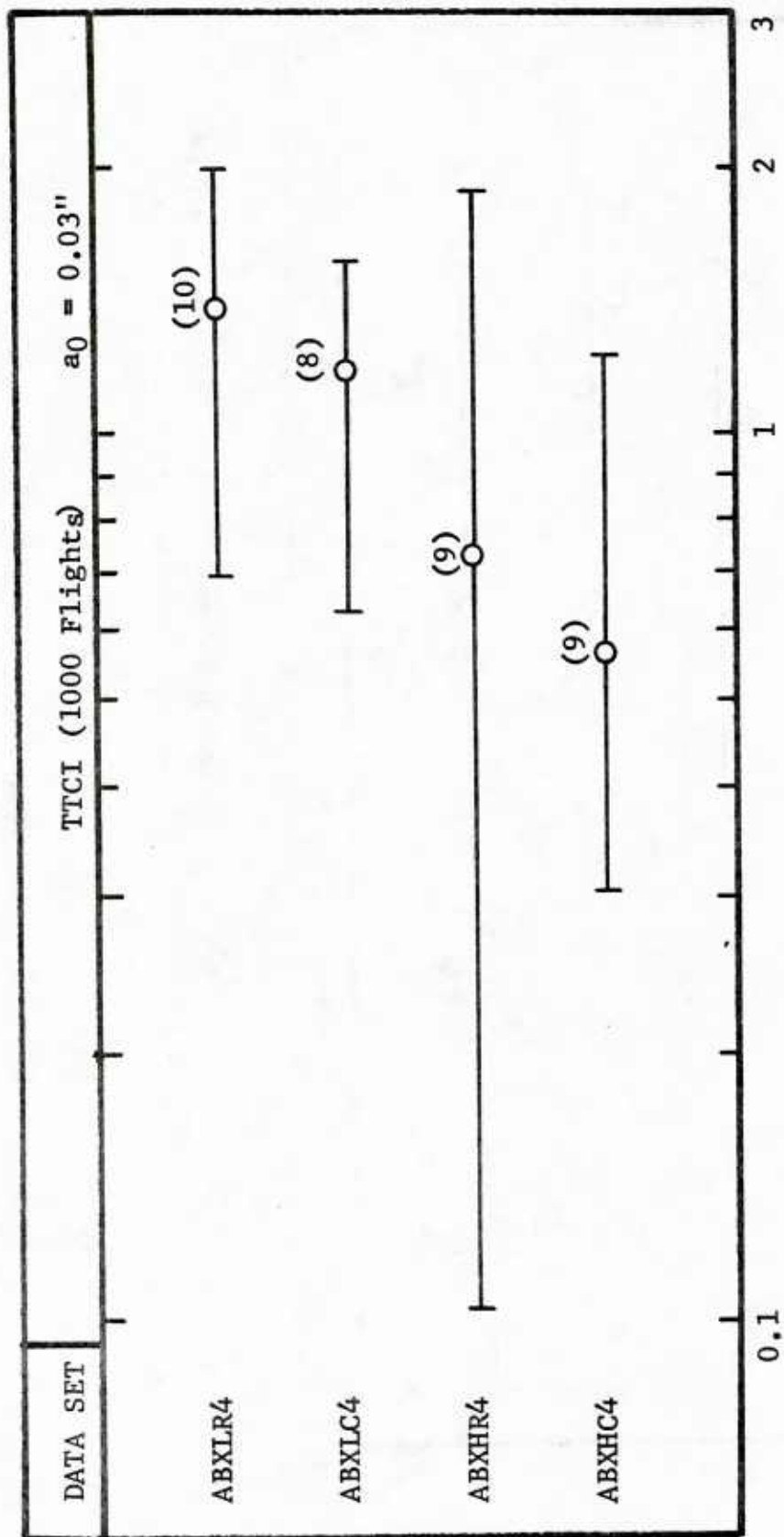


Fig. 27 TTI Comparisons for Selected 15% Load Transfer Data Sets
(7475-T7351 Aluminum; B-1 Spectrum; $a_0 = 0.03$ ")

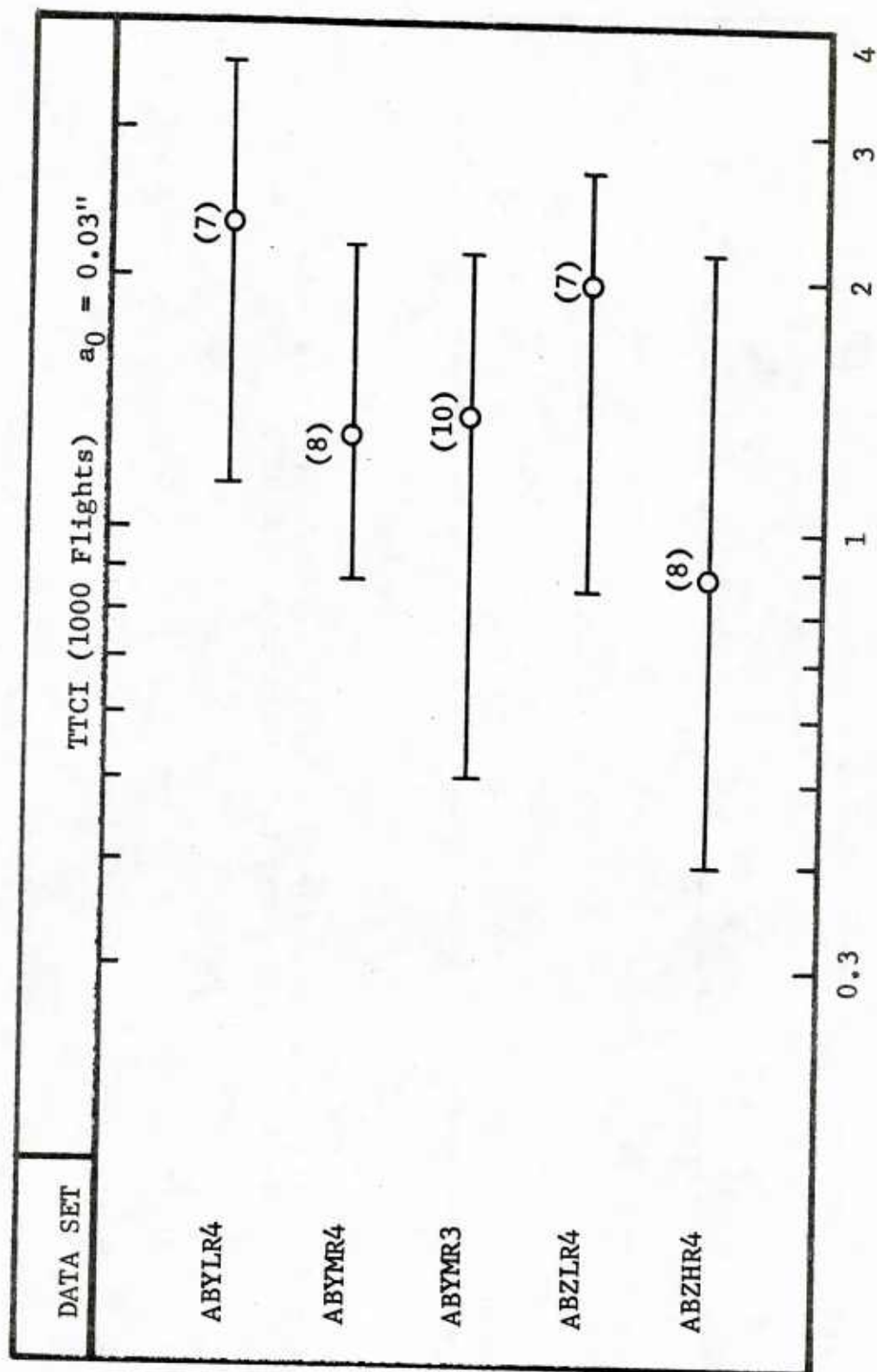


Fig. 28 TTCI Comparisons for Selected 30% and 40% Load Transfer Data Sets (7475-T7351 Aluminum; B-1 Bomber Spectrum; $a_0 = 0.03$)

**7475-T7351 ALUMINUM
400 HR BLOCK F-16 FIGHTER SPECTRUM**

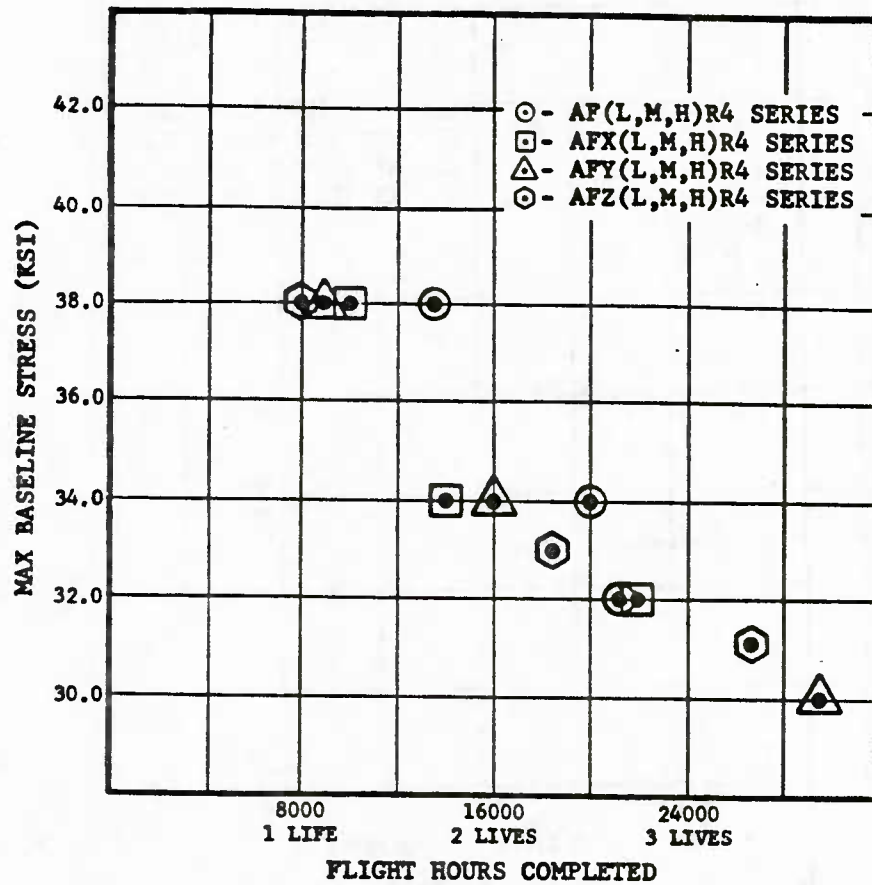


Fig. 29 Fatigue Life as a Function of Stress Level for F-16 400-Hour Spectrum

7475-T7351 ALUMINUM
B-1 BOMBER SPECTRUM

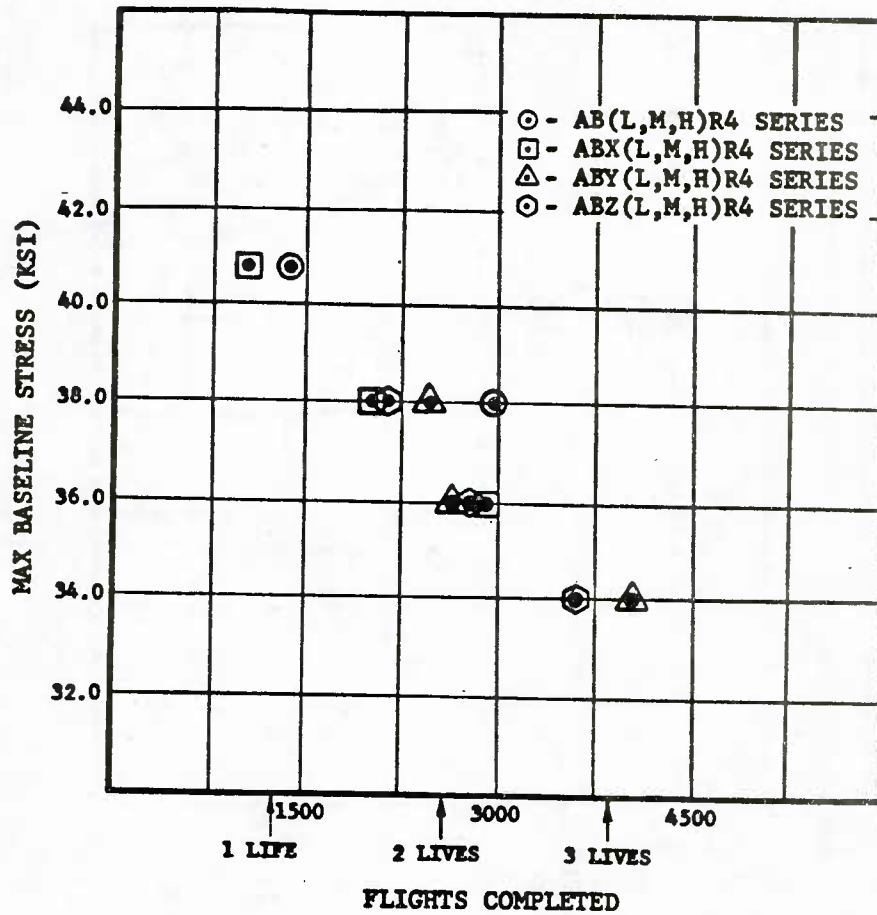


Fig. 30 Fatigue Life as a Function of Stress Level for B-1 Bomber Spectrum

are also shown in Fig. 29 at stress levels of 32 and 34 ksi and in Fig. 30 at stress levels of 38 and 36 ksi. For example, in Fig. 29 the average fatigue life for the 30% load transfer data set (AFYMR4) is larger than that for the 15% load transfer data set (AFXMR4) at the 34 ksi stress level. Further analyses are required in this case to evaluate the effects of scatter and percent load transfer on fatigue life.

6.2.3 Test Results for D6ac Steel

Seventeen D6ac no-load transfer specimens (Fig. 21) were tested using the F-16 400-hour block spectrum. All holes were 1/4-inch diameter with NAS-6204 straight shank bolts installed. Test results are summarized in Table 12 and further details, including fractographic results, are given in Ref. 6. The size of the largest fatigue crack in a fastener hole and the corresponding number of flight hours to failure are shown for each specimen in Table 12. Fatigue crack initiation sites are also indicated. The fatigue life as a function of stress level is shown in Fig. 31.

6.2.4 Discussion

Test results for the dog-bone specimens are discussed in this section in terms of the specimens and test variables. This discussion is limited to general observations and understandings reached during Phase II. Further evaluation of the test results [6] is recommended.

The "load-transfer" specimens (see Figs. 18-20) were designed for 15%, 30%, and 40% load transfer through the fasteners. These specimens were designed by equalizing the axial deformation for the upper and lower dog bones between the lug pin and fastener. Pins and fasteners were also assumed to be rigid and to "perfectly fit" their mating holes. Due to normal hole size variations and clearance fits, the actual percentage of load transfer obtained varied from specimen-to-specimen and depended on the magnitude of the applied load. A typical free-body diagram is shown in Fig 22.

Table 12 Test Results for D6ac Steel Specimens

Data Set ①	Specimen Number	Max. Baseline Stress (ksi) ②	Flight Hours Completed Before Failure	Final Crack Size (In)	Crack Initiation Site ③
SFLP4	714	85	> 16,000	< 0.050	----
SFLP4	708 709 710 711 712 713	100 ↓	8,406 6,346 12,035 8,748 10,759 10,278	0.2487 0.2443 0.1836 0.3008 0.2357 0.2100	Corner, Bore Corner Bore Bore Bore Bore
SFMP4	715 716 717 718 719	110 ↓	5,469 6,806 8,439 4,835 6,806	0.2558 0.1768 0.2042 0.1881 0.2152	Bore Bore Bore Corner Bore
SFHP4	707 720 721 722 723	125 ↓	1,878 2,806 2,992 3,959 4,663	0.1935 0.1631 0.1612 0.2063 0.2456	Corner Corner Bore Bore Bore

Notes

① Ref. 21 pp. B-125 - B-133 for fractography

② Gross section; F-16 400 hour spectrum

③ Ref. Fig. 34

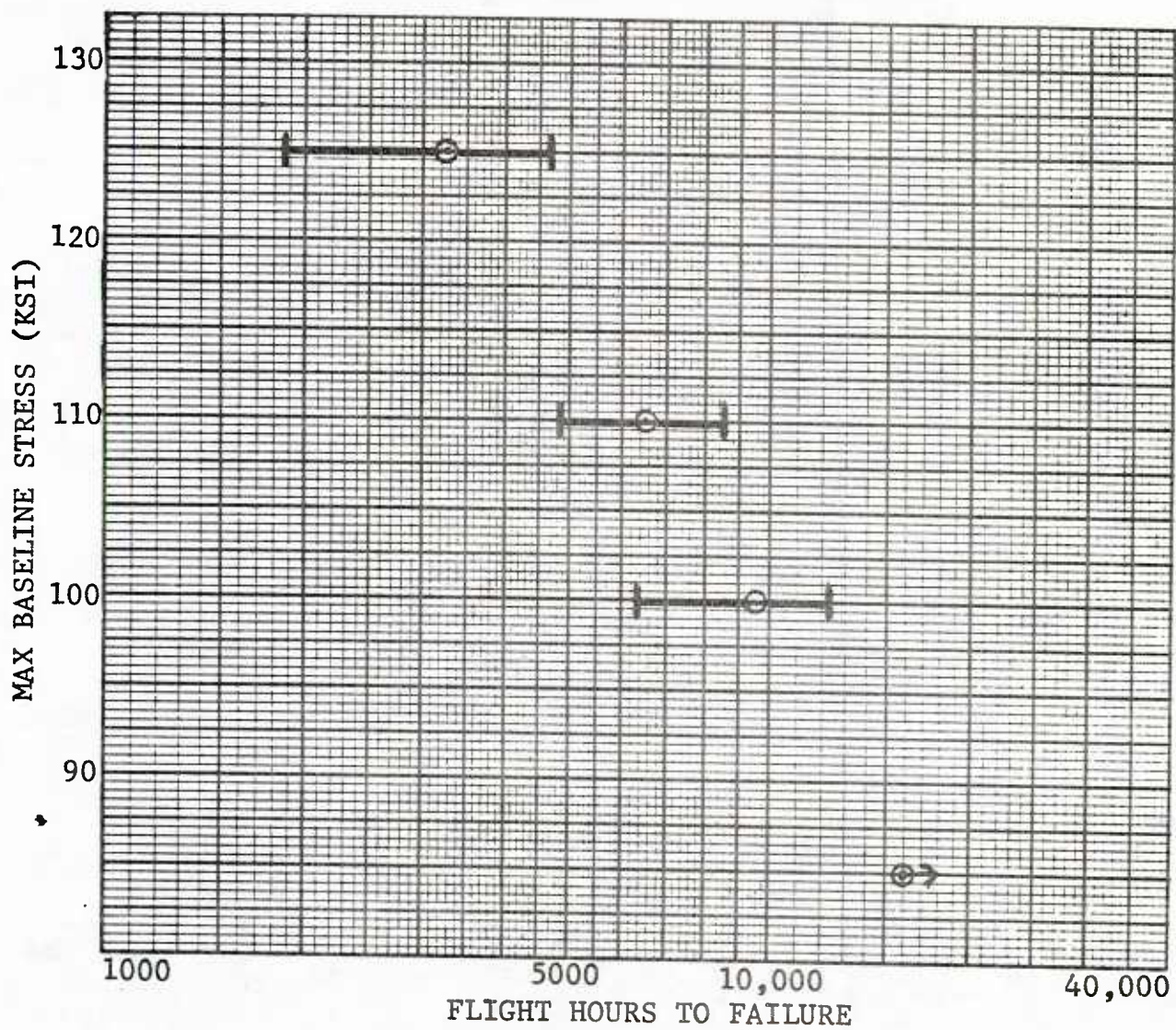


Fig. 31 Fatigue Life as a Function of Stress Level for D6ac Steel Specimens (F-16 400-Hour Spectrum)

The lug end dimensions for the different percent load transfer specimens were determined using the conditions described above. Since the test load frames were limited to a maximum pin-to-pin dimension of 13.0", the lug ends for the 30% and 40% load transfer specimens had to be "bulkier" than those for the 15% load transfer specimens. As a result, for the same fastener fits, the 30% and 40% load transfer specimens required a larger applied load than the 15% load transfer specimens before the bolts could start transferring load. Since the magnitude of the specimen loads varied depending on the load spectrum and stress level, the actual percentage of load transferred through the bolts also varied.

The 15% load transfer specimens seemed to perform very well for the Phase II tests. However, the 30% and 40% load transfer specimens did not reach the design percent load transfer consistently. The reverse, double dog-bone type specimen for bolt load transfer does not assure the "design" percent bolt load transfer will be obtained for each load in the spectrum. To assure the desired percent bolt load transfer, the specimen should be designed to transfer load directly to the bolt rather than indirectly by relative deformations.

The actual percent bolt load transfer in aircraft structure also varies depending on the fastener type/fit and the applied load levels. In order to quantitatively assess the effects of load transfer on the TTCI and TTF, the percent of load transfer must be controlled. Further tests and analyses are required to develop a better understanding of the effects of bolt load transfer on the TTCI and TTF.

Two different types of countersunk fasteners were used for the test program. This included the MS-90353 blind, pull-through rivet (3/16" and 1/4" dia.) and the NAS-1580 bolt (1/4" dia.). When the MS-90353 rivet is installed, it acts more like a clearance-fit bolt because the shank of the rivet does not fill the hole like a typical "bucked" rivet. In terms of clearance between fastener and hole, for the nominal 1/4-inch diameter MS-90353 steel rivet, the diameter can range from 0.258-inch to 0.260-inch while the hole diameter according to General Dynamics Specification M-198 is 0.260-inch to 0.263-inch. This allows a hole tolerance ranging from 0 to 0.005-inch clearance. For the nominal 1/4-inch diameter NAS-1580 bolt, the fastener diameter can range from 0.2485-inch to 0.2495-inch while the hole diameter varies from 0.250-inch to 0.254-inch. This allows a hole tolerance from 0.0005-inch to 0.0055-inch clearance, therefore, a slightly sloppier fit can be obtained with the NAS-1580 bolt. In aluminum alloy load transfer specimens, a decrease in fatigue life with increase in clearance fit has been

observed in clearance fit holes [47]. In general, specimens with the larger diameter MS-90353 rivet had slightly longer fatigue lives than the smaller diameter rivet. Clamp-up normally increases for larger diameters with an accompanying increase in fatigue life. Urzi [44] has studied the effects of clamp-up on fatigue life and concluded that the fatigue life decreases as the stacking-thickness to fastener diameter ratio increases.

It has been shown [46] that as the countersink depth approaches the thickness of the material, the stress concentration factor, K_t , increases. For countersink depth/sheet thickness ratios greater than 0.5, K_t increases from a range of 2-4 to a range of 8-10. For our no load transfer specimens, this ratio was ~0.29 for the 0.375-inch coupons, and ~0.44 for the 0.250-inch thickness specimens, therefore little increase in stress concentration factor would be expected. Countersink depths were approximately the same for each type of 1/4-inch diameter fastener (0.105-inch with the MS90353 rivet and 0.111-inch with the NAS-1580 bolt). In the load-transfer coupon, the countersink depth/sheet thickness ratio was ~0.58 for the 1/4-inch diameter fasteners, therefore, a slight increase in K_t would be expected in this area.

For the same maximum baseline stress level, the fatigue life was longer for specimens tested using the B-1 bomber spectrum than for those tested using the F-16 400-hour block fighter spectrum. For example, at a maximum baseline stress of 34 ksi, the average fatigue life for the fighter spectrum tests was approximately 2 lives while specimens tested under the B-1 bomber spectrum survived approximately 3 lives.

Several specimens were tested using the F-16 500-hour random spectrum. This is the same spectrum used to test the F-16 durability test article, and is a little less severe than the F-16 400-hour block spectrum. Both 0% and 15% load transfer, 7475 aluminum specimens were tested. All specimens were fastened with the MS-90353 steel rivet. In many cases, failures did not occur during testing and only final crack sizes were recorded [6].

Specimens with two different widths and thicknesses were fatigue tested. No conclusions were reached on the effects of specimen thickness on TCI and TTF. However, the 1.5" wide specimens generally had slightly longer fatigue lives than the 2" wide specimens. The effects of scatter need to be investigated.

Two different aluminum alloys were tested in this program, 7475-T7351 and 2024-T851. Since both alloys are used on the F-16 aircraft, considerable in-house crack growth data have been generated [48]. In order to be compatible with results obtained for the "Fastener Hole Quality" program [41], more testing was done

using 7475-T7351 material than 2024-T851 aluminum. Considerable spectrum fatigue data on 2024-T851 has been obtained on two other programs [47,49].

Previous tests with an F-16 spectrum on 2124-T851 showed longer fatigue life than similar testing with 7475-T7651 material [50]. However, it has been shown that overaging the 7475-T651 alloy to the T7351 condition improves crack growth resistance under spectrum loading considerably at the expense of reduced yield strength [51].

6.3 COMPLEX SPLICE

Twenty-four complex splice specimens (Fig. 15) were fatigue tested using a B-1 bomber load spectrum. Specimens were tested without intermediate lateral support between the lug ends using servo-controlled, hydraulically-actuated load frames. This same specimen design, for a different aluminum alloy (2124-T851), had been previously tested with and without lateral support [42]. Results of the strain survey from Ref. 42 showed a negligible effect of the lateral support on the resulting strains.

Complex splice test results from Ref. 6 are summarized in Table 13. Fractographic results for fastener hole fatigue cracks, fastener hole dimensions, final crack sizes for the outer row fastener holes and other testing details are given in Ref. 6.

All specimens were fatigue tested to failure except one (CBS& 22 ksi; ref. Table 13). All failures occurred in the outer row of holes in the net section except for specimen number 731 (Table 13), which failed in the inner row of holes. Fretting appeared to be the major cause of failure in specimen 731.

Following the fatigue test, all fastener holes in the outer row of each specimen were inspected for fatigue cracks visually and by the eddy current technique. The size of the largest fatigue crack in each outer row fastener hole (10 holes per specimen) were measured [6]. A fractographic evaluation was then performed for the largest fatigue crack in any one of ten holes per specimen.

In Table 13 the size of the largest fatigue crack per specimen in an outer row fastener hole and the corresponding number of flights are shown. The location of the fastener hole with the largest fatigue crack and fatigue crack initiation sites are also noted. Crack initiation sites were difficult to determine in those cases where cracks from adjoining holes overlapped. Also, locations of the fatigue crack origins varied, ranging from the countersink-bore intersection area to the faying surface.

TABLE 13 Complex Splice Test Results

① DATA SET	SPECIMEN NO.	BASELINE STRESS ② (ksi)	NO. FLTS. COMPLETED ③	FINAL CRACK SIZE (IN) ④	⑤ HOLE NO. (OUTER ROW)	FATIGUE CRACK ⑥ ORIGIN LOCATION
CBSL	726	22	3840	0.0276	3	-----
CBSL ↓	725	25 ↓	2273	0.4142	2	(C.S.-B) Intersection
	727		1319	0.2711	2	(C.S.-B) "
	728		1769	0.2875	4	Countersink Area
	729		1979	0.3087	4	Corner
	730		2079	0.2698	4	Bore
	731		2304	0.1690	4	Bore
	732		2159	0.3434	3	Bore
	733		1954	0.3600	4	Bore
	734		2589	0.3253	2	-----
	735		1539	0.3166	4	-----
	736		1839	0.2919	2	Corner (C.S.-B) Intersection
CBSH ↓	724	30 ↓	1079	0.2070	3	Countersink Area
	737		759	0.2283	2	Bore
	738		769	0.2849	4	(C.S.-B) Intersection
	739		899	0.2572	3	Multi: Bore
	740		3162	0.2955	4	Corner
	741		827	0.3010	2	(C.S.-B) Location
	742		779	0.3183	2	(C.S.-B)
	743		1059	0.3037	4	-----
	744		939	0.2613	4	(C.S.-B) Location
	745		729	0.2854	2	Corner, (C.S.-B)
	746		769	0.2724	4	Bore
	747		979	0.2570	4	Bore

NOTES

- ① Ref. 6, pp C-175-C-186 for fractography
- ② Gross section stress at outer row of fasteners
- ③ B-1 Bomber Spectrum: 1280 flights=13500 flight hours=1 service life
- ④ Largest fatigue crack in outer row/specimen measured in direction of crack propagation
- ⑤ Fastener hole with largest fatigue crack at end of test. Ref. Fig 38 for locations
- ⑥ Ref. Fig. 34

The number of flights to failure versus the maximum baseline stress is plotted in Fig. 32 for each specimen tested. Except for one outlier at the 30 ksi stress level (specimen no. 740; see Table 13), the results look very consistent.

Crack growth rates were much faster at the stress levels tested than would have been expected based on the load-transfer coupon data. Possible explanations for this behavior are:

1. During testing significant lateral bending was observed in the lug plates near the outer row of fastener holes. The resulting bending stress on the lug plate at the outer row of fastener holes could have significantly increased the localized stress.

2. A significant increase in the amount of fretting was observed in the complex splice specimens compared to the load transfer specimens.

6.4 CRACK INITIATION ORIGINS AND TRENDS

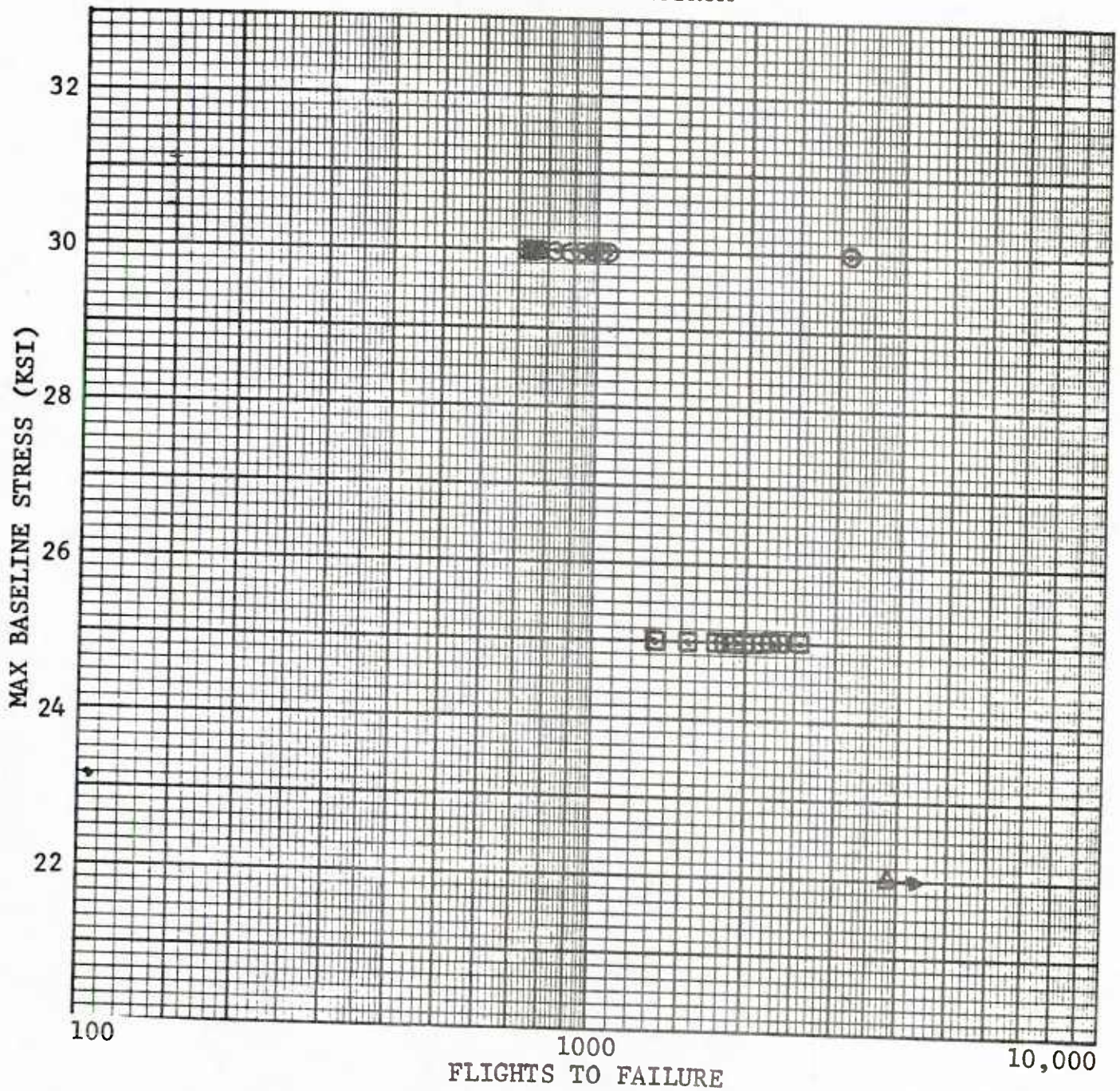
Fatigue crack origins and trends were discussed in this section for the no-load (0%), 15%, 30%, and 40% load transfer specimens and for the complex splice specimens. These observations are based on the comprehensive fractographic evaluations performed during Phase II [6]. All fracture surfaces considered were examined to determine, if possible, the origin of the dominant fatigue crack. In many cases, fatigue crack origins were difficult to determine due to the coalescence of multiple fatigue cracks (Fig. 33).

A coding system, shown in Fig. 34, was developed to identify fatigue crack origins for straight-bore and countersunk fastener holes. This system applies to test specimens with and without a bolt load transfer. For example, in Fig 34 the coding for the no-load transfer specimens applies to only one section and the one with the applicable type of fastener hole (i.e., countersunk or straight-bore).

6.4.1 No-Load Transfer Specimens

Most of the observed fatigue crack origins were randomly distributed in the bore of the hole. In general, origin locations in specimens tested with the fighter spectrum were consistent with those tested using the B-1 bomber spectrum.

COMPLEX SPLICE SPECIMEN
B-1 BOMBER SPECTRUM



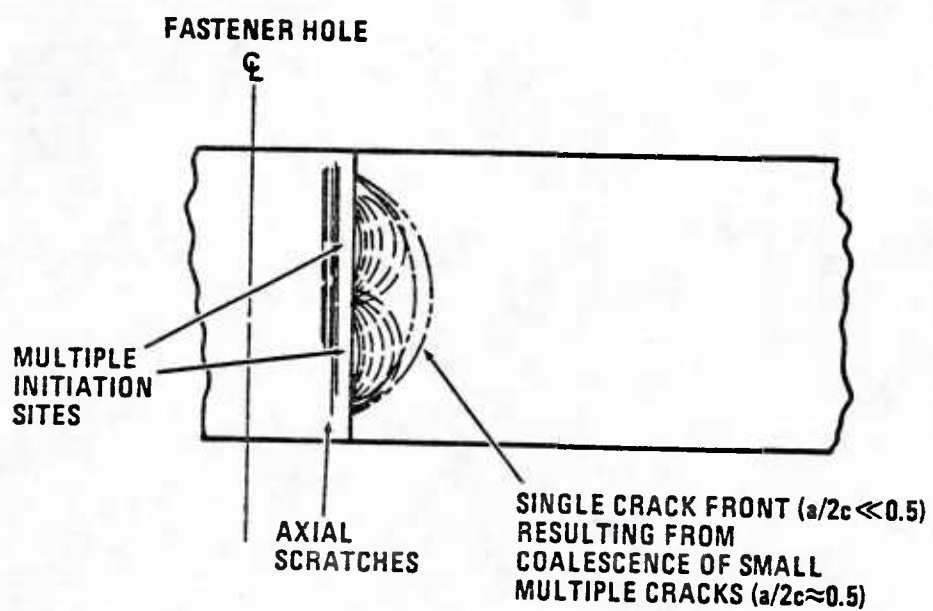
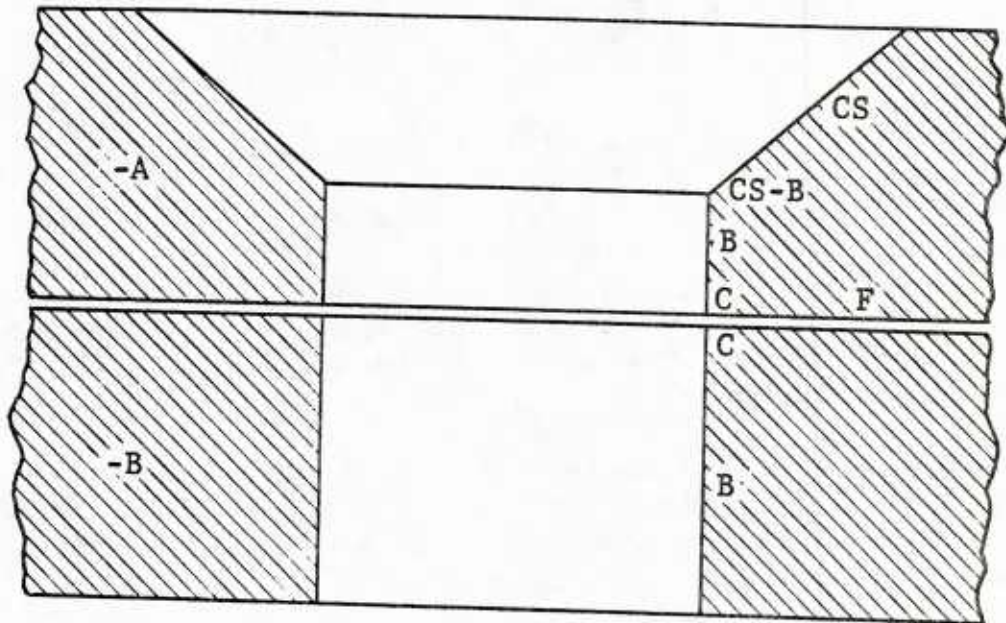


Fig. 33 Coalescence of Multiple Cracks to Form a Single Large Crack



CS - Countersink Region
CS-B - Countersink-Bore Intersection
B - Bore of the Hole
C - Corner
F - Faying Surface

Fig. 34 Fatigue Crack Origin Location Designations

Fatigue cracking was distributed between the countersink and straight bore portions of the hole. Typical crack origins are shown in Fig. 35. Similar trends were observed in Ref. 41 for straight-bore holes.

Early fatigue failures appeared to be due to: (1) multi-initiation sites coalescing to cause rapid crack propagation, (2) large initiation sites where crack growth is unstable until an $a/2c$ ratio of 0.5 is obtained, and (3) large fatigue cracks on opposite sides of a fastener hole.

6.4.2 15% Load Transfer Specimens

Several conclusions can be made about crack origins and failure modes in the 15% load transfer specimens.

1. Most fatigue crack initiation sites were located at or near the fastener hole-faying surface intersection. Typical crack origins are shown in Fig. 36.

2. Failures frequently occurred in the hole section containing the countersink. The countersink depth/section thickness ratio was greater than 0.5. Therefore, a slight increase in stress concentration would be expected in this area.

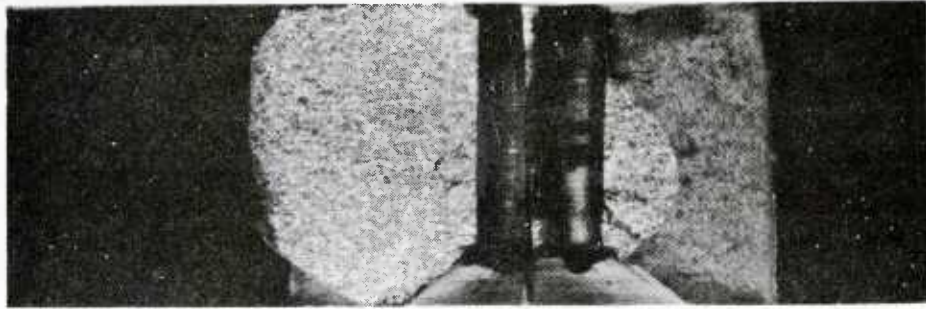
3. Consistent with results obtained from no load transfer specimens, load transfer specimens with multiple initiation sites also had shorter fatigue lives. In general, the multi-origins caused a broader crack front at an earlier stage of propagation. An example of a corner crack converging with a crack in the bore of the hole is shown in Fig. 37. Again, as was found in no-load transfer specimens, faster crack growth rate and earlier fatigue failure was observed in holes with large cracks on opposite sides of the hole.

4. Similar crack origins and trends were observed for the specimens tested in Ref. 41.

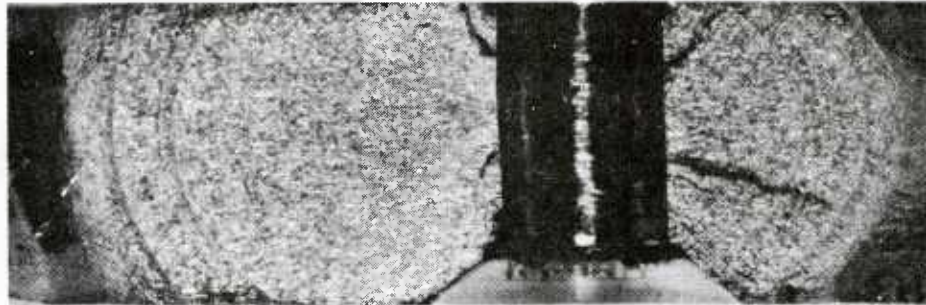
5. Since a surface treatment was not applied to the faying surfaces, some fatigue damage due to fretting occurred. Fretting is normally a more serious problem at low fatigue stresses, since at higher stresses cracks initiate rapidly even without fretting. No significant difference was observed in the failure modes of the 15% load transfer specimens at two different stress levels (i.e., 32 ksi and 40.8 ksi).

F-16 400 HOUR SPECTRUM
NO LOAD TRANSFER

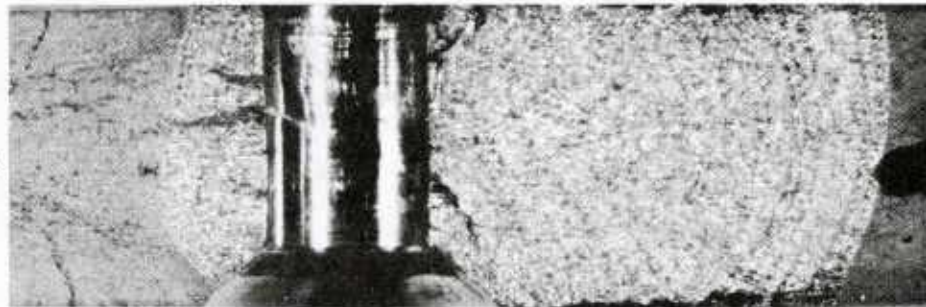
99A
32 KSI



99B



100A
32 KSI



100B

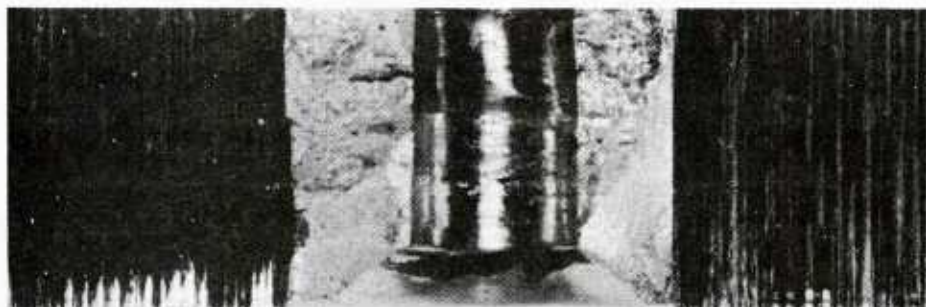
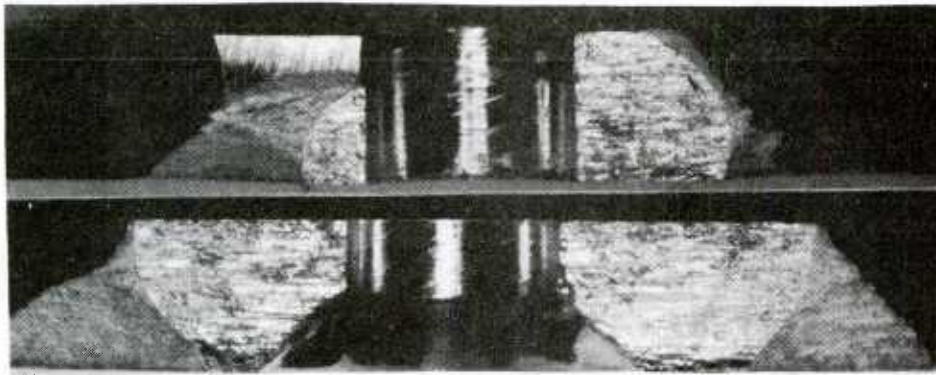


Fig. 35 Typical Fatigue Crack Origins in No-Load Transfer Specimen



232TA

232HB

Fig. 36 Typical Fracture Surface for 15% Load Transfer Specimen (ABXMR4(A); $\sigma = 38\text{ksi}$; B-1 Bomber Spectrum)

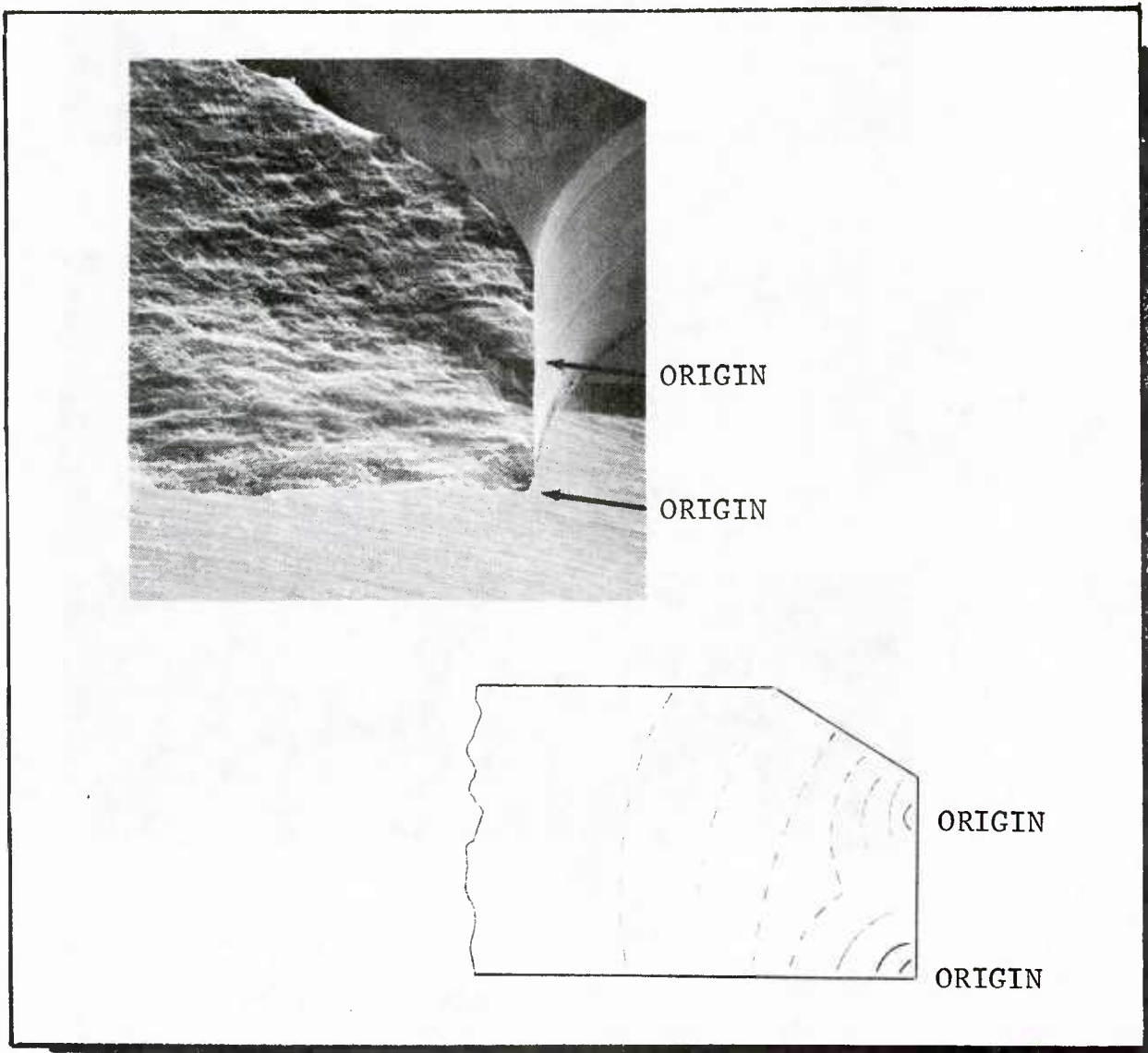


Fig. 37 Convergence of Crack Fronts Causing Rapid Crack Growth

6.4.3 30% and 40% Load Transfer Specimens

Fatigue crack initiation sites varied in these specimens. Many cracks originated at or near the fastener hole-faying surface intersection. A large number were also found at or near the countersink-bore intersection. Several early failures were due to broad origins around the countersink-bore intersections.

In a few of the 40% load transfer specimens (AFZLR4, AFZMR4, ABZLR4, and ABZMR4), cracks initiated on the faying surface rather than in the fastener hole.

6.4.4 Complex Splice

Fatigue crack initiation sites were difficult to determine when cracks from adjacent holes overlapped. Also fatigue crack origins varied, ranging from the countersink-bore intersection area to the faying surface (see Table 13).

Most of the largest fatigue cracks in the outer row of fastener holes occurred in the three holes near the center (i.e., hole number 2, 3, 4, in Fig. 38). In 20 out of 24 specimens, the largest fatigue crack in the outer row of fastener holes occurred in either hole number 2 or 4 (ref. Fig. 38 and Table 13).

Considerable fretting was observed in most specimens. In two cases, surface cracks were initiated on the faying surface away from the bore of the hole.

6.5 F-16 LOWER WING SKIN TEAR-DOWN INSPECTION

The full-scale F-16 wing box structure in Fig. 39 was fatigue tested under the F-16 durability certification program [52,53]. Both the right and left hand wing boxes were fatigue tested the same way (i.e., lab air, same load spectrum, stress levels, etc.) using the F-16 500-hour spectrum.

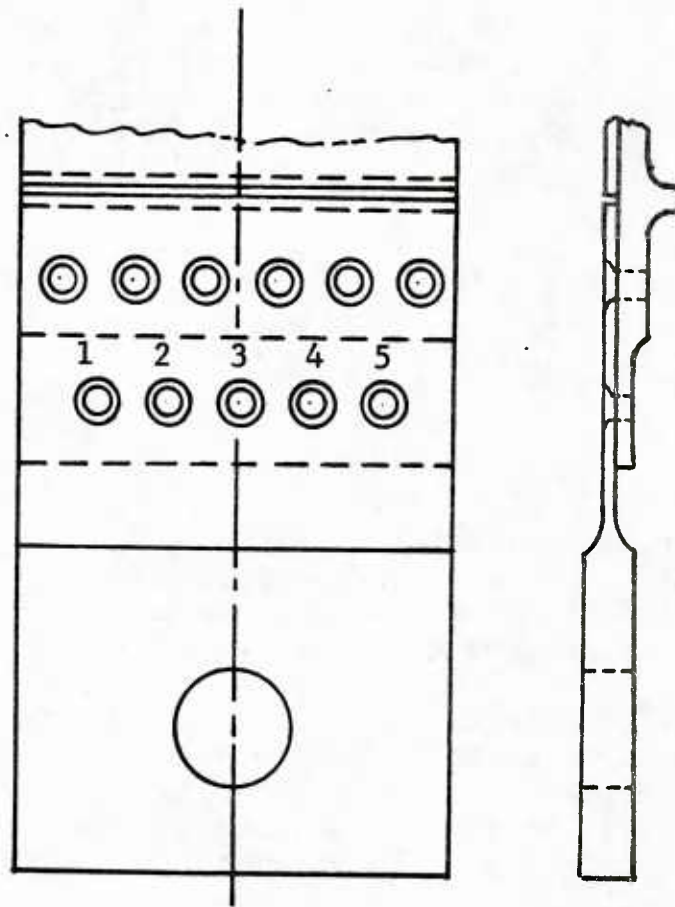


Fig. 38 Identification of Fastener Holes in Outer Row of Complex Splice Specimen

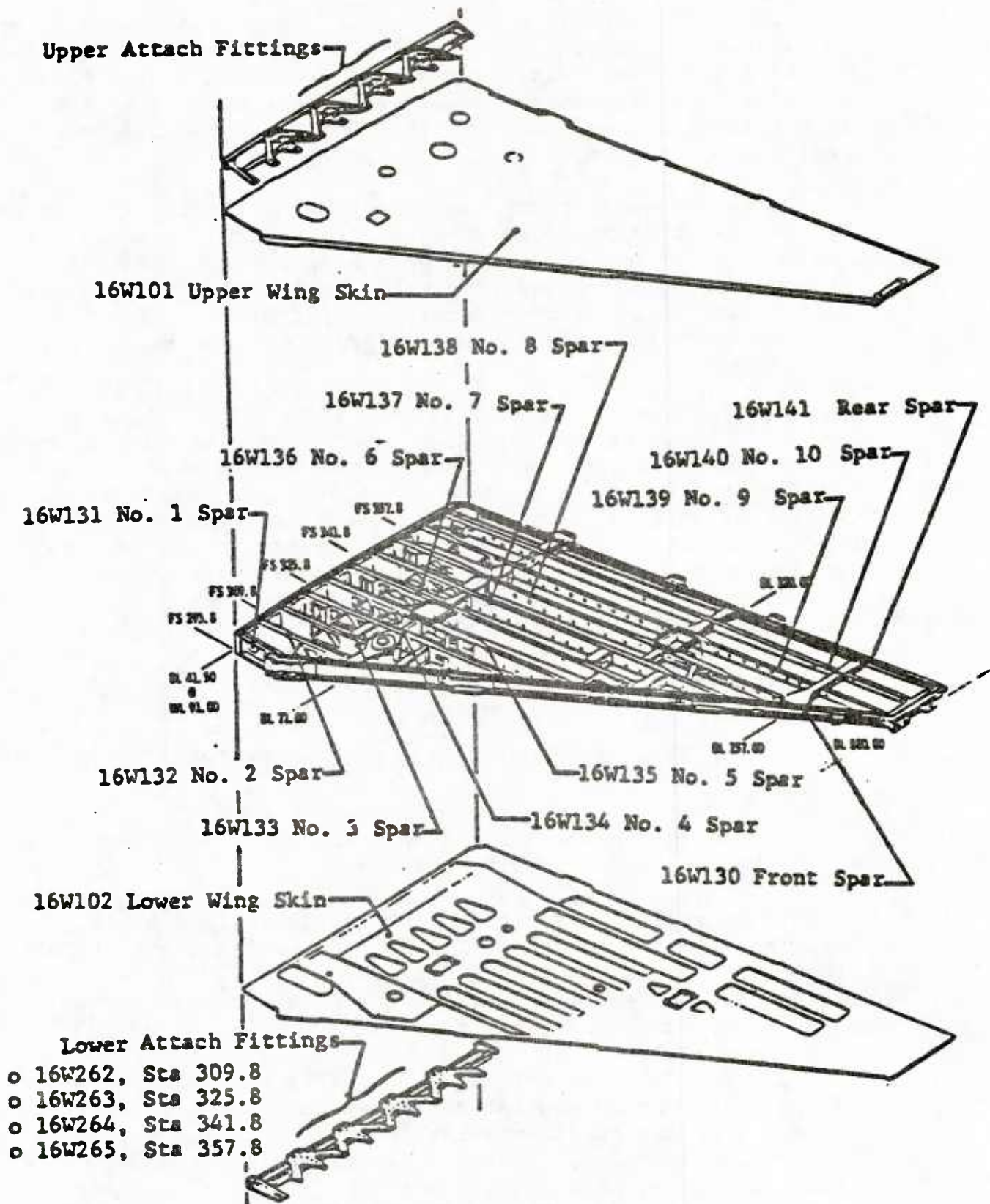


Fig. 39 F-16 Basic Wing Box Structure

The F-16 durability test article (wings) was fatigue tested to two service lives (i.e., 16000 flight hours) using the F-16 500 hour spectrum. After successfully completing the F-16 durability certification requirements, the durability test article (wings) was dedicated to the "Durability Methods Development" (DMD) program.

A tear-down inspection of the F-16 durability test article (wings) was performed under Phase II of the DMD program. All fastener holes and cutouts in both wing lower skins (7475-T7351 aluminum) were inspected (over 3000 holes) using eddy current techniques. Also, approximately forty fastener holes per spar (20 upper and 20 lower at the inboard end) were inspected.

All fastener holes in the lower wing skins with an indicated crack were broken open and then evaluated fractographically. Fastener holes with an indicated crack after 16000 hours of fatigue testing (F-16 500 hour spectrum) are identified in Figs. 40 and 41 for the right hand and left hand lower wing skin, respectively. Fractographic results are summarized in Tables 14 through 17. Results of the F-16 wing tear-down inspection were used to demonstrate the durability analysis methodology [21, 34, 36]. The tear-down inspection is also documented in Volume VIII and elsewhere [11,15,18].

6.6 CONCLUSIONS AND RECOMMENDATIONS

The following conclusions and recommendations are based on the Phase II test program and results [6].

1. A wealth of fatigue crack initiation and crack propagation data for clearance-fit fastener holes has been developed and documented under this program [6]. These results can be used to determine the IFQ for clearance-fit fastener holes for future durability analyses.

2. The "ton" of data in Volume VIII needs to be further evaluated to better understand the effects and significance of various test and specimen variables on the TTCI and TTF (e.g., % bolt load transfer, fastener type/size/fit, specimen size, clamp-up, etc.). A statistical analysis of the data is needed to evaluate the effects of scatter and to determine trends.

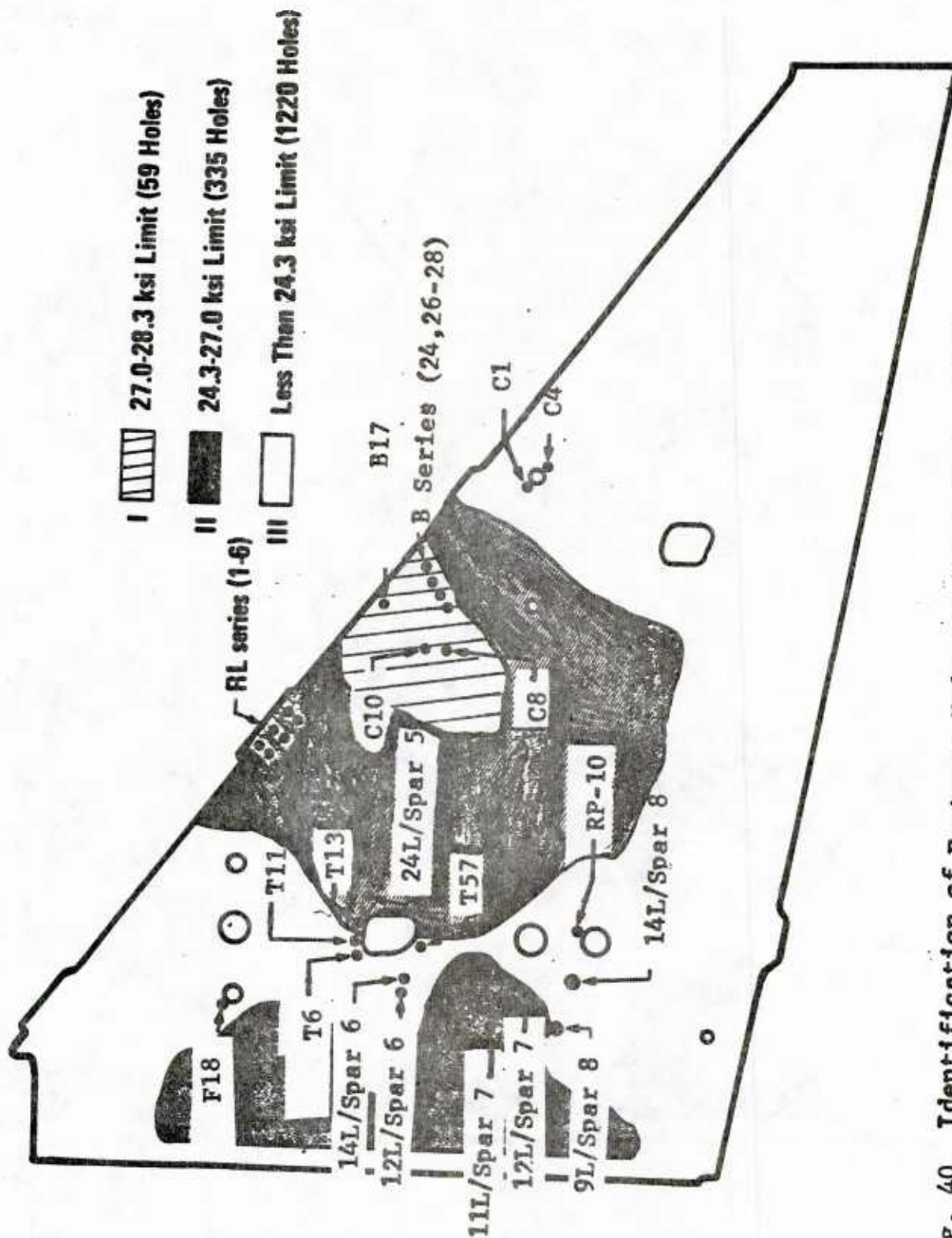


Fig. 40 Identification of Fastener Holes in the F-16 Durability Component Lower Right Hand Wing Skin with Observed Cracks (After 16000 Hrs. of Testing with F-16 500-Hour Spectrum)

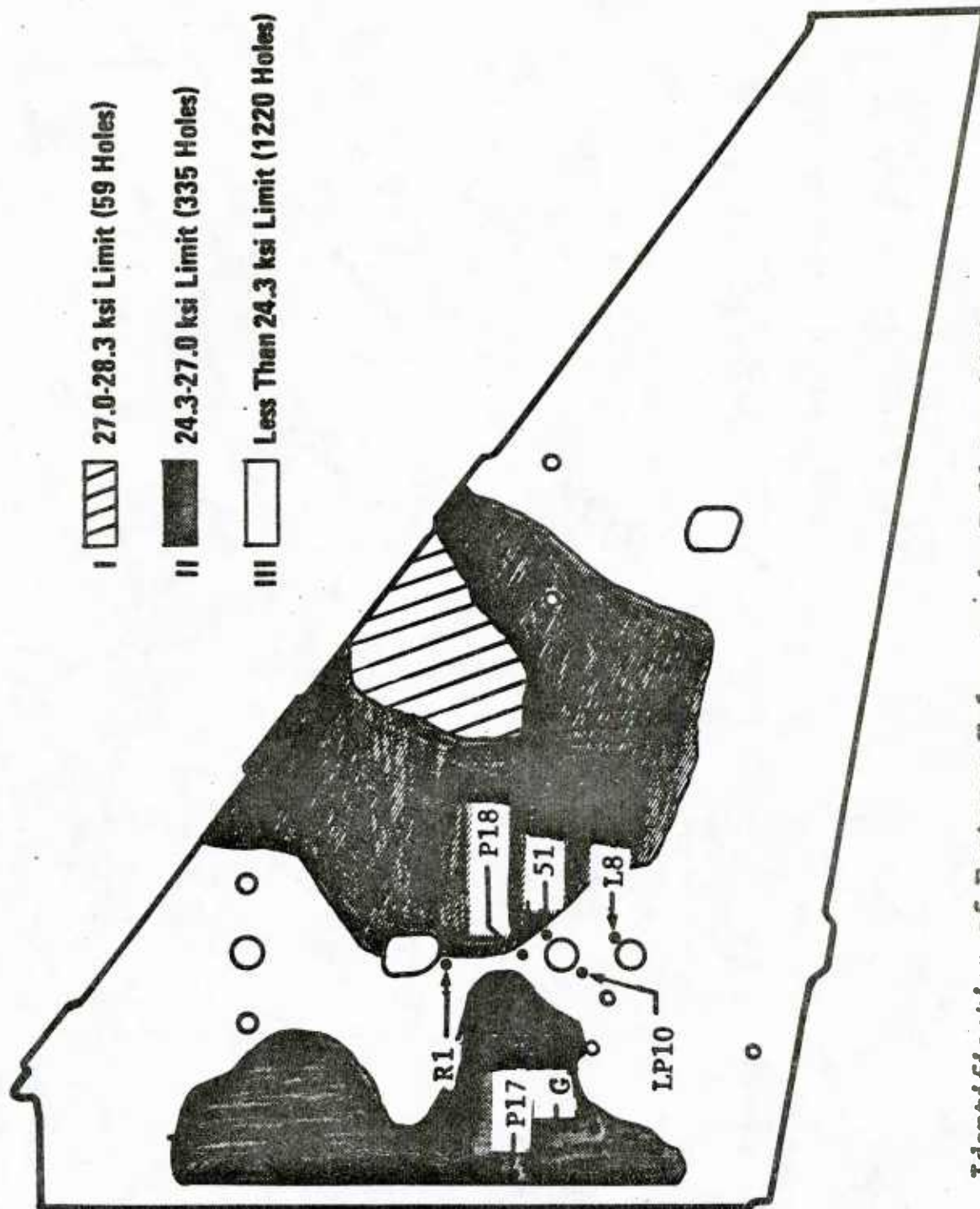









Fig. 41 Identification of Fastener Holes in the F-16 Durability Component Lower Left Hand Wing Skin 4th Observed Cracks (After 16000 Hrs. of Testing with F-16 500-Hour Spectrum)

Table 14 Fractographic Results for F-16 Lower Wing Skin (Right Hand; Durability Test Article) - Stress Zone I











Hole No	Crack Length (IN) ***						
*Flight Hours	C8	C10	B17	B24	B26	B27	B28
16000	0.0177	0.1482	0.0634	0.1495	0.1560	0.0423	0.2744
15000	0.0154	0.0988	0.0435	0.0975	0.0949	0.0304	0.1928
14000	0.0137	0.0637	0.0314	0.0598	0.0585	0.0254	0.1337
13000	0.0123	0.0403	0.0218	0.0340	0.0338	0.0207	0.0969
12000	0.0109	0.0293	0.0139	--	--	0.0153	0.0724
11000	0.0094**	0.0208	--	--	--	0.0115	0.0573
10000	--	--	--	--	--	--	0.0437
9000	--	--	--	--	--	--	0.0319
8000	--	--	--	--	--	--	0.0197**
7000	--	--	--	--	--	--	--
6000	--	--	--	--	--	--	--
5000	--	--	--	--	--	--	--
							

* F-16 500-Hour Block Spectrum

** Vague

*** Perimeter dimensions along direction of crack growth/crack measurements

Table 15 Fractographic Results for F-16 Lower Wing Skin (Right Hand; Durability Test Article) - Stress Zone II





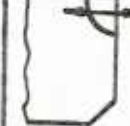

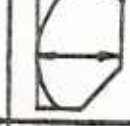



Hole No	Crack Length (IN) ***									
	RL-1	RL-2	RL-3	RL-4	RL-5	RL-6	T13	11L/Spar 7	12L/Spar 7	24L/Spar 5
*Flight Hours										
16000	0.0413	0.0362	0.0353	0.0297	0.2160	0.2016	0.1814	0.0481	0.0401	0.1339
15000	0.0297	0.0294	0.0270	0.0229	0.1448	0.1354	0.0893	0.0247	0.0267	0.0965
14000	0.0217	0.0245	0.0205	0.0178	0.1152	0.1094	0.0446	0.0130	0.0155	0.0677
13000	0.0129	0.0204	0.0144	0.0133	0.0893	0.0922	0.0202	--	0.0076	0.0461
12000	0.0068**	0.0177**	--	--	0.0691	0.0806	--	--	0.0020**	0.0302
11000	--	0.0149**	--	--	0.0533	--	--	--	--	0.0216
10000	--	--	--	--	0.0418	--	--	--	--	0.0144
9000	--	--	--	--	--	--	--	--	--	--
8000	--	--	--	--	--	--	--	--	--	--
7000	--	--	--	--	--	--	--	--	--	--
6000	--	--	--	--	--	--	--	--	--	--
5000	--	--	--	--	--	--	--	--	--	--
										

* F-16 500-Hour Block Spectrum

*** Perimeter dimensions along direction of crack growth/crack measurements

** Vague

Table 16 Fractographic Results for F-16 Lower Wing Skin (Right Hand; Durability Test Article) - Stress Zone III

Hole No	Crack Length (IN) ***									
*Flight Hours	C1	C4	F18	RP-10	T6	T11	T57	12L/Spar 6	14L/Spar 6	14L/Spar
16000	0.1456	0.0239	0.1833	①	0.0308	0.0369	0.1613	0.3456	0.1079	0.0157
15000	0.0884	0.0183	0.1407	0.1430	0.0210	0.0247	0.1382	0.2822	0.0832	0.0110
14000	0.0520	0.0147	0.1043	0.0923	0.0149	0.0187	0.1181	0.2246	0.0663	0.0082
13000	--	0.0117	0.0863	0.0520	0.0107	0.0134	0.0980	0.1786	0.0507	0.0056
12000	--	0.0098	0.0587	0.0280	0.0074	0.0094**	0.0806	0.1426	0.0390	0.0038*
11000	--	0.0082	0.0398	0.0143	--	--	0.0648	0.1094	0.0286	--
10000	--	--	0.0294	--	--	--	0.0490	0.0835	0.0208	--
9000	--	--	--	--	--	--	0.0360	0.0634	--	--
8000	--	--	--	--	--	--	--	0.0504	--	--
7000	--	--	--	--	--	--	--	0.0374	--	--
6000	--	--	--	--	--	--	--	0.0288	--	--
5000	--	--	--	--	--	--	--	0.0230	--	--
										


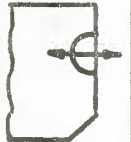





* F-16 500-Hour Block Spectrum

** Vague

*** Perimeter dimension along direction of crack growth/crack measurements

① Perimeter Beyond Readings

Table 17 Fractographic Results for F-16 Lower Wing Skin (Left Hand; Durability Test Article)

Hole No	Crack Length (IN) ***						
	G	P17	51	L8	LP10	P18	R1
*Flight Hours							
16000	0.0815	0.0252	0.0327	0.0590	0.065	0.0741	0.0406
15000	0.0616	0.0176	0.0244	0.0409	0.0533	0.0533	0.0227
14000	0.0455	0.0119	0.0197	0.0297	0.0429	0.0377	0.0137
13000	0.0349	0.0083	0.0131	0.0178	0.0325	0.0273	0.0069
12000	0.0217	0.0054	--	0.0083	0.0234	0.0189	--
11000	0.0165	--	--	--	0.0176	0.0130	--
10000	0.0123	--	--	--	0.0130	--	--
9000	0.0094	--	--	--	--	--	--
8000	--	--	--	--	--	--	--
7000	--	--	--	--	--	--	--
6000	--	--	--	--	--	--	--
5000	--	--	--	--	--	--	--
							
	Stress Zone II			Stress Zone III			

*F-16 500-Hour Block Spectrum

*** Perimeter dimension along direction of crack growth/crack measurements

3. Other fractographic data sources for fastener holes [e.g., 47, 49, 54, 55] should also be evaluated and compared with the results in Volume VIII [6].

4. Variable percentages of bolt load transfer were obtained using the double, reverse dog-bone type specimens (see Figs. 18-20). The actual amount of bolt load transfer for each specimen depends on factors such as the fastener type and fit, load spectrum, stress level, etc. Since the actual percentage of bolt load transfer varies for clearance-fit fastener holes in aircraft components, test specimens with variable percentages of bolt load transfer may be satisfactory for generating the IFQ for fastener holes. The effects of bolt load transfer on the TTCI and IFQ need to be investigated further, using specimens with a controlled load applied directly to the bolt.

5. Specimens with countersunk fastener holes typically exhibited more "scatter" in the fractographic results than those for straight bore holes [e.g., 41]. The increased scatter for the countersunk fastener holes is probably due to differences in : (1) fit for countersunk and protruding head fasteners and (2) crack initiation origins.

6. The following crack initiation origins and trends were observed:

- (1) No-load transfer Specimens - Most origins were in the bore of the hole. Multiple fatigue cracks converging into a single crack front were also observed.
- (2) 15% Load Transfer Specimens - Fatigue cracks generally originated at the faying surfaces - bore intersection. Signs of fretting were also observed in several specimens.
- (3) 30% and 40% Load Transfer Specimens - Origins of failure varied considerably. Many origins were at or near the fastener hole-faying surface intersection and at or near the countersink-bore intersection. Signs of fretting were observed but the problem appeared to be no worse than that for the 15% load transfer specimens.

- (4) Complex Splice Specimens - Fatigue crack origins varied considerably, ranging from the countersink-bore intersection area to the faying surface (see Table 13). Initiation sites were particularly difficult to determine when cracks from adjacent holes overlapped. Most of the largest fatigue cracks occurred in the outer row of fastener holes near the centerline. Considerable evidence of fretting was observed.

7. Early fatigue failures were observed when cracks of approximately equal size occurred on both sides of the hole. Fractographic results were obtained for the largest fatigue crack per specimen and for selected secondary cracks. A small fatigue crack (e.g., ≤ 0.10 ") for one side of a fastener hole does not appear to have a significant effect on the crack initiation for a crack on the opposite side of the hole and vice versa. The effects of cracks on both sides of the hole and crack geometry on TTCI and TTF need to be investigated further.

8. The wealth of available fractographic data for fastener holes [e.g., 6, 24, 41, 47, 49, 54, 55] should be used to determine suitable IFQ model parameters for durability analysis. IFQ Model parameters should be determined for pooled fractographic data sets and the accuracy of the extent of damage predictions evaluated to increase confidence in the durability analysis methodology.

SECTION VII

CONCLUSIONS AND RECOMMENDATIONS

7.1 CONCLUSIONS

The durability analysis methodology developed in Phase I of this program has been evaluated and refined in Phase II. This methodology has been demonstrated for coupon data, full-scale fighter aircraft structure (i.e., F-16 lower wing skin) and a complex splice subjected to a B-1 bomber spectrum. The analytical tools developed under this program can be used to analytically assure design compliance with the U.S. Air Force's durability design requirements. Although the methodology has been demonstrated only for fastener hole cracking, the basic durability strategy and concepts apply to cracking in any structural detail (e.g., cutouts, lugs, fillets, etc.). The methodology has been demonstrated for quantifying the extent of damage in grouped fastener holes due to relatively small sub-critical cracks (e.g. $\leq 0.10''$). Further work is required to demonstrate the methodology for larger crack sizes.

A large fractographic data base has been developed for cracking in fastener holes. Much has been learned about IFQ characterization and the associated parameters involved. An effective IFQ model has been developed, evaluated and refined for quantifying the IFQ for structural details susceptible to fatigue cracking. The IFQ model is a very promising tool for quantifying the initial manufactured state of structural details in terms of equivalent initial flaw sizes.

The following conclusions and observations are based on the results and investigations of this program:

1. Several useful applications of the durability analysis tools developed are: (1) evaluate durability design trade-offs in terms of structural design variables, (2) evaluate structural maintenance requirements before or after aircraft is committed to service, and (3) provide aircraft user options affecting life-cycle-costs, structural maintenance requirements, and operational readiness.

2. The IFQ model is simply a "mathematical tool" for quantifying the IFQ of structural details. Therefore, the resulting EIFS's must be considered in the context of the

IFQ model and the fractographic results used to calibrate the model parameters. EIFS's should be considered as hypothetical cracks used to make crack exceedance predictions rather than actual initial cracks per se.

3. Back extrapolations of fractographic data must be done consistently to put the EIFS's on a common baseline for different data sets. Inconsistent EIFS results will be obtained if the EIFS distribution is determined by back extrapolating the fractographic results for individual specimens and then fitting a statistical distribution to the EIFS results for different data sets. Two problems result if this approach is used: (1) the EIFS's are not on a common baseline for different data sets, and (2) the resulting EIFS distribution is not statistically compatible with the TTCI distribution and the fatigue wear out process. The resulting EIFS distribution should be statistically compatible with the TTCI distribution. The IFQ model developed satisfies this requirement.

4. The IFQ model developed can be used to define the EIFS cumulative distribution using suitable fractographic results. The parameters α and $Q_1^* \beta_1$ provide the basis for putting fractographic results on a common baseline for quantifying the initial fatigue quality. α and $Q_1^* \beta_1$ should be constants for different fractographic data sets (same material, fastener type/fit, and drilling technique but different loading spectra, stress level and percent load transfer).

5. For generic EIFS, α and $Q_1^* \beta_1$ should be constants. Encouraging results have been obtained to justify the use of the same EIFS cumulative distribution for making crack exceedance predictions for different design conditions. Further research is required to confirm the IFQ distributions for different materials, load spectra, stress levels, fastener types/diameters/fit, % load transfer, etc. A considerable amount of fractographic results exist which need to be evaluated using the IFQ model [e.g., 6, 41, 47, 49, 54, 55].

6. Theoretically, the IFQ model can be used to quantify the EIFS cumulative distribution for various structural details so long as fractographic results are available for the details to be included in the durability analysis. The IFQ model has been evaluated using fractographic results for fastener holes. Suitable specimens and guidelines need to be developed for generating crack initiation and crack growth results for details such as, cutouts, fillets, lugs, etc. Fractographic results should be developed and evaluated for such details so that the durability analysis

methods described can be efficiently applied to different types of structural details in typical aircraft structures.

7. The accuracy of crack exceedance predictions, based on the same EIFS cumulative distribution, needs to be evaluated for different design conditions. Also, IFQ model parameter sensitivity studies need to be performed to better understand the average parameter values and variances and the impact of these parameters on the IFQ for different fractographic data sets.

8. The durability analysis method was developed for making crack exceedance predictions for relatively small crack sizes (e.g., $\leq 0.10"$) in structural details. The largest crack in each detail was assumed to be statistically independent to justify using the binomial distribution for combining crack exceedance predictions for structural details. If the largest crack in a given detail doesn't significantly affect the growth of cracks in neighboring details, perhaps the proposed durability analysis method can be extended to crack sizes $> 0.10"$. The simplistic crack growth rate equation (Eq. 2) used in the IFQ model may not be suitable for defining the EIFS cumulative distribution for crack sizes $> 0.10"$. Other functional forms for crack growth rate may be required to justify the same EIFS distribution for both small and large crack sizes. Eq. 2 may be acceptable for making $p(i, \tau)$ predictions for larger crack sizes if the "EIFS master curve" is curve fit to the larger crack sizes. This would result in a different EIFS cumulative distribution for the small and large crack size range. Further research is required to extend the probabilistic fracture mechanics approach developed to larger crack sizes.

9. Two different $F_a(0)(x)$ equations (i.e., Eqs. 8 and 13) were presented for representing the IFQ. Either equation is valid but Eq. 13 is recommended for two reasons: (1) it assures all EIFS's in the IFQ distribution will be > 0 , and (2) the crack growth rate parameter, Q or Q_i^* , can be easily determined from the fractographic results and the resulting Q_i^* values for different data sets will be directly comparable. If Eq. 8 is used, a common b parameter (Eq. 2) must be imposed for different fractographic data sets to put the $Q_i^* \beta_i$ values on a comparable baseline. As long as $b > 1$, all EIFS's in Eq. 8 will be ≥ 0 .

10. The EIFS cumulative distribution $F_a(0)(x)$ is independent of the TTCI reference crack size, a_0 , used (ref. Eqs. 8 and 13). By using consistent fractographic data

pooling procedures, results for different data sets can be put on a common baseline.

11. Fractographic results for cracks in given structural details are required to calibrate the IFQ model parameters. The IFQ distribution is based on the observed fractographic results without direct consideration of small crack kinetics. This means that the IFQ, or EIFS distribution, can be determined without addressing directly the question of small crack growth behavior. The effects of small crack growth, if desired, could be accounted for in the EIFS master curve used to define the IFQ distribution. Due to the generality of the IFQ model concepts, IFQ can be determined using state-of-the-art understandings of the crack growth behavior.

12. The EIFS concept is convenient for quantifying IFQ. Care and judgment must be exercised when defining the IFQ distribution to assure EIFS results are on a comparable basis for different data sets. One of the most important lessons learned from this program is that EIFS's must be defined using pooled fractographic results to make the EIFS's for one data set comparable with those for another data set. If a constant α can be justified for the pooled fractographic data sets, this provides a simple way to put the TTCI results on a compatible basis. In order to obtain compatible EIFS results for different fractographic data sets, the EIFS master curve must also be defined in a consistent manner. This is very important because the resulting IFQ distribution depends on the transformation of the TTCI distribution using the applicable EIFS master curve.

13. The EIFS master curve depends on the fractographic crack size range used and the acceptable curve fit criterion. If the EIFS master curve changes, the resulting EIFS's also change. Therefore, different EIFS's can be obtained for the same set of TTCI's. Use consistent procedures and fractography data pooling for defining EIFS's to make results directly comparable -- otherwise EIFS comparisons will be meaningless.

14. Be sure to use consistent fractographic crack size ranges for different fractographic data sets when defining the corresponding EIFS master curves. For example, a crack size range from 0.005" to 0.100" appears reasonable for quantifying the IFQ. Consistent crack size ranges must be used to obtain compatible EIFS master curves for different fractographic data sets.

15. The durability analysis methodology has been demonstrated for the F-16 lower wing skin and for a complex splice specimen subjected to a B-1 bomber spectrum. In both cases, fractographic results for load transfer coupon specimens were used directly to predict the extent of damage for the corresponding full-scale structures. Excellent correlations were obtained without considering scale-up effects (i.e., coupon structure to full-scale structure). However, such effects should be investigated further to determine their significance for durability analyses.

16. Fractographic data are available for countersunk fasteners for two different diameters (Vol. VIII). The effects of fastener diameter on the IFQ distribution have been studied but further research is needed to reach a better understanding.

17. IFQ model calibration studies (see Appendices A and B) were made using fractographic results for straight bore [41] and countersunk fastener holes [6]. These studies were based on the $Q[a(t)]^b$ model for the EIFS master curve. The following observations are based on these studies for 7475-T7351 aluminum:

- o α and b appear to be material constants independent of load spectra and stress level.
- o Typical α values ranged from approximately 4.4 for straight bore holes to 2.5 for countersunk holes. More scatter in the results were observed for countersunk holes than for the straight bore holes.
- o Typical b values of 0.88 and 0.61 were observed for straight bore and countersunk holes, respectively.
- o Average $Q_1^* \beta_i$ values of 2.8 and 0.62 were observed for straight bore and countersunk bore holes, respectively ($a_0=0.03"$).
- o $Q_1^* \beta_i$ appeared to be independent of load spectra, stress level, and percent load transfer.

Further studies are needed to evaluate the IFQ distribution based on the $Q[a(t)]$ model for the EIFS master curve. A better understanding of the IFQ model parameter sensitivities to design variables is needed. Further studies should be made using available fractographic data [e.g., 6, 41, 47, 49, 54, 55].

18. Variable shear load transfer through the fasteners was obtained for the various % load transfer fractographic data sets. This variability was apparently due to the following:

- o Variable clearance between fasteners and mating holes (test section and lugs).
- o insufficient axial deformation under applied spectrum loading to obtain full design load transfer in specimen for each load in spectrum.

Real aircraft structure will also have variable % load transfer due to variable fits between fasteners and holes. However, to properly assess the effects of fastener shear load transfer on IFQ, fatigue cracking in fastener holes should be obtained under controlled % load transfer conditions.

7.2 RECOMMENDATIONS

1. Further work is needed to evaluate the accuracy and sensitivity of $p(i, \tau)$ predictions based on a given IFQ distribution and service crack growth master curves determined using a suitable analytical crack growth program [e.g., 37-40]. This research is necessary to increase confidence in the $p(i, \tau)$ predictions for a wide range of "real world" durability applications.

2. The IFQ of fastener holes should be studied further using the IFQ model developed. Existing fractographic results from various sources should be used to evaluate IFQ model parameters (i.e., α , β , ϵ , Q and b) and to establish, on a statistical basis, suitable IFQ distributions for durability design applications. A wealth of fractographic results are available from this program (Vol. VIII). Other fractographic data sources are also available [e.g., 24, 41, 47, 49, 54, 55].

3. The accuracy of crack exceedance predictions, based on the same EIFS cumulative distribution, need to be evaluated for different design conditions. Also, IFQ model parameter sensitivity studies need to be performed to better understand the average parameter values and variances and the impact of these parameters on the IFQ for different fractographic data sets.

4. Fractographic data from various sources should be pooled and IFQ model parameters determined. Model parameters should be analyzed statistically and a "generic" EIFS distribution for IFQ should be determined, if possible, for a wide range of durability design applications.
5. Further research is required to confirm the IFQ distributions for different materials, load spectra, stress levels, fastener types/diameters/fit, % load transfer, etc. A considerable amount of fractographic results exists which need to be evaluated using the IFQ model.
6. The durability analysis methodology developed under this program needs to be clinically evaluated using the wealth of fractographic data available. Basic assumptions, analysis procedures, design guidelines and overall implementation need to be critically reviewed and the methodology appropriately refined if necessary.
7. The effects of fretting, clamp-up, corrosion, size effect (scale-up from coupon to component), faying surface sealant, interference-fit fasteners, residual stresses, etc., on IFQ need to be investigated and guidelines should be determined for durability design applications.
8. The feasibility of using no-load transfer specimens with multiple holes for quantifying the IFQ should be evaluated using spectrum and constant amplitude loading. This could provide an economical way to generate the fractographic results needed to quantify the IFQ distributions.
9. The effect of percent fastener load transfer on IFQ should be investigated further. The "load transfer" specimens for this program were designed for 15%, 30% and 40% load transfer assuming a perfect fit between fasteners and holes as well as lug pins and holes. Since the fit varies from hole to hole, the % load transfer also varies. Therefore, to quantitatively evaluate the effects of load transfer on IFQ, specimens need to be fatigue tested in such a way to assure a specified % shear load transfer through the fastener.
10. The effect of scale-up (e.g., coupon-component) on $p(i,r)$ predictions needs to be investigated further, including an assessment of the accuracy of the predictions for different design conditions.
11. The effect of fastener size on IFQ needs to be investigated further.

12. The durability design handbook [21] should be expanded to include more "durability design data" for different materials and for the key structural details governing durability.

13. Evaluate and verify the durability analysis methodology developed under this program for cutouts, lugs and fillets. Refine the methodology if required.

14. Develop suitable test specimens and guidelines for generating crack initiation and crack growth data needed to quantify the IFQ for cutouts, lugs and fillets.

15. Generate fractographic results for cutouts, lugs and fillets for different materials and design conditions (e.g., load spectra, stress level, environment, etc.). Use these data to determine the corresponding IFQ for cutouts, lugs and fillets. Study the resulting IFQ model parameters and develop understanding for design applications.

16. The durability analysis methodology developed under this program should be extended to larger crack sizes (e.g., $a > 0.10"$) and verified for key structural details governing durability (i.e., fastener holes, cutouts, lugs, and fillets).

17. Further work is needed to determine reasonable durability crack size limits and guidelines for the economical repair of cutouts and fillets. Repair crack size limits are needed for applicable structural details to quantify the extent of damage predictions on a rational basis.

18. Allowable extent of damage limits for airframe structures and guidelines need to be developed so that "economic life" can be defined in meaningful terms for analytically demonstrating design compliance with the U.S. Air Force's durability design requirements.

19. An efficient, general-purpose plotting capability should be developed for presenting durability analysis results in various useful formats. An automated plotting capability has been developed under this program but improvements are needed to obtain plots more efficiently. The program should be able to handle large amounts of fractographic data. This capability could be used to economically generate useful durability design data for the durability design handbook and to evaluate the accuracy of durability analysis predictions.

20. Durability analysis workshops should be conducted to transfer the technology developed under this program to various user levels. For example, such workshops would be useful to aerospace engineers who are directly concerned with aircraft structural durability analyses and compliance with the U.S. Air Force's durability design requirements. This would provide an excellent forum for exchanging ideas and explaining the application of the durability analysis methodology developed. Such exchanges should lead to methodology improvements and further advance the durability analysis state-of-the-art.

APPENDIX A

EVALUATION OF IFQ MODEL PARAMETERS FOR STRAIGHT-BORE FASTENER HOLES

A.1 INTRODUCTION

The IFQ model described in Section 3.5 is evaluated in this Appendix using fractographic results for straight-bore fastener holes [41]. Similar results for countersunk fastener holes are documented in Appendix B of this report. Model parameters were determined for both individual and pooled fractographic data sets using the procedures described in section 4.3.

The basic objective of this study was to compare IFQ model parameters for different fractographic data sets for consistency and trends and to learn more about the application of the model. A secondary objective was to evaluate possible relationships for Q and β , Q and σ and β and σ . The IFQ model parameters for this study were determined using preliminary calibration procedures rather than those recommended in the Durability Design Handbook [21]. However, this study and others [e.g., 11-19, 31-36] provided the "experience" needed to develop the final understanding for the program [21].

The fractographic data sets used for this study are described in Table A1 and details are given in Ref. 41. Specimen details for the no-load transfer and the 15% load transfer specimen are shown in Fig. A1. All specimen fastener holes were drilled using a modified Winslow spacematic drill and holes were not deburred. NAS 6204($\frac{1}{4}$ " dia.) protruding head bolts (clearance-fit) were installed

TABLE A1 FHQ DATA SETS USED

DATA SET	% LOAD TRANSFER	NO. SPECIMENS	σ (ksi)	TEST SPECTRUM	MATERIAL
WPF	0	37	34	F-16 400-Hr	7475-T7351
XWPF	15	33	34	Block	
HYWPF	15	10	40.8	↓	
LYWPF	15	10	30.6	↓	
WPB	0	32	34	B-1	
XWPB	15	31	34	↓	
HYWPB	15	10	40.8	↓	
LYWPB	15	10	30.6	↓	

Notes

1. Fractographic results from Ref. 41.
2. NAS 6204 ($\frac{1}{2}$ dia) protruding head bolt.

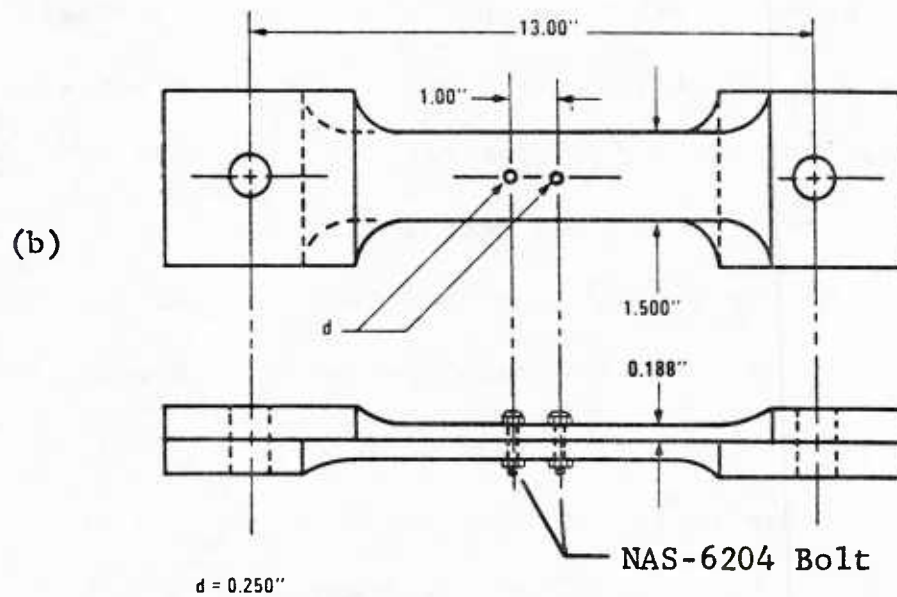
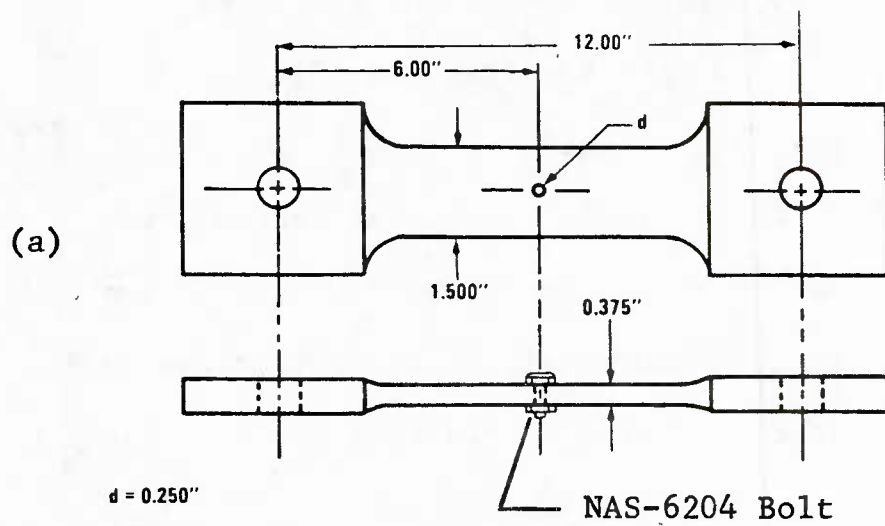


Fig. A1 Fastener Hole Quality Specimens; (a) No-Load Transfer and (b) 15% Load Transfer

in the fastener holes as shown in Fig. A1.

This study also reflected the following:

- o $\epsilon = 0$ and $a_0 = x_u$ (ref. Eq. 8)
- o $b \neq 1$ form of Eq. 2
- o two fractographic crack size ranges used:
 $0.005" \leq a(t) \leq 0.10"$ and $0.005" \leq a(t) \leq 0.050"$.

IFQ model parameter values are summarized herein. Further details of the study and conclusions are given in subsection 4.8.1.

A.2 IFQ MODEL PARAMETERS FOR INDIVIDUAL DATA SETS

In Table A2, IFQ model parameters are summarized for individual fractographic data sets. These parameters were determined using the fractographic results from Ref. 41 and the calibration procedures described in section 4.3. Only the fractography for the largest fatigue crack per specimen was used to determine the IFQ model parameters (i.e., $\ell_i=1$; no β scaling used).

The notation for the IFQ Model parameters shown in Table A2 is consistent with Ref. 21. For example,

α_i = Weibull shape parameter for the i th TCI data set.

b_i^*, Q_i^* = crack growth constants in $\frac{da(t)}{dt} = Q_i^* [a(t)]^{b_i^*}$
for the i th fractographic data set.

β_{ℓ_i} = Weibull scale parameter for the i th TCI data set.

Note:

$$\beta_i = \beta_{\ell_i} (\ell_i)^{1/\alpha_i} \quad (\text{Ref. Section 4.4}).$$

TABLE A2 Model Parameters for Unpooled FHQ Data Sets (Straight Bore Holes; 0.005"-0.100" Crack Size Range)

Data Set	No. Specimens	σ (ksi)	% LT	α_i	b_i^*	β_{ℓ_i}	$Q_i^* \times 10^4$	Load Spectra
WPF	37	34	0	4.408	0.8399	16992	1.306	F-16 400 Hr. ↓
XWPF	33	34	15	5.349	0.8613	11352	1.964	
HYWPF	10	40.8	15	4.157	0.8277	4230	4.218	
LYWPF	10	30.6	15	3.039	0.9765	25386	1.924	
WPB	32	34	0	4.619	0.9211	37092	1.096	B-1 ↓
XWPB	31	34	15	4.375	0.9224	16956	1.793	
HYWPB	10	40.8	15	3.934	0.7166	7672	1.602	
LYWPB	10	30.6	15	4.671	1.0574	34428	1.937	

- Notes: 1. Material: 7475-T7351 Aluminum
2. NAS-6204 ($\frac{1}{2}$ dia.) Protruding Head Bolt
3. $a_0 = x = 0.03"$
4. $\beta_i = \beta_{\ell_i}(\ell_i)^{1/\alpha_i}$ (Ref. Section 4.4)

A.3 IFQ MODEL PARAMETERS FOR POOLED DATA SETS

IFQ Model parameters were determined using the pooled fractographic results for different data sets and data set combinations. Two different fractographic crack size ranges were used, i.e., $0.005'' \leq a(t) \leq 0.100''$ and $0.005'' \leq a(t) \leq 0.050''$. The computed IFQ Model parameters for the different fractographic crack size ranges are summarized in Tables A3 and A4.

In Table A3 and A4, α and b were determined using the pooled fractographic results for the data sets indicated. Given " α ", the corresponding β_{ℓ_i} value for each data set pooled was determined using the procedures described in Section 4.3. Q_i^* for each data set was determined using the applicable " b " value for the pooled data sets.

The product $Q_i^* \beta_{\ell_i}$ is tabulated in Table A3 and A4 for each data set and data pooling combination. Also, the average $Q_i^* \beta_{\ell_i}$ and the standard deviation and coefficient of variation for $Q_i^* \beta_{\ell_i}$ are shown.

α and β_{ℓ_i} depend on the TTCIs for a given a_0 . However, in some cases fractographic results for selected fatigue cracks had to be extrapolated to obtain TTCI values for $a_0 = 0.03''$. Extrapolations were made using the generalized crack size-time relationship based on Eq. 2 and $b \neq 1$. Since the corresponding " Q " and " b " values for a given fatigue crack depends on the fractographic crack size range used, this explains the small difference

TABLE A3 Model Parameters for Pooled FHQ Data Sets (Straight Bore Holes; 0.005"-0.100" Crack Size Range.)

CASE	DATA SET	NO. SPECIMENS	σ (ksi)	Z LT	a	b	β_{ℓ_1}	$Q_1^* \times 10^4$	$Q_1^* \beta_{\ell_1}$	$Q_1^* \beta_{\ell_1}$		
										AVE.	STD. DEV.	C.O.V. (%)
I	XWPF	33	34	15	4.245	0.8706	11152	2.045	2.281	2.566	0.588	22.9
	HYWPF	10	40.8	15	↓	↓	4240	5.129	2.175	↓	↓	↓
	LYWPF	10	30.6	15	↓	↓	26789	1.211	3.243	↓	↓	↓
II	XWPB	31	34	15	4.299	0.9422	16930	1.952	3.304	3.499	0.419	12.0
	HYWPB	10	40.8	15	↓	↓	7761	4.138	3.212	↓	↓	↓
	LYWPB	10	30.6	15	↓	↓	34174	1.165	3.981	↓	↓	↓
III	WPF	37	34	0	4.309	0.8707	16952	1.503	2.549	2.566	0.484	18.8
	XWPF	33	34	15	↓	↓	11164	2.046	2.284	↓	↓	↓
	HWYFPF	10	40.8	15	↓	↓	4247	5.132	2.179	↓	↓	↓
	LYWPF	10	30.6	15	↓	↓	26859	1.211	3.253	↓	↓	↓
IV	WPB	32	34	0	4.430	0.9322	36942	1.149	4.247	3.583	0.549	15.3
	XWPB	31	34	15	↓	↓	16974	1.869	3.174	↓	↓	↓
	HYWPB	10	40.8	15	↓	↓	7793	3.968	3.092	↓	↓	↓
	LYWPB	10	30.6	15	↓	↓	34265	1.114	3.819	↓	↓	↓
V	XWPF	33	34	15	4.269	0.8902	11157	2.228	2.486	2.798	0.453	16.2
	HYWPF	10	40.8	↑	↓	↓	4243	5.611	2.380	↓	↓	↓
	LYWPF	10	30.6	↓	↓	↓	26816	1.319	3.538	↓	↓	↓
	XWPB	31	34	↓	↓	↓	16920	1.562	2.643	↓	↓	↓
	HYWPB	10	40.8	↓	↓	↓	7754	3.325	2.578	↓	↓	↓
	LYWPB	10	30.6	15	↓	↓	34153	0.926	3.162	↓	↓	↓
VI	WPF	37	34	0	4.364	0.8826	16974	1.588	2.695	2.800	0.449	16.1
	XWPF	33	34	15	↓	↓	11174	2.156	2.409	↓	↓	↓
	HYWPF	10	40.8	15	↓	↓	4253	5.419	2.305	↓	↓	↓
	LYWPF	10	30.6	15	↓	↓	26918	1.276	3.435	↓	↓	↓
	WPB	32	34	0	↓	↓	36889	0.928	3.425	↓	↓	↓
	XWPB	31	34	15	↓	↓	16952	1.512	2.563	↓	↓	↓
	LYWPB	10	30.6	15	↓	↓	34219	0.895	3.064	↓	↓	↓
	HYWPB	10	40.8	15	↓	↓	7777	3.221	2.505	↓	↓	↓

TABLE A4 Model Parameters for Pooled FHQ Data Sets (Straight Bore Holes; 0.005-0.050" Crack Size Range)

Case	Data Set	No. Specimens	σ (ksi)	Z LT	α	b	β_{ℓ_i}	$Q^* \times 10^4$	$Q^* \beta_{\ell_i}$	$Q^* \beta_{\ell_i}$		
										Ave.	Std. Dev.	C.O.V. (%)
I	XWPF	33	34	15	4.557	0.8224	11209	1.764	1.977	2.122	0.475	22.4
	LYWPF	10	30.6				24973	1.062	2.653			
	HYWPF	10	40.8				4282	4.055	1.736			
II	XWPF	31	34		4.229	0.9677	16939	2.072	3.510	3.744	0.624	16.7
	LYWPF	10	30.6				34153	1.304	4.452			
	HYWPF	10	40.8				7761	4.214	3.271			
III	WPF	37	34	0	4.536	0.8222	16931	1.213	2.053	2.103	0.389	18.5
	XWPF	33	34	15			11206	1.762	1.974			
	HYWPF	10	40.8				4279	4.051	1.734			
	LYWPF	10	30.6				24958	1.061	2.649			

Notes: 1 Material: 7475-T7351 Aluminum

2 NAS 6204 ($\frac{1}{4}$ dia.) Protruding Head Bolts

3 $a_0 = x_u = 0.03"$

in the α and β_{ℓ_i} values for comparable cases in Tables A3 and A4.

$Q_i^{*\beta_{\ell_i}}$ should be a constant for the EIFS distribution to be "generic". Since $Q_i^{*\beta_{\ell_i}}$ depends on " α " and " b ", the $Q_i^{*\beta_{\ell_i}}$ values are comparable only for the data sets pooled. For example, in Table A3 the $Q_i^{*\beta_{\ell_i}}$ values for Case I are not directly comparable with any of the other cases in the table.

Individual $Q_i^{*\beta_{\ell_i}}$ values from Table A3, as well as average, standard deviation and coefficient of variation values for $Q_i^{*\beta_{\ell_i}}$, are tabulated for comparison in Tables A5 and A6. The $Q_i^{*\beta_{\ell_i}}$ values don't vary significantly for different stress levels, load spectra and % load transfer. This suggests that $Q_i^{*\beta_{\ell_i}}$ values are independent of load spectra, stress level and % load transfer through the fastener.

A.4 STUDY IFQ MODEL RELATIONSHIPS

The IFQ model parameters from Table A3 for pooled data sets were used to evaluate the following assumed relationships.

$$Q = K\beta^A \quad (A1)$$

$$\beta = k\sigma^J \quad (A2)$$

$$Q = \xi\sigma^\gamma \quad (A3)$$

In Eqs. A1 through A3, A , K , k , J , ξ and γ are empirical constants and σ =gross stress. Results are summarized in Table A7 and plots are presented in Figs. A2 through A6.

TABLE A5 Comparison of $Q_i^* \beta_{\ell_i}$ Values for Different Spectra and Stress Levels
(15% LT, Straight Bore Holes)

% LT	σ (ksi)	$Q_i^* \beta_{\ell_i}$		α	b
		F-16 400 Hr.	B-1		
15	30.6	3.538	3.162	4.269	0.8902
↓	34	2.486	2.643	↓	↓
↓	40.8	2.380	2.578	↓	↓
	Ave. $Q_i^* \beta_{\ell_i}$	2.801	2.794		
	$S(Q_i^* \beta_{\ell_i})$	0.640	0.320		
	% C.O.V.	22.8	11.4		

TABLE A6 Comparison of $Q_i^* \beta_{\ell_i}$ Values for Different % LT, Stress Levels
and Spectra (Straight Bore Holes)

% LT	σ (ksi)	$Q_i^* \beta_{\ell_i}$		α	b
		F-16 400 Hr.	B-1		
0	34	2.695	3.425	4.364	0.8826
15	30.6	3.435	3.064	↓	↓
↓	34	2.409	2.563	↓	↓
↓	40.8	2.305	2.505	↓	↓
	Ave. $Q_i^* \beta_{\ell_i}$	2.711	2.889		
	$S(Q_i^* \beta_{\ell_i})$	0.510	0.437		
	% C.O.V.	18.8	15.1		

Table A7 Summary of Model Parameters and Empirical Constants for Pooled Data Sets

Data Set	σ (ksi)	α	b	$\beta_{\ell 1}$	$Q_I^* \times 10^4$	$Q_I^* = K \beta_{\ell 1}^A$		$\beta_{\ell 1} = k \sigma^J$		$Q_I^* = \xi \sigma^{\gamma}$	
						K	A	$k \times 10^{-13}$	J	$\xi \times 10^{12}$	γ
XWPF	34	4.245	0.8706	11152	2.045						
HYWPF	40.8	↓	↓	4240	5.129	0.3462	-0.7861	5.3848	-6.2860	5.5623	4.9414
LYWPF	30.6	↓		26789	1.211						
XWPB	34	4.299	0.9422	16930	1.952						
HYWPB	40.8	↓	↓	7761	4.138	0.8698	-0.8571	0.10404	-5.0562	43.5987	4.3337
LYWPB	30.6	↓		34174	1.165						
WPF	34	4.309	0.8707	16952	1.503						
XWPF	34	↓	↓	11164	2.046	0.3931	-0.8018	9.2179	-6.4169	2.4984	5.1451
HYWPF	40.8	↓	↓	4247	5.132						
LYWPF	30.6	↓		26859	1.211						
WPB	34	4.430	0.9322	36942	1.149						
XWPB	34	↓	↓	16974	1.869	0.5485	-0.8116	0.35384	-5.3531	35.8564	4.3445
HYWPB	40.8	↓	↓	7793	3.968						
LYWPB	30.6	↓		34265	1.114						
XWPF	34	4.269	0.8902	11157	2.228					13.162	4.724
HYWPF	40.8	↓	↓	4243	5.611			0.6006	↓	↓	
LYWPF	30.6	↓		26816	1.319	0.5600	-0.8317	0.9266	-5.672	8.729	
XWPB	34	↓	↓	16920	1.562			↓			
HYWPB	40.8	↓	↓	7754	3.325						
LYWPB	30.6	↓		34153	0.926						

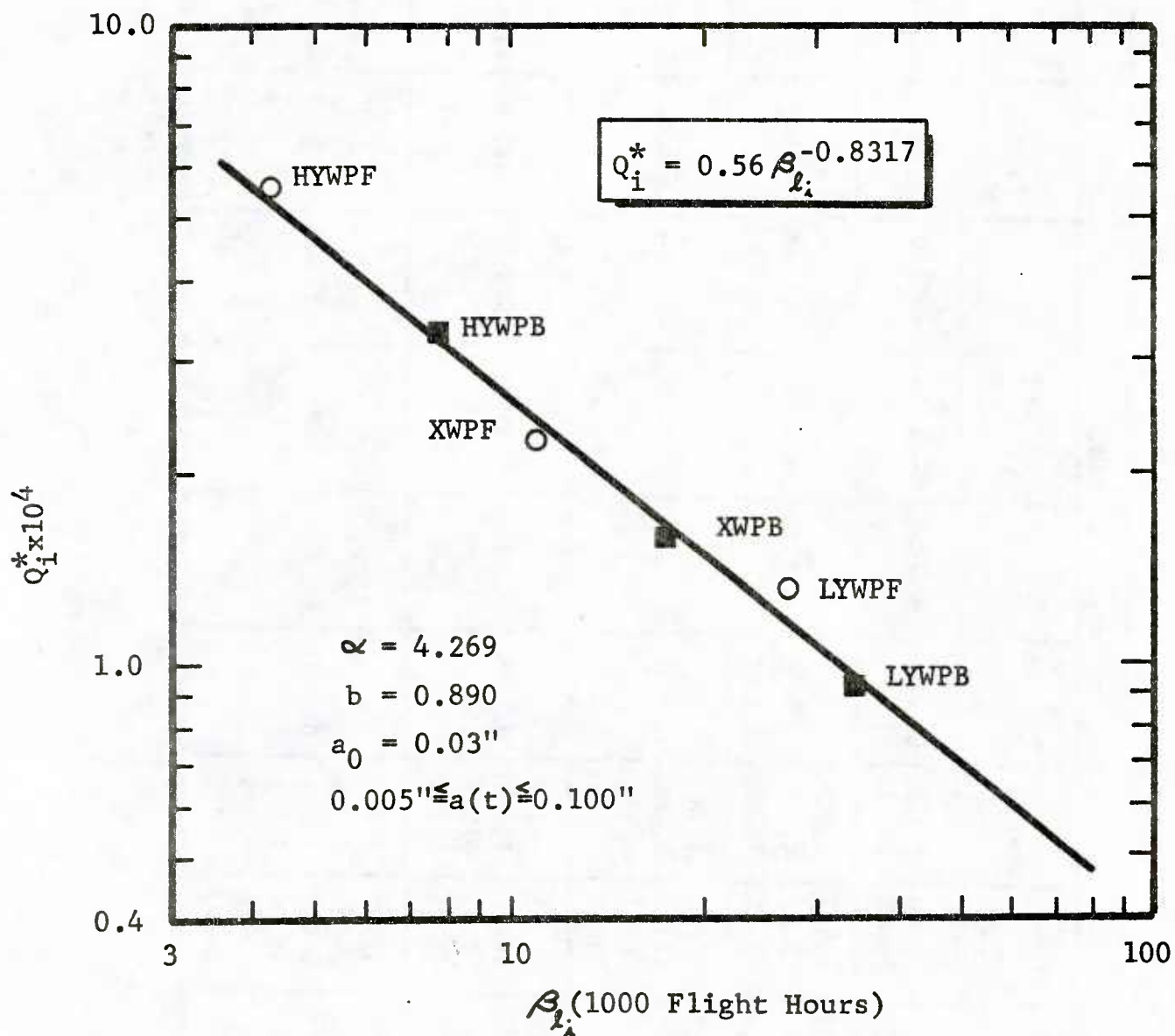


Fig. A2 $\ln Q_i^*$ Versus $\ln \beta_i$ for Pooled Data Sets (Case V; Table A3)

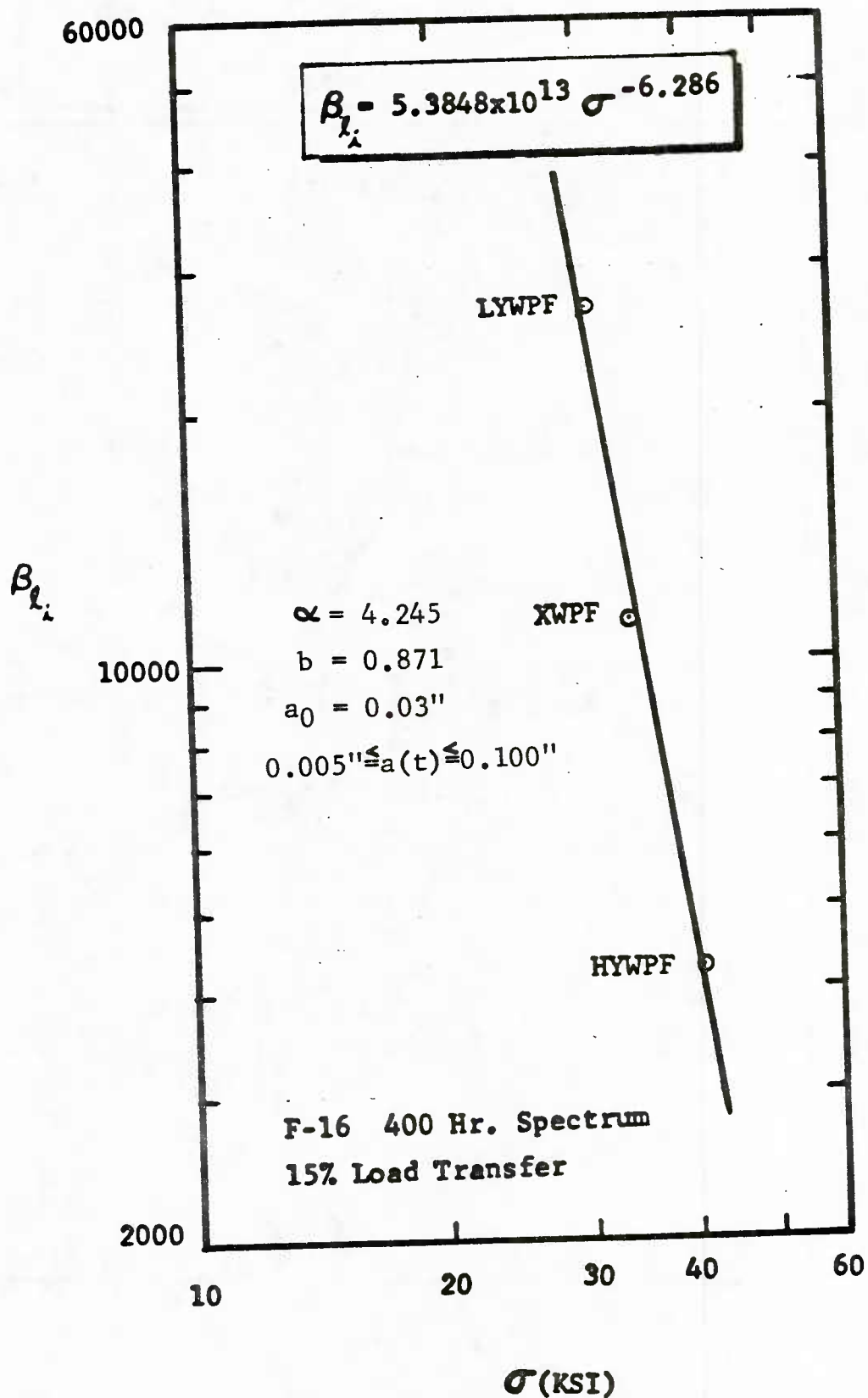


Fig. A3 $\ln \beta_{Li}$ Versus $\ln \sigma$ for Pooled Data Sets (Case I; Table A3)

$$\beta = k\sigma^j$$

$$A_{Li}(F-16) = 6.006 \times 10^{12} (\sigma)^{-5.672}$$

$$\beta_{Li}(B-1) = 9.266 \times 10^{12} (\sigma)^{-5.672}$$

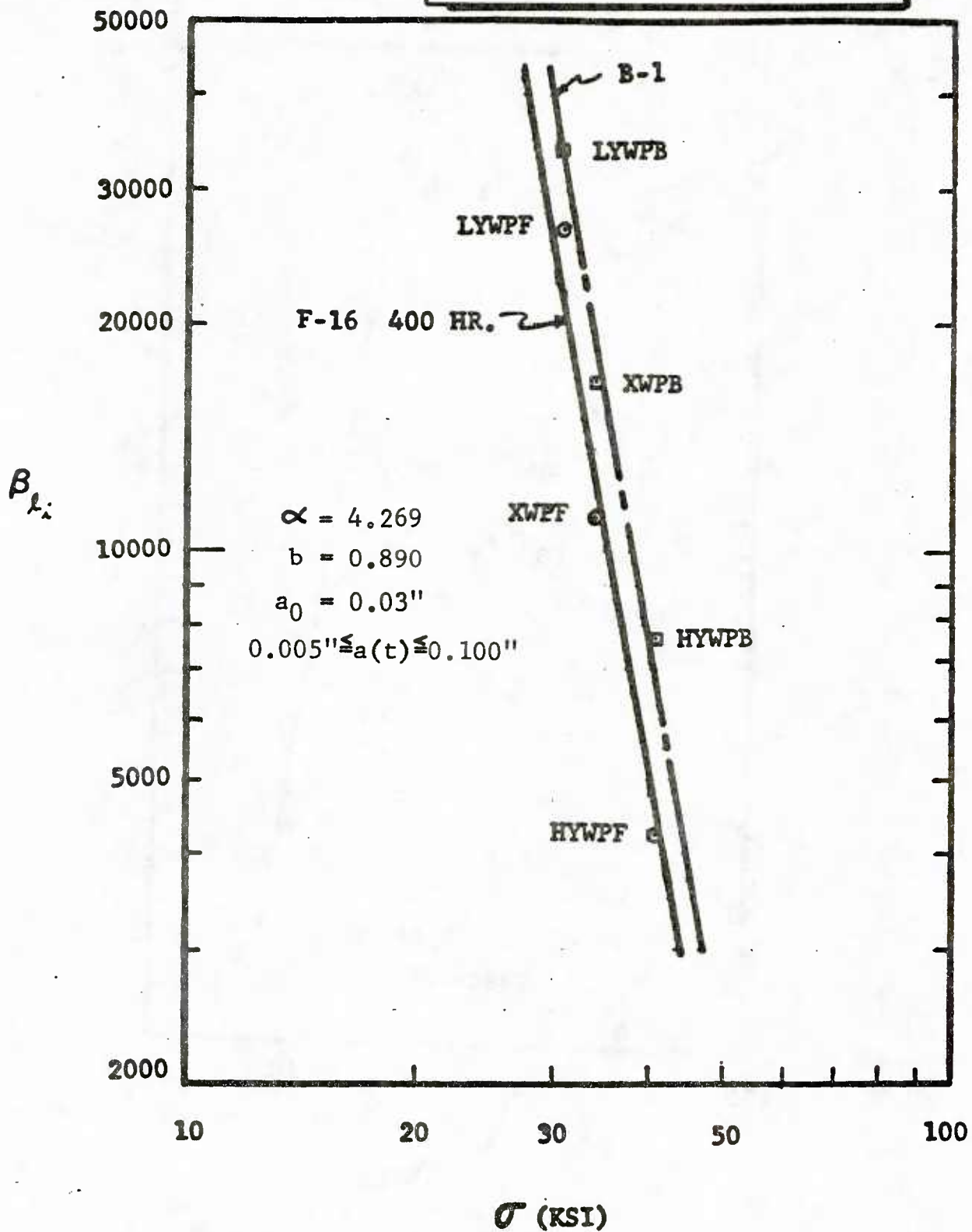


Fig. A4 $\ln \beta_{Li}$ Versus $\ln \sigma$ for Pooled Data Sets (Case V; Table A3)

$$Q_i^* = (5.5623 \times 10^{-12}) (\sigma)^{4.9414}$$

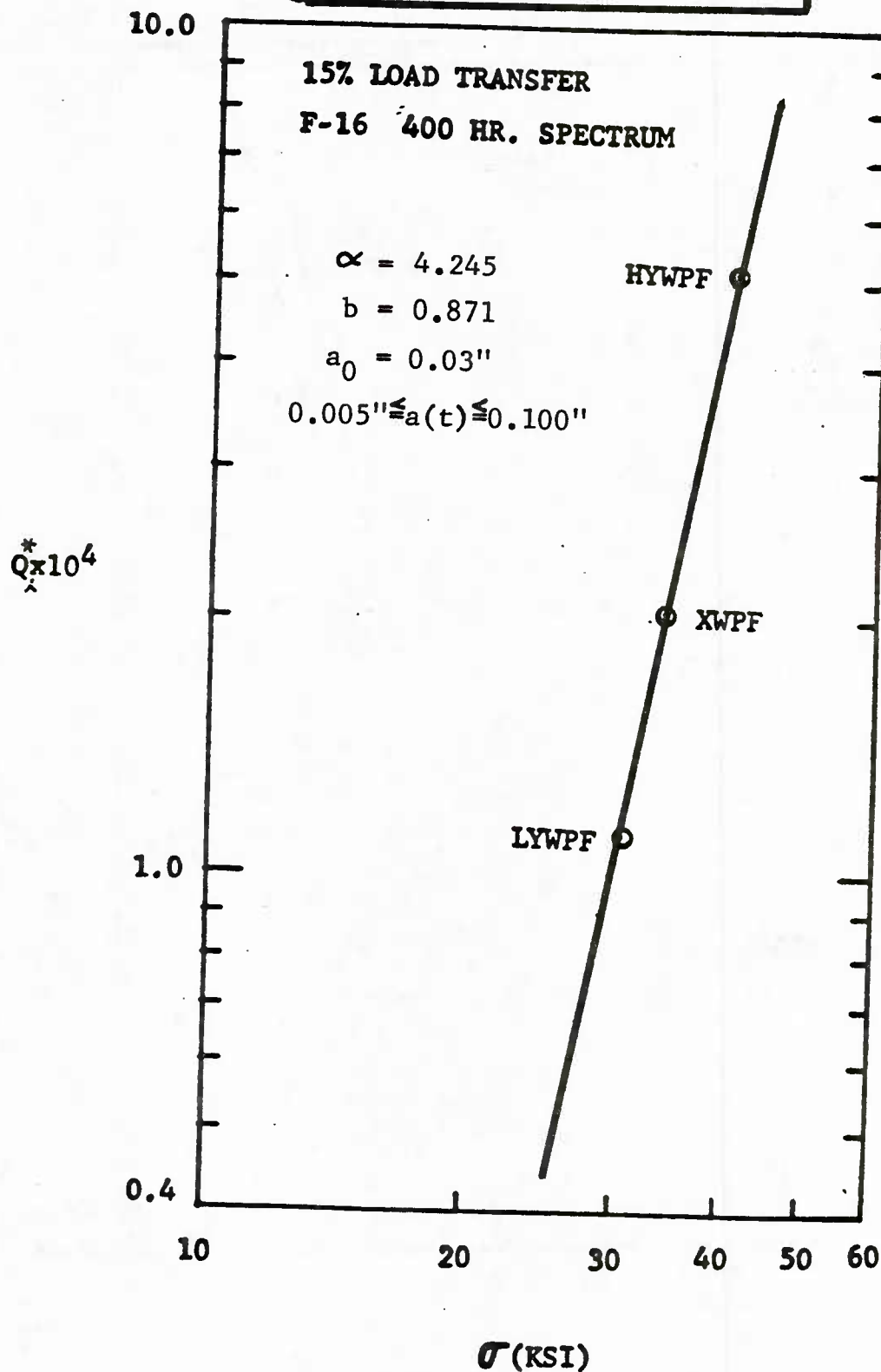


Fig. A5 $\ln Q_i^*$ Versus $\ln \sigma$ for Pooled Data Sets (Case I; Table A3)

$$Q = \xi \sigma^\gamma$$

$$Q_i^* \text{ (F-16)} = 13.165 \times 10^{-12} (\sigma)^{4.724}$$

$$Q_i^* \text{ (B-1)} = 8.729 \times 10^{-12} (\sigma)^{4.724}$$

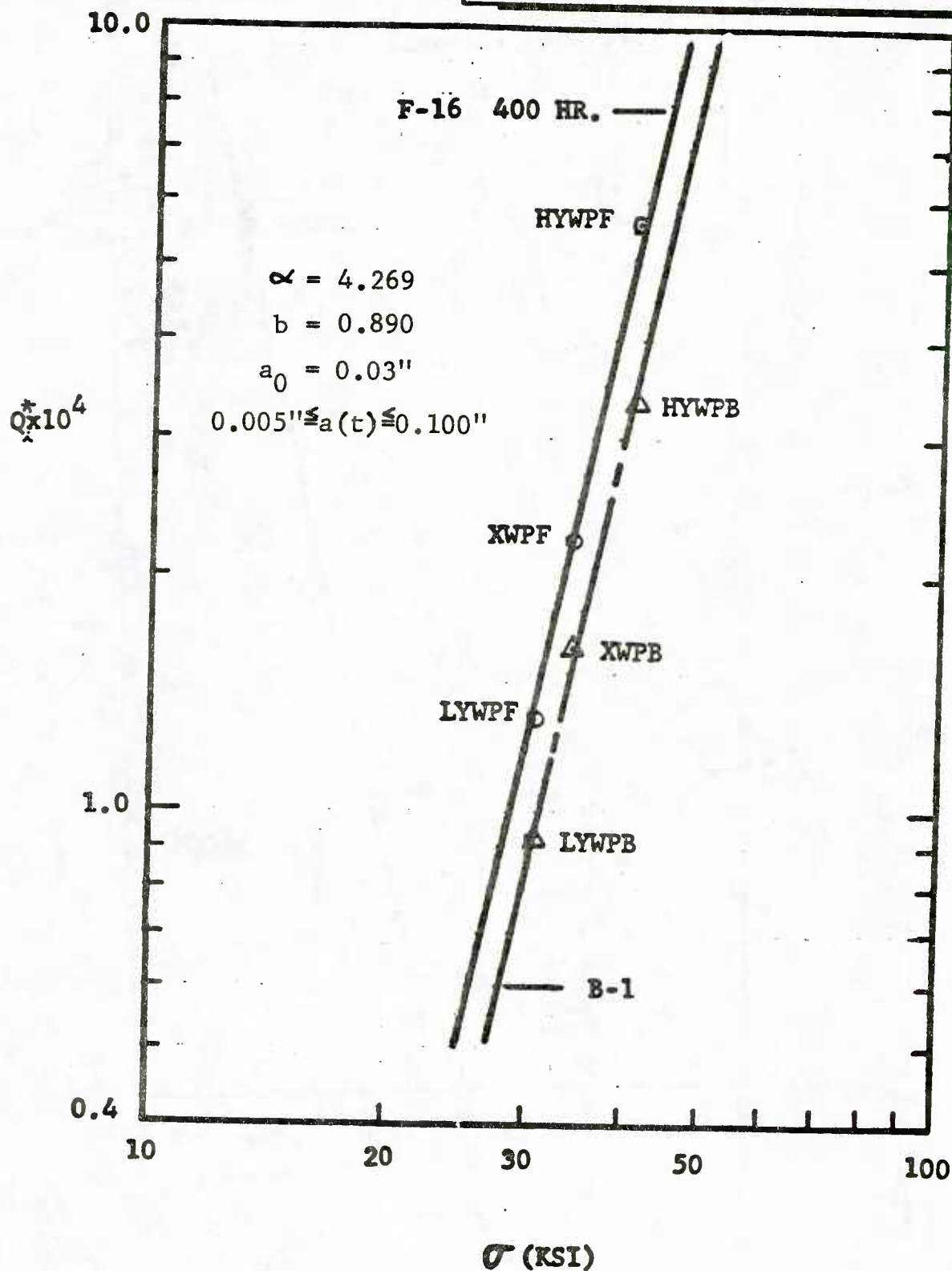


Fig. A6 $\ln Q_i^*$ Versus $\ln \sigma$ for Pooled Data Sets (Case V; Table A3)

$Q_i^* \beta_{\ell_i}$ values should be constant for different data sets for EIFS values to be "generic". This means the constant "A" in Eq. A1 should be -1.0 for a generic EIFS. A typical plot of $\ln Q_i^*$ versus $\ln \beta_{\ell_i}$ is shown in Fig. A2 for Case V. "A" values, summarized in Table A7 for various cases, vary from -0.7861 to -0.8571.

Q_i^* versus β_{ℓ_i} values from Table A3 are plotted in Fig. A2 for selected fighter and bomber data sets. This plot suggests that: (1) Q and β values for different data sets are directly comparable when they are determined using consistent data pooling procedures, (2) Eq. A1 is a promising relationship and (3) $Q_i^* \beta_{\ell_i}$ is independent of load spectra and stress level.

Plots for $\ln \beta_{\ell_i}$ versus $\ln \sigma$ (ksi) are shown in Figs. A3 and A4. The plot in Fig. A3 is for three fighter data sets and the plot in Fig. A4 is for pooled fighter and bomber data sets. Two parallel straight lines are shown in Fig. A4 for the fighter and bomber data sets. These lives were determined using a least square fit with Eq. A2 and a common slope (i.e., a constant J value) imposed. Eq. A2 correlates very well with the plotted results.

Plots for $\ln Q_i^*$ versus $\ln \sigma$ (ksi) are shown in Figs. A5 and A6. Eq. A3, based on a least squares fit, fits the plotted results very well. Constants ξ and γ are summarized for various data set combinations in Table A7.

A service crack growth master curve is needed to make $p(i, \tau)$ predictions using the EIFS cumulative distribution, $F_{a(0)}(x)$. Eq. A3 could be particularly useful for durability analyses if the $Q[a(t)]^b$ model is acceptable for defining the service crack growth master curve for different design stress levels. For example, Eq. A3 might be used to help define $y_{1i}(\tau)$ (i.e., the EIFS value corresponding to a crack size x_1 at service time τ) for different stress levels than the fractographic data base used to define the IFQ distribution. Such an approach has been used for the final demonstration of the durability methodology for the F-16 lower wing skin [36].

APPENDIX B

EVALUATION OF IFQ MODEL PARAMETERS FOR COUNTERSUNK FASTENER HOLES

B.1 INTRODUCTION

A similar study to the one documented in Appendix A is presented in this appendix for countersunk fastener holes. In this study the IFQ model parameters were determined for different combinations of pooled fractographic data sets. The model parameters were determined using the preliminary calibration procedures described in Section 4.3, the fractographic data from Ref. 6 and the computer program from Ref. 7. Also, the empirical relationships of Eqs. A1-A3 (Appendix A) were also evaluated.

The fifteen fractographic data sets used for this study are described in Table B1 and details are given in Ref. 6. Details for the 15%, 30% and 40% load transfer specimens are shown in Figs. 19-21. All fastener holes were drilled with a modified Winslow spacematic drill and the holes were not deburred.

This study reflected the following:

- o $\epsilon=0$ and $a_0=x_u$ (ref. Eq. 8)
- o $b \neq 1$ form of Eq. 2
- o a fractographic crack size range of $0.005'' \leq a(t) \leq 0.10''$ was used.

It should be noted that the procedures used to determine the IFQ Model parameters herein deviated slightly from those recom-

TABLE B1 FRACTOGRAPHIC DATA SETS USED

DATA SET	DIA* (IN)	% LOAD TRANSFER	σ (ksi)	TEST SPECTRUM	MATERIAL
AFXLR3	3/16	15	32	F-16 400	7475-T7351
AFXMR3	↓	↓	34	HR BLOCK	Aluminum
AFXHR3	↓	↓	38	↓	↓
AFXLR4	1/4	↓	32	↓	↓
AFXMR4	↓	↓	34	↓	↓
AFXHR4	↓	↓	38	↓	↓
ABXLR4	1/4	↓	36	B-1	↓
ABXMR4	↓	↓	38	Bomber	↓
ABXHR4	↓	↓	40.8	↓	↓
ABYLR4	↓	30	34	↓	↓
ABYMR4	↓	↓	36	↓	↓
ABYHR4	↓	↓	38	↓	↓
ABZLR4	↓	40	34	↓	↓
ABZMR4	↓	↓	36	↓	↓
ABZHR4	↓	↓	38	↓	↓

*MS90353 Countersunk Rivet (Blind, Pull-through)

mended in the Durability Design Handbook [21]. This study and others (e.g., 11-19, 31-36) provided the "experience" needed to develop the recommended calibration procedures and guidelines for the program [21].

IFQ model parameters are summarized herein. Further details about the study and conclusions are given in subsection 4.8.1.

B.2 IFQ MODEL PARAMETERS FOR INDIVIDUAL DATA SETS

IFQ Model parameters are summarized in Table B2 for pooled fractographic data sets. The parameters were determined using the fractography for the largest fatigue crack per specimen (i.e., $\ell_i=1$; no β scaling used).

In Table B2, the IFQ Model parameter notations are consistent with those of Ref. 21. Refer to Section A2 of Appendix A for a description of the subscripted/superscripted notations.

The α and b values in Table B2 were determined using the pooled fractographic data sets indicated. Once the pooled " α " value had been determined, the corresponding β_{ℓ_i} value for each data set pooled was determined using the computer program of Ref. 7.

$Q_i^* \beta_{\ell_i}$ values are tabulated in Table B2 for various fractographic data pooling combinations. In Table B2, the average, standard deviation and coefficient of variation for $Q_i^* \beta_{\ell_i}$ are also shown.

TABLE B2 Model Parameters for Pooled Data Sets (Csk Rivets: 0.005"-0.100" Crack Size Range)

CASE	Data Set ①	No. Specimens	a ₀	λ LT	② Dia.	σ (ksi)	α	b	c	P _{xi}	Q _x × 10 ⁴	Q _x β _{xi}			C.O.V. (%)
												Ave.	Std. Dev.		
I	AFXLR4	9	0.03	15	1/4	32	2.363	0.5999	-0.4901	13718	0.2603	0.357			
	AFXMR4	9				34				8322	0.3942	0.328	0.110	27.2	
	AFXHR4	9				38				5479	0.9708	0.532			
II	AFXLR4	9	0.05			32	2.644	0.5099	-0.4901	16965	0.2603	0.442			
	AFXMR4	9				34				10958	0.3942	0.432	0.126	24.7	
	AFXHR4	9				38				6744	0.9708	0.655			
III	AFXLR3	9	0.03		3/16	32	3.306	0.6886	-0.3114	12718	0.8506	1.082			
	AFXMR3	9				34				7984	1.069	0.853	0.193	21.9	
	AFXHR3	6				38				4367	1.601	0.699			
IV	ABXLR4	11			1/4	36	2.010	0.6209	-0.3791	14783	0.4663	0.689			
	ABXMR4	11				38				10495	0.5459	0.573	0.059	9.3	
	ABXHR4	11				40.8				8636	0.7583	0.655			
V	ABYLR4	10		30		34	2.571	0.6522	-0.3478	25895	0.3091	0.739			
	ABYMR4	10				36				13574	0.4518	0.533	0.106	16.3	
	ABYHR4	10				38				13431	0.5706	0.678			
VI	ABZLR4	10		40		34	2.137	0.5200	-0.4800	19916	0.2033	0.405			
	ABZMR4	8				36				15790	0.2831	0.447	0.040	8.9	
	ABZHR4	10				38				10917	0.444	0.485			
VII	AFXLR4	9		15		32	2.237③	0.5546	-0.4454	13999④	0.2991	0.419			
	AFXMR4	9				34				8269	0.4577	0.378			
	AFXHR4	9				38				5136	1.1212	0.598	0.093	18.9	
VIII	ABXLR4	11				36				16164	0.3736	0.604			
	ABXMR4	11				38				10649	0.4384	0.467			
	ABXHR4	11				40.8				7859	0.6126	0.481			
VIII	AFXLR4	9		15		32	2.683	0.5757	-0.4243	14014	0.3195	0.448			
	AFXMR4	9				34				8541	0.4913	0.419			
	AFXHR4	9				38				5632	1.2000	0.676	0.129	23.4	
VIII	AFXLR3	9			3/16	32				12398	0.5905	0.732			
	AFXMR3	9				34				7780	0.7444	0.579			
	AFXHR3	6				38				4237	1.1030	0.467			

Notes: ① Material: 7475-T7351 Aluminum

② MS 90353 Countersunk Rivet (Blind, Pull-Through)

③ Average α

④ β = $\bar{X}/\Gamma (1 + 1/\alpha)$; \bar{X} = Average TTCl

TABLE B2 Model Parameters for Pooled Data Sets (Csk Rivets: 0.005-0.100" Crack Size Range)
(Continued)

Case	Data Set	No. Specimens	a_0	z LT	σ (ksi)	α	b	c	β_{L_2}	$Q_A \times 10^4$	$Q_A^* \beta_{L_2}$	$Q_A^* \beta_{L_2}^2$		
												Ave.	Std. Dev.	C.O.V. (%)
IX	ABXLR4	11	0.03	15	36	2.239③	0.5996	-0.4004	16170④	0.4343	0.702	→	→	→
	ABXMR4	11	→	→	38	→	→	→	10654	0.5089	0.542	→	→	→
	ABXHR4	11	→	→	40.8	→	→	→	7862	0.7082	0.557	→	→	→
	ABYLR4	10	→	30	34	→	→	→	26997	0.2584	0.698	→	→	12.1
	ABYMR4	10	→	→	36	→	→	→	13317	0.3791	0.505	→	→	→
	ABYHR4	10	→	→	38	→	→	→	13409	0.4855	0.648	→	→	→
	ABZLR4	10	→	40	34	→	→	→	21048	0.2644	0.557	→	→	→
	ABZMR4	8	→	→	36	→	→	→	14946	0.3669	0.548	→	→	→
X	ABZHR4	10	→	→	38	→	→	→	10781	0.5775	0.623	→	→	→
	AFXLR4	9	→	15	32	2.477③	0.60969	-0.39031	13983④	0.3553	0.497	→	→	→
	AFXMR4	9	→	→	34	→	→	→	8259	0.5506	0.455	→	→	→
	AFXHR4	9	→	→	38	→	→	→	5329	1.3399	0.714	→	→	→
	AFXLR3	9	→	3/16	32	→	→	→	12859	0.6591	0.848	→	→	→
	AFXMR3	9	→	3/16	34	→	→	→	8184	0.8301	0.679	→	→	→
	AFXHR3	6	→	3/16	38	→	→	→	4295	1.2341	0.530	→	→	→
	ABXLR4	11	→	1/4	36	→	→	→	16145	0.4492	0.725	→	→	17.3
	ABXMR4	11	→	→	38	→	→	→	10637	0.5261	0.559	→	→	→
	ABXLR4	10	→	→	40.8	→	→	→	7849	0.7315	0.574	→	→	→
	ABYLR4	10	→	30	34	→	→	→	26955	0.2674	0.721	→	→	→
	ABYMR4	9	→	→	36	→	→	→	13297	0.3921	0.521	→	→	→
	ABYHR4	10	→	→	38	→	→	→	13388	0.4990	0.668	→	→	→
	ABZLR4	10	→	40	34	→	→	→	21015	0.2733	0.574	→	→	→
	ABZMR4	8	→	→	36	→	→	→	14923	0.3790	0.566	→	→	→
	ABZHR4	10	→	→	38	→	→	→	10765	0.5969	0.643	→	→	→

- Notes: ① Material: 7475-T7351 Aluminum
 ② MS 90353 Countersunk Rivet (Blind, Pull-Through)
 ③ Average α
 ④ $\beta = \bar{X}/\Gamma (1 + 1/\alpha)$; \bar{X} = Average TTCT

One of the conditions for a "generic" EIFS distribution is that $Q_i^* \beta_{\ell_i}$ should be a constant for a given material, drilling procedure, fastener type and fit [21]. Since $Q_i^* \beta_{\ell_i}$ values depend on the applicable " α " and " b ", the $Q_i^* \beta_{\ell_i}$ values are comparable only for the data sets pooled. For example, in Table B2 the average $Q_i^* \beta_{\ell_i}$ values for Cases V and VI are not compatible because the " α " and " b " values are different for each case. It has also been shown that Q and b are cross correlated constants [33], i.e., Q depends on b and vice versa.

$Q_i^* \beta_{\ell_i}$ values and statistics for selected fractographic data sets for case X of Table B2 are compared in Tables B3-B5. For example, individual $Q_i^* \beta_{\ell_i}$ values are shown for different situations and the average, standard deviation and coefficient of variation for $Q_i^* \beta_{\ell_i}$ are also shown. $Q_i^* \beta_{\ell_i}$ values are compared for different stress levels and load spectra, for different hole diameters ($D = 1/4"$ and $3/16"$) and for different % load transfer and stress levels in Tables B3, B4 and B5, respectively.

B.3 STUDY IFQ MODEL RELATIONSHIPS

Empirical relationships, given by Eqs. A1-A3, were evaluated using results for Case X from Table B2. Plots for $\ln Q_i^*$ versus $\ln \beta_{\ell_i}$, $\ln Q_i^*$ versus $\ln \sigma$ and $\ln \beta_{\ell_i}$ versus $\ln \sigma$ are presented in Figs. B1, B2 and B3, respectively. The empirical constants for each figure were determined using a least squares fit.

*
TABLE B3 Comparison of $Q_i \beta_{\lambda_i}$ Values for Different Stress Levels and Spectra
(15% LT. 1/4" Dia. Csk Hole)

% LT	σ (ksi)	$Q_i \beta_{\lambda_i}$		α	b
		F-16 400 Hr.	B-1		
15 ↓	32	0.497	--- ①	2.477 ↓	0.6097 ↓
	34	0.455	--- ①		
	36	--- ①	0.725		
	38	0.714	0.559		
	40.6	--- ①	0.574		
Ave. $Q_i \beta_{\lambda_i}$		0.555	0.619		
S($Q_i \beta_{\lambda_i}$)		0.139	0.092		
% C.O.V.		25.0	14.8		

Note: ① No fractographic data for given stress level.

TABLE B4 ^{*}
Comparison of $Q_i \beta_{\ell_i}$ Values for Different Hole Diameters
(F-16 400-Hour Spectrum; Csk Hole)

Z LT	σ (ksi)	[*] $Q_i \beta_{\ell_i}$		α	b
		D=1/4"	D=3/16"		
15 ↓	32 34 38	0.497 0.455 0.714	0.843 0.679 0.530	2.477 ↓	0.6097 ↓
Ave. $Q_i^* \beta_{\ell_i}$		0.555	0.686		
S($Q_i^* \beta_{\ell_i}$)		0.139	0.159		
% C.O.V.		25.0	23.2		
Ave. $Q_i^* \beta_{\ell_i}$		0.620			
S($Q_i^* \beta_{\ell_i}$)		0.151			
% C.O.V.		24.4			

TABLE B5 Comparison of $Q_i^* \beta_{\ell_i}$ Values for Different % LT and Stress Levels
(B-1 Bomber Spectrum; Csk Hole)

% LT	σ (ksi)	$Q_i^* \beta_{\ell_i}$	Ave. $Q_i^* \beta_{\ell_i}$	$S(Q_i^* \beta_{\ell_i})$	C.O.V. (%)
15 ↓	36 38 40.8	0.725 0.559 0.574	↑ 0.619 ↓	↑ 0.092 ↓	↑ 14.8 ↓
30 ↓	34 36 38	0.721 0.521 0.668	↑ 0.637 ↓	↑ 0.104 ↓	↑ 16.3 ↓
40 ↓	34 36 38	0.574 0.566 0.643	↑ 0.594 ↓	↑ 0.042 ↓	↑ 7.1 ↓
Ave. $Q_i^* \beta_{\ell_i}$		0.617			
$S(Q_i^* \beta_{\ell_i})$		0.075	$\alpha = 2.477$		
% C.O.V.		12.1	$b = 0.6097$		

$$\alpha = 2.477$$

$$b = 0.609$$

$$a_0 = 0.03''$$

$$0.005'' \leq a(t) \leq 0.100''$$

$$Q_i^* = 0.312 \beta_{xi}^{-0.928}$$

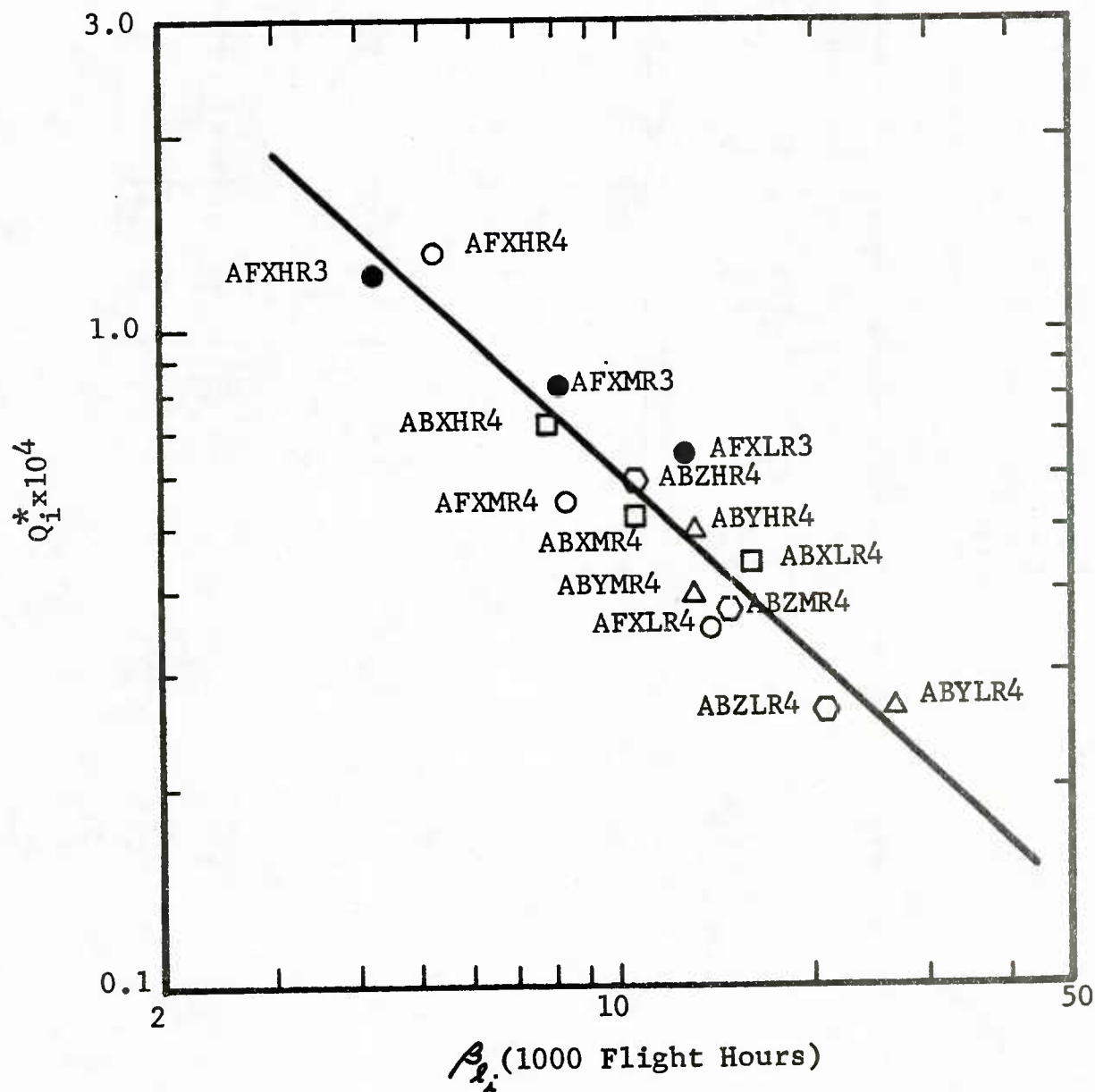


Fig. B1 $\ln Q_i^*$ Versus $\ln \beta_{xi}$ for Pooled Data Sets (Case X; Table B2)

$$\alpha = 2.477$$

$$b = 0.609$$

$$a_0 = 0.03''$$

$$0.005'' \leq a(t) \leq 0.100''$$

$$Q_i^* \text{ (F-16)} = 1.579 \times 10^{-13} (\sigma)^{5.638}$$

$$Q_i^* \text{ (B-1)} = 0.656 \times 10^{-13} (\sigma)^{5.638}$$

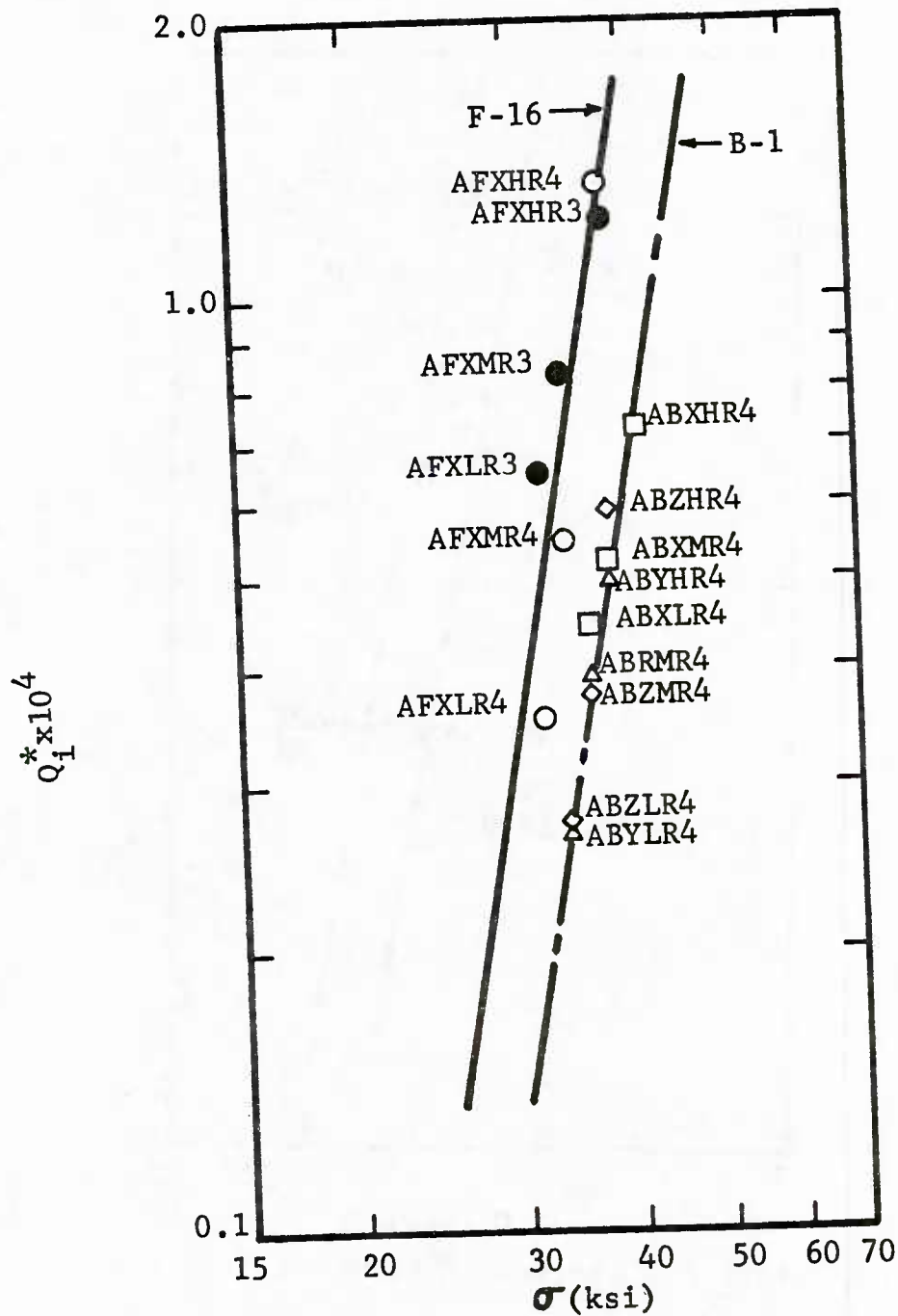


Fig. B2 $\ln Q_i^*$ Versus $\ln \sigma$ for Pooled Data Sets (Case X; Table B2)

$$\alpha = 2.477$$

$$b = 0.609$$

$$a_0 = 0.03''$$

$$0.005'' \leq a(t) \leq 0.100''$$

$$\beta_i(\text{F-16}) = 1.140 \times 10^{13} (\sigma)^{-5.935}$$

$$\beta_i(\text{B-1}) = 2.625 \times 10^{13} (\sigma)^{-5.935}$$

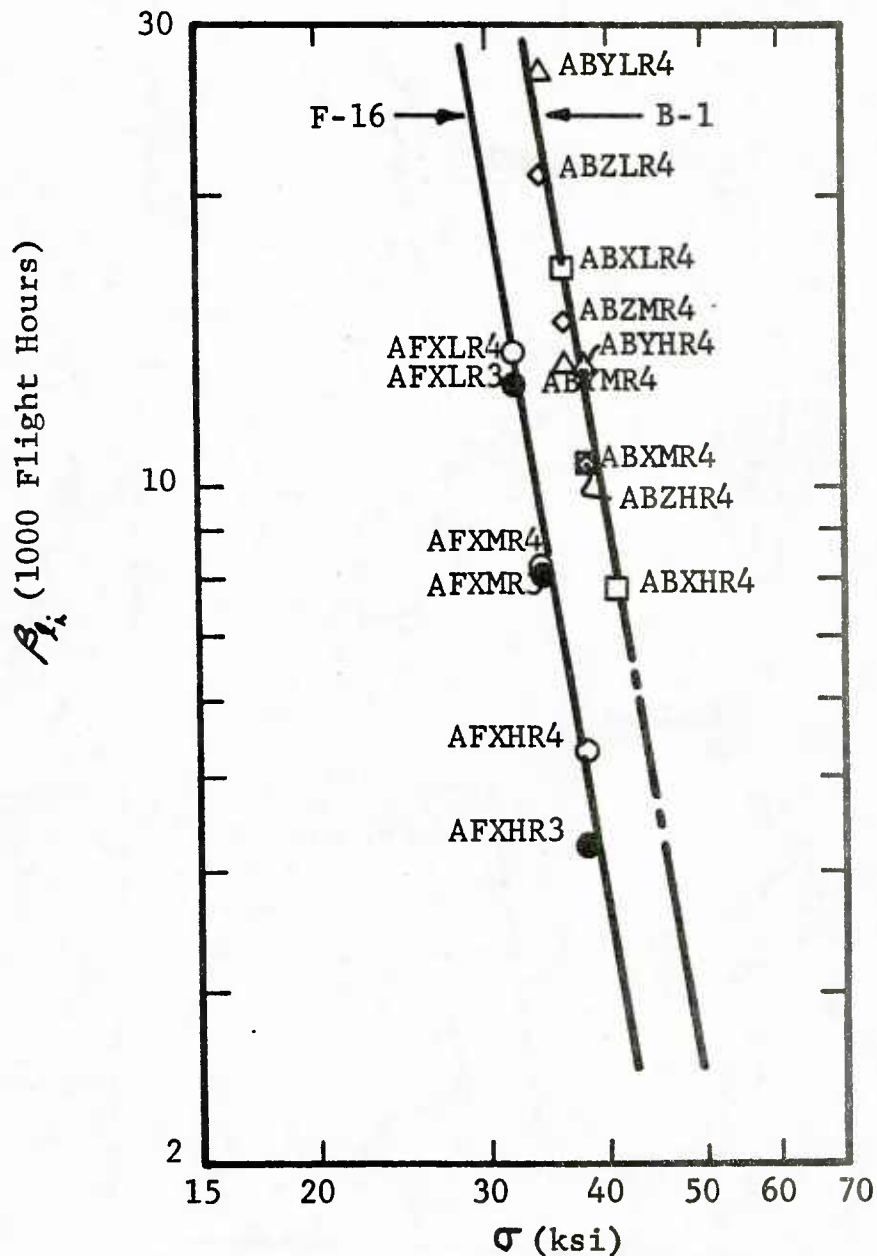


Fig. B3 $\ln \beta_i$ Versus $\ln \sigma$ for Pooled Data Sets (Case X; Table B2)

APPENDIX C

RELATED DURABILITY STUDIES

C.1 SCALE-UP EFFECTS AND HOLE INTERACTION

C.1.1 Introduction

In general, experimental results on the crack growth observed in coupon specimens, full-scale structural components and prototype structures manifest scale-up and interaction effects. When these test specimens have fastener holes, it is reasonable to assume that, under the usual loading conditions, the crack growth always concentrates at the points of highest stress concentration around the fastener holes.

The following list indicates the major sources of the scale-up effects.

- A. Increase in the number of fastener holes
- B. Change in stress field
- C. Increased variability in workmanship
- D. Increased variability in material properties

Preliminary analytical models for the scale-up effects resulting from these sources are proposed in the following. It appears, however, that the interaction effects can be disregarded since the crack size to be dealt with in the present durability study is at most of the order of 50 mils while the distances between the two closest adjacent fastener holes are obviously much larger than 50 mils.

C.1.2 Scale-Up Effect Due to Increase in Number of Fastener Holes

Consider a set of nominally identical wing skin panels, each with N fastener holes subjected to the same state of stress. Let $p(x,t)$ denote

the probability that the crack size around a fastener hole will be larger than x at time t and $N(x,t)$ the number of holes with such a crack size at time t . Then, the expected value $\bar{N}(x,t)$ of $N(x,t)$ can be shown to be

$$\bar{N}(x,t) = N p(x,t) \quad (C1)$$

and the variance $\sigma_N^2(x,t)$ of $N(x,t)$

$$\sigma_N^2(x,t) = N p(x,t) [1 - p(x,t)] \quad (C2)$$

if the probability $p(x,t)$ associated with one fastener hole is independent of the probabilities associated with other fastener holes, while

$$\sigma_N^2(x,t) = N^2 p(x,t) [1 - p(x,t)] \quad (C3)$$

if the probability is completely dependent. It is recognized, however, that reality lies between these two extreme cases and so does the true variance. The following observations can be made from Eqs. C1 - C3: (a) While the expected value of the number $N(x,t)$ of fastener holes with cracks larger than x at time t increases proportionally to the number N of the holes in the panel, the variance $\sigma_N^2(x,t)$ of $N(x,t)$ is proportional to N or N^2 contingent upon whether the crack growth probability $p(x,t)$ is independent or dependent, and (b) this makes it possible to determine whether the probability is closer to the case of ideal independence or to that of complete dependence by estimating the variance from experiments performed on a set of nominally identical panels.

C.1.3 Scale-Up Effect Due to Change in Stress Field

The probability $p(x,t)$ that each hole has a crack larger than x at

time t depends on the state of stress around the hole. Therefore, if the i -th fastener hole is subjected to the stress state unique to that hole, the probability $p(x,t)$ for this hole should reflect such a state of stress and can be denoted by $p_i(x,t,s)$ in which s symbolically represents the state of stress around the hole. Under the assumption that the probability $p_i(x,t,s)$ is independent of $p_j(x,t,s)$ ($j \neq i$), it can be shown that

$$\bar{N}(x,t) = \sum_{i=1}^N p_i(x,t,s) \quad (C4)$$

$$\sigma_N^2(x,t) = \sum_{i=1}^N p_i(x,t,s) [1 - p_i(x,t,s)] \quad (C5)$$

C.1.4 Scale-Up Effect Due to Variability in Workmanship

The spatial variability in workmanship is expected to produce variability in the stress state around each fastener hole. Therefore, Eqs. C4 and C5 can also be used in this case as the expected value and variance of $N(x,t)$, respectively.

• C.1.5 Scale-Up Effect Due to Variability in Material Properties

The existence of nonhomogeneity in the material properties requires, in principle, that the parameters of the crack growth equation be adjusted accordingly and thus that different master curves be used for individual fastener holes. Therefore, the probability $p(x,t)$ that the crack size will be larger than x around a fastener hole at time t varies from fastener hole to fastener hole, and hence it will be denoted by $p_i(x,t)$. Then, Eqs. C4 and C5 are again valid for the expected value and variance of $N(x,t)$.

C.1.6 Concluding Remarks

The analytical expressions for the expected value and variance of the number of fastener holes with a crack larger than x at time t are derived in terms of the total number of fastener holes in the specimen and the probability that such a crack will be found around a fastener hole at time t . This probability can be estimated from a crack growth analysis based on the fracture mechanics theory and experimental evidence. The significance of the dependence and independence of the same probabilities associated with individual fastener holes has been pointed out. The way in which these probabilities depend on the change in the stress field and the variabilities due to workmanship and material properties has also been indicated. Development of a data base for more detailed theoretical and numerical analysis is strongly recommended.

C2. DEVELOPMENT OF TRANSFER FUNCTIONS

C.2.1 Introduction

Figure C1 schematically shows five crack growth curves for a crack of initial crack size c_0 under five different load spectra I, II, ..., V. These crack growth curves imply that the intensity of load spectrum I is the highest, that of II the second highest and so on. A question immediately arises as to how such a (spectral) intensity can be quantitatively defined. One possible way in which this can be achieved is to use a single parameter indicator of the intensity such as the root mean square (rms) value $\sqrt{\Delta\sigma^2}$ of the rise and fall of the stress history. Other indicators involving two or more parameters may be found to be desirable. However,

since the present study places its emphasis on the exploratory development of transfer function methodology, the rms value of the rise and fall of a stress history is used for the definition of the spectral intensity primarily because of its simplicity.

Figure C2 also schematically shows the relationship between the spectral intensity and the flight hours needed for a crack to grow from its initial size c_0 to $5c_0$ (Curve A), $10c_0$ (Curve B) and $20c_0$ (Curve C). For example, Curve B indicates that T_1, T_2, \dots, T_5 flight hours are required for a crack of initial size c_0 to grow to that of size $10c_0$ under the spectral intensity associated with the spectra I, II, ..., V, respectively.

Both Figs. C1 and C2 show the transfer characteristics among load spectra; Fig. C1 may be used to trace the process of crack growth under a combined load spectrum. For example, the initial crack of size c_0 , subjected to load spectrum III, grows to $10c_0$ (Point P_1 in Fig C1) after T_3 flight hours. This crack of size $10c_0$ then grows under spectrum II to $20c_0$ after T'_2 flight hours ($P_2 \rightarrow P_3$). If this crack of size $20c_0$ is further subjected to load spectrum IV, it will grow to the critical size c_{cr} after T'_4 flight hours ($P_4 \rightarrow P_5$). On the other hand, Fig C2 can be used to establish a crack growth curve corresponding to a load spectrum, say, I_0 , for which no crack growth curve is available. This can be done by assuming that under spectrum I_0 , the initial crack of size c_0 will grow to $5c_0$, $10c_0$ and $20c_0$ after, respectively, T_{Q1} , T_{Q2} and T_{Q3} flight hours and interpolating curve I_0 through the points Q_1 , Q_2 and Q_3 plotted in Fig C1 which corresponds to the points Q_1 , Q_2 and Q_3 in Fig. C2. In the following, the curves in Fig. C2 are referred to as generalized S-N curves for their obvious similarity to the well-known S-N fatigue curves.

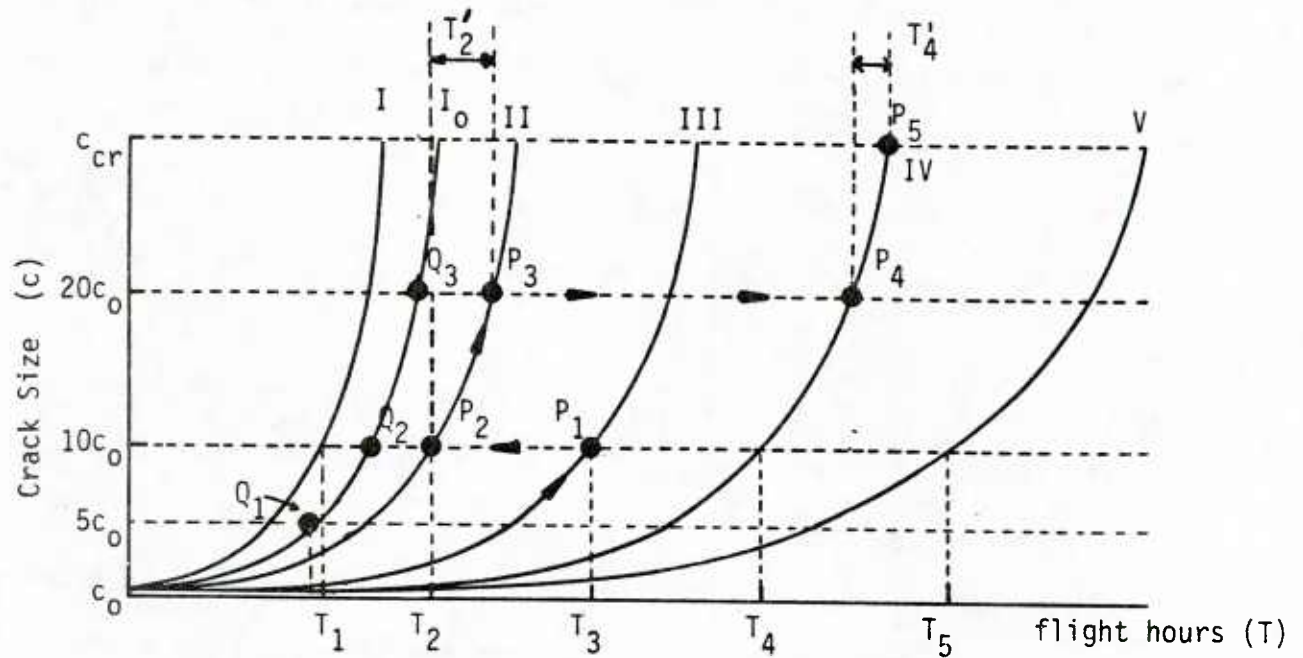


Fig. C1 Schematic Comparisons of Crack Growth Curves for Different Load Spectra

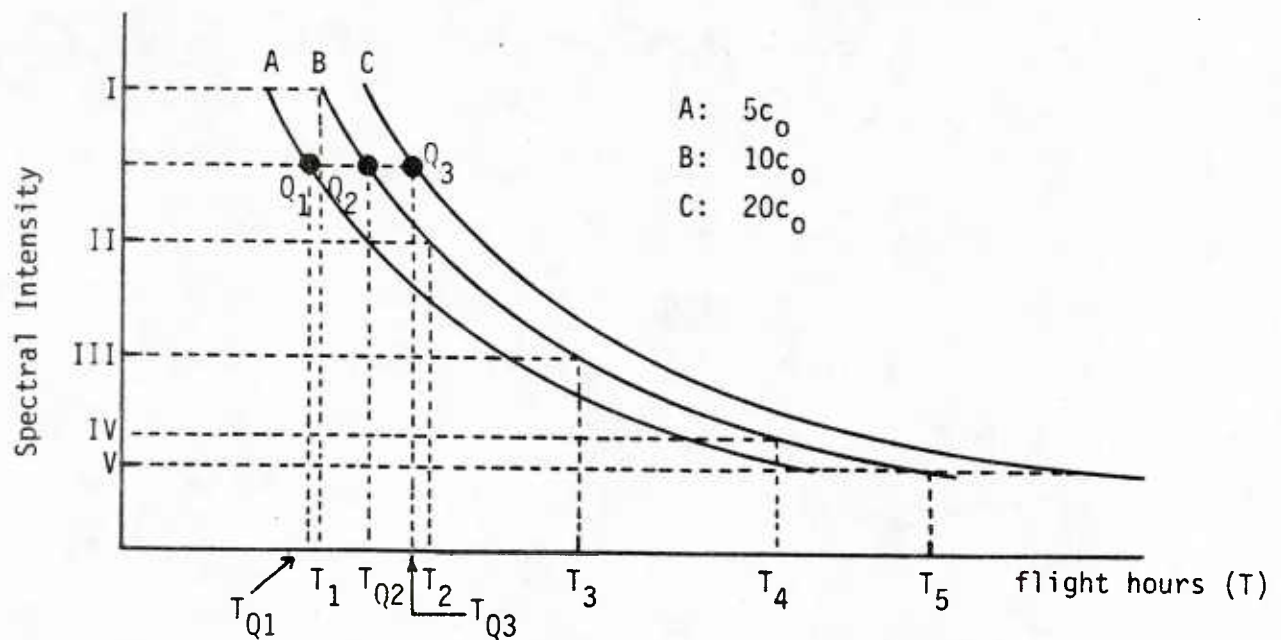


Fig. C2 Relationship Between Spectral Intensity and Flight Hours

C.2.2 Development of Crack Growth and Generalized S-N Curves

A computer program named "CYCGRO" was originally developed by the Rockwell International Corporation and later modified by Modern Analysis Inc. to accommodate a random stress sequence as the input [C1]. The program computed the size of a crack, as it grows from its initial size c_0 , by integrating the cycle-by-cycle (differential) equation representing the crack growth rate in terms of the range of the stress intensity factor, current crack size, R-factor, etc. The modified version of the program also includes a routine in which a crack growth curve is constructed by evaluating the rate of crack growth per flight (rather than per cycle) at various values of the existing crack size with the aid of the unit block approach [C2].

The CYCGRO program, together with the unit block approach, is also utilized in the present investigation to construct crack growth curves and corresponding generalized S-N curves. Five of the more realistic load spectra are considered as listed below. In all cases, the initial crack size is assumed to be $c_0 = 0.01$ ".

ID	LOAD SPECTRA	RMS
I	F-15 (Air-Air; $\sigma_{LIM} = 40$ ksi)	14.8 ksi
II	GD 400 hr ($\sigma_{LIM} = 34$ ksi)	9.93 ksi
III	GD 400 hr ($\sigma_{LIM} = 28.9$ ksi)	8.44 ksi
IV	B-1 (Combat)	5.80 ksi
V	B-1 (Crew Training)	5.18 ksi

Load spectrum I is defined by the random stress sequence listed in Table C1 which represents a block of fifty flights (totaling 46 flight hours) used in the unit block analysis approach. Each stress level of this sequence is in terms of the percentage of the limit stress σ_{LIM} which, for numerical purposes, is taken as 40 ksi. Load spectra II and III are also given in the form of a random stress sequence in Table C2 with each stress level again indicating the percentage of σ_{LIM} . Load spectra II and III are obtained by setting $\sigma_{LIM} = 34$ ksi and $\sigma_{LIM} = 28.9$ ksi, respectively, in this sequence. In each case, the size of one unit block used for computing the flight-by-flight crack growth rate involves 400 flight hours. Table C3 shows a representative stress sequence in one complete flight under spectrum IV while Table C4 lists the same under spectrum V. In both cases, the size of one unit flight consists of fifty flights. However, one unit block is equivalent to 450 and 200 flight hours for spectra IV and V, respectively. The rms values associated with the load spectra listed above are evaluated directly from these stress histories. The crack growth curves for all the load spectra are computed using the CYCGRO program and are shown in Fig. C3. From these crack growth curves, the time T (flight hours) needed for the initial crack size $c_0 = 0.01$ " to grow to the sizes $c = 2c_0, 4c_0, 6c_0, 8c_0$ and $10c_0$ are read and plotted for each load spectrum which is now represented in terms of the rms stress intensity value as shown in Fig. C4: The five different values of T needed for c_0 to reach $2c_0, 4c_0, 6c_0, 8c_0$ and $10c_0$ at each load spectrum intensity level. Smooth curves are then drawn by interpolation through the five sets of five points in Fig. C4, with each set indicating a generalized S-N curve or the relationship between the spectral intensity and the flight hours T needed to produce a specific value of c : For

Table C1 F-15 Load Spectrum (Air-Air)

Notes: Random spectrum.

A block of fifty (50) flights (46 hrs. in block).

Percentage of σ_{LIM}									
σ_{min}	σ_{max}	σ_{min}	σ_{max}	σ_{min}	σ_{max}	σ_{min}	σ_{max}	σ_{min}	σ_{max}
-5.0	70.0	16.1	54.1	20.1	45.5	25.0	52.3	34.0	58.7
28.2	44.5	18.6	48.6	24.5	81.9	8.6	29.4	17.8	52.4
17.5	29.5	10.2	79.9	18.6	50.6	32.5	53.7	17.3	65.7
50.6	63.5	3.1	67.5	10.9	60.6	-44.0	54.9	16.2	49.1
14.7	34.0	20.4	58.4	31.2	45.6	27.8	63.5	9.4	69.7
36.1	58.2	-5.0	79.4	27.6	42.9	27.9	41.0	9.4	33.5
16.0	40.2	5.2	39.1	19.5	51.9	9.3	31.4	19.1	48.6
0.4	27.6	16.9	36.2	11.8	28.7	9.3	33.2	1.8	13.2
1.4	50.2	18.6	31.8	19.1	48.8	34.0	63.7	29.9	86.8
22.5	42.7	12.2	40.8	22.0	41.9	21.2	42.2	16.3	26.6
-3.6	27.3	11.9	45.3	-5.0	42.8	14.7	48.6	23.6	57.2
36.4	58.3	32.7	48.7	27.1	41.5	29.7	81.1	29.3	60.7
19.8	43.5	28.5	74.9	19.2	48.5	22.4	38.3	9.1	52.8
34.0	45.0	14.7	46.4	3.0	34.8	19.8	48.7	33.4	54.2
25.4	38.7	18.3	36.0	18.5	63.7	17.7	56.1	11.7	29.3
-7.5	41.4	15.3	33.8	9.7	36.1	-5.0	61.7	16.3	50.9
30.1	47.9	25.4	52.1	24.9	65.2	10.3	50.7	12.6	44.6
32.1	47.0	24.3	38.4	19.6	46.2	23.4	42.3	3.5	52.9
35.8	64.4	16.9	30.6	19.1	47.2	8.4	74.1	12.2	90.2
28.8	45.6	12.7	46.2	15.3	39.2	20.2	46.4	36.3	58.6
3.8	60.0	11.9	44.6	29.5	41.3	11.5	40.4	-5.0	47.4
6.9	44.3	32.4	58.2	16.3	55.1	-4.6	83.3	0.8	37.5
24.1	57.7	16.2	34.8	22.2	65.7	24.8	47.5	13.4	55.9
42.5	64.5	24.9	38.5	-22.0	61.8	36.2	66.4	39.4	60.9
39.4	56.8	25.5	51.2	34.5	54.9	28.8	39.5	9.7	81.0
-1.8	47.0	12.5	59.6	8.3	53.9	7.7	45.3	29.7	66.4
-5.0	49.2	5.5	33.5	15.0	36.1	2.7	58.5	2.8	40.9
13.8	38.1	13.2	51.7	4.0	33.3	9.4	29.3	11.6	68.5
18.7	37.3	19.3	40.6	1.1	25.6	8.3	67.1	32.8	71.0
19.0	45.4	30.9	45.9	13.5	48.1	21.1	57.3	13.9	35.2
21.5	51.4	12.5	42.8	11.3	41.4	22.8	47.5	17.9	48.9
17.5	55.1	-5.0	41.4	12.2	79.3	15.1	50.4	28.7	45.8
34.3	59.1	28.3	45.5	29.1	52.9	12.0	65.1	30.9	48.0
9.2	66.8	47.6	61.6	15.0	31.1	14.3	50.6	7.7	93.2
39.7	68.1	6.8	20.5	6.2	56.5	9.3	75.7	12.6	52.7
31.3	55.7	17.4	57.7	22.3	61.7	29.0	51.7	39.8	55.5
12.2	42.6	8.1	25.8	-5.0	60.0	13.5	56.0	16.8	83.7
21.6	32.8	20.3	43.4	9.7	48.1	33.5	45.2	-7.3	47.1
8.4	77.9	45.9	58.8	10.3	71.8	10.6	38.2	23.3	46.2
-9.8	40.3	4.9	41.1	17.9	42.7	9.1	41.8	27.2	58.7
29.8	42.9	13.3	46.0	1.2	26.5	-4.5	51.3	9.4	26.6
15.4	38.3	8.6	39.0	5.3	60.3	-5.0	42.2	13.0	34.4
15.8	55.6	12.7	40.8	23.6	49.4	38.7	53.9	29.7	41.0
18.2	33.3	22.5	46.5	3.0	44.7	6.4	39.8	22.5	64.3
24.5	57.0	26.3	53.4	9.8	33.3	0.9	46.4	0.3	48.9
24.5	47.4	22.3	47.2	6.3	77.9	29.9	74.7	19.7	84.1
22.7	58.6	4.7	72.1	7.6	72.3	17.5	53.0	-5.0	59.3
15.0	42.4	27.8	41.6	17.3	70.0	12.9	47.5	25.4	66.3

Table C1 F-15 Load Spectrum (Air-to-Air) (Continued)

50.3	89.9	-0.2	89.5	47.1	60.2	13.1	88.1	11.6	71.4
18.7	53.3	18.2	35.5	10.7	42.3	5.6	61.4	23.5	49.3
19.1	51.0	1.3	45.7	15.9	32.5	20.9	43.4	29.9	47.3
22.5	46.1	21.8	52.4	36.4	61.3	8.7	57.5	39.3	54.9
-5.0	39.9	28.4	50.2	8.9	31.0	13.8	55.9	47.8	75.9
16.6	50.3	34.6	46.2	11.4	66.4	11.7	55.5	-6.0	50.9
37.8	51.0	22.5	37.5	14.6	24.7	1.2	33.1	8.7	26.6
1.5	42.0	0.5	41.0	11.2	47.8	19.5	37.6	9.6	49.7
-0.4	40.1	29.0	44.2	23.4	60.8	14.2	40.4	23.3	45.3
24.3	56.8	-5.0	67.8	22.8	66.8	32.9	52.2	24.9	56.5
28.3	58.5	25.0	55.9	38.0	60.4	23.8	68.7	24.0	61.6
18.8	85.3	21.5	49.1	6.8	30.4	1.0	58.5	17.4	29.3
8.8	42.3	31.6	49.6	34.8	48.4	25.7	46.8	16.8	41.3
-0.7	61.2	8.6	42.7	5.1	44.9	16.0	59.0	-0.7	64.7
21.5	55.4	17.6	36.6	-5.0	36.9	7.5	55.0	24.8	51.4
2.2	72.7	1.3	32.2	-3.8	70.1	8.8	73.8	21.9	49.6
38.6	54.0	41.3	56.3	27.5	38.1	25.3	49.5	9.6	60.9
13.9	93.4	14.9	36.7	15.9	41.8	15.3	38.3	14.8	58.7
28.7	46.8	19.0	55.2	8.9	49.2	5.9	49.6	19.9	55.6
-0.1	21.5	-8.9	27.4	12.2	51.4	-5.0	59.9	16.8	78.8
-2.5	40.2	3.7	80.9	7.5	62.3	31.2	60.0	37.3	54.7
28.2	42.3	30.5	57.2	13.4	26.6	9.6	29.9	12.5	23.8
-0.7	55.7	-4.2	37.7	18.1	56.9	36.3	56.8	27.5	41.8
-0.6	47.0	23.3	62.3	10.0	50.8	30.6	50.0	15.0	57.6
20.2	37.6	21.7	53.2	37.1	65.4	18.7	57.7	-5.0	37.8
24.6	42.7	1.6	40.1	13.4	62.1	4.4	52.7	2.6	68.3
6.2	34.7	-0.9	38.9	24.2	59.2	2.4	47.6	12.3	36.2
9.1	52.4	2.4	16.6	-5.1	56.3	35.8	53.2	1.7	52.1
35.6	70.2	28.3	40.0	25.2	49.2	20.9	35.2	17.6	37.4
26.4	93.7	20.7	34.3	8.1	45.5	34.6	48.7	23.9	88.7
-5.0	82.4	21.1	54.4	30.2	60.1	5.8	35.7	14.5	60.4
23.2	48.4	19.9	49.7	5.5	68.3	42.8	54.9	24.5	48.8
23.8	42.7	5.8	43.6	26.00	74.2	12.6	34.2	24.3	37.5
24.9	36.9	26.5	55.5	22.5	66.8	52.5	65.0	23.9	56.2
12.7	61.0	27.4	53.4	13.3	37.9	20.5	33.2	22.3	40.3
25.7	62.8	-5.0	53.4	21.5	67.9	24.8	48.5	6.9	31.1
18.1	41.4	14.8	27.1	10.4	61.2	8.5	53.4	9.1	27.7
15.0	44.5	14.9	66.4	35.8	59.1	30.2	71.3	24.0	76.1
28.3	92.1	14.8	69.1	40.5	73.0	8.4	56.3	27.9	37.6
17.2	60.1	6.2	36.5	16.9	57.2	10.1	42.2	21.2	67.9
5.3	63.4	34.3	47.4	-5.0	52.9	21.4	57.5	17.5	38.7
10.0	56.2	26.1	45.5	27.9	60.4	25.5	41.8	14.7	56.5
24.9	37.0	24.6	47.5	17.2	92.5	5.3	44.1	5.4	20.5
-0.3	37.7	26.0	39.8	3.3	23.9	3.2	42.6	-1.9	57.6
42.5	82.9	19.4	74.2	13.4	68.8	23.2	52.5	26.4	37.7
9.1	35.9	22.0	69.2	32.4	54.8	-5.0	94.0	14.5	53.6
12.8	38.9	21.4	53.7	28.6	49.5	39.2	60.8	26.1	52.5
8.7	81.4	21.5	43.1	19.7	91.6	4.8	24.1	11.9	47.8
14.6	34.3	10.4	35.8	10.2	21.6	9.0	41.6	17.7	51.8
10.1	36.5	16.7	54.3	35.0	73.8	34.4	71.1	38.3	52.0

Table C1 F-15 Load Spectrum (Air-to-Air) (Continued)

20.9	38.5	28.7	48.7	24.9	44.6	28.0	48.0	-9.0	62.3
45.4	74.7	33.8	46.3	21.4	53.4	8.9	45.9	-3.5	48.8
15.6	58.4	32.2	48.8	9.6	48.7	15.3	26.4	3.0	57.5
15.4	31.7	15.3	41.5	7.9	27.7	14.7	71.6	6.4	24.7
3.0	54.2	-0.8	46.7	11.5	34.2	-2.9	32.1	-0.3	47.9
3.1	31.1	9.6	55.2	5.7	50.7	27.8	38.6	9.6	63.1
-5.0	49.0	31.0	61.7	43.5	65.7	6.3	47.8	23.1	71.9
10.0	76.6	22.7	38.0	5.2	31.1	17.5	70.8	35.3	61.6
26.8	56.5	7.2	54.9	17.4	30.1	9.2	19.9	5.9	17.9
6.2	65.2	-1.9	76.0	5.9	55.9	13.8	63.4	37.4	59.9
33.4	45.6	23.8	50.1	21.7	54.7	12.2	46.3	32.0	44.1
6.6	70.8	-5.0	48.4	23.9	45.7	20.3	52.5	6.2	35.3
20.3	61.8	8.1	47.5	28.7	41.5	18.8	34.2	6.3	84.1
25.8	47.9	30.3	59.6	20.5	64.6	38.3	55.0	27.8	43.2
26.0	62.8	17.1	40.1	17.6	30.6	12.8	65.8	9.5	59.6
34.4	67.6	-4.2	60.6	0.9	63.5	12.8	37.9	7.7	69.5
10.7	42.4	25.9	42.3	-5.0	54.1	24.7	66.4	23.2	49.9
12.4	34.5	23.5	50.5	25.5	44.1	22.4	45.7	26.1	74.2
39.4	61.1	28.2	45.7	18.3	53.7	20.6	34.1	32.1	67.6
23.4	62.3	28.4	80.2	19.1	48.7	29.4	55.9	19.7	79.2
11.2	43.8	21.7	48.2	20.9	71.9	33.9	63.3	34.9	52.7
29.8	60.6	10.7	65.8	17.5	64.9	-5.0	41.7	11.5	34.0
-22.0	26.3	11.0	30.7	19.0	40.1	29.5	47.3	2.7	60.1
26.0	59.6	28.2	64.9	21.9	52.8	34.7	49.6	27.5	55.8
30.2	57.5	23.3	62.3	3.2	46.9	11.1	35.2	16.7	35.3
7.1	45.9	15.4	46.9	22.0	50.0	24.0	36.6	13.8	52.0
4.1	17.7	-4.2	36.9	6.0	36.1	5.3	59.4	-5.0	67.1
19.0	48.0	19.8	78.5	21.8	45.9	21.9	45.8	9.5	67.8
17.8	37.8	18.5	85.2	24.5	35.3	20.3	56.2	31.6	62.8
8.7	50.2	10.5	65.9	20.0	42.2	9.2	34.2	11.9	52.6
21.4	64.7	-0.1	10.4	-3.7	62.3	6.6	44.1	9.8	41.6
24.3	39.6	19.4	31.1	15.8	32.8	-0.2	48.3	15.5	45.0
-5.0	41.0	16.2	45.2	34.1	58.6	26.5	48.3	10.5	59.9
9.8	61.8	5.4	53.0	26.9	44.4	2.1	57.4	28.3	49.5
18.3	56.5	-2.9	49.3	36.9	68.0	49.3	74.5	34.2	44.8
21.6	54.1	12.5	52.3	12.8	46.1	29.1	71.4	34.0	69.0
30.4	42.4	14.7	39.9	6.6	27.4	11.9	77.7	27.1	53.9
16.3	70.1	-5.0	67.1	43.0	63.1	7.7	27.8	8.7	46.0
8.8	54.7	25.8	53.5	22.6	48.9	33.4	47.8	35.2	74.6
43.2	53.3	21.5	69.1	21.7	83.9	10.9	43.6	18.9	34.3
7.6	45.9	32.7	54.3	9.3	50.3	2.6	35.7	16.2	43.8
29.9	52.5	13.8	58.6	16.2	83.3	29.5	49.1	9.2	38.5
16.4	57.4	-0.1	65.3	-5.0	65.0	32.1	53.7	27.4	45.1
33.7	65.3	15.4	31.6	5.3	22.3	7.8	45.0	-3.7	25.6
2.1	68.4	7.4	63.3	10.9	22.3	2.8	58.8	19.3	49.8
8.0	56.9	7.5	38.5	-1.1	41.8	12.8	61.7	3.3	36.2
25.1	51.8	20.6	58.3	42.7	63.7	25.9	49.2	11.7	48.3
28.4	54.7	23.2	46.2	14.7	46.7	-9.0	18.7	-19.0	48.8
-5.8	39.7	-2.7	64.8	1.0	41.2	29.8	49.8	29.4	39.5
9.1	40.2	4.5	51.5	20.8	54.8	22.4	59.8	7.8	25.2

Table C1 F-15 Load Spectrum (Air-to-Air) (Continued)

5.6	24.8	13.5	38.4	28.2	43.7	12.3	29.3	12.3	63.5
30.4	45.0	22.7	75.1	30.8	49.9	23.8	43.8	2.1	70.7
3.5	36.2	10.4	48.9	25.1	41.5	28.6	44.1	-5.0	66.4
21.8	49.5	28.1	56.1	-6.9	44.9	20.3	65.4	44.0	71.0
11.6	51.9	6.3	58.1	22.0	41.8	24.6	53.5	14.2	63.4
11.1	41.1	13.7	32.6	11.4	75.6	2.5	64.5	10.0	43.3
28.8	57.7	-4.7	73.5	12.7	41.9	18.6	46.0	24.6	36.9
14.6	41.7	30.7	67.3	28.5	71.2	15.4	49.9	21.4	59.2
-5.0	47.9	22.9	66.1	15.4	47.0	31.7	43.6	20.8	34.2
8.5	20.4	0.0	42.3	-14.3	48.6	21.2	43.3	-7.2	80.1
27.6	55.3	32.2	66.5	2.1	43.4	9.2	62.8	22.8	51.9
0.4	43.8	19.7	56.8	8.7	20.8	3.0	45.7	13.3	36.2
15.9	41.4	9.1	47.9	18.6	29.4	12.8	66.8	-7.5	45.8
29.6	61.3	-5.0	46.3	19.5	35.3	11.4	55.4	2.4	22.3
7.2	48.1	33.8	50.1	23.3	49.8	19.3	42.2	25.2	57.0
43.0	38.5	15.9	52.5	29.0	58.1	23.9	40.2	29.0	70.8
27.9	52.1	14.5	44.8	16.6	44.7	28.1	66.9	10.2	43.4
21.1	41.8	2.0	62.5	9.6	36.1	3.5	60.9	21.4	46.7
33.7	47.5	14.4	54.5	-5.0	60.9	16.4	32.1	17.3	80.2
6.8	26.9	9.9	55.7	13.5	65.1	41.8	53.3	20.7	39.4
28.2	40.6	8.6	63.2	23.0	45.3	22.3	36.1	21.0	65.7
27.6	40.2	22.5	43.0	31.8	77.5	-0.2	74.3	24.8	93.4
28.1	45.1	31.2	67.5	21.2	35.4	4.1	25.5	14.0	36.3
10.3	56.6	7.7	31.4	7.3	47.6	-5.0	15.1	1.1	36.7
7.4	49.4	16.9	45.9	10.4	22.4	10.6	23.1	8.4	20.8
6.9	50.6	1.5	34.4	-6.0	58.3	3.1	43.3	26.1	38.2
21.9	42.9	27.1	48.3	11.2	34.4	21.0	69.4	14.2	79.2
-10.1	67.5	11.1	49.8	8.9	51.4	18.2	52.6	19.8	81.3
30.8	48.6	15.3	56.3	15.2	49.6	22.6	48.5	-5.0	51.5
11.8	59.0	14.9	43.0	31.9	43.1	24.1	39.9	8.1	53.9
9.4	55.0	21.7	49.9	18.2	66.0	8.7	47.9	27.4	43.8
11.1	46.1	34.6	77.4	-8.6	64.6	4.6	70.9	19.1	48.6
32.6	65.4	8.3	64.2	32.3	54.9	10.5	39.7	3.0	37.7
27.3	38.1	24.3	50.3	29.5	43.4	4.1	42.8	19.6	57.9
-5.0	50.8	37.0	47.6	3.3	57.6	28.1	48.6	36.7	51.1
0.0	49.8	32.6	64.3	11.3	50.7	10.8	23.4	11.1	36.2
38.8	54.4	14.5	27.6	7.9	30.8	20.4	45.0	14.3	54.4
18.2	34.0	8.0	56.3	15.7	48.5	14.5	56.7	44.3	62.6
13.3	49.0	22.7	42.1	16.1	38.2	8.0	49.6	-7.1	24.9
6.5	45.2	-5.0	47.7	15.7	37.8	9.3	57.4	19.5	61.6
29.1	48.6	17.7	49.8	3.6	66.9	14.6	26.9	-0.5	35.5
13.6	25.7	15.2	60.6	1.1	35.8	14.5	81.0	30.4	46.5
9.8	19.9	7.2	44.2	22.7	33.6	11.6	40.9	4.8	67.1
16.2	74.6	10.0	23.2	1.0	21.3	1.9	73.9	1.8	42.2
30.1	61.6	13.6	39.7	-5.0	50.3	32.4	70.4	20.6	66.0
25.8	56.5	42.0	55.6	10.9	48.5	17.1	37.8	3.4	32.5
4.2	41.9	16.4	46.9	11.8	46.7	20.5	52.1	1.7	52.4
32.4	49.1	24.7	70.4	18.8	64.8	-1.8	49.5	-9.3	23.9
12.0	48.2	22.9	37.3	10.8	31.5	16.8	40.2	20.3	48.5
26.7	59.9	21.7	52.3	11.1	35.8	-5.0	49.2	5.4	25.2

Table C1 F-15 Load Spectrum (Air-to-Air) (Continued)

12.8	47.9	29.3	41.9	3.4	57.8	-28.0	39.6	-9.2	31.0
7.8	37.0	8.3	37.0	13.0	67.2	5.6	45.6	8.9	33.7
4.4	67.4	15.9	46.6	36.1	46.6	18.3	59.3	38.2	64.7
13.5	39.2	16.4	49.9	12.1	54.3	-20.9	42.1	-17.3	43.1
11.5	51.2	19.2	39.1	12.0	44.9	23.4	34.3	-5.0	61.3
9.0	48.7	8.8	39.1	24.4	42.4	15.5	45.8	21.5	35.9
24.8	38.9	13.4	47.2	20.8	52.2	-17.6	53.4	-34.2	53.7
19.6	38.5	22.5	67.3	8.2	38.0	25.5	44.1	30.3	42.3
23.4	46.6	35.0	68.8	40.8	52.6	13.5	32.7	12.0	60.7
32.0	49.7	33.7	46.6	-27.7	49.5	38.1	55.1	-2.3	44.9
-5.0	41.7	22.2	47.1	33.8	55.4	10.8	49.0	38.4	49.8
9.8	56.9	27.4	53.7	31.9	60.6	8.0	51.0	26.1	61.8
39.6	77.7	34.8	53.2	-22.6	34.4	-9.2	35.0	-29.2	42.3
15.6	41.5	18.8	45.7	34.1	45.0	26.0	47.5	26.0	44.1
21.6	33.2	20.2	37.6	13.5	39.3	23.0	48.7	7.5	33.7
22.6	-5.0	29.6	44.7	16.3	64.5	7.8	55.8	-4.2	30.6
20.2	44.8	34.1	54.0	20.7	41.1	26.6	72.3	25.5	55.5
30.0	72.5	7.3	38.1	25.1	39.0	17.6	62.8	8.2	35.2
-4.4	19.3	0.8	53.2	-8.3	50.2	-5.7	63.9	-4.0	49.7
27.7	38.3	-1.0	27.3	2.3	55.9	16.5	59.5	24.0	50.6
9.5	41.5	2.8	-5.0	18.1	52.2	16.0	50.9	35.2	56.7
-2.4	52.7	8.3	26.1	-12.8	32.6	-15.1	60.6	-6.6	62.7
-1.8	43.9	14.7	50.2	33.8	56.7	24.2	56.9	3.3	53.8
41.4	69.1	31.5	41.7	23.0	48.9	38.5	78.3	10.6	37.5
23.0	53.0	31.9	48.0	-9.9	35.6	-15.7	65.1	-35.2	51.4
11.2	45.0	33.1	46.8	23.9	-5.0	35.1	58.2	-3.1	62.8
13.1	72.2	19.6	76.3	36.8	68.3	17.9	68.6	0.7	64.9
35.0	67.2	17.1	35.1	6.8	29.4	-12.4	45.8	-15.1	43.2
2.7	40.8	9.7	50.0	20.4	46.0	23.2	50.5	15.4	83.0
17.4	30.2	19.6	38.4	26.5	77.5	19.8	52.2	10.0	83.5
6.3	79.2	16.0	29.4	-4.1	68.5	31.2	50.8	-5.0	52.4
9.9	40.1	10.5	24.4	13.1	39.5	23.7	53.5	7.6	74.8
16.7	68.6	4.8	49.5	28.1	45.7	25.9	47.0	13.1	54.8
24.4	56.8	27.4	49.7	34.2	65.5	-17.2	69.9	-8.2	30.7
11.8	51.1	31.7	48.1	19.2	29.3	18.8	65.6	23.8	68.8
56.2	74.6	38.4	56.8	28.1	54.3	31.5	59.4	45.9	61.3
-5.0	57.0	36.9	71.7	34.1	67.1	43.7	61.0	-24.7	47.3
33.4	66.3	30.3	43.7	21.8	47.6	14.4	43.6	-6.8	55.2
2.5	37.8	19.4	46.3	9.8	63.4	-12.7	5.0	-5.2	39.6
12.1	30.3	17.4	53.8	21.6	55.5	-17.7	45.1	-16.8	54.3
9.8	93.0	12.7	38.0	21.5	50.1	33.6	66.7	17.5	35.4
25.0	44.8	-5.0	40.6	29.8	47.3	11.3	40.7	23.7	60.7
3.9	43.4	19.9	50.6	5.7	51.8	-1.3	55.1	-17.0	82.5
34.2	61.6	40.6	54.5	14.1	60.9	14.2	50.4	19.4	62.3
2.9	79.2	41.9	53.9	11.6	28.1	13.2	26.9	-4.2	50.6
7.9	49.3	4.5	19.9	-10.2	43.7	29.5	40.3	13.6	41.3
15.3	47.4	12.3	71.6	-5.0	50.6	24.0	51.6	32.9	44.4
17.2	55.1	13.3	37.0	13.0	39.3	1.3	27.7	7.3	36.7

Table C1 F-15 Load Spectrum (Air-to-Air) (Continued)

7.6	41.3	30.3	47.2	26.2	41.0	4.7	61.4	19.3	35.5
23.3	33.4	10.2	43.5	27.0	51.8	16.3	26.9	11.7	69.1
0.6	59.4	-2.9	56.8	-1.1	43.4	34.8	33.7	27.4	40.4
23.4	55.2	44.5	60.2	21.6	70.9	-5.0	56.3	18.4	61.4
28.2	41.1	20.6	58.0	37.0	49.1	13.4	45.5	-0.6	59.0
7.5	64.9	17.6	53.8	39.1	63.7	14.1	51.0	-0.6	59.2
15.9	61.8	16.8	60.2	24.8	52.2	26.5	57.3	9.5	21.4
4.3	55.0	2.9	49.4	16.5	41.8	10.1	47.6	33.7	67.7
9.4	53.3	32.4	47.5	17.9	74.1	29.2	59.0	-9.0	34.6
18.7	52.7	12.7	28.1	17.1	41.8	8.5	44.7	30.1	49.6
0.5	48.1	29.0	40.5	21.4	35.5	13.4	38.2	10.0	57.7
18.6	35.8	23.9	42.0	26.4	52.8	23.8	36.5	-9.6	55.1
14.3	43.4	30.1	49.8	23.4	56.1	18.4	44.6	7.8	51.0
35.9	59.7	37.2	51.7	33.6	47.7	37.0	59.2	32.5	54.9

Notes: Percentage of σ_{LIM}

σ_{min}	σ_{max}	<u>cycles</u>
15.3	53.7	10.
10.0	25.0	3.0
15.3	47.8	22.
10.0	16.1	1.
6.7	29.7	64.
11.9	51.0	11.
14.2	37.1	49.
14.5	40.2	0.1
11.5	41.0	0.5
13.4	27.1	1.
6.3	17.8	1.
11.5	53.8	10.
11.5	41.3	27.
9.6	27.0	18.
6.9	14.5	1.
7.3	18.8	1.
11.5	26.3	76.
-6.7	6.9	1.
-2.7	92.3	9.
13.4	31.8	1308.
11.5	35.0	49.
-2.7	100.	1.2
13.4	49.3	618.
13.8	44.4	38.
15.3	53.7	11.
15.3	51.0	302.
14.9	95.3	1.4
12.4	40.6	305.
11.7	44.2	95.
6.1	15.3	1.
13.4	43.6	3.
15.3	33.7	77.
-22.6	11.9	1.
14.5	40.2	15.
13.4	26.1	1.
11.5	34.5	0.1
9.6	37.9	5.
15.3	56.3	32.
-18.4	15.3	1.
13.4	41.3	1129.
14.9	50.5	43.
-2.7	54.9	80.
10.4	16.8	1.
15.3	54.4	0.2
-19.5	13.4	1.
15.3	37.5	350.
15.3	64.9	27.
11.5	38.8	1.

Table C2 F-16 400-Hour Spectrum (FHQ Program) (Continued)

-2.7	83.5	30.
15.3	51.0	7.
12.4	51.8	0.05
-13.4	38.9	6.
7.1	13.5	1.
13.8	33.0	321.
-1.5	14.2	1.
13.4	51.5	211.
11.9	80.8	0.5
3.1	11.9	1.
14.9	36.6	54.
11.5	43.3	5.
15.3	55.2	9.
11.9	37.1	15.
11.9	30.1	57.
11.9	44.2	1.
15.3	59.0	89.
11.9	64.4	3.
15.3	58.1	0.5
9.6	59.8	13.
15.3	47.8	43.
11.5	41.9	3.
11.9	64.4	4.
-2.7	57.8	21.
15.3	21.4	1.
-12.3	9.6	1.
15.7	65.0	3.
-12.6	15.3	6.
11.5	28.0	57.
6.9	25.7	56.
13.4	53.1	591.
9.6	14.5	1.
9.4	20.9	11.
15.3	33.7	347.
11.9	64.4	1.
11.5	36.6	98.
10.0	29.7	880.
11.9	67.8	28.
13.4	37.5	1.
15.3	33.7	74.
11.5	34.5	5.
9.6	27.1	52.
-2.7	59.0	13.
12.7	19.1	1.
12.4	48.6	0.1
11.5	35.0	8.
11.9	44.0	44.
14.5	20.7	1.
5.6	21.7	99.
9.6	49.3	1.
14.5	35.6	42.

Table C2 F-16 400-Hour Spectrum (FHQ Program) (Continued)

11.9	77.5	0.05
-3.8	11.9	1.
10.0	72.0	80.
14.9	63.3	22.
-2.7	67.6	6.
10.0	54.5	416.
15.3	55.2	2.
12.4	17.6	1.
10.5	16.9	1.
11.9	18.3	1.
11.9	30.1	347.
-2.7	82.3	2.
15.3	79.2	14.
11.9	57.7	7.
11.9	71.6	2.
14.9	77.5	6.
13.8	79.3	3.
13.4	31.6	24.
11.9	57.7	2.
13.4	29.9	6.
12.4	53.5	1.
-21.4	15.3	1.
11.5	34.5	876.
13.8	70.3	23.
14.5	35.6	125.
4.2	14.2	1.
4.0	15.5	1.
13.4	30.9	156.
10.0	42.1	760.
6.9	37.7	48.
12.4	33.3	5.
11.5	30.3	4.
-34.5	28.7	3.
15.3	47.8	8.
13.4	50.5	1.
13.4	31.8	3.
14.5	40.2	29.
13.8	44.6	1082.
13.4	49.5	1.
15.3	56.3	2.
-20.3	11.9	1.
6.9	49.7	27.
11.9	44.0	6.
9.6	37.9	45.
-17.6	9.6	1.
14.2	34.3	57.
11.9	56.9	593.

Table C2 - F-16 400-Hour Spectrum (FHQ Program) (Continued)

-6.1	15.3	17.
11.5	16.9	1.
-8.8	11.9	1.
11.5	30.3	19.
13.8	67.6	153.
-2.7	78.3	4.
10.1	26.2	189.
11.5	33.3	22.
7.3	13.8	1.
-23.0	11.9	1.
11.9	68.5	10.
-13.8	14.2	1.
15.7	37.7	16.
11.9	37.1	36.
11.9	71.6	0.5
-8.4	11.5	1.
12.4	45.5	2.
13.4	27.1	1.
13.4	48.4	2.
15.3	55.2	7.
1.1	24.1	18.
11.5	28.0	43.
2.3	18.4	11.
11.9	31.6	4.
-4.1	18.8	5.
6.9	68.0	5.
11.5	41.0	1.
12.4	30.3	885.
15.3	56.9	1.
13.4	37.5	0.1
15.3	40.6	36.
11.1	22.6	1.
12.4	47.1	30.
13.4	28.2	17.
13.4	30.9	12.
15.3	40.8	87.
11.5	39.7	36.
13.4	34.1	15.
15.3	36.0	3.
14.5	48.2	0.2
15.7	65.0	5.
13.8	33.0	132.
15.3	56.9	3.
-1.3	6.9	1.
13.8	33.0	1353.
6.9	23.0	11.
13.8	53.9	7.
9.6	63.9	6.

Table C2 F-16 400-Hour Spectrum (FHQ Program) (Continued)

13.4	41.3	8.
15.3	37.5	122.
10.0	67.0	224.
13.4	52.2	1.
11.9	57.7	9.
15.3	75.8	5.
15.3	51.0	34.
7.6	49.3	25.
-2.7	60.8	3.
13.4	19.1	1.
15.3	56.0	138.
-12.3	6.9	1.
13.8	44.4	3.
13.4	34.5	29.
13.4	29.3	57.
-7.6	14.2	1.
2.1	34.3	4.
6.9	61.9	14.
15.7	51.4	17.
13.4	33.7	2.
12.4	27.4	30.
14.2	40.4	47.
11.9	71.6	4.
13.4	41.3	52.
0.0	15.3	57.
15.7	37.5	69.
11.9	30.1	76.
11.5	44.2	14.
4.4	15.9	1.
-14.2	13.4	1.
2.7	11.9	1.
11.5	38.8	479.
15.7	50.7	5.
11.9	44.0	22.
13.4	16.9	1.
12.4	39.2	2.
15.3	58.1	6.
11.9	51.0	26.
15.3	58.1	3.
-2.7	11.5	1.
11.9	30.3	1014.
11.9	32.0	109.
14.5	44.4	6.
15.3	53.7	26.
3.1	19.2	7.
-7.1	43.5	1.
-7.1	43.5	1.

Table C3 B-1 Load Spectrum (Combat)

Notes: All fractional cycles have been replaced by unit cycles.
This is a complete flight (= 9 hrs.).

MISSION SEGMENT	WING ANGLE	LOAD TYPE	GROSS STRESS (KSI)		CYCLES/ MISSION
			MAXIMUM	MINIMUM	
GROUND	15		20.00	-5.00	1.00
POST TAKE OFF	15	MANEUVER	17.66	10.09	0.10
			16.88	11.07	1.00
WING SWEEP	15	1G	13.67	13.87	1.00
	25		11.26	11.26	1.00
SUBSONIC CLIMB	25	MANEUVER	16.69	4.77	0.10
			15.16	7.46	1.00
			13.67	11.26	4.00
			11.26	8.85	3.00
SUBSONIC CRUISE	25	GUST	15.79	6.40	0.10
			14.39	7.80	1.00
			13.19	9.00	1.00
		MANEUVER	16.40	7.19	0.10
			16.20	7.49	1.00
			14.80	11.09	19.00
WING SWEEP	25	1G	11.26	11.26	1.00
	67.5		7.70	7.70	1.00
SUPERSONIC CLIMB	67.5	MANEUVER	14.26	2.02	0.10
			12.32	4.03	1.00
			10.25	8.17	8.00
			8.17	6.64	7.00
SUPERSONIC CRUISE	67.5	MANEUVER	12.62	1.92	0.10
			10.46	3.46	1.00
			8.47	6.33	5.00
			6.33	4.80	2.00
SUPERSONIC DESCENT	67.5	MANEUVER	12.64	1.57	0.10
			10.65	3.97	1.00
			8.87	7.17	8.00
			7.17	5.53	7.00
WING SWEEP	67.5	1G	7.70	7.70	1.00
	25		11.00	11.09	1.00
REFUEL	25	MANEUVER	15.69	5.99	0.10
			14.69	6.89	1.00

Table C3 B-1 Load Spectrum (Combat) (Continued)

MISSION SEGMENT	WING ANGLE	LOAD TYPE	GROSS STRESS (KSI)		CYCLES/ MISSION
			MAXIMUM	MINIMUM	
REFUEL	25	MANEUVER	13.59	11.09	10.00
			11.09	8.39	15.00
SUBSONIC CRUISE	25	MANEUVER	18.30	5.22	0.10
			16.92	6.30	1.00
			13.38	10.92	26.00
			10.92	8.17	8.00
SUBSONIC DESCENT	25	MANEUVER	16.03	4.50	0.01
			15.34	5.07	0.10
			13.89	6.00	1.00
			12.52	9.78	4.00
			9.78	7.21	3.00
WING SNEEP	25	IG	9.78	9.78	1.00
	67.5		7.17	7.17	1.00
LOW LEVEL NAVIGATION	67.5	GUST	8.49	0.27	0.01
			7.73	0.89	0.10
			6.97	1.65	1.00
			6.21	2.41	10.00
			5.70	2.92	17.00
			11.59	2.48	0.01
			10.70	3.30	0.10
			9.94	4.12	1.00
			9.25	4.82	10.00
			8.61	5.45	61.00
			15.12	6.64	0.01
			14.36	7.40	0.10
			13.80	8.16	1.00
			12.91	8.86	10.00
			12.34	9.43	26.00
FLY UP	67.5	3.06	18.01	7.03	1.00
		2.56	15.24	7.03	1.00
LOW LEVEL NAVIGATION	67.5	MANEUVER	13.45	5.54	1.00
			12.83	4.72	11.00
			12.88	4.31	29.00
			11.96	4.00	46.00
			10.83	3.75	75.00
LOW LEVEL BOMBING	67.5	GUST	9.80	3.59	86.00
			9.94	2.52	0.10
			9.41	3.06	1.00
			8.63	3.83	10.00
			7.85	4.61	62.00
		MANEUVER	8.30	4.16	0.10

Table C3 B-1 Load Spectrum (Combat) (Continued)

MISSION SEGMENT	WING ANGLE	LOAD TYPE	GROSS STRESS (KSI)		CYCLES/ MISSION
			MAXIMUM	MINIMUM	
LOW LEVEL BOMBING	67.5	MANEUVER	8.01	4.45	1.00
			7.59	4.87	3.00
		GUST	11.29	1.68	0.01
			10.92	2.06	0.10
			10.54	2.44	1.00
			10.28	2.69	4.00
		MANEUVER	8.33	4.64	1.00
			8.18	4.84	6.00
			7.92	5.05	8.00
			7.67	5.30	9.00
WING SWEEP	67.5	IG	6.49	6.49	1.00
	25		9.80	9.80	1.00
SUBSONIC CLIMB	25	MANEUVER	16.98	2.71	0.01
			16.00	3.86	0.10
			15.03	4.83	1.00
			12.14	10.02	10.00
			10.02	7.90	8.00
SUBSONIC CRUISE	25	MANEUVER	17.05	3.96	0.01
			16.52	4.66	0.10
			15.21	5.87	1.00
			12.94	9.80	12.00
			9.80	8.18	3.00
SUBSONIC DESCENT	25	MANEUVER	12.07	1.69	0.01
			11.45	2.15	0.10
			10.21	3.00	1.00
			8.97	6.41	10.00
			6.41	4.09	8.00
WING SWEEP	25	IG	8.80	8.80	1.00
	15		9.25	9.25	1.00
PRE-LANDING	15	GUST	16.97	1.53	0.01
			15.75	2.75	0.10
			13.89	4.62	1.00
			12.02	6.49	87.00
		MANEUVER	17.63	2.60	0.01
			16.49	3.24	0.10
			14.40	4.88	1.00
			11.71	9.25	17.00
			9.25	3.85	13.00
			7.45	9.25	1.00

Table C4 B-1 Load Spectrum (Crew Training)

Notes: All fractional cycles have been replaced by unit cycles.
This is a complete flight (= 4 hrs.).

MISSION SEGMENT	WING ANGLE	LOAD TYPE	GROSS STRESS (KSI)		CYCLES/ MISSION
			MAXIMUM	MINIMUM	
GROUND	15		20.00	- 5.00	1.00
POST TAKE OFF	15	MANEUVER	17.05	7.00	0.01
			15.57	8.48	0.10
			14.36	9.69	1.00
WING SWEEP	15	IG	12.02	12.02	1.00
	25		10.02	10.02	1.00
SUBSONIC CLIMB	25	MANEUVER	16.00	3.66	0.01
			15.03	4.83	0.10
			13.36	6.76	1.00
			12.14	7.90	2.00
SUBSONIC CRUISE	25	GUST	15.90	7.00	0.01
			14.40	5.21	0.10
			12.50	7.11	1.00
		MANEUVER	15.65	5.36	0.01
			14.78	6.23	0.10
			12.94	8.18	1.00
			12.24	9.60	2.00
REFUEL	25	MANEUVER	14.68	3.86	0.01
			14.08	4.66	0.10
			12.94	6.23	1.00
			11.91	9.00	7.00
			9.80	7.92	11.00
SUBSONIC CRUISE	25	MANEUVER	16.52	4.06	0.01
			15.48	5.53	0.10
			13.64	7.00	1.00
			12.24	9.80	5.00
			9.80	7.97	1.00
SUBSONIC DESCENT	25	MANEUVER	15.34	5.07	0.01
			14.31	5.75	0.10
			12.52	7.21	1.00
			11.57	7.99	1.00
WING SWEEP	25	IG	9.78	9.78	1.00
	67.5		7.17	7.17	1.00

Table C4 B-1 Load Spectrum (Crew Training) (Continued)

MISSION SEGMENT	WING ANGLE	LOAD TYPE	GROSS STRESS (KSI)		CYCLES/ MISSION
			MAXIMUM	MINIMUM	
LOW LEVEL NAVIGATION	67.5	GUST	8.11	0.51	0.01
			7.73	0.89	0.10
			6.97	1.65	1.00
			6.21	2.41	10.00
			5.70	2.92	17.00
			11.14	2.92	0.01
			10.70	3.36	0.10
			9.94	4.12	1.00
			9.25	4.82	10.00
			8.61	5.45	61.00
			14.80	6.96	0.01
			14.36	7.40	0.10
			13.60	8.16	1.00
			12.91	8.86	10.00
			12.34	9.43	26.00
FLY UP	67.5	3.0G	18.01	7.03	1.00
		2.5G	15.24	7.03	1.00
LOW LEVEL NAVIGATION	67.5	MANEUVER	13.29	3.03	0.01
			13.45	3.44	0.10
			12.83	3.59	1.00
			12.88	3.75	10.00
			11.96	4.00	25.00
			10.83	4.31	60.00
			9.80	4.72	60.00
			8.73	5.54	60.00
LOW LEVEL BOMBING	67.5	GUST	10.92	2.06	0.01
			10.54	2.44	0.10
			9.84	3.13	1.00
			9.02	3.95	5.00
			8.19	4.78	17.00
		MANEUVER	8.18	4.84	0.01
			7.92	5.05	0.10
			7.67	5.30	1.00
WING SWEEP	67.5	IG	6.49	6.49	1.00
	25		8.80	8.80	1.00
SUBSONIC CLIMB	25	MANEUVER	14.03	3.41	0.01
			13.19	4.41	0.10
			11.68	6.00	1.00
			10.62	6.98	2.00
SUBSONIC CRUISE	25	MANEUVER	14.50	4.20	0.01

Table C4 B-1 Load Spectrum (Crew Training) (Continued)

MISSION SEGMENT	WING ANGLE	LOAD TYPE	GROSS STRESS (G)		CYCLES/ MISSION
			MAXIMUM	MINIMUM	
SUBSONIC CRUISE	25	MANEUVER	13.52	4.96	0.10
			12.09	6.25	1.00
			10.80	8.67	5.00
			8.67	7.09	1.00
SUBSONIC DESCENT	25	MANEUVER	11.45	2.15	0.01
			10.52	1.69	0.10
			8.97	4.09	1.00
			8.12	4.79	1.00
WING SWEEP	25	IG	8.80	8.80	1.00
	15		9.25	9.25	1.00
PRE-LANDING	15	GUST	10.97	1.53	0.01
			15.75	2.75	0.10
			13.89	4.62	1.00
			12.42	6.08	10.00
			11.28	7.22	93.00
		MANEUVER	17.63	2.60	0.01
			16.49	3.24	0.10
			14.40	4.88	1.00
			12.30	9.25	20.00
			9.25	6.38	15.00
GROUND	15	TAXI	-1.61	-0.76	1.00
FLY AROUND	15	MANEUVER	14.40	4.88	1.00
GROUND	15	TAXI	-1.61	-0.76	1.00
FLY AROUND	15	MANEUVER	14.40	4.88	1.00
GROUND	15	TAXI	-1.61	-0.76	1.00
FLY AROUND	15	MANEUVER	14.40	4.88	1.00
GROUND	15	TAXI	-1.61	-0.76	1.00
FLY AROUND	15	MANEUVER	14.40	4.88	1.00
			7.45	9.25	1.00

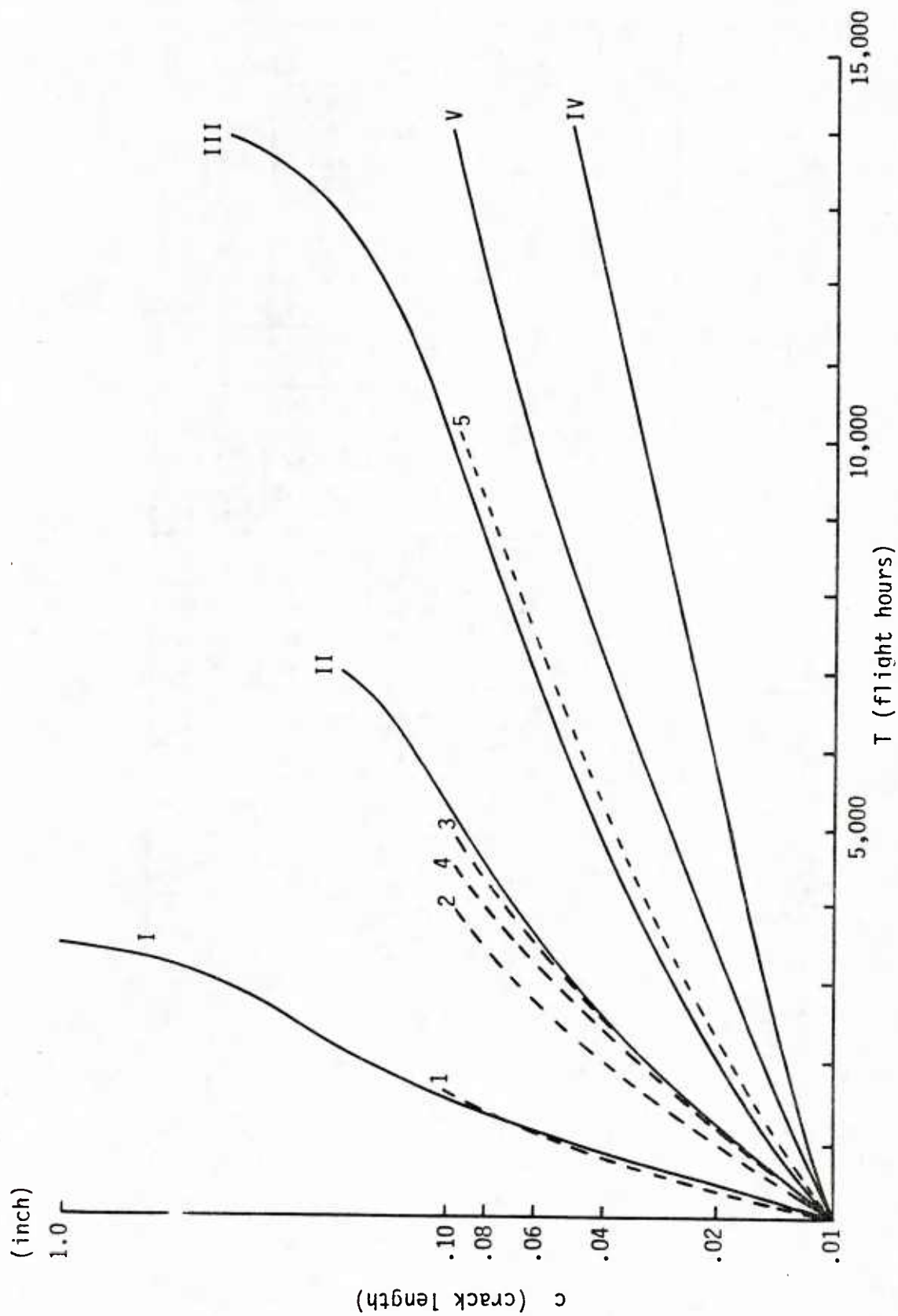


Fig. C3 Crack Growth Curves for Five Load Spectra
Based on CYCGRO Program

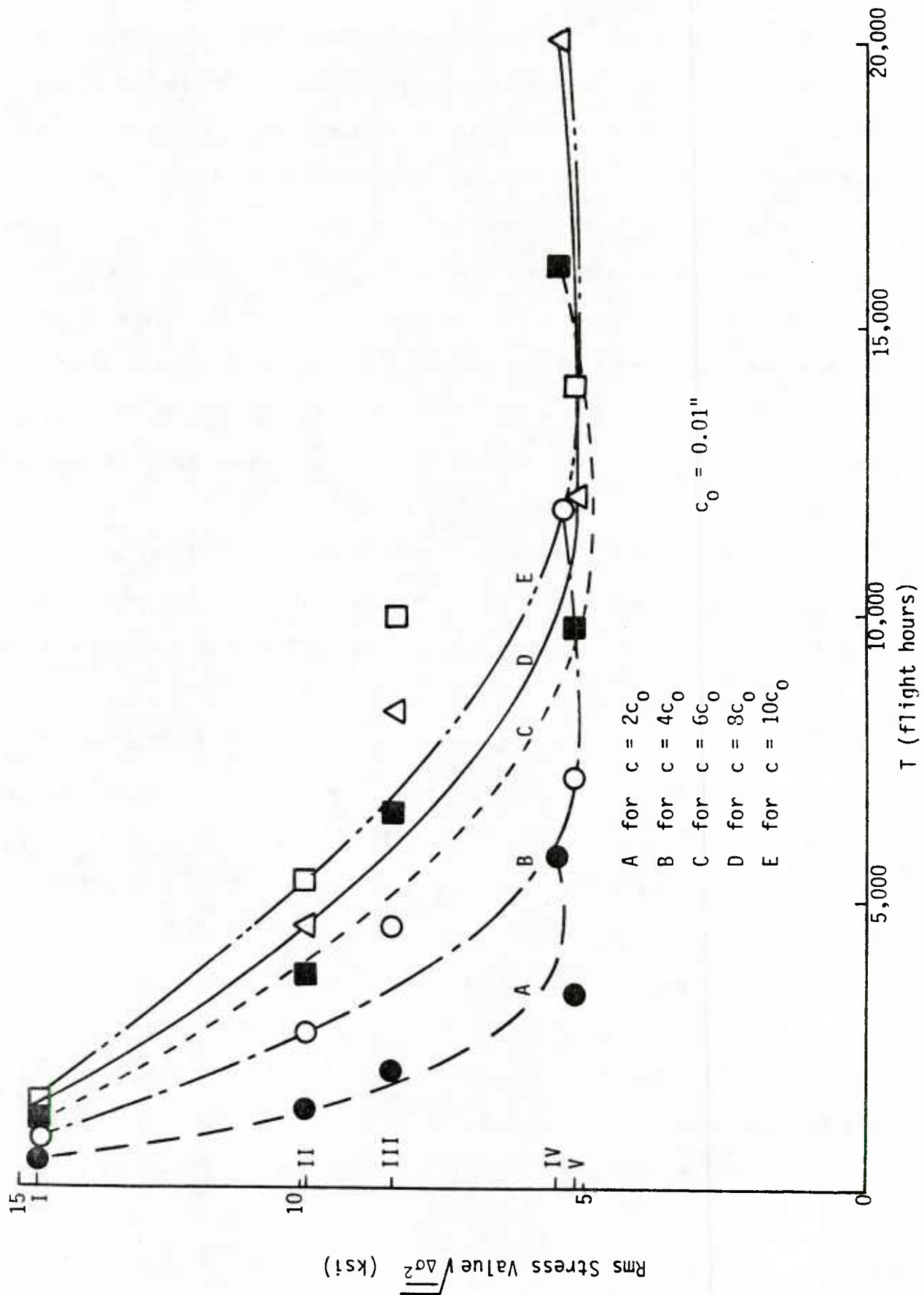


Fig. C4 Rms Stress Value - Flight Hour Relationship

example, Curve A for $c = 2c_0$. These curves appear to be reasonable in representing the $T-\sqrt{\Delta\sigma^2}$ relationships for the various crack sizes, except in the lower range of the spectral intensities. Indeed, when the rms stress values are small, the crack grows slowly and the relationships may become highly sensitive to the definition of the spectral intensity. In fact, under load spectrum IV with an rms stress value of 5.80 ksi, the crack grows more slowly than under load spectrum V with a smaller rms stress value of 5.18 ksi. This particular anomaly can be explained, however: one flight for load spectrum IV is nine (9) hours in duration, while one flight for load spectrum V is four (4) hours. Therefore, although the rms value is smaller, load spectrum V has a larger number of air-ground cycles and, apparently because of this, produces a slightly larger amount of damage for each flight hour than load spectrum IV does. Such anomalies may be rectified by redefining (or revising the current definition of) the spectral intensity. For example, a spectral intensity definition that reflects the effect of the mean stress or of the ratio R of the maximum to minimum stress (in addition to the rise and fall) may alleviate this difficulty. This is indeed an interesting subject to be investigated. It is pointed out again, however, that the $T-\sqrt{\Delta\sigma^2}$ relationships in Fig.C4 present no anomalous features in the high intensity range where the fighter load spectral intensities are expected to lie, particularly when each load spectrum involves approximately the same number of flight hours for one flight.

At any rate, the curves in Figs.C3 and C4 represent, in approximation, the transfer characteristics as explained earlier: For example, the crack growth curve under a load spectrum with, say, $\sqrt{\Delta\sigma^2} = 12.5$ ksi, can be constructed approximately on the basis of Fig.C4 by reading the values of T

at $c = 2c_0$, $4c_0$, etc., respectively, as 850 hrs, 1,700 hrs, etc. As also indicated previously, it is important to note that these curves establish the equivalent flight hours for the various load spectra. For example, from Fig.C3, one observes that 1,300 hours of flight under load spectrum II is equivalent to 2,250 hours of flight under load spectrum III, since, in both cases, the initial crack $c_0 = 0.01$ " will grow into $c = 0.02$ " during their respective flight hours.

In a further application of this concept of equivalent flight hours, a simplified spectrum consisting only of a few stress cycles (including, however, an air-ground stress cycle) can be constructed for, say, experimental purposes. Fig.C5 depicts such a simplified spectrum whose parameters are σ_{\max} , σ_{\min} , σ'_{\min} and n (number of stress cycles). For example, adjusting these parameter values, one can construct five types of load spectra identified by ID Numbers 1 through 5 in Table C5. The designation of these spectra as A-A (severe), A-A, A-G, Composite and I-N, is rather arbitrary, however. Under the assumption that one flight involves 1.3 flight hours for A-A, 0.92 hours for A-G, 1.22 hours for Composite and 2.07 hours for I-N, the crack growth curves are constructed and plotted in Fig.C3 (dashed curves). Comparing curves 1 ~ 5 with curves I ~ V in Fig.C3, one observes that spectra 1 (simplified A-A, severe) and 3 (simplified A-G) are almost equivalent to spectra I (F-15, A-A) and III (GD 400 hours with $\sigma_{LIM} = 34$ ksi), respectively, at least up to $c = 0.1$ ", and spectrum 5 (simplified I-N) somewhat underestimates the crack growth associated with spectrum III (GD 400 hours with $\sigma_{LIM} = 28.9$ ksi). The other simplified spectra 6 ~ 15 are also listed in Table C5 with the corresponding crack growth curves plotted in Fig.C6. Comparison of Fig.C6 with Fig.C3 shows, among other things, that simplified

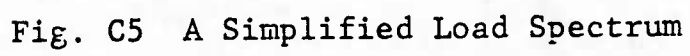


Table C5 Simplified Amplitude Flight-by-Flight Load Spectra ($\sigma_{LIM} = 40$ ksi)

ID #	Mission	σ_{min} , ksi	σ'_{min} , ksi	σ_{max} , ksi	$(\overline{\Delta\sigma^2})^{1/2}$, ksi	n, cycles
1	A - A (severe)	-2	4	20	16.28	24
2	A - A	-2	4	16	12.30	24
3	A - G	-4	4	16	12.52	19
4	Composite	-3	4	16	12.40	21
5	I - N	-.8	1.6	14	12.64	10
6	Composite	-3	6	16	10.58	21
7		-3	8	16	8.80	
8		-3	12	16	5.63	
9		-3	6	14	8.62	
10		-3	6	18	12.55	
11		-3	6	20	14.53	
12		-3	6	22	16.52	
13		0	4	16	12.21	
14		-.4	4	16	12.23	
15		-1.6	4	16	12.31	

Note: A-A; 1 flight = 1.3 hrs
 A-G; 1 flight = 0.92 hrs
 Composite; 1 flight = 1.22 hrs
 I-N; 1 flight = 2.07 hrs

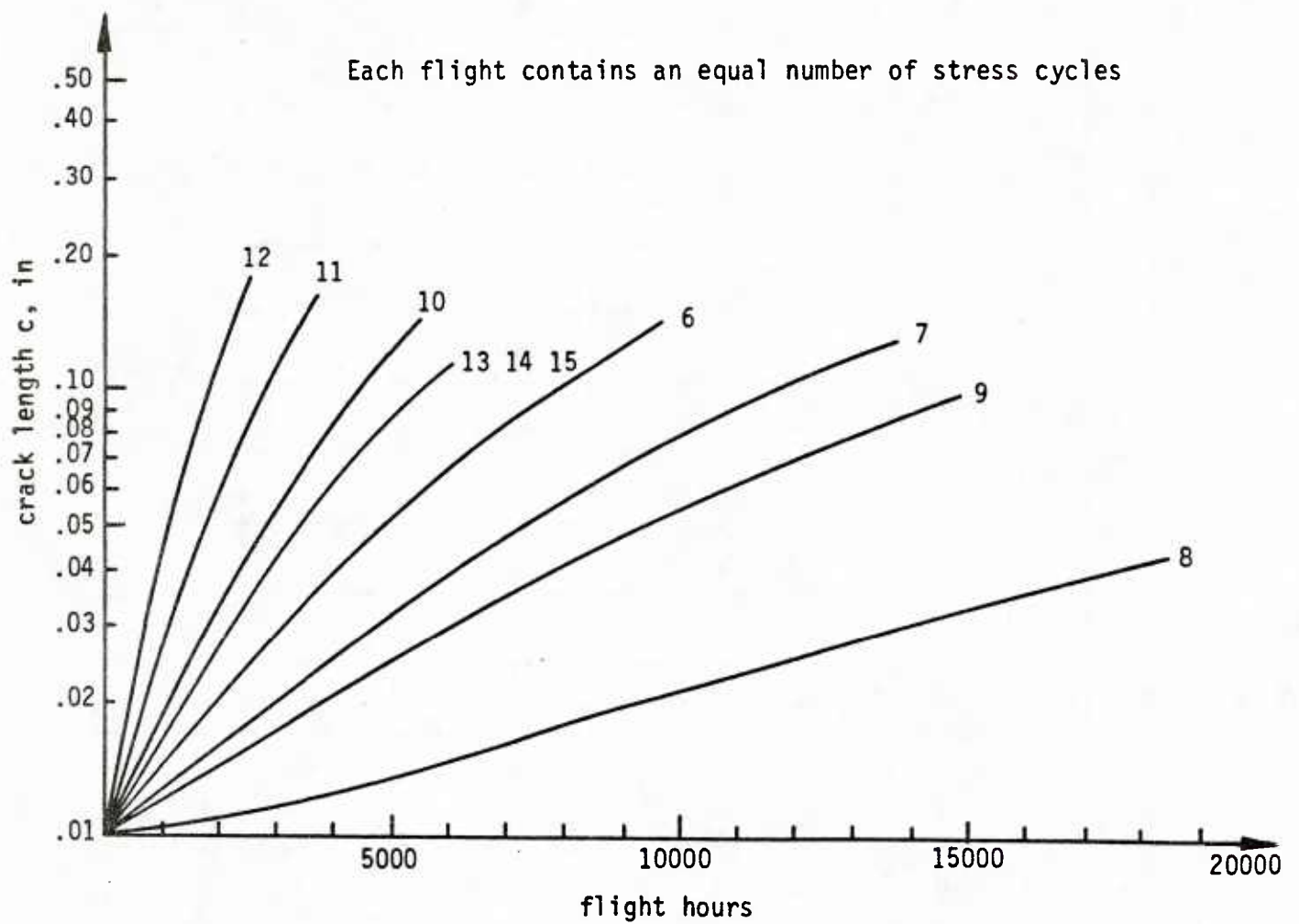


Fig. C6 Crack Growth Under Simplified Spectra (Missions 6-15)

spectra 7 and 9 are equivalent in approximation to spectrum V (B-1, Crew Training), with spectrum 7 overestimating and spectrum 9 underestimating the crack growth associated with spectrum V.

C.2.3 Concluding Remarks

The transfer characteristics among load spectra are described with the aid of crack growth and generalized S-N curves. The generalized S-N curve is defined as showing the relationship between the load spectral intensity (S) and the flight hours (N) required for a crack of initial size c_0 to grow to a specific size $c(> c_0)$. For simplicity, the rms value of the rise and fall of the stress history representing each load spectrum is used in this investigation as the indicator of the spectral intensity. For the five more realistic load spectra I ~ V, crack growth and generalized S-N curves are constructed. Similarly, the crack growth curves for the simplified load spectra 1 ~ 15 are constructed for the purpose of further comparison.

C.3 PARAMETRIC SENSITIVITY ANALYSIS

In the preceding sections, a number of analytical models are introduced primarily with respect to the crack propagation law, the distribution function of TICI and the corresponding distribution function of EIFS for the purpose of evaluating the probability $p(x,t)$ that, say, a fastener hole will have a dominant crack of a size larger than x at time t . Obviously, the value of $p(x,t)$ depends on these analytical models. However, these models are constructed on the basis of the current (and therefore not necessarily perfect) state of engineering knowledge on the subject matters involved, with due consideration not only for analytical and numerical tractability

but also for data availability. Therefore, it is highly desirable to investigate the sensitivity of the probability to these models. Such sensitivity studies can be performed in terms of numerical examples for those items for which competing or alternative models are proposed. For example, a significant difference in the probability may result depending on whether one chooses a Weibull compatible distribution or a log-normal compatible distribution for the EIFS. Such results are highly useful in numerically assessing the significance of the various models described in the preceding sections.

After the decision is made to choose a particular model among the alternatives proposed, it is not unusual to face uncertainties of a statistical or other nature under which the values are to be assigned to the parameters of the model. Then, sensitivity studies are again desirable with respect to these parameters for the purpose of identifying the more important parameters in terms of their contributions to the probability. Such a parameter sensitivity analysis, which is the main theme of this sub-section, is more straightforward than a model sensitivity analysis, at least in principle.

Writing these parameters as X_1, X_2, \dots, X_n , the probability $P = p(x, t)$ can be formally written as a function of X_1, X_2, \dots, X_n once the analytical models to be used are decided upon;

$$P = P(X_1, X_2, \dots, X_n) \quad (C6)$$

In actuality, the dependence of P on the parameters is obviously highly complex as seen from the analysis developed in the preceding sections.

Treating the uncertainties associated with these parameters as if they were all from statistical origins (or treating X_1, X_2, \dots, X_n as random

variables), the sensitivity of the probability $p(x,t)$ to each of these parameters is evaluated with the first order and second moment approach. Within the framework of this approach, the most reliable value of the parameter X_i is treated as its expected value and written as \bar{X}_i , whereas its uncertainty is expressed in terms of the coefficient of variation $V_{X_i} = \sigma_{X_i} / \bar{X}_i$ with σ_{X_i} being the standard deviation of X_i . The expected value \bar{P} and coefficient of variation V_P of P are then obtained from

$$\bar{P} = P(\bar{X}_1, \bar{X}_2, \dots, \bar{X}_n) \quad (C7)$$

$$V_P^2 = \sum_{i=1}^n \alpha_i^2 V_{X_i}^2 \quad (C8)$$

where α_i is referred to as the sensitivity index and is given by

$$\alpha_i = \left(\frac{\partial P}{\partial X_i} \right) \left(\frac{\bar{X}_i}{\bar{P}} \right) \quad (C9)$$

where the partial derivatives are evaluated at $X_i = \bar{X}_i$ ($i=1,2,\dots,n$). If \bar{P} and V_P are interpreted as representing the most reliable value of P and its uncertainty, respectively, the sensitivity index α_i indicates the contribution of the uncertainty associated with the parameter X_i to the uncertainty of \bar{P} through Eq. C8.

As mentioned earlier, the dependence of P on X_1, X_2, \dots, X_n is highly complex and the analytical evaluations of the partial derivatives in Eq. C9 may not be possible. Therefore, these derivatives are numerically evaluated as

$$\left(\frac{\partial P}{\partial X_i}\right)_{X_i=\bar{X}_i} = \{P(\bar{X}_1, \bar{X}_2, \dots, \bar{X}_i + \Delta X_i, \dots, \bar{X}_n) - P(\bar{X}_1, \bar{X}_2, \dots, \bar{X}_i, \dots, \bar{X}_n)\} / \Delta X_i$$

$$(i=1,2,\dots,n) \quad (C10)$$

Similarly, a parameter sensitivity analysis can be performed with respect to the mean $\bar{N}(x,t)$ and variance $\sigma_N^2(x,t)$ of the number N of the fastener holes. In fact, it may be more sensible to perform a parameter sensitivity analysis for these quantities since they are more directly related to the durability performance.

With respect to a sensitivity analysis, the present investigation has been limited in its scope to a general discussion. In view of the fact that the present state of knowledge is always imperfect and involves uncertain factors, it is highly recommended that a future durability study address itself exclusively to the problem of model as well as parameter sensitivity, and that it examine the range of the resulting numerical solutions in order to establish engineering, if not mathematical, confidence in the models and their parameter values to be used in the durability analysis as developed in the preceding sections.

References (Appendix C Only)

- C1. M. Szamossi, "Crack Propagation Analysis by Vroman's Model, Program EFFGRO, A-72-94, Rockwell International, Los Angeles 1972.
- C2. Private communication to S. D. Manning (General Dynamics, Fort Worth Division) from R. Vaicaitis (Columbia University), June 16, 1982.

REFERENCES

1. S. D. Manning, J. N. Yang, M. Shinozuka, and W. R. Garver, "Durability Methods Development, Volume I - Phase I Summary," Air Force Flight Dynamics Lab., AFFDL-TR-79-3118, September 1979.
2. S. D. Manning, M. A. Flanders, W. R. Garver, and Y. H. Kim, "Durability Methods Development, Volume II, Durability Analysis: State-Of-The-Art Assessment," Air Force Flight Dynamics Lab., AFFDL-TR-79-3118, September 1979.
3. B. J. Pendley, S. P. Henslee, and S. D. Manning, "Durability Methods Development, Volume III, Structural Durability Survey: State-Of-The-Art Assessment," Air Force Flight Dynamics Lab., AFFDL-TR-79-3118, September 1979.
4. M. Shinozuka, "Durability Methods Development, Volume IV - Initial Quality Representation," Air Force Flight Dynamics Lab., AFFDL-TR-79-3118, September 1979.
5. J. N. Yang, S. D. Manning, and W. R. Garver, "Durability Methods Development, Volume V, Durability Analysis Methodology Development," Air Force Flight Dynamics Lab., AFFDL-TR-79-3118, September 1979.
6. S. M. Speaker, D. E. Gordon, et al, "Durability Methods Development, Volume VIII - Test and Fractography Data," Air Force Flight Dynamics Lab., AFFDL-TR-79-3118, November 1982.
7. J. W. Norris, "Durability Methods Development, Volume IX - Documentation of Durability Analysis Computer Program," Air Force Flight Dynamics Lab., AFFDL-TR-79-3118, November 1982.
8. MIL-STD-1530A, "Aircraft Structural Integrity Program" December 1975.
9. MIL-A-8867B, "Airplane Strength and Rigidity Ground Tests," 22 August 1975.
10. MIL-A-8866B, "Airplane Strength, Rigidity and Reliability Requirements; Repeated Loads and Fatigue," August 1975.

52. "F-16 Durability Test Airplane, Volume I, Certification Test Plan," General Dynamics, Fort Worth Division, Report 16PR310-1, 17 February 1977.
 53. "F-16 Durability Test Airplane Certification Test Report," General Dynamics, Fort Worth Division, Report 16PR801, Vol. I-IV, 30 March 1979.
 54. W. R. Garver and R. D. Bruner, "Spectrum Fatigue Testing of Mechanical Fasteners for Structural and Fuel Integrity," General Dynamics, Fort Worth Division, ERR-FW-2069, April 1981.
 55. "Fractographic Examination of A-7D ASIP Initial Quality Specimens," Vought Aerospace Corp., Report ETR-53452-078, 19 June 1975.
-

U212878